5-2013

Chemical characterization and anion exchange properties of a west Tennessee loess soil

Jessica Lynn Ottinger
jottinge@utk.edu

To the Graduate Council:

I am submitting herewith a thesis written by Jessica Lynn Ottinger entitled "Chemical characterization and anion exchange properties of a west Tennessee loess soil." I have examined the final electronic copy of this thesis for form and content and recommend that it be accepted in partial fulfillment of the requirements for the degree of Master of Science, with a major in Environmental and Soil Sciences.

Michael E. Essington, Major Professor

We have read this thesis and recommend its acceptance:

Jaehoon Lee, Donald D. Tyler

Accepted for the Council:
Carolyn R. Hodges

Vice Provost and Dean of the Graduate School

(Original signatures are on file with official student records.)

CHEMICAL CHARACTERIZATION AND ANION EXCHANGE PROPERTIES OF A WEST TENNESSEE LOESS SOIL

A Thesis Presented for the
Master of Science
Degree
The University of Tennessee, Knoxville

Jessica Lynn Ottinger
May 2013

DEDICATION

I dedicate this Master's thesis to my parents, David Lynn and Carla Mason Ottinger, who always encouraged me to pursue my dreams and never gave up on me. I love you both.

ACKNOWLEDGEMENTS

This thesis was far from a solo act. I owe many thanks to those who have helped me in achieving this goal. First, I would like to thank my Major Professor, Dr. Michael E. Essington for believing in me even when I did not. My gratitude is also extended to my committee members, Dr. Donald D. Tyler and Dr. Jaehoon Lee for their guidance and support. I also give a special thank you to Galina Melnichenko for being a delight to work with and becoming a lifelong friend.

To my lab family, Melanie Stewart, Kalyn Vergeer, Lyndsye Benfield, Sarah Sheffel, Chad Tague, Candace Wilson, and Chloe Ashley, thank you all for being my rock and always helping me when I needed you. I cherish each and every one of you and hope to keep you all in my life forever.

I must also acknowledge my wonderful family and friends for their ongoing support and encouragement. To my parents, David Lynn and Carla Mason Ottinger, I love you both so much and appreciate all the sacrifices you have made for me to allow me to accomplish my goals. To my precious German Shepherd, Bristol, I love you more than words, and thank you for being my protector. To Joe, thank you for showing me there is still good ones left in the world. There are truly too many people to list that I owe thanks to. Thank you to all those people who are not mentioned by name who never left my side. I could never have finished this without you.

ABSTRACT

Loess soils of west Tennessee may potentially contain large amounts of subsoil metal oxides (Fe, Al, and Mn) which may retain and restrict the movement of conservative anions, such as nitrate (NO_3). The potential utilization of large quantities of flue gas desulfurization (FGD) gypsum on these soils may displace subsoil NO_3, releasing it to adversely impact sensitive aquatic environments. This research examines the depth distribution of Fe-, Al, and Mn-oxyhydroxides, pH, particle size distribution, and of the cation and anion exchange capacity and exchange phase composition to identify depths that have the greatest potential for anion exchange. The metal oxide content of depth incremented soil samples was determined using the citrate- bicarbonate-dithionite (CBD) and ammonium oxalate (AAO) extraction methods. The effective anion exchange capacity (EAEC), effective cation exchange capacity (ECEC), and anion and cation exchange phase compositions were determined using modified standard extraction methods. Both CBD and AAO extractable Fe, Al, and Mn were found to peak at two different depths within the soil profiles: in the Bt horizons (30 to 46 cm), and in the C horizon that underlie the loess deposits (244 to 259 cm). The depth- distribution of ECEC and EAEC follow the same trend as the extractable metal oxides. Based on these characterization data, the 30 to 46 cm and 245 to 261 cm depth increments are expected to be reactive to anions. This study also examined the anion exchange characteristics of binary and ternary nitrate, sulfate, and chloride systems in these high Fe-oxide horizons in the loess soils. Exchange isotherms were constructed by adding varying ratios

of two (binary) or three (ternary) ions to soil samples, allowing them to equilibrate, and displacing exchanged anions on the exchange phase. Exchange isotherms indicate that chloride and nitrate are preferred relative to sulfate, and that chloride is preferred relative to nitrate where preference is established by the Vanselow selectivity coefficients. Although not preferred, sulfate predominates on the anion exchange phase due to its divalent charge. These findings will enhance our knowledge of how the addition of sulfate to soil will impact conservative anion behavior in loess soils.

TABLE OF CONTENTS

LIST OF TABLES

CHAPTER II PAGE

CHAPTER III

LIST OF FIGURES

CHAPTER II PAGE

CHAPTER III

CHAPTER I

INTRODUCTION

INTRODUCTION

Agriculture has always been a viable repository for society's waste by-products. These by-products, which include sewage sludge, dairy and swine manure, poultry litter, yard waste, and paper mill residues, have been used to improve the nutrient status and physical characteristics of agricultural soils.

Increasing energy demand in the US, in addition to the implementation of Clean Air Act standards, has resulted in greater flue gas desulfurization (FGD) gypsum production, causing added strain on landfills and gypsum consumers (Clark et al., 2001). This material is created during coal-combustion power generation. Sulfur-laden flue exhaust gases are pumped into a scrubber where they are met by oxygenated limestone-water slurry. Gypsum is a by-product of this combination, and treated air is emitted from the top of the scrubber. The resulting gypsum slurry in the bottom of the scrubber is then sent to a dewatering station where it is "dried". In 1998, 98 million metric tons of coal combustion products (CCPs) were produced in the US, of which 34% was fly ash, 31% was bottom ash, and 10% was FGD gypsum that was used beneficially in both agricultural application and industrial uses such as construction, road, and structural fill (Clark et al., 2001). In 2009, the total production of CCPs had increased to 122.2 million metric tons (ACAA, 2011). FGD gypsum accounted for 13.3% (16.3 million metric tons) of the CCPs produced, and approximately 50% of that was utilized in concrete, cement, embankments and structural filling, mining application, paneling, waste stabilization, and agriculture (ACAA, 2011).

In the past, gypsum has been used in agriculture as a liming agent, sulfur source, and as an amendment to improve soil aggregation and mitigate soil erosion (Truman et

al., 2010). Soil amendments of FGD gypsum have also been shown to increase soil moisture retention by increasing infiltration rates, resulting in decreased runoff and sediment pollution in local streams (Truman et al., 2010).

Loess soils of the southeastern United States are susceptible to runoff and erosion (Truman et al., 2010). The application of gypsum to erosive soils generally results in decreased erosion and runoff with increased flocculation, dependent on soil properties such as texture, clay mineralogy, cation exchange capacity, and organic matter content (Lee et al., 2010). The loess-derived soils of the Mississippi Valley also contain variable charge Fe- and Al-oxide minerals, such as goethite, hematite, gibbsite, and kaolinite. These minerals contribute net positive surface charge under nearly all pH conditions, resulting in anion exchange capacity (Donn and Menzies, 2005). It has been shown that the presence of variable charge minerals results in the retention of otherwise mobile anions through outer-sphere (anion exchange) retention mechanisms. Specifically, long-term studies have shown that loess soils in west Tennessee accumulate nitrate (NO_3) and bromide (Br) in subsoil horizons (Ammons et al., 1994; Tyner et al., 2007). This is thought to be due to the presence of hydrous Fe-oxides acting as a barrier against NO_3 and Br leaching into the groundwater.

The addition of sulfate by gypsum amendment has the potential to affect the fate of bound NO_3. If the NO_3 is displaced from the anion exchange phase it may leach through the soil profile to adversely impact sensitive aquatic environments. Nitrate leaching into groundwater and subsequently into surface water has been linked to eutrophication in streams (He et al., 2011). Eutrophication occurs when increased amounts of fugitive fertilizers (e.g., NO_3) enter the waterway and result in a rapid

increase in algal growth, called an algal bloom. When this mass of algae dies they decompose and increase the biochemical oxygen demand (BOD) in the water. With the oxygen being used in the decomposition process there is less available for the use of the aquatic organisms, resulting in their suffocation. Research shows that NO_3 concentrations in groundwater and surface water are significantly higher in areas with extensive agricultural activity due to fertilizer use on cropland (He et al., 2011).

The chemical characterization of surface soils located at the Milan Research and Education Center (MREC) in Milan, Tennessee have been well documented, but the subsoil chemical characteristics have not been well characterized (Essington and Howard, 2000;Suba and Essington, 1999). Soils at the MREC are a part of the Memphis Catena and include the Grenada (fine-silty, mixed, active, thermic Oxyaquic Fraglossudalfs), Loring (fine-silty, mixed, active, thermic Oxyaquic Fragiudalfs), and Memphis (fine-silty, mixed, active, thermic Typic Hapludalfs) soils. These soils are highly erodible due to their fine-silty texture. The identification of reactive subsoil horizons is necessary to evaluate the impact of anion fate and behavior, specifically that of NO_3.

Accessory minerals, such as goethite, hematite, gibbsite, kaolinite, and Mn-oxides bear reactive surface hydroxyl groups that may develop net positive charge by protonation (Sumner and Davidtz,1965; Singh and Kanehiro, 1969; Hingston et al., 1972; Uehara and Gillman, 1980; Grove et al., 1982; Bellini et al., 1996). This net positive charge results in the retention of NO_3 and Br due to coulombic attraction. Iron and aluminum oxides bear net positive charge when soil solution pH is less than approximately 9, which leads to anion exchange capacity (AEC).

The objective of this study was to characterize the chemical and mineralogical characteristics of west Tennessee loess soils, and to identify the depths with the greatest potential for anion retention. This was accomplished by determining pH, particle size distribution, crystalline and amorphous metal oxide content, anion exchange capacity and composition, and cation exchange capacity and composition.

The ability to predict how the addition of sulfate from FGD gypsum ($CaSO_4$) will affect nitrate retention can be evaluated by examining anion exchange behavior. Exchange isotherm, plots of the equivalent fraction of an ion on the exchange phase (E) versus the equivalent fraction of that ion in the aqueous phase (Ẽ), will be developed (Essington, 2003). These isotherms can be constructed for binary exchange (two ions present) or for ternary exchange (three ions present). In addition, the Vanselow selectivity coefficient (K_V) can be determined. In general,an anion exchange reaction may be described as:

$$aB^{b-}(aq) + bAX_a(ex) \rightarrow aBX_b(ex) + bA^{a-}(aq) \quad [1]$$

where X^+ represents an equivalent of anion exchanger. The Vanselow selectivity coefficient for this reaction is:

$$K_V = \frac{N_B^a (A^{a-})^b}{N_A^b (B^{b-})^a} \quad [2]$$

where, (A^{a-}) and (B^{b-}) are the activities of the soluble species, and N_A and N_B represent the mole fractions of A^{a-} and B^{b-} on the exchange complex. If K_V is greater than 1 for the reaction in Eq. [1], B^{b-} is preferred on the exchange complex; whereas, if K_V is less than 1, A^{a-} is preferred (Essington, 2003). The exchange isotherm illustrates both the

preference and magnitude of K_V. Exchange isotherms commonly include the nonpreference isotherm: a theoretically derived line which represents the condition where K_V is equal to 1(neither A^{a-} or B^{b-} are preferred by the exchange phase). The data are then evaluated relative to the nonpreference isotherm to establish preference.

Based on the literature available, NO_3 should be effectively displaced from soil followed by Cl then SO_4. In order to test this hypothesis, binary and ternary anion exchange isotherms will be developed for the soil depth increments that contain elevated concentrations of iron and aluminum oxides.

CHAPTER II

A CHEMICAL EVALUATION OF SOILS LOCATED AT THE MILAN RESEARCH AND EDUCATION CENTER IN MILAN, TENNESSEE

ABSTRACT

Loess soils of West Tennessee may potentially contain large amounts of subsoil metal oxides (Fe, Al, and Mn) which may retain and restrict the movement of conservative anions, such as nitrate (NO_3). The potential utilization of large quantities of flue gas desulfurization (FGD) gypsum on these soils may displace subsoil NO_3, releasing it to potentially adversely impact sensitive aquatic environments. This research examines the depth distribution of Fe-, Al-, and Mn-oxyhydroxides, pH, particle size distribution, and of the cation and anion exchange capacity and exchange phase composition to identify depths that have the greatest potential for anion retention. The metal oxide content of depth incremented soil samples was determined using the citrate-bicarbonate-dithionite (CBD) and ammonium oxalate (AAO) extraction methods. The effective anion exchange capacity (EAEC), cation exchange capacity (CEC), effective cation exchange capacity (ECEC), and anion and cation exchange phase compositions were determined using modified standard extraction methods. Both CBD and AAO extractable Fe, Al, and Mn were found to peak at two different depths within the soil profiles: in the Bt horizons (30 to 46 cm), and in the C horizon that underlie the loess deposits (244 to 259 cm). The depth-distribution of CEC, ECEC and EAEC follow the same trend as the extractable metal oxides. The average CEC was 6.46 $cmol_c\,kg^{-1}$ ranging from 5.4 to 10.02 $cmol_c\,kg^{-1}$. The average ECEC was 9.9 $cmol_c$/kg, ranging from 7.2 to 18.5 $cmol_c$/kg. On average, the ECEC consisted of 78% Ca followed by 6.8% K, 14.8% Mg, and 0.4% Na. The average EAEC was 0.13 $cmol_c$/kg, ranging from 0.09 to 0.21 $cmol_c$/kg. On average, the anion exchange phase is dominated by SO_4 (59% of the EAEC), while Cl accounts for 25%, and NO_3 for 16%. Silt dominates the particle size

distribution with an average of 69.5%, ranging from 40.7% to 86.6%. It is followed by an average of 22.0% sand and 8.4% clay. The pH ranged from 4.55 to 7.02 with an average of 6.24. Based on the characterization data generated, depths of 30 to 46 cm and 245 to 261 cm are expected to be the most reactive relative to anion retention.

INTRODUCTION

The chemical characteristics of surface soils of the Milan Research and Education Center (MREC) in Milan, Tennessee have been well documented (Essington, 2003; Essington and Howard, 2000; Suba and Essington, 1999). However, the subsoil chemical characteristics have not been thoroughly studied. The soils present at MREC include soils from the Memphis Catena; specifically, the moderately well-drained Grenada (fine-silty, mixed, active, thermic Oxyaquic Fraglossudalfs), moderately well-drained Loring (fine-silty, mixed, active, thermic Oxyaquic Fragiudalfs), and the well-drained Memphis (fine-silty, mixed, active, thermic Typic Hapludalfs) soils (Rhoton et al.,1998). Soils included in a Catena are said to have been developed from similar parent material under similar climatic conditions, but whose characteristics differ because of variations in relief and drainage (Brady and Weil, 2002).These soils were deposited during the Cretaceous, Tertiary, and Quaternary sea level fluctuations (Van Arsdale and Cox, 2007). These deep loess deposits in parts of western Tennessee were transported by wind and exposed by water erosion. The soils are highly erodible due to their fine-silty texture. Essington and Howard (2000) reported that the clay content of the Memphis Catena soils varied from 10% to greater than 20%, depending on depth. They also reported that the clay mineralogy consist of hydroxyl-interlayered vermiculite, vermiculite, kaolinite, and mica. Previous studies have also shown that the average cation exchange capacity (CEC) of the MREC soils range between 3 to greater than 15 cmol kg^{-1} with the majority of the exchange complex being dominated by Ca^{2+} with lesser amounts of Mg^{2+} (Suba and Essington, 1999; Essington, 2003).

Although surface soils of the Memphis Catena have been extensively characterized, there has been very little characterization of subsoil properties, particularly those that impact the fate and behavior of anions. Essington (2003) showed that 0 – 15 cm surface samples had an average of 152 mg kg^{-1} Mehlich-3 (M3) extractable K, 121 mg kg^{-1} extractable Mg, 238 mg kg^{-1} extractable Mn, and 52 mg kg^{-1} extractable P. Essington (2003) also reported an average surface soil pH of 5.57 (representing 236 samples) and an average ECEC summation of exchangeable Ca^{2+}, Mg^{2+}, K^{+}, Na^{+}, Mn^{2+}, and Al^{3+} of 7.46 mol_c kg^{-1}. The soil organic carbon content range from 6.28 to 13.46 g kg^{-1}, with an average of 8.96 g kg^{-1}.

The identification of reactive subsoil horizons in soils subjected to sulfate additions from flue-gas desulfurization (FGD) gypsum is necessary to evaluate the impact of anion fate and behavior, specifically that of nitrate. Many soil minerals, such as goethite, hematite, gibbsite, kaolinite, and Mn-oxides bear reactive surface hydroxyl groups (Sumner and Davidtz, 1965; Uehara and Gillman, 1980; Grove et al., 1982; Bellini et al., 1996). These groups may develop positive surface charge by protonation reactions. Thus, these minerals may be responsible for the retention of NO_3^- and Br^- and other conservative anions due to coulombic attraction (Hingston et al., 1972; Singh and Kanehiro, 1969). The iron and aluminum oxide minerals commonly bear net positive charge when soil solution pH is less than approximately 9 (Bolland et al., 1976; Bowden et al., 1977; Qafoku et al., 2004; Donn and Menzies, 2000a, 2000b) resulting in anion exchange capacity (AEC). The AEC of soil typically increases with decreasing soil pH and increasing electrolyte concentration (Wong and Wittwer, 2009). Net positive surface charge is present on minerals when the pH is less that the zero point of charge

(ZPC) (Toner et al., 1989). The ZPC of metal oxide minerals occurs at a soil pH of 9.0 for goethite, 8.5 for hematite, 8.9 for gibbsite, 4.7 for kaolinite, and 3.76 for birnessite (Essington, 2003).

It has been shown that NO_3 is retained in weathered tropical soils that contain iron and aluminum oxides (Singh and Kanehiro, 1969; Kinjo and Pratt, 1971a,b; Kinjo et al., 1971; Espinozo et al., 1975). It has also been shown that NO_3 and Br are retained in the subsoil horizons of west Tennessee soils (Ammons et al., 1994). The retention of NO_3 is important because it affects crop nutrient uptake, fertilizer application rates, and the potential impact to sensitive aquatic ecosystems.

Nitrogen leaching from agricultural soils affects sensitive aquatic ecosystems by introducing a flux of a limiting nutrient into either groundwater or surface waters. Increases in bioavailable nitrogen into estuaries and coastal oceans have been linked to eutrophication and hypoxia the Gulf of Mexico, and in other sensitive aquatic environments (Turner and Rabalais, 1994; Diaz, 2001; He et al., 2011). Eutrophication causes hypoxia and the subsequent suffocation of aquatic wildlife. Algal blooms (eutrophication) leads to a decrease in available oxygen that results when the algae die and decompose, resulting in fish kills. Nitrate concentrations in groundwater and surface streams are recorded as being higher in areas with extensive agricultural activity with irresponsible fertilization techniques versus a pristine area with no source of nutrient contaminants (He et al., 2011). Further, global agriculture activities have also been known to significantly impact the presence of NO_3 in aquatic environments (He et al., 2011).

The objectives of this study were to chemically characterize the loess soils of west Tennessee, and to identify the depths with the greatest potential for anion retention. This was accomplished by evaluating pH, particle size distribution, metal oxide content, anion exchange capacity and composition, and cation exchange capacity and composition using standard methods. These characterizations will also identify the soil horizons for the anion exchange study.

MATERIALS AND METHODS

Soil samples were collected from the Milan Research and Education Center (MREC) (35°54'57''N latitude and 88°45'29'' longitude; 129 m altitude) located in Milan, Tennessee. The soil series within the study area include the Grenada (fine-silty, mixed, active, thermic Oxyaquic Fraglossudalfs), Loring (fine-silty, mixed, active, thermic, Oxyaquic Fragiudalfs), and Memphis (fine-silty, mixed, active, thermic, Typic Hapludalfs). These soils are highly erodible loess soils used for the production of cotton, soybean, wheat, and switchgrass.

The field experiment site was divided into 40 plots designed to represent both till and no-till management of cotton under 5 rates of annual FGD gypsum application (0, 2.2, 4.5, 6.7, and 11.2 Mg ha^{-1}, which are equivalent to 0, 1, 2, 3, and 5 tons per acre). Ten of the forty plots were sampled to a depth of 261 cm in 15 cm increments. Once sampled, each sample was air-dried, placed into a plastic Whirl-Pak, and transported from MREC to the University of Tennessee in Knoxville. Upon arrival, the samples were disaggregated and sieved to pass 2 mm. The soil pH was measured on each sample

using a Thermo Orion Expandable IonAnalyzer EA 490 pH meter (Thermo Fisher Scientific, Waltham, MA) and a Thermo Orion Ross Series combination pH electrode in a 1:1 soil-to-solution using 0.1 M $CaCl_2$ (McLean, 1982). Particle size analysis was conducted in duplicate on all soil samples using the Beckman Coulter LS 13 320 Laser Diffraction Particle Size Analyzer with the Beckman Coulter Sonication Control Unit (Brea, CA). All reagents were analytical grade or better and all solutions were made using Type-I deionized water (18Ω).

Metal Oxide Determination

The total metal oxide content of the soil samples was determined in triplicate using the sodium citrate-bicarbonate-dithionite (CBD) extraction method (Mehra and Jackson, 1960). In this method, sodium dithionite dissolves into hydrogen sulfite gas. The dithionite is a strong reductant and reduces the Fe^{3+} in oxide minerals to soluble Fe^{2+} at pH values below 10 (Borggaard, 1988). A 5 g soil sample was placed into a 250 ml low-density polyethylene (LDPE) Nalgene centrifuge bottle and combined with 40 mL of 0.3 *M* sodium citrate [$Na_3C_6H_5O_7 \cdot 2H_2O$] and 5 mL of 0.1 *M* sodium bicarbonate [$NaHCO_3$]. The bottles were placed in a water bath and brought to a temperature of 75°C - 80°C. After this temperature was reached, 1 g of sodium dithionite powder [$Na_2S_2O_4$] was added and the suspension was immediately stirred with a glass rod for 5 minutes. An additional 1 g of $Na_2S_2O_4$ was then added and the suspension was allowed to sit for 10 minutes in the water bath with intermittent mixing. The bottles were then removed and 10 mL of a saturated NaCl solution was added and the suspension stirred with a glass rod. The bottles were then capped, centrifuged for 5 minutes at ~3000 x g,

and the supernatant was collected into a 500 mL volumetric flask. The remaining soil sample was centrifuge washed with 50 mL of the sodium citrate-bicarbonate mixture two more times, and the supernatant solution combined into the volumetric flask. The flasks were then brought to volume with Type I water and analyzed on a Spectro Ciros (Mahwah, NJ) inductively coupled argon-plasma atomic emission spectrometer (ICP-AES) for Fe, Mn, Si, and Al.

Differential x-ray diffraction (DXRD) was conducted by comparing the x-ray diffractograms of iron-oxide free soils (CBD treated) to those of corresponding untreated soil samples. Random powder mounts were prepared and subjected to DXRD using a Brüker AXS x-ray diffractometer (Karlsruhe, Germany) set at 40 kV and 30 mA using Ni-filter, CuKα radiation. Using Brüker software, iron-oxide free soil XRD patterns were subtracted from corresponding untreated soil patterns. The resulting difference patterns were then compared to the Joint Committee on Powder Diffraction Standards (JCPDS) files of the iron oxide minerals.

Microcrystalline Metal Oxide Determination

The microcrystalline metal oxide content of the Milan soils was determined using a modified version of the acid ammonium oxalate (AAO) extraction method using Tamm's Reagent (Schwertmann, 1964; McKeague & Day, 1966). Each of the metal oxides will react with ammonium oxalate to some extent, but the reactions proceed at different rates depending on particle size and surface reactivity (Schwertmann, 1991). A 0.5 g, 100-mesh (<149 μm) sieved soil sample was placed in an aluminum foil wrapped, 50 mL polypropylene centrifuge tube and treated with 30 mL of pH 3.0 0.2 *M*

ammonium oxalate [$(NH_4)_2C_2O_4 \cdot H_2O$]. This reaction is preformed in the dark to prevent photoreduction and to retard the rate of dissolution of the crystalline metal oxides. Each tube was then capped and placed on a reciprocal shaker for 2 hours. The tubes were then removed, centrifuged for 5 minutes at ~3000 x g, and the supernatant solutions collected in a 100 mL volumetric flask. The soil samples were then washed three additional times with 10 mL 0.5 *M* ammonium carbonate [$(NH_4)_2CO_3$] aliquots, and the supernatant solutions were combined in the 100 mL volumetric flask. Finally, the soil was washed with 5 mL of $(NH_4)_2CO_3$ and 5 mL of Type I water and the supernatant combined in the volumetric flask. The combined extracts were brought to volume with Type I water and analyzed using ICP-AES for Fe, Mn, Si, and Al.

Cation and Anion Exchange Capacities and Cation Composition

The cation exchange capacity (CEC), anion exchange capacity (AEC), and cation exchange phase composition were determined using an unbuffered salt extraction method (Zelazny et al., 1996). A 5 g soil sample was placed into a preweighed 50 mL polypropylene centrifuge tube and combined with a 30 mL aliquot of 0.2 M NH_4Cl. The tubes were capped, shaken for 5 minutes, and centrifuged for 5 minutes at ~3000 x g. The clear supernatant was decanted through Whatman #2 filter paper into a 250 mL volumetric flask. A second 30 mL volume of 0.2 M NH_4Cl was added and the samples were resuspended using a vortex mixer, shaken for 5 minutes, and centrifuged. The supernatant liquid was then filtered through Whatman #2 filter paper into the volumetric flask. The soil was centrifuge washed the additional times with 0.2 M NH_4Cl and the supernatant filtered into the volumetric flasks. The volumetric

flasks were brought to volume with 0.2 M NH_4Cl and the solution analyzed for exchangeable cations (Na, K, Ca, Mg, Mn, and Al) using ICP-AES. The summation of the exchangeable cation composition, in $cmol_c\,kg^{-1}$, resulted in a computed effective cation exchange capacity (ECEC). The remaining NH_4-saturated soil was then treated with a 30 mL volume of 0.04 M NH_4Cl. The tubes were capped, vortexed, shaken for 5 minutes, and centrifuged for 5 minutes at ~3000 x g and the supernatant discarded. The centrifuge washing with 0.04 M NH_4Cl was repeated and additional three times, and the supernatant discarded each time. The tubes were then weighed to determine the volume of entrained 0.04 M NH_4Cl. Finally, 30 mL of 0.2 M KNO_3 was added to the tubes, which were vortexed, shaken for 5 minutes, and centrifuged. The supernatant was filtered into a 250 mL volumetric flask. The centrifuge washing with 0.2 M KNO_3 was repeated an additional four times, and the supernatant liquids were combined into the volumetric flask. The volumetric flask was brought to volume with 0.2 M KNO_3. The displaced NH_4 and Cl are equivalent to the CEC and AEC of the soil. The solution was then analyzed for NH_4 using a Skalar San^{++} Automated Wet Chemistry Analyzer – Continuous Flow Analyzer (CFA) (Buford, GA) and Cl using Dionex Model Ion Chromatography ICS-5000 Reagent-Free™ system (Sunnyvale, CA). The Dionex was equipped with Dionex IonPak AS18 Analytical separation column (4 x 250) with associated guard column. Suppression was achieved using a Dionex Suppressor ASRS 4mm. The instrument was operated in isocratic mode at 30°C with current of 57A and a flow rate 1.0 mL min^{-1}. The mobile phase was 23 mM KOH. The eluent was prepared from Potassium Hydroxide Eluent Generator Cartridge. The method detection limit for Cl was 1.0 µmol L^{-1}, and sample replicates and standard checks were within ±10%. Dionex

Chromeleon 7.1 Chromatography Data System software was used for system control and data processing.

The exchanger phase composition of each cation ($\frac{cmol_c}{kg}$) was determined by:

$$\frac{cmol_c}{kg} = \frac{mg}{L} \times \frac{0.25L}{0.005kg} \times \frac{dF}{mw} \times 0.1 \frac{cmol}{mmol} \times \frac{Z\ cmol_c}{cmol}$$

where $\frac{mg_C}{L}$ is the concentration of the cation in the volumetric flask, dF is the dilution factor (if needed), mw is the molecular mass of the cation in units of $\frac{mg}{mmol}$, and Z is the cation charge. Cation exchange capacity (CEC, $\frac{cmol_c}{kg}$) was determined by:

$$CEC = 0.2775 \times NH_4 - 0.80 \times V_{en}$$

where NH_4 is the concentration NH_4 in the combined extract (in mg/L), and V_{en} is the volume of entrained solution (in mL). Anion exchange capacity (AEC, $\frac{cmol_c}{kg}$) was determined by:

$$AEC = 0.14 \times Cl - 0.80 \times V_{en}$$

where Cl is the concentration of Cl in the combined extract (in mg/L), and V_{en} is the volume of entrained solution (in mL).

Effective Anion Exchange Capacity and Composition

Effective anion exchange capacity (EAEC) is the summation of anion charge from NO_3^-, SO_4^{2-}, and Cl^- present on the exchange complex. Anion exchange phase composition was determined using a modified unbuffered $C_2H_3O_2K$ extraction method

(United States Salinity Laboratory Staff, 1954). The original method called for the use of KBr as the extractant. This was change to potassium acetate due to high levels of chloride contamination in the KBr that masked the concentrations of exchangeable chloride in the soil samples. A 5 g sample of soil was placed in a preweighed 50 mL polypropylene centrifuge tube with 30 mL of 0.2 *M* $C_2H_3O_2K$. The tubes were capped, shaken for 5 minutes on a reciprocal shaker, and centrifuged for 5 minutes at ~3000 x g. Then the clear supernatant was filtered through Whatman #2 filter paper into a 250 mL volumetric flask. The centrifuge washing of the soil with 0.2 *M* $C_2H_3O_2K$ was repeated an additional four times and supernatant solution collected into the volumetric flask. The volumetric flask was then brought to volume with 0.2 *M* $C_2H_3O_2K$ and the solution analyzed for exchangeable anions (Cl, NO_3, and SO_4) using the Skalar (CFA) for NO_3^- and DIONEX ion chromatography for Cl^- and SO_4^{2-}.

The exchanger phase composition of each anion ($\frac{cmol}{kg}$) was determined by:

$$\frac{cmol}{kg} = \frac{mg}{L} \times \frac{0.25L}{0.005kg} \times \frac{dF}{mw} \times 0.1 \frac{cmol}{mol} \times \frac{cmol_c}{cmol}$$

where $\left(\frac{mg}{L}\right)$ is the concentration of anion in the volumetric flask, dF is the dilution factor (if needed), mw is the molecular mass of the anion in units of $\frac{mg}{mmol}$, and Z is the anion charge. The EAEC was then computed by the summation of the anion charge:

$$EAEC = \frac{cmol_{c,Cl^-}}{kg} + \frac{cmol_{c,NO_3^-}}{kg} + \frac{cmol_{c,SO_4^{2-}}}{kg}$$

Particle Size Analysis

Particle size analysis was conducted on six plots for all depth increments to a depth of 261 cm. Samples were suspended in 10 ml of 5 g L^{-1} sodium-hexametaphosphate (HMP) solution. The samples were analyzed by the Backman Coulter LS 13 320 Laser Diffraction Particle Size Analyzer (Brea, CA).

RESULTS AND CONCLUSIONS

pH

The pH ranged from 4.56 in the 198 to 213 cm depth increment to 7.02 in the 15 to 30 cm increment (Fig. 1). The average was 6.24 ± 0.04 across all 10 depth-incremented plots. Essington (2003) reported an average surface pH of 5.57, compared to an average of 6.59 ± 0.14 for the surface 15 cm in the present study.

Particle Size Analysis

The mean percentages of clay, silt, and sand in the 6 plots are found on Table 1. The minimum percentage of clay was 3.7 ± 0.9% and was located in the 213 to 229 cm depth increment, and the maximum percentage of clay was 14.2 ± 0.8% in the 30 to 46 cm increment. The average percentage of clay (Fig. 2) present among all depth increments was 8.4 ± 1.0%. The minimum percentage of silt was 40.7 ± 12.8% in the 213 to 229 cm depth increment, and the maximum was 86.6 ± 0.7% located in the 61 to 76 cm increment. The average silt percentage among all depth increments (Fig. 3) was 69. 6 ± 5.8%. The minimum sand percentage of 2.1 ± 0.3% was located at a depth of 30

to 46 cm, and its maximum of 55.6 ± 13.5% was located at a depth of 213 to 229 cm. The average sand percentage (Fig. 4) among all plots was 22. 0 ± 6.3%.

All plots (Figs. 5 to 10) are dominated by silt which represents roughly 70% of the particle size distribution, followed by sand with 22% and clay with 8%. This supports the premise that west Tennessee loess soils are composed of large percentages of fine-silty material that is easily erodible.

The National Resources Conservation Service (NRCS) reports loess deposits in depths down to122 cm, clay content in the range of 25 – 30% in the upper 51 cm, and less than 5% sand content to a depth of 123 cm for the Memphis soil series. The maximum clay content in the Loring series occurs in the Bt horizon and there is less than 10% sand throughout the profile. The Grenada soil contains 18 – 30% clay and less than 10% sand.

CBD-Extractable Metal Oxide Content

The average concentrations of CBD-extractable metals from the ten depth-incremented plots is presented in Table 2. Average CBD-extractable iron concentrations (Fig. 11) ranged from a minimum of 7.19 ± 0.2 g kg^{-1} in the surface 15 cm, to a maximum of 16.89 ± 0.2 g kg^{-1} at a depth of 30 to 46 cm. The mean extractable iron concentration among all plots and depths was 11.88 ±0.3 g kg^{-1}.

The depth distribution of CBD-extractable aluminum was similar to that of CBD-extractable iron (Fig. 12). The minimum CBD Al was located at the surface with 864 ± 25 mg kg^{-1} and the maximum was located 30 to 46 cm increment with a concentration of 2287 ± 48 mg kg^{-1}. The mean extractable aluminum concentration among all 10 plots and depths was 1386 ± 39 mg kg^{-1}.

Extractable manganese (Fig. 13) did not follow the same trend with depth as iron or aluminum. The minimum CBD Mn was located in the 76 to 91 cm depth increment with a concentration of 461 ± 13 mg kg^{-1}. The maximum CBD Mn was located in the surface 15 cm increment (1220 ± 25 mg kg^{-1}). The mean extractable manganese concentration among all 10 plots and depths was 628 ± 45 mg kg^{-1}.

Extractable silicon (Fig. 14) did not follow the same trend with depth as the other elements. The minimum CBD Si concentration of 471 ± 28 mg kg^{-1} was located in the 245 to 261 cm depth increment. The maximum CBD Si concentration was 642 ±25 mg kg^{-1} located 137 to 152 cm increment. The mean extractable silicon concentration for all 10 plots and depths was 557 ± 32 mg kg^{-1}.

AAO-extractable Metal Oxide Content

The average concentrations of AAO-extractable metals from the ten depth-incremented plots is presented in Table 3. The average concentrations of AAO-extractable iron (Fig. 11) ranged from 1515 ± 87 mg kg^{-1} in the 245 to 261 cm increment to 2958 ± 101 mg kg^{-1} in the 30 to 46 cm increment. The average concentration among all plots and depths was 2172 ± 151 mg kg^{-1}. The maximum concentrations of CBD and AAO exchangeable Fe were found in the same depth increment. However, minimum CBD and AAO-exchangeable Fe were observed at different depths.

The average concentrations of AAO-extractable aluminum (Fig. 12) ranged from 707 ± 19 mg kg^{-1} at the surface, to 1372 ± 24 mg kg^{-1} in the 30 to 46 cm increment. The average concentration among all plots and depths was 911 ± 33 mg kg^{-1}. These

maximum and minimum AAO-Al depths coincided with the depths of the maximum and minimum values obtained by the CBD extraction method.

The average AAO-extractable manganese concentrations (Fig. 13) ranged from 271 ± 13 mg kg^{-1} in the 76 to 91 cm depth, to 1021 ± 39 mg kg^{-1} at the surface. The average among all plots and depths was 485 ± 36 mg kg^{-1}. The AAO Mn levels were similar to the CBD Mn concentrations throughout the profile.

The average minimum concentration for AAO-extractable silicon (Fig. 14) was 179 ± 20 mg kg^{-1} located in the surface 15 cm. The average maximum was 344 ± 13 mg kg^{-1} found in the 46 to 61 cm depth. The average concentration of AAO-extractable silicon in all plots and depths was 290 ± 20 mg kg^{-1}. These values for amorphous silicon are not correlated to the concentrations of CBD silicon.

Effective Anion Exchange Capacity and Composition

The anion exchange capacity (AEC) of the soils was below detectable levels for the methodology employed. The EAEC and anion exchange phase composition data are presented in Table 4. The minimum average EAEC (Fig. 15) of 0.94 ± 0.05 $mmol_c$ kg^{-1} was found in the 46 to 61 cm depth. The maximum average EAEC was 2.1 ± 0.09 $mmol_c\,kg^{-1}$ located in the surface 15 cm. In general, the EAEC in the 15 to 100 cm increments averaged 1.0 $mmol_c\,kg^{-1}$, while that of the 100 to 260 cm increments averaged 1.4 $mmol_c$ kg^{-1}. The average EAEC among all plots and depths was 1.35 ± 0.1 $mmol_c$ kg^{-1}. The maximum distribution of EAEC with depth was not correlated with either the CBD-extractable and AAO-extractable metal concentrations. The EAEC of the individual plots is illustrated in Figs. 16 through 25. On average, the EAEC was

dominated by SO_4, which accounted for 65% of the total EAEC, followed by Cl (27%), and NO_3 (8%).

Average exchangeable sulfate concentrations (Fig. 26) ranged from 0.44 ± 0.04 $mmol_c\,kg^{-1}$ in the 30 to 61 cm increment, to 1.13 ± 0.14 $mmol_c\,kg^{-1}$ in the 137 to 152 cm increment. The average exchangeable SO_4 concentration among all plots and depths was 0.80 ± 0.09 $mmol_c\ kg^{-1}$. Average concentrations of exchangeable nitrate (Fig. 27) ranged from 0.07 ± 0.007 $mmol_c\,kg^{-1}$ in the 213 to 245 cm depths to 0.15 ± 0.007 $mmol_c\ kg^{-1}$ at the surface. The average exchangeable NO_3 concentration among all 10 plots and depths was 0.09 ± 0.01 $mmol_c\ kg^{-1}$.The minimum average exchangeable chloride concentration (Fig. 28) was 0.21 ± 0.02 $mmol_c\,kg^{-1}$ in the 15 to 30 cm depth increment. The maximum average exchangeable Cl concentration of 0.40 ± 0.02 $mmol_c\,kg^{-1}$ was found in the 152 to 168 cm increment. The average exchangeable Cl concentration among all 10 plots and depths was 0.33 ± 0.04 $mmol_c\ kg^{-1}$. The exchangeable anion composition of all plots as a function of depth is illustrated in Figs. 29 through 38.

Cation Exchange Capacity, Effective Cation Exchange Capacity, and Composition

The mean CEC, ECEC, and cation exchange phase composition data are presented in Table 5. The mean ECEC by depth (Fig. 39) varied from 7.25 ± 0.1 $cmol_c\ kg^{-1}$ in the 213 to 229 cm depth to 18.50 ± 0.9 $cmol_c\ kg^{-1}$ in the15 to 30 cm depth. The average among all 10 plots and depths was 9.94 ± 0.3 $cmol_c\ kg^{-1}$. The ECEC was dominated by Ca (78.0%), followed by Mg (14.8%), K (6.8%), Na (0.4%), and Mn (0.16%). The mean CEC by depth (Fig. 39) approximately 5.4 $cmol_c\ kg^{-1}$ in the 183 to 229 cm increments to 10.02 ± 0.69 $cmol_c\ kg^{-1}$ in the 30 to 46 cm depth. The average

among all 10 plots and depths was 6.46 ± 0.42 $cmol_c\ kg^{-1}$. The CEC and ECEC of all plots as a function of depth are illustrated in Figs. 40 through 49.

The average exchangeable calcium concentration (Fig. 50) varied from 4.42 ± 0.2 $cmol_c\ kg^{-1}$ in the 213 to 229 cm depth to 17.35 ± 0.9 $cmol_c\ kg^{-1}$ in the 15 to 30 cm depth. The average among all 10 plots and depths was 7.73 ± 0.3 $cmol_c\ kg^{-1}$. In general, Ca decreased with depth. The exchangeable The average exchangeable potassium concentrations (Fig. 51) ranged from 0.42 ± 0.02 $cmol_c\ kg^{-1}$ in the 76 to 91 cm depth to 0.97 ± 0.1 $cmol_c\ kg^{-1}$ in the 245 to 261 cm depth, which was the deepest sample collected. The average among all 10 plots and depths was 0.67 ± 0.06 $cmol_c\ kg^{-1}$. Mean magnesium concentrations (Fig. 52) ranged from 0.43 ± 0.01 $cmol_c\ kg^{-1}$ at the surface to 2.16 ± 0.06 $cmol_c\ kg^{-1}$ in the 245 to 261 cm depth. The average among all 10 plots was 1.46 ± 0.1 $cmol_c\ kg^{-1}$. The exchangeable Mg levels also increased with depth. The exchangeable K concentrations generally increased with depth. The average exchangeable manganese concentrations (Fig. 53) ranged from 0.003 ± 0.001 $cmol_c\ kg^{-1}$ at a depth of 76 to 91 cm to 0.028 ± 0.009 $cmol_c\ kg^{-1}$ at a depth of 137 to 152 cm. The average among all 10 plots and depths was 0.015 ± 0.005 $cmol_c\ kg^{-1}$. Exchangeable sodium concentrations (Fig. 54) ranged from 0.03 ± 0.002 $cmol_c\ kg^{-1}$ at the surface to 0.06 ± 0.006 $cmol_c\ kg^{-1}$ in the 137 to 152 cm depth. The average among all 10 plots and depths was 0.04 ± 0.03 $cmol_c\ kg^{-1}$. In general, exchangeable Na and Mn displayed similar distributions with depth. Concentrations of exchangeable aluminum and iron were generally at or below detection limits of <0.001 $cmol_c\ kg^{-1}$. The exchange phase composition of all plots is illustrated in Figs. 55 through 64.

SUMMARY

The chemical and particle size characteristics of Memphis Catena soils were characterized by determining pH, particle size distribution, sodium citrate-bicarbonate-dithionite (CBD) extractable metal oxides, ammonium oxalate (AAO) extractable metal oxides, effective anion exchange capacity and composition, and effective cation exchange capacity and composition as a function of depth. The average pH of 6.24 indicates that iron and aluminum oxides may bear net positive surface charge and participate in anion retention (Bolland et al., 1976; Bowden et al., 1977; Qafoku et al., 2004; Donn and Menzies, 2000a, 2000b). Particle size distribution is dominated by silt with approximately 70%, in the shallow horizons; sands are significant in the >150 cm depths. The CBD and AAO extractable metal oxides identified the depths of 30 to 46 cm and 245 to 261 cm have the highest concentrations of metal oxides. The EAEC of 1.35 ± 0.052 $mmol_c\ kg^{-1}$ was dominated by SO_4 (65%) followed by Cl (27%)and NO_3 (8%); however, the exchangeable anion composition did not correlate with CBD or AAO metal levels. The average ECEC of 9.94 ± 1.39 $cmol_c\ kg^{-1}$ was dominated by Ca (78.0%), followed by Mg (14.8%), K (6.8%), Na (0.4%) and Mn (0.16%).

The characterization of the Memphis Catena soils identifies the depths with the greatest potential for anion retention and indicates the horizons for additional study by anion exchange isotherm analysis.

LITERATURE CITED

Ammons, J.T., A.O. Gallagher, R.L. Livingston, J.L. Branson, and R.J. Lewis. 1994.Background levels of nitrate-nitrogen and selected heavy metals for the Ames Plantation watershed project. Tenn. Farm Home Sci. 169:30-33.

Assimakopoulos, J.H., D.P. Kalivas, and V.J. Kollias. 2003. A GIS-based fuzzy classification for mapping the agricultural soils for N-fertilizers use. Sci. Total Environ. 309:19-33.

Bellini, G., M.E. Sumner, D.E. Radcliffe, and N.P. Qafoku. 1996. Anion transport through columns of highly weathered acid soil: Adsorption and retardation. Soil Sci. Soc. Am. J.60:132-137.

Bolland, M.D.A., A.M. Posner, and J.P. Quirk. 1976. Surface charge on kaolinites in aqueous suspension. Australian Journal of Soil Research. 14:197-216.

Borggaard, O.K. 1988. Phase identification by phase dissolution techniques. P.83-98. *In* J.W. Stucki et al. (ed.) Iron in soils and clay minerals. Reidel, Dordrecht, the Netherlands.

Bowden, J.W., A.M. Posner, and J.P. Quirk. 1977. Ionic adsorption on variable charge mineral surfaces. Theoretical-charge development and titration curves. Australian Journal of Soil Research. 15:121-136

Brady, N.C., and R.R. Weil. 2002. The nature and properties of soils. Prentice Hal, Upper Saddle River, NJ.

Diaz, R.J. 2001. Overview of hypoxia around the world. Journal of Environmental Quality. 30:275-281.

Donn, M.J., and N.W. Menzies. 2005a. Simulated rainwater effects on anion exchange capacity and nitrate rentention in Ferrosols. Australian Journal of Soil Research. 43:33-42.

Donn, M.J., and N.W. Menzies. 2005b. The effect of ionic strength variation and anion competition on the development of nitrate accumulations in variable charge subsoils. Australian Journal of Soil Research. 43:43-50.

Espinoza, W., R.G. Gast, and R.S. Adams, Jr. 1975. Charge characteristics and nitrate retention by two Andepts from South-central Chile. Soil Sci. Soc. Am. Proc. 39:842-846.

Essington, M.E. 2003. Soil and water chemistry: an integrated approach. CRC Press, Boca Raton, FL.

Essington, M.E., and D.D. Howard. 2000. Phosphorus availability and speciation in long-term no-till and disk-till soil. Soil Sci. 165:144-152

Gillman, G.P. 1979. A proposed method for the measurement of exchange properties of highly weathered soils. Australian Journal of Soil Research. 17:129-139.

Grove, J.H., C.S. Fowler, and M.E. Sumner. 1982. Determination of the charge character of selected acid soils. Soil Sci. Soc. Am. J. 46:32-38.

Hansen, B., E.S. Kristensen, R. Grant, H.H. Jensen, S.E. Simmelsgaard, and J.E. Olesen. 2000. Nitrogen leaching from conventional versus organic farming systems – a systems modeling approach. Eur. J. Agron. 13:65-82.

He, B., S. Kanae, T. Oki, Y. Hirabayashi, Y. Yamashiki, and K. Tarara. 2011. Assessment of global nitrogen pollution in rivers using an integrated biogeochemical modeling framework. Water Research. 45:2573-2586.

Hendershot, W.H., and M. Duquette. 1986. A simple barium chloride method for determining cation exchange capacity and exchangeable cations. Soil Sci. Soc. Am. J. 50:605-608.

Hillin, C.K., and P.F. Hudak. 2003. Nitrate contamination in the seymour aquifer, north-central Texas, USA. Bull. Environ. Contam. Toxicol. 70:674-679.

Hingston, F.J., A.M. Posner, and J.P. Quirk. 1972.Influence of potassium chloride on nitrification in Bedford loam. J. Soil Sci. 23:117-192.

Jalali, M. 2005. Nitrates leaching from agricultural land in Hamadan, western Iran. Agr. Ecosyst. Environ. 110:210-218.

Kinjo, T., and P.F. Pratt. 1971a. Nitrate adsorption: I. In some acid soils of Mexico and South America. Soil Sci. Soc. Am. Proc. 35:722-725.

Kinjo, T., and P.F. Pratt. 1971b. Nitrate adsorption: II. In competition with chloride, sulfate, and phosphate. Soil Sci. Soc. Am. Proc. 35:725-728.

Kinjo, T., P.F. Pratt, and A.L. Page. 1971. Nitrate adsorption: III. Desorption, movement and distribution in Adepts. Soil Sci. Soc. Am. Proc. 35:728-732.

Lui, H.B., Z.H. Li, Y.G. Zhang, W.L. Zhang, and B. Lin. 2004. Characteristics of nitrate distribution and accumulation in soil profiles under main agro-land use types in Beijing. Scientia Agricultura Sinica. 34:692-698.

McKeague, J.A., and J.H. Day. 1966. Dithionite- and oxalate-extractable Fe and Al as aids in differentiating various classes of soils. Can. J. Soil Sci. 46:13-22.

McLean, E.O. 1982, Soil pH and lime requirement. p. 199-224. *In* J.M. Bartels (ed.) Methods of soil analysis. Part 3. Chemical methods. ASA, SSSA, Madison, WI.

Mehra, O.P., and M.L. Jackson. 1960. Iron oxide removal from soils and clays by a dithionite-citrate system buffered with sodium bicarbonate. *In* Clays and Clay Minerals, Proc. 7th Conf., pp. 317-327. Natl. Acad. Sci.-Natl. Res. Council Publ., Washington, D.C.

Qafoku, N.P., E. van Ranst, A. Noble, and G. Baert. 2004.Variable charge soils: their mineralogy, chemistry and management. Advances in Agronomy. 84:159-215.

Rhoton, F.E., D.L. Lindbo, and M.J.M. Romkens. 1998. Iron oxides erodibility interactions for soils of the Memphis catena. Soil Sci. Soc. Am. J. 62:1693-1703.

Schwertmann, U. 1964. The differentiation of iron oxide in soils by a photochemical extraction with acid ammonium oxalate. Z. Pflanzenernaehr. Dueng. Bodenkund. 105:194-201.

Schwertmann, U. 1991. Solubility and dissolution of iron oxides. P. 3-27. *In* Y. Chen and Y. Hadar (ed.) Iron nutrition and interactions in plants. Kluwer, Dordrecht, the Netherlands.

Schwertmann, U., D.G. Schulze, and E. Murad. 1982. Identification of ferrihydrite in soils by dissolution kinetics, differential x-ray diffraction and Mössbauer spectroscopy. Soil Sci. Soc. Am. J. 46:869-875.

Singh, B.R., and Y. Kanehiro. 1969. Adsorption of nitrate in amorphous and kaolinitic Hawaiian soils. Soil Sci. Soc. Am. Proc. 33:681-683.

Suba, J.D., and M.E. Essington. 1999. Adsorption of Mercury(II) by variable charged surfaces of quartz and gibbsite. Soil Sci. 164:145-155

Sumner, M.E., and J.C. Davidtz. 1965. Positive and negative charges in some Natal soils. S. Afr. J. Agric. Sci. 8:1045-1050.

Toner, IV, C.V., D.L. Sparks, and T.H. Carski. 1989. Anion exchange chemistry of Middle Atlantic soils: Charge properties and nitrate retention kinetics. Soil Sci. Soc. Am. J. 53:1061-1067.

Turner, R.E., and N.N. Rabalais. 1994.Coastal eutrophication near the Mississippi River Delta. Nature. 268:619-621.

Uehara, G., and G.P. Gillman. 1980. Charge characteristics of soils with variable and permanent charge minerals: II. Experimental. Soil Sci. Soc. Am. J. 44:252-255.

United States Salinity Laboratory Staff, 1954. Diagnosis and improvement of saline and alkali soils. USDA Handbook No. 60. Washington, D.C.

Van Arsdale, R.B., and R.T. Cox. 2007. The Mississippi's curious origins. Scientific America. 76-82.

Wong, M.T.F., and K. Wittwer. 2009. Positive charge discovered across western Australian wheatbelt soils challenges key soil and nitrogen management assumptions. Australian Journal of Soil Research. 47:127-135.

Zelazny, L.W., L. He, and A.M. Vanwormhoudt. 1996. Charge analyses of soils and anion exchange. p. 1231-1254. *In* D.L. Sparks et al. (eds.) Methods of soil analysis. Part 3. SSSA Book Ser. 5. SSSA, Madison, WI.

APPENDIX I

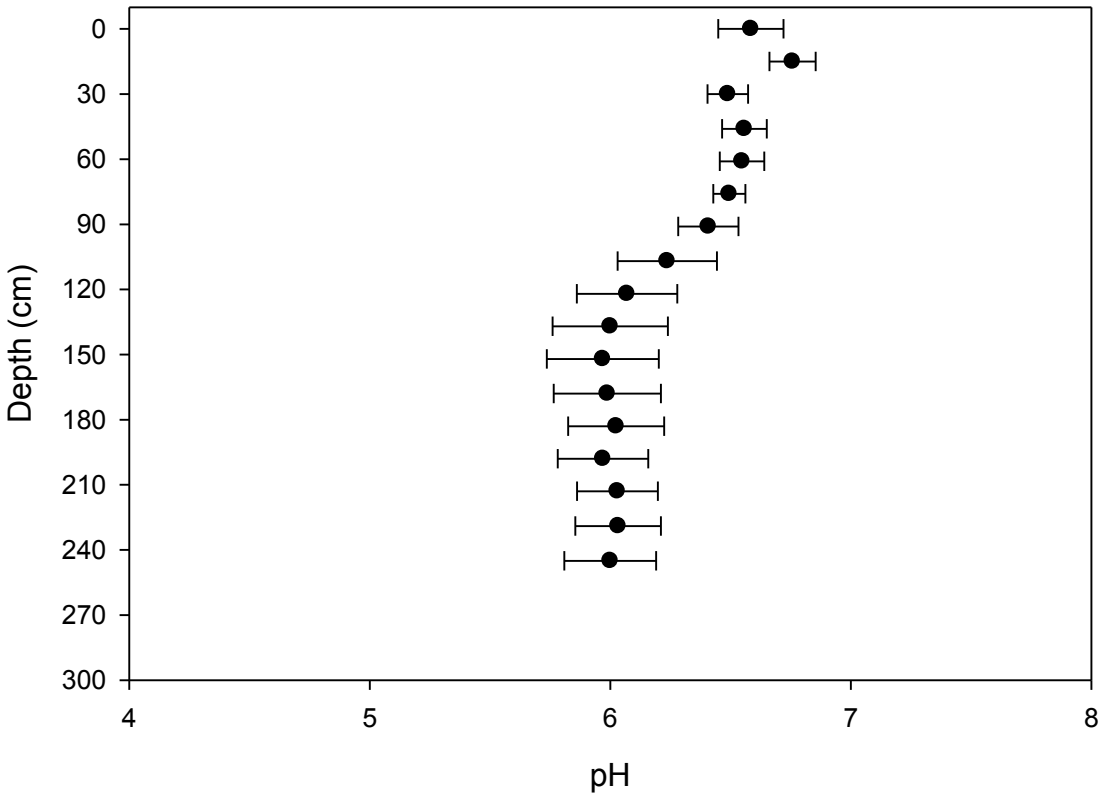

Figure 1. The mean pH of 1:1 soil-to-0.1 M $CaCl_2$ extracts of six depth incremented soil profiles. The error bars represent standard error.

Table 1. Mean particle size distribution of 6 plots. †

Depth	Clay	Silt	Sand
cm	%		
0-15	7.9 ± 0.7	77.2 ± 1	14.8 ± 2
15-30	12.0 ± 1.0	78.8 ± 5	9.2 ± 6
30-46	14.2 ± 0.8	83.7 ± 1	2.1 ± 0.3
46-61	12.9 ± 1.4	84.3 ± 1	2.9 ± 1
61-76	10.4 ± 0.9	86.6 ± 1	3.1 ± 1
76-91	10.2 ± 0.5	86.4 ± 0.3	3.4 ± 0.3
91-107	9.5 ± 0.9	84.8 ± 1	5.8 ± 2
107-122	10.2 ± 0.5	85.8 ± 1	3.9 ± 0.4
122-137	7.7 ± 0.8	74.5 ± 5	17.8 ± 6
137-152	6.4 ± 0.8	68.2 ± 11	25.4 ± 11
152-168	5.4 ± 1.2	58.8 ± 10	35.8 ± 11
168-183	5.8 ± 1.3	57.6 ± 11	36.6 ± 12
183-198	6.2 ± 1.2	59.0 ± 10	34.8 ± 11
198-213	7.4 ± 1.1	61.5 ± 8	31.1 ± 8
213-229	3.7 ± 0.9	40.7 ± 13	55.6 ± 14
229-245	6.7 ± 2.1	47.3 ± 14	46.0 ± 16
245-261	6.8 ± 1.0	47.3 ± 7	45.9 ± 8

† Mean ± standardard error

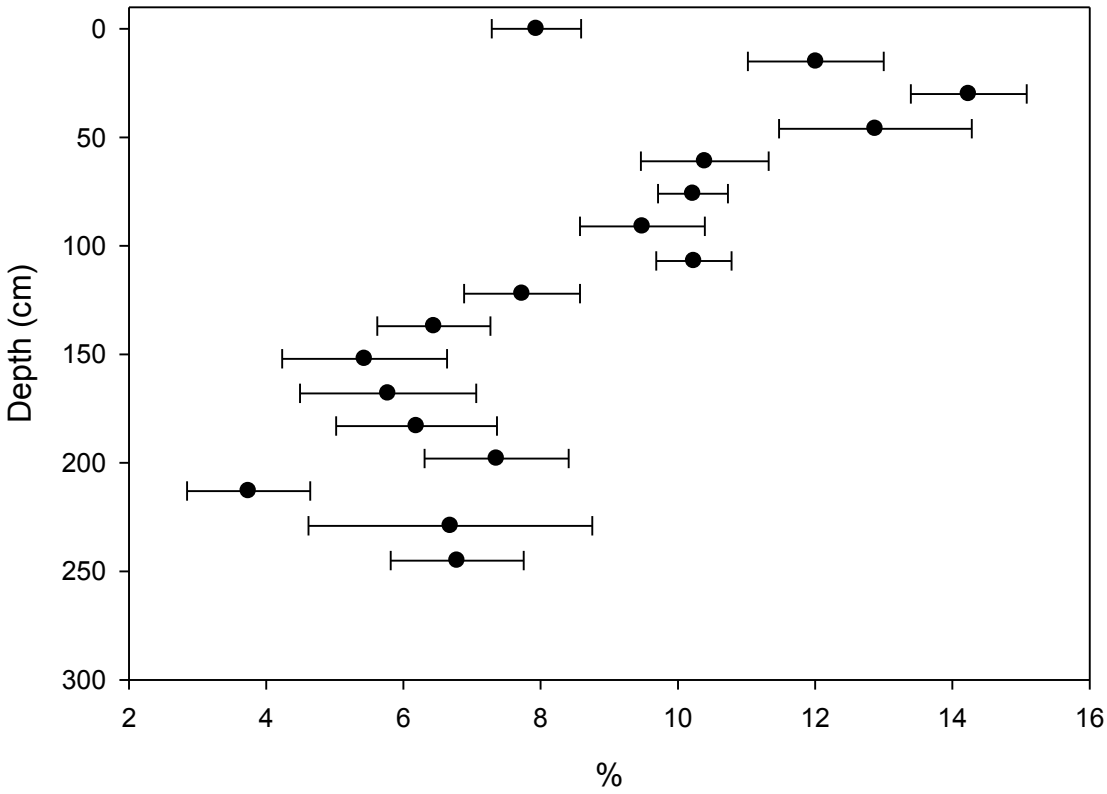

Figure 2. Mean clay particle size distribution of 6 depth-incremented plots. Error bars represent standard error.

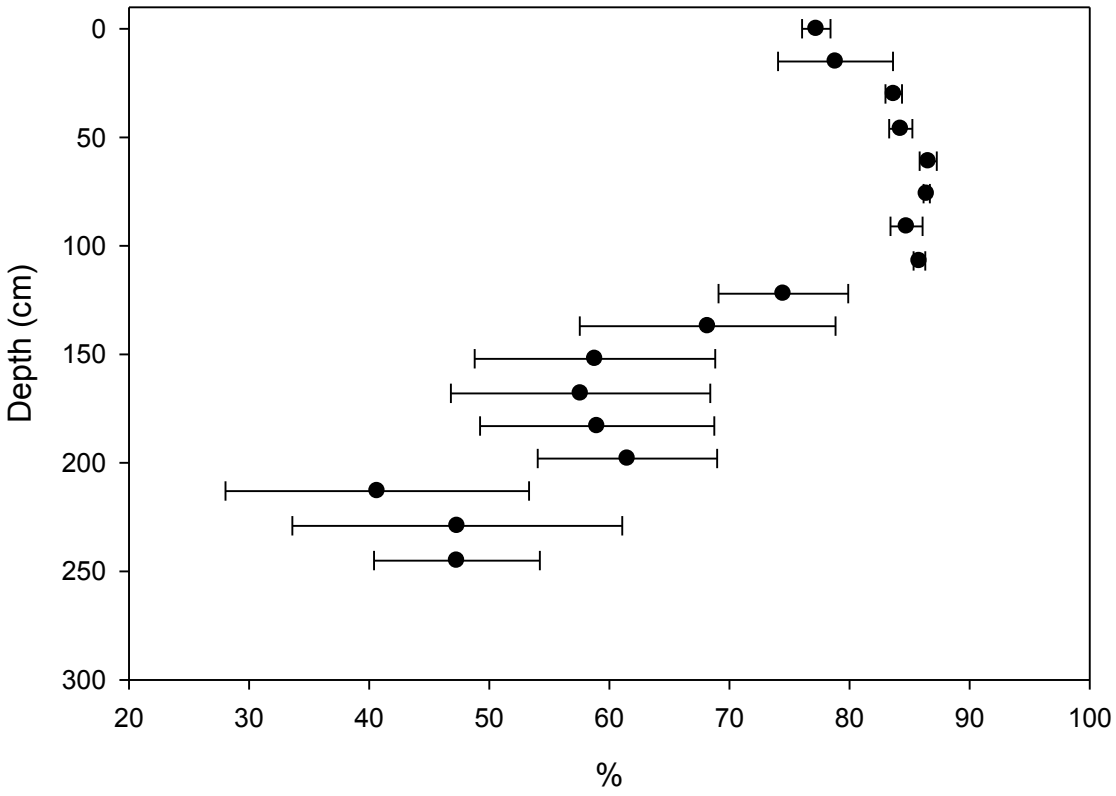

Figure 3. Mean silt particle size distribution of 6 depth-incremented plots. Error bars represent standard error.

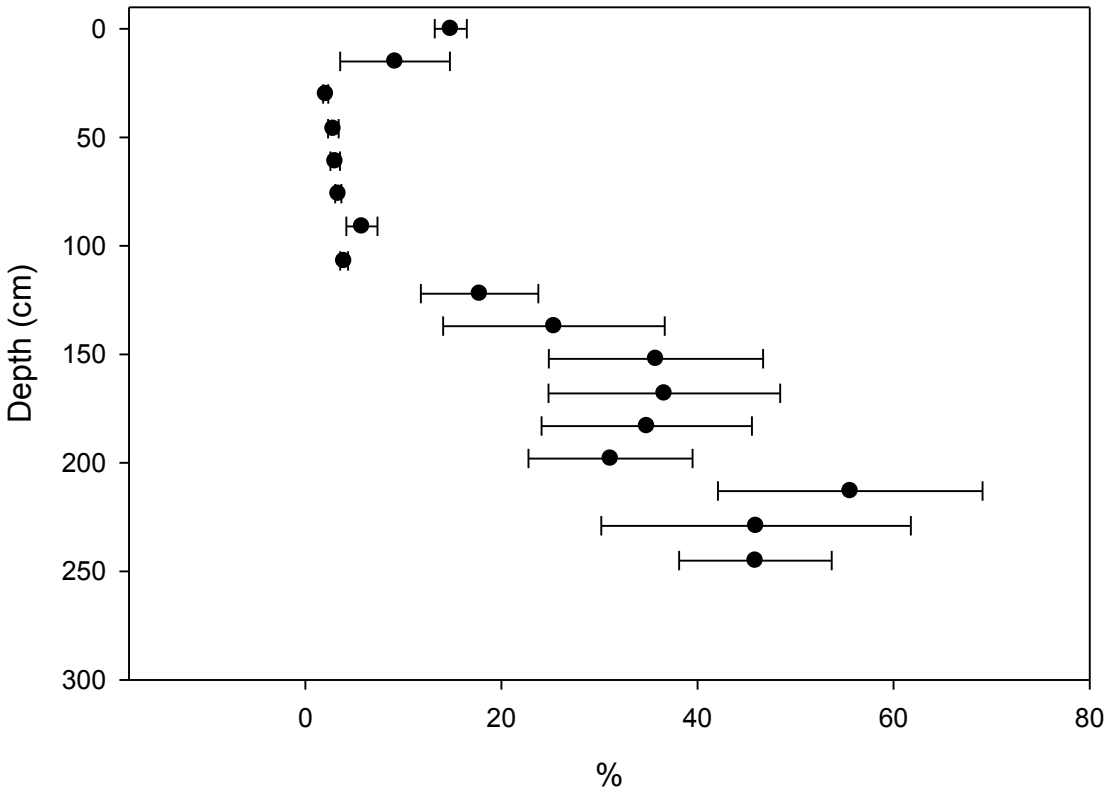

Figure 4. Mean sand particle size distribution of 6 depth-incremented plots. Error bars represent standard error.

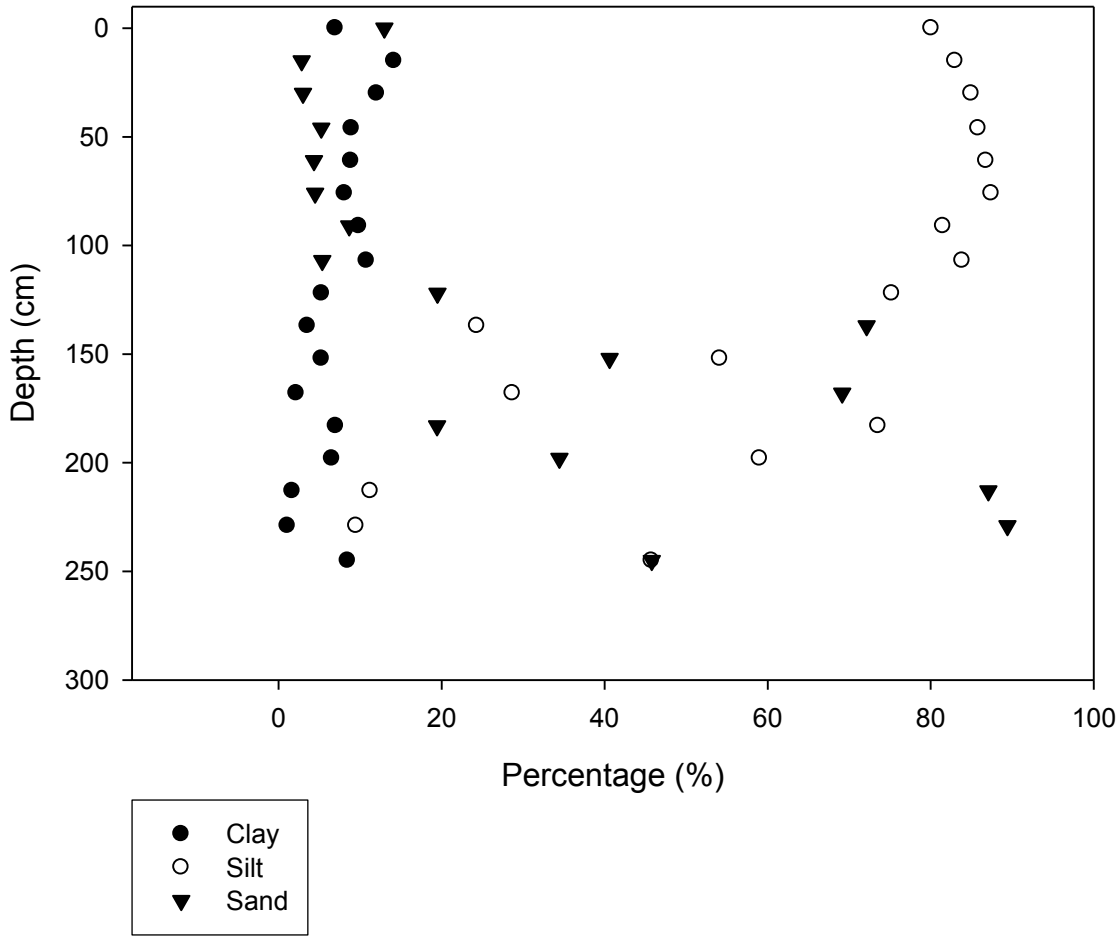

Figure 5. Particle size distribution in Plot 1.

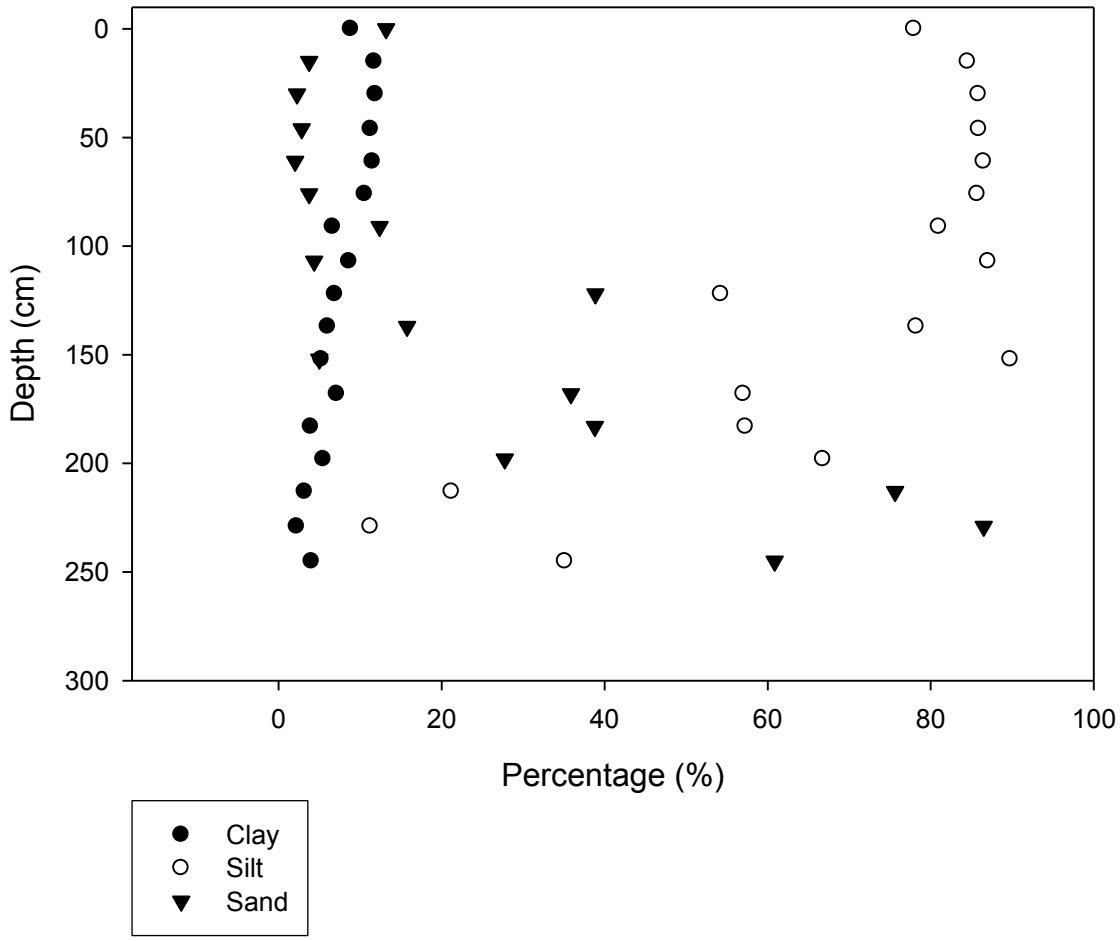

Figure 6. Particle size distribution in Plot 2.

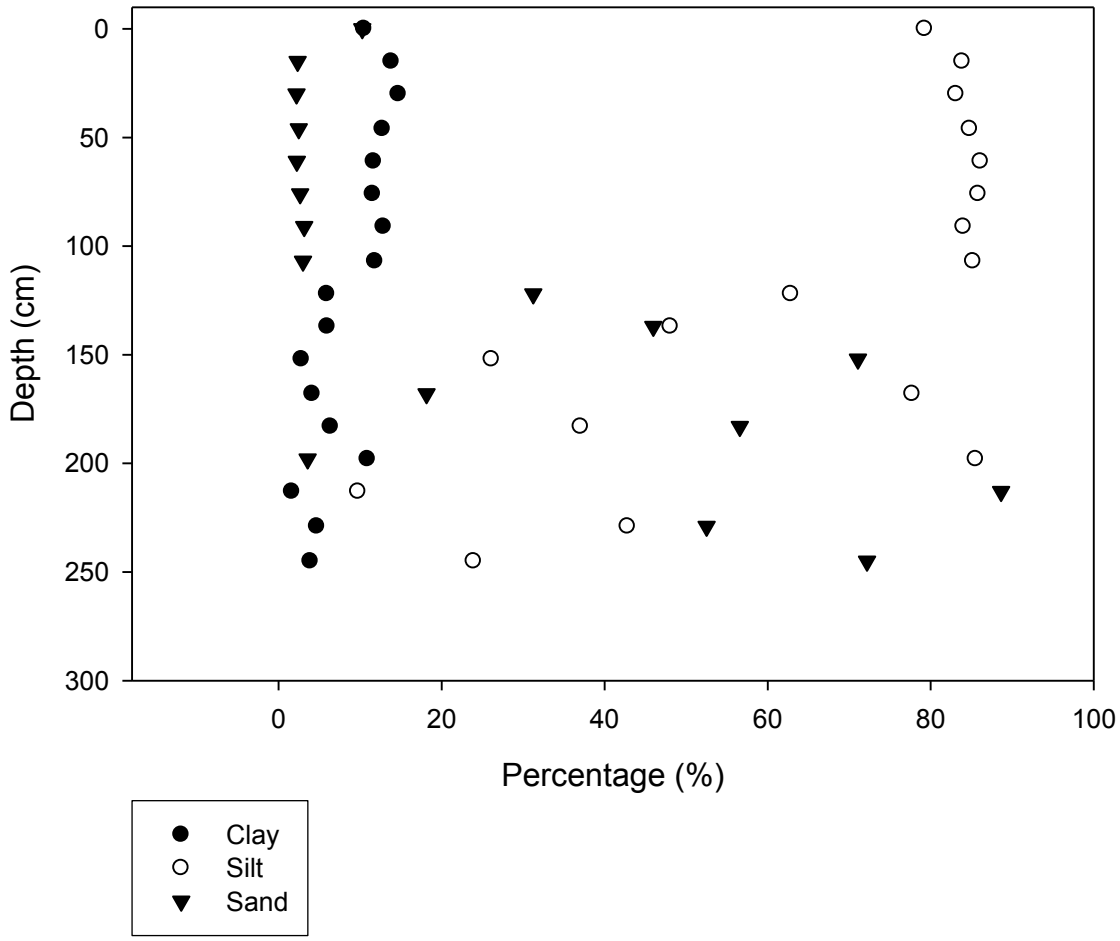

Figure 7. Particle size distribution in Plot 3.

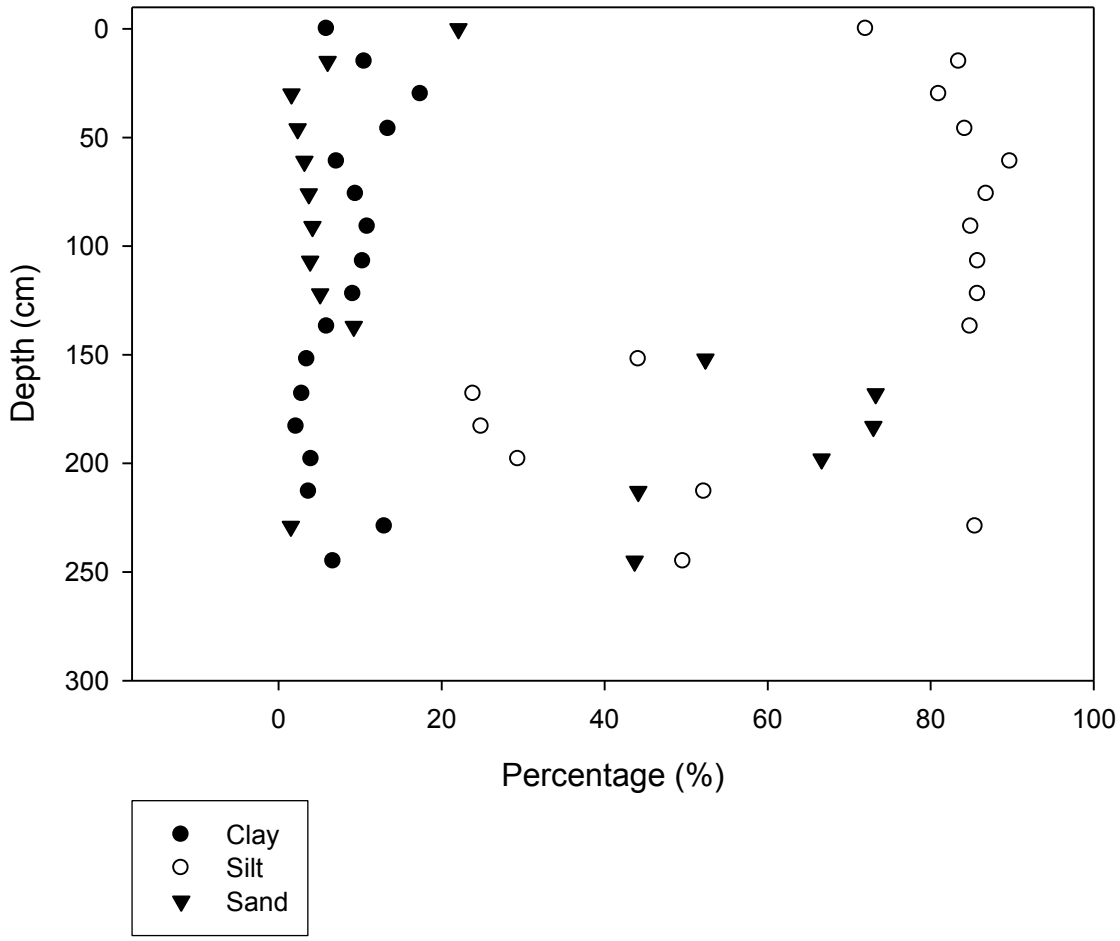

Figure 8. Particle size distribution in Plot 4.

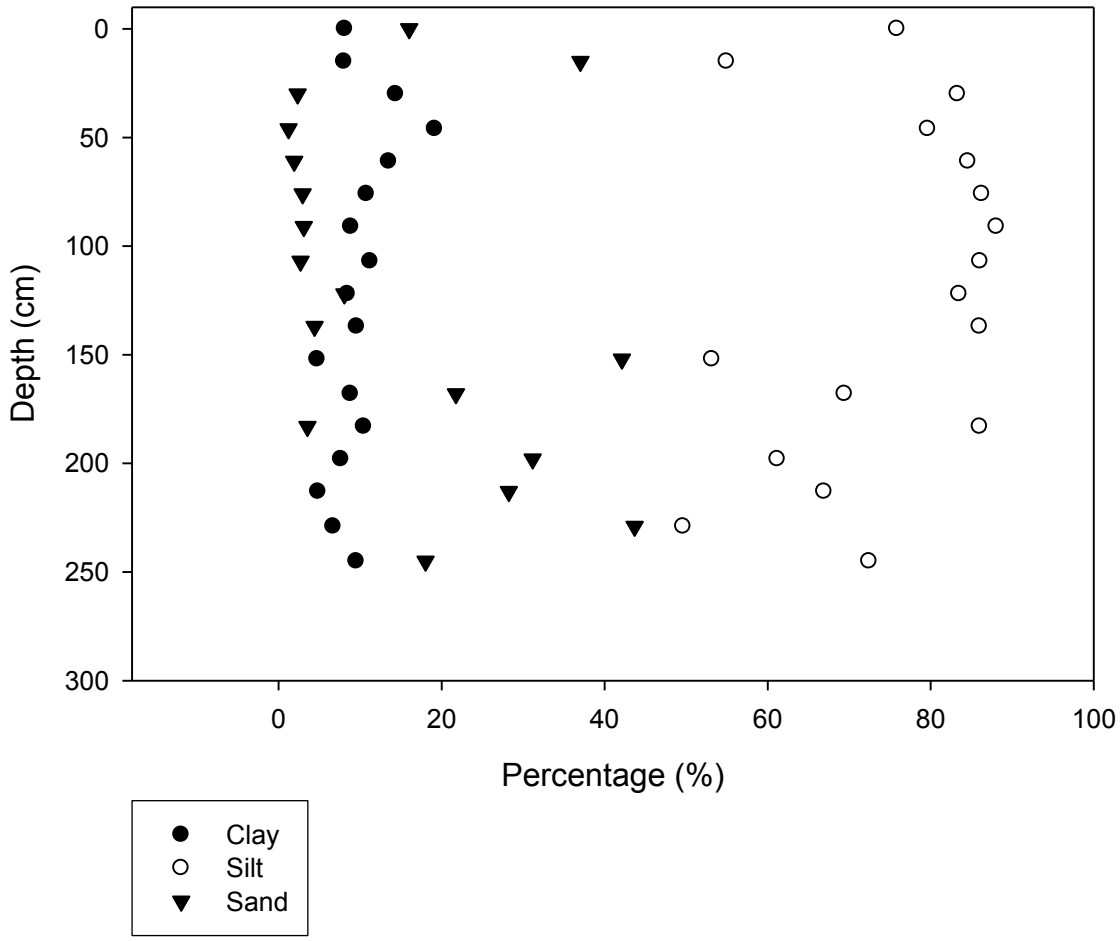

Figure 9. Particle size distribution in Plot 5.

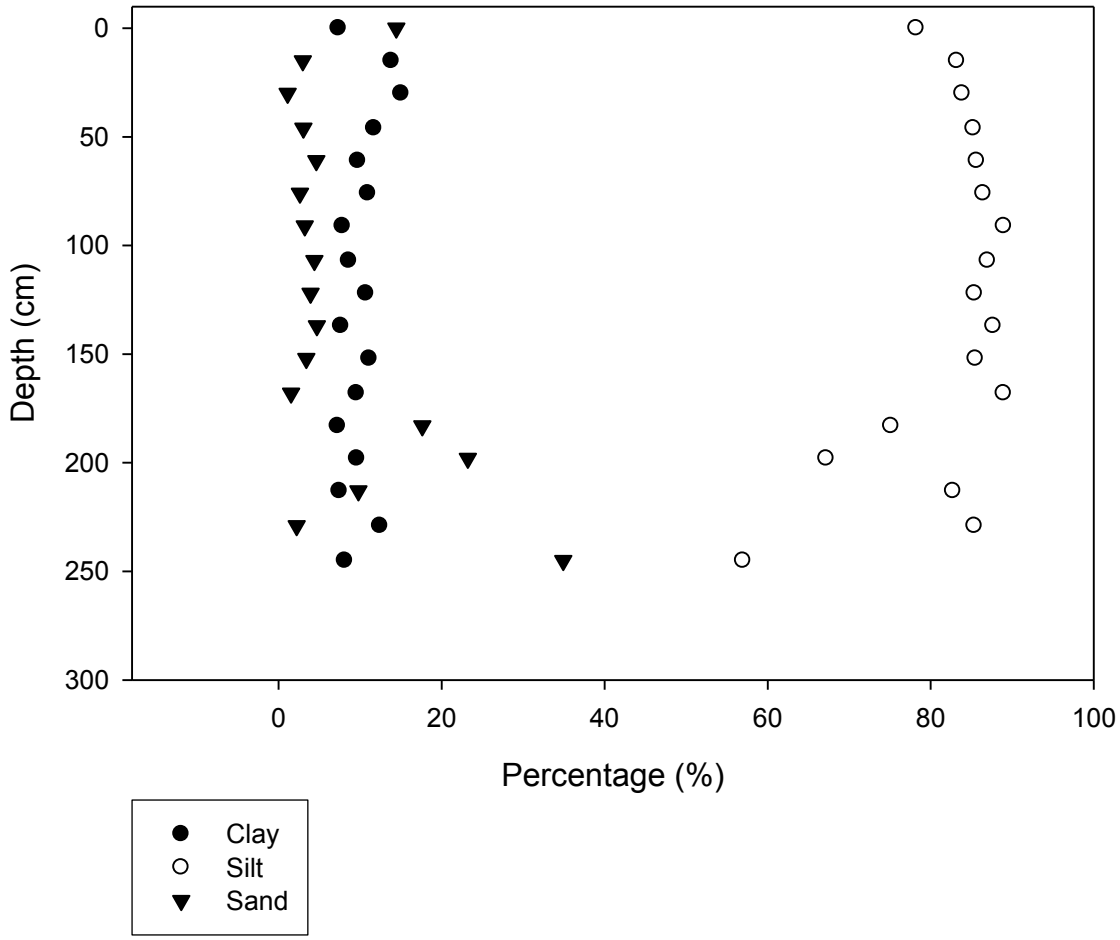

Figure 10. Particle size distribution in Plot 6.

Table 2. Mean concentrations of extractable (standard error) Fe, Al, Mn, and Si for the 10 depth-incremented plots using the sodium citrate-bicarbonate-dithionite (CBD) method.

Depth	Fe	Al	Mn	Si
cm	g/kg	——————————mg/kg ——————————		
0-15	7.19 ± 0.2	864 ± 25	1220 ± 25	485 ± 33
15-30	12.51 ± 0.4	1630 ± 39	884 ± 24	592 ± 34
30-46	16.89 ± 0.2	2287 ± 48	684 ± 24	634 ± 44
46-61	15.75 ± 0.3	2139 ± 49	592 ± 20	572 ± 36
61-76	13.66 ± 0.4	1759 ± 49	538 ± 35	509 ± 33
76-91	12.44 ± 0.2	1485 ± 33	461 ± 13	505 ± 30
91-107	12.11 ±0.2	1345 ± 25	534 ± 24	556 ± 27
107-122	11.90 ± 0.2	1314 ± 30	576 ± 30	635 ± 47
122-137	11.11 ± 0.2	1167 ± 19	600 ± 29	634 ± 24
137-152	10.30 ± 0.2	1087 ± 22	553 ± 32	642 ± 25
152-168	9.76 ± 0.2	1051 ± 18	559 ± 21	604 ± 29
168-183	9.83 ± 0.2	1058 ± 27	564 ± 24	610 ± 23
183-198	10.48 ± 0.2	1101 ± 20	621 ± 22	539 ± 37
198-213	10.97 ± 0.2	1162 ± 22	634 ± 36	501 ± 34
213-229	11.36 ± 0.2	1227 ± 28	580 ± 48	510 ± 26
229-245	12.36 ± 0.2	1361 ± 27	554 ± 74	483 ± 34
245-261	13.37 ± 0.2	1524 ± 23	525 ± 93	471 ± 28

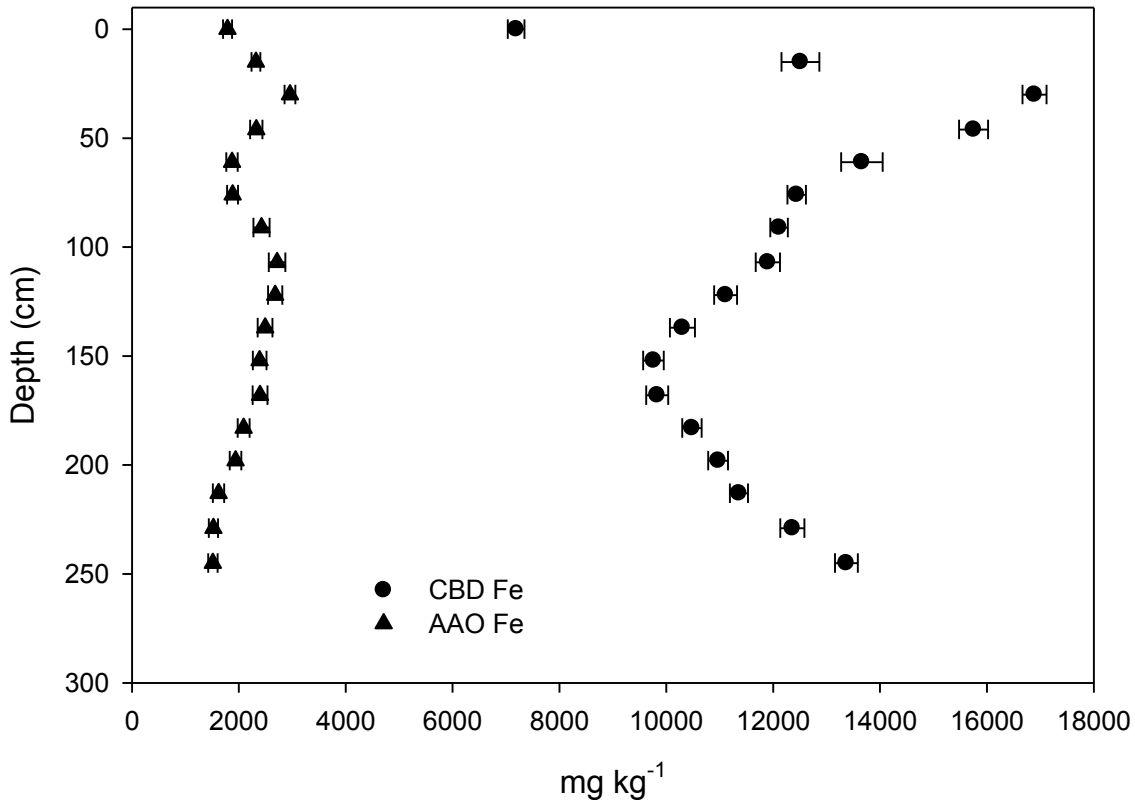

Figure 11. Mean concentration of extractable iron by sodium citrate-bicarbonate-dithionite (CBD) and ammonium oxalate (AAO) methods. The error bars represent standard error.

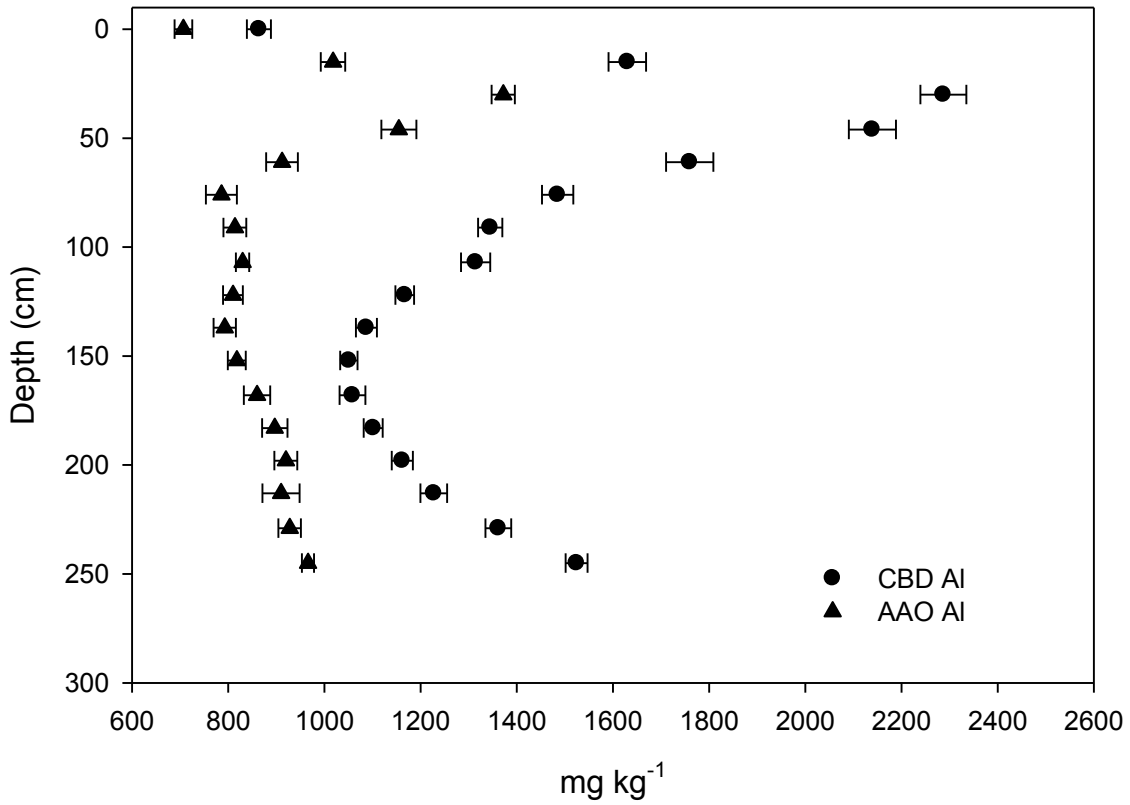

Figure 12. Mean concentration of extractable aluminum by sodium citrate-bicarbonate-dithionite (CBD) and ammonium oxalate (AAO) methods. The error bars represent standard error.

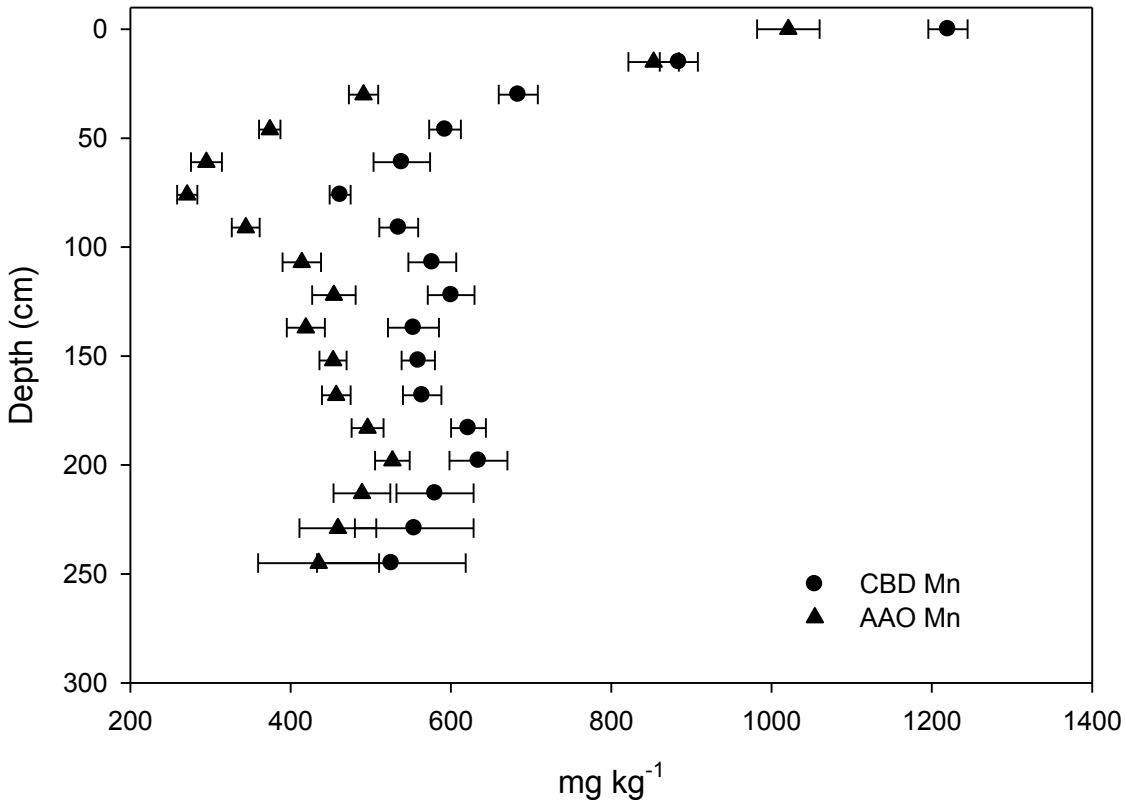

Figure 13. Mean concentration of extractable manganese by sodium citrate-bicarbonate-dithionite (CBD) and ammonium oxalate (AAO) methods. The error bars represent standard error.

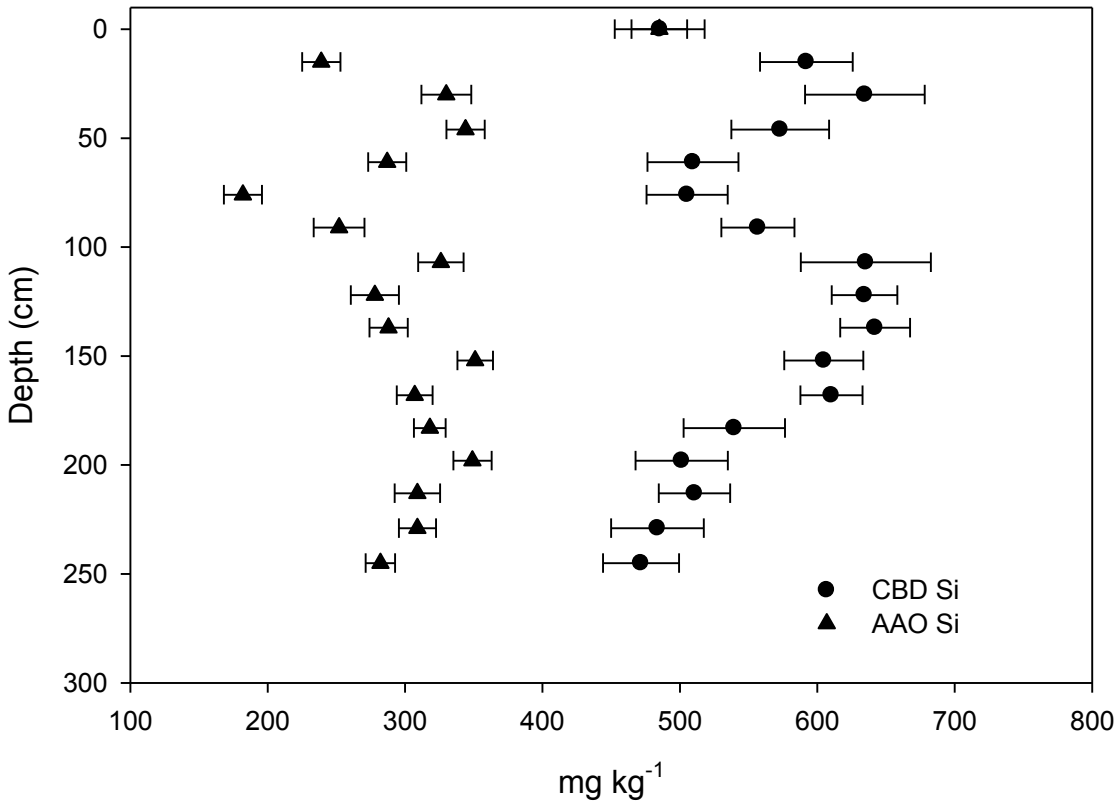

Figure 14. Mean concentration of extractable silica by sodium citrate-bicarbonate-dithionite (CBD) and ammonium oxalate (AAO) methods. The error bars represent standard error.

Table 3. Mean concentrations of extractable (standard error) Fe, Al, Mn, and Si for the 10 depth-incremented plots using the ammonium oxalate (AAO) method.

Depth	Fe	Al	Mn	Si
cm	mg/kg			
0-15	1789 ± 83	707 ± 19	1021 ± 39	179 ± 20
15-30	2320 ± 84	1018 ± 25	853 ± 31	239 ± 14
30-46	2958 ± 101	1372 ± 24	491 ± 18	330 ± 18
46-61	2327 ± 114	1155 ± 36	374 ± 13	344 ± 14
61-76	1872 ± 105	912 ± 33	295 ± 19	287 ± 14
76-91	1883 ± 104	786 ± 32	271 ± 13	182 ± 14
91-107	2424 ± 151	814 ± 24	344 ± 17	252 ± 18
107-122	2717 ± 156	830 ± 14	414 ± 24	326 ± 17
122-137	2680 ± 132	810 ± 21	454 ± 27	278 ± 18
137-152	2492 ± 139	793 ± 23	419 ± 24	288 ± 14
152-168	2390 ± 127	818 ± 19	453 ± 17	351 ± 13
168-183	2397 ± 140	860 ± 27	457 ±18	307 ± 13
183-198	2090 ± 112	897 ± 26	496 ± 20	318 ± 12
198-213	1938 ± 108	920 ± 24	527 ± 22	349 ± 13
213-229	1620 ± 106	910 ± 338	489 ± 35	309 ± 17
229-245	1525 ± 85	928 ± 23	459 ± 48	309 ± 13
245-261	1515 ± 87	966 ± 12	435 ± 75	282 ± 11

Table 4. Mean anion exchange capacity (EAEC) and exchange phase composition for the 10 depth-incremented plots using the potassium acetate extraction method. †

Depth	SO_4 ‡	NO_3	Cl	EAEC
cm	———	$mmol_c/kg$	———	
0-15	0.57 ± 0.08	0.15 ± 0.007	0.26 ± 0.03	2.10 ± 0.09
15-30	0.48 ± 0.07	0.07 ± 0.007	0.21 ± 0.02	1.04 ± 0.07
30-46	0.44 ± 0.04	0.12 ± 0.001	0.21 ± 0.02	1.38 ± 0.04
46-61	0.44 ± 0.06	0.07 ± 0.005	0.25 ± 0.03	0.94 ± 0.05
61-76	0.55 ± 0.07	0.08 ± 0.005	0.29 ± 0.02	1.04 ± 0.07
76-91	0.52 ± 0.05	0.07 ± 0.003	0.29 ± 0.02	1.00 ± 0.07
91-107	0.61 ± 0.08	0.07 ± 0.004	0.27 ± 0.01	1.05 ± 0.09
107-122	0.89 ± 0.11	0.09 ± 0.009	0.31 ± 0.02	1.35 ± 0.13
122-137	0.98 ± 0.16	0.09 ± 0.009	0.35 ± 0.02	1.43 ± 0.18
137-152	1.13 ± 0.14	0.10 ± 0.010	0.34 ± 0.02	1.55 ± 0.15
152-168	0.86 ± 0.05	0.10 ± 0.005	0.40 ± 0.02	1.41 ± 0.07
168-183	0.92 ± 0.06	0.10 ± 0.005	0.38 ± 0.03	1.40 ± 0.08
183-198	1.03 ± 0.06	0.11 ± 0.005	0.37 ± 0.03	1.52 ± 0.06
198-213	0.93 ± 0.07	0.09 ± 0.005	0.31 ± 0.03	1.32 ± 0.06
213-229	1.05 ± 0.04	0.10 ± 0.008	0.34 ± 0.03	1.46 ± 0.15
229-245	1.08 ± 0.02	0.09 ± 0.007	0.33 ± 0.02	1.48 ± 0.11
245-261	1.06 ± 0.06	0.10 ± 0.012	0.31 ± 0.03	1.48 ± 0.16

† EAEC = summation of $cmol_C/kg$ from exchangeable NO_3, Cl, and SO_4

‡ Error term is the standard error

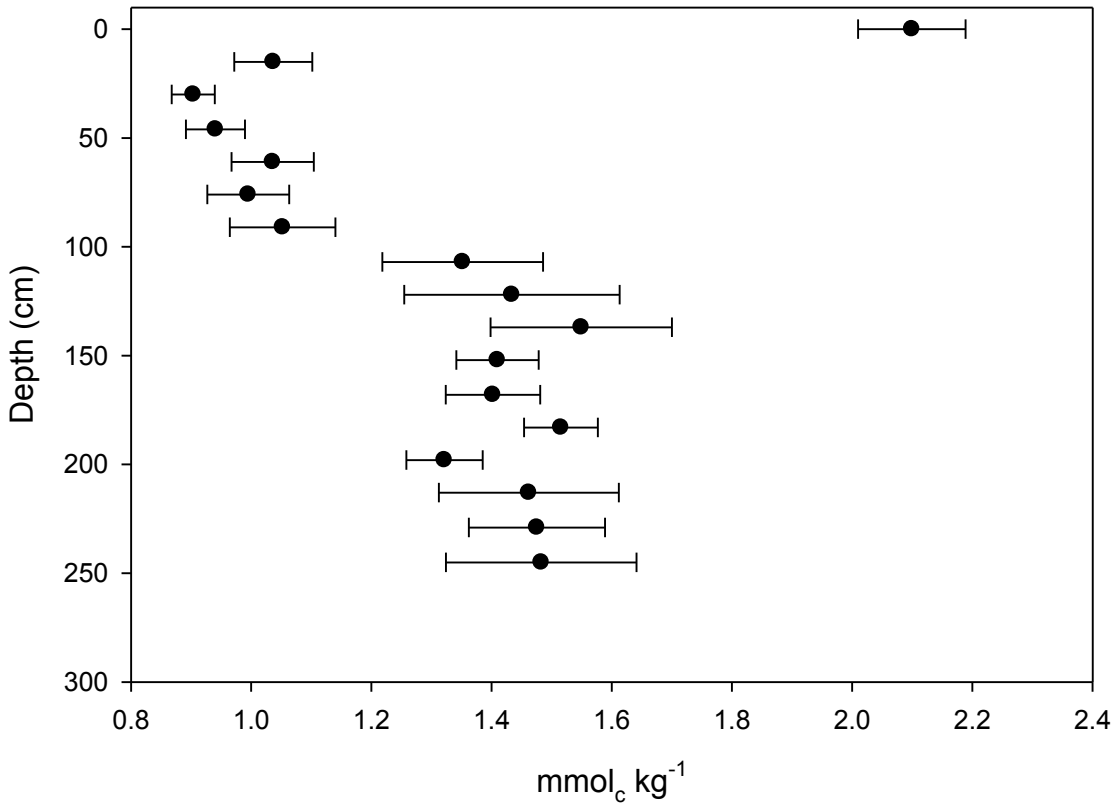

Figure 15. Mean effective anion exchange capacity (EAEC) of the 10 depth-incremented plots. Error bars represent standard error.

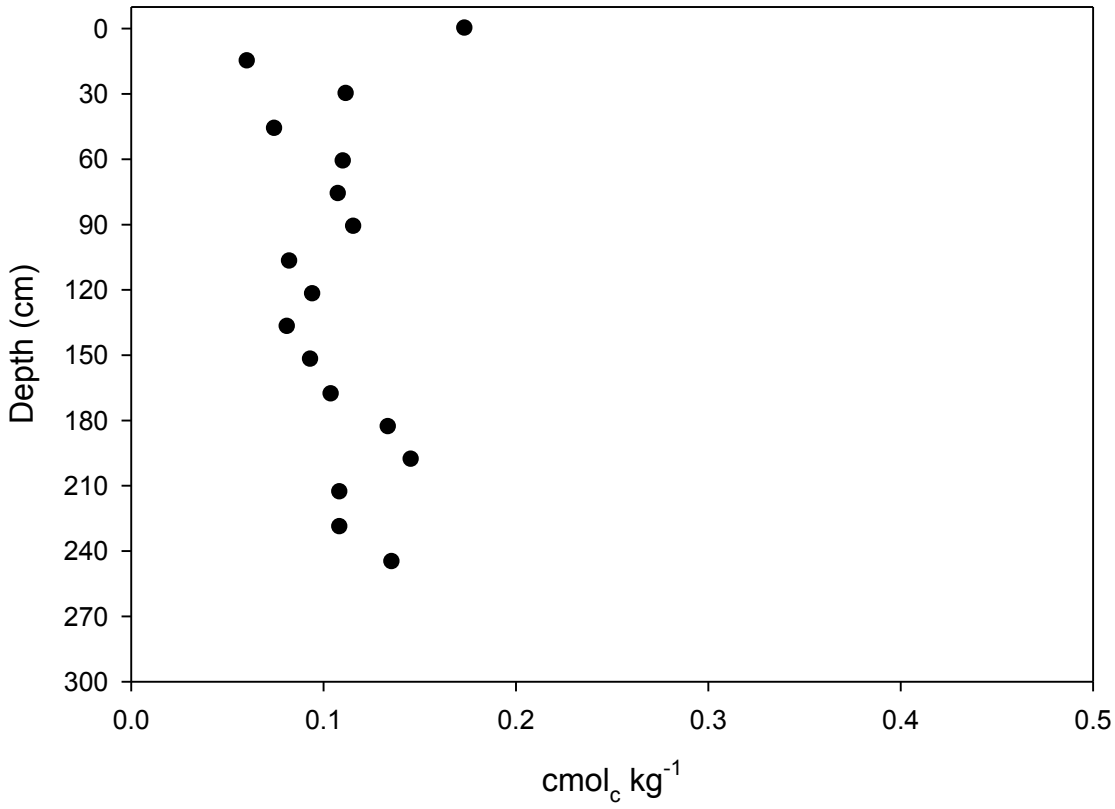

Figure 16. Effective anion exchange capacity (EAEC) of Plot 1

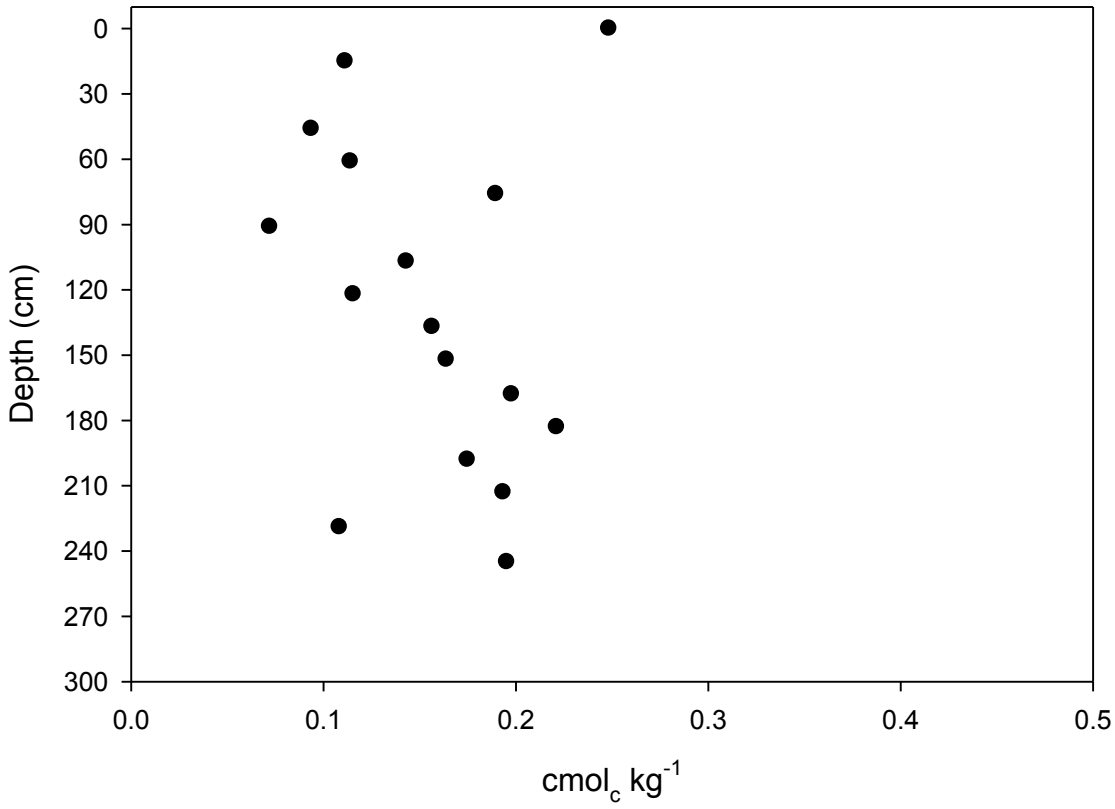

Figure 17. Effective anion exchange capacity (EAEC) of Plot 2

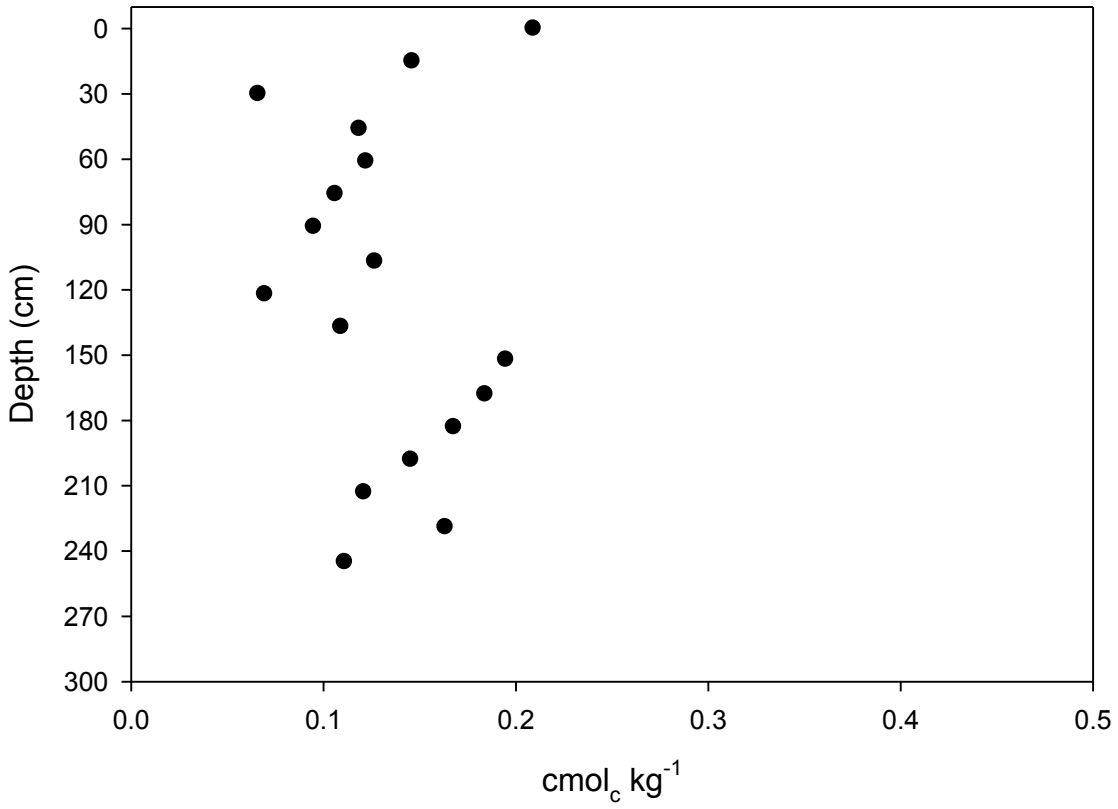

Figure 18. Effective anion exchange capacity (EAEC) of Plot 3

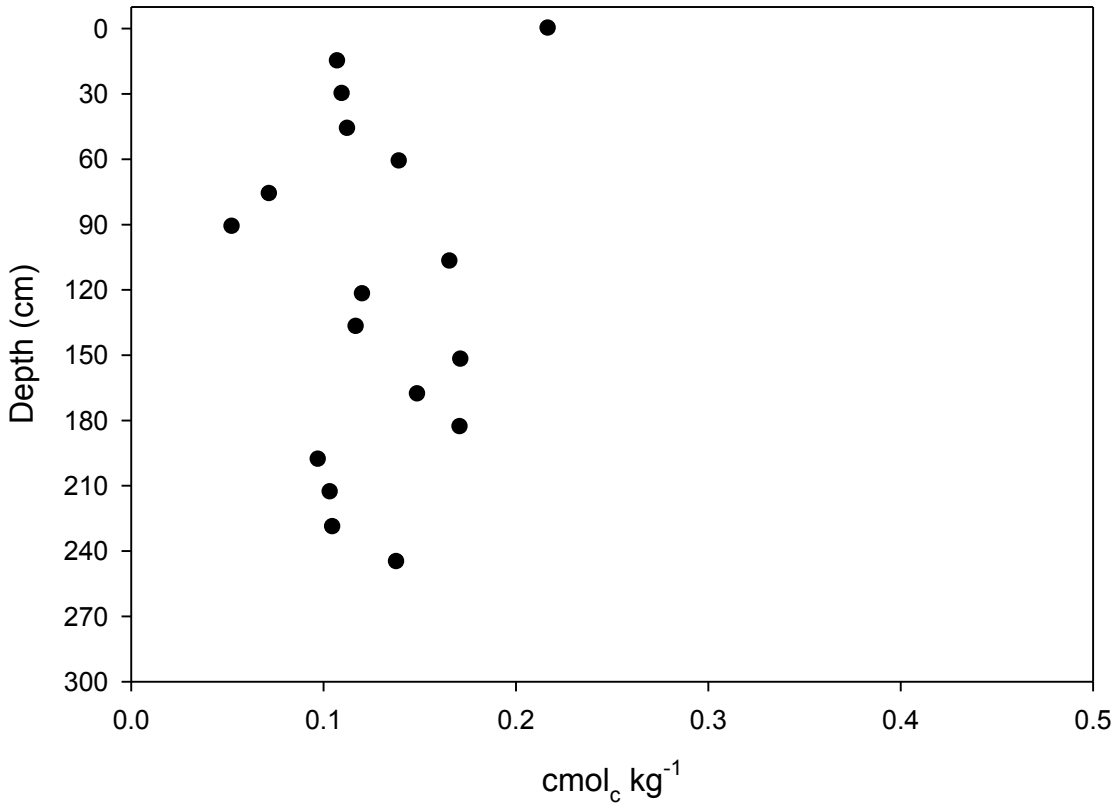

Figure 19. Effective anion exchange capacity (EAEC) of Plot 4

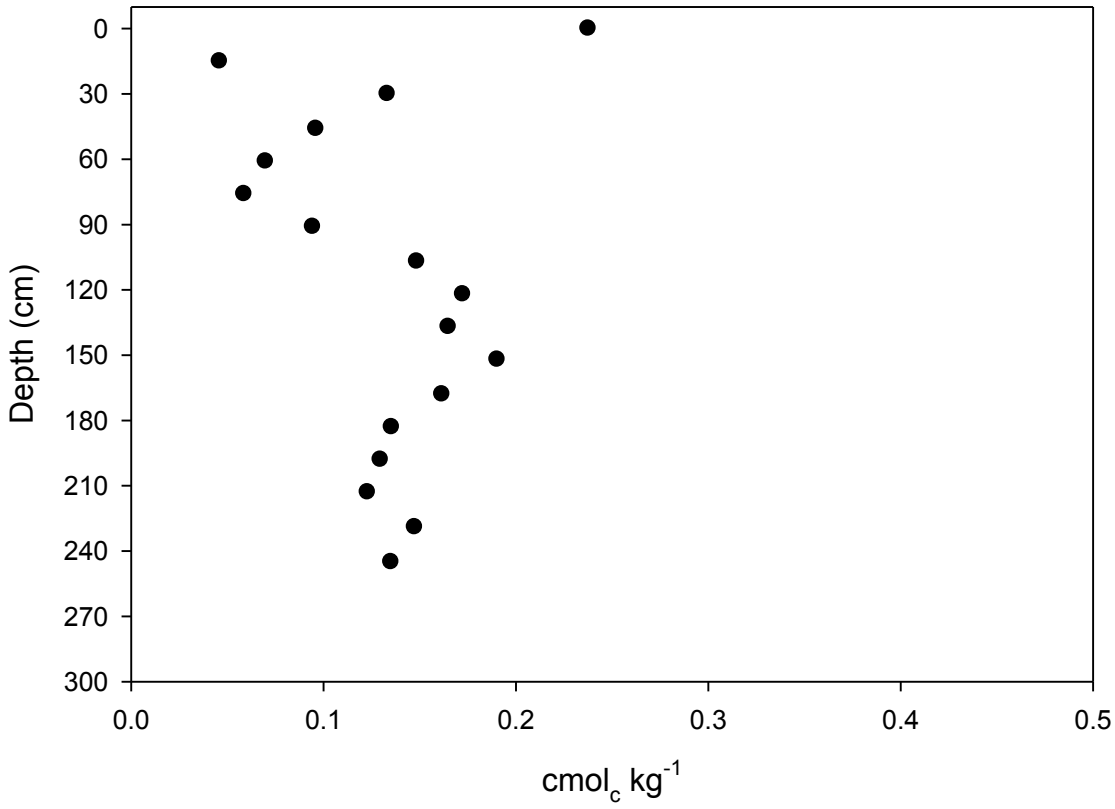

Figure 20. Effective anion exchange capacity (EAEC) of Plot 5

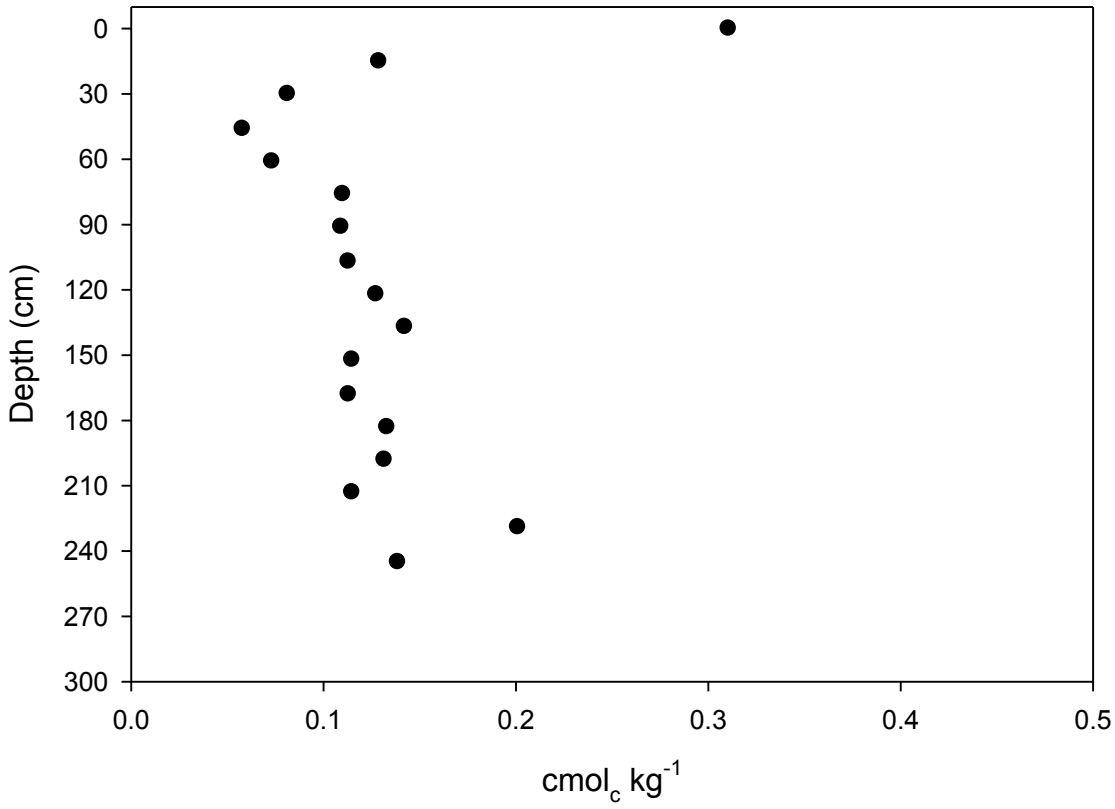

Figure 21. Effective anion exchange capacity (EAEC) of Plot 6

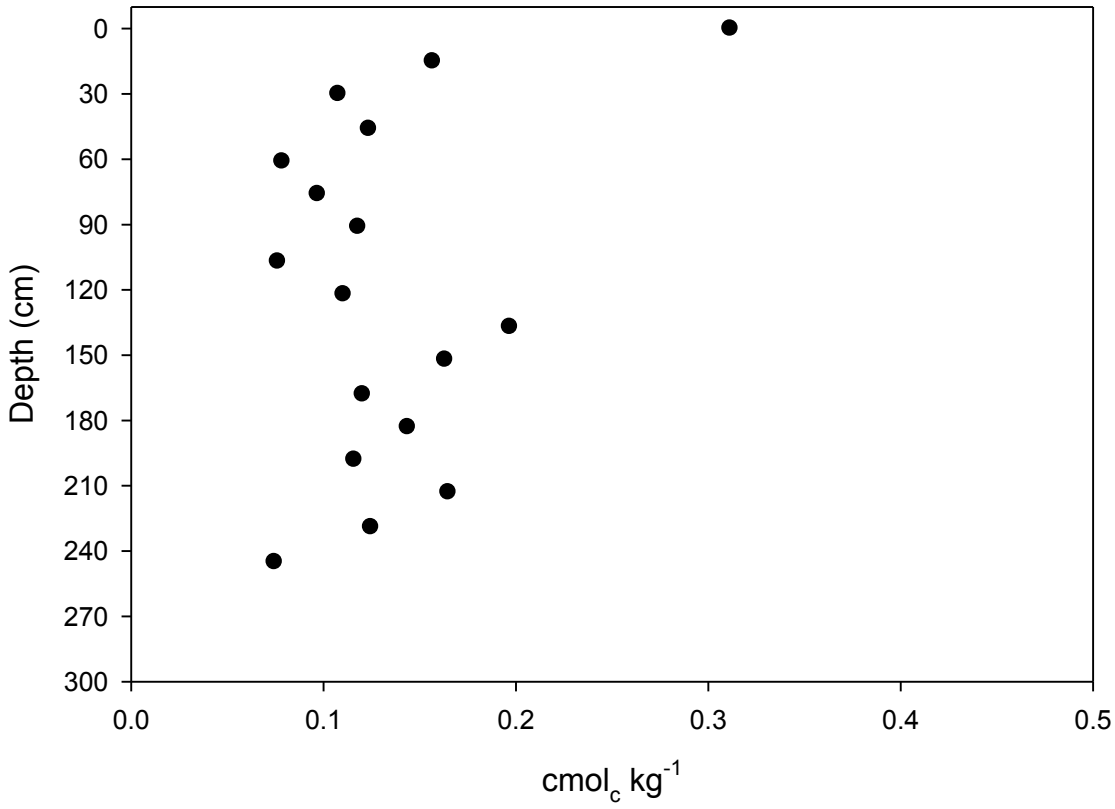

Figure 22. Effective anion exchange capacity (EAEC) of Plot 7

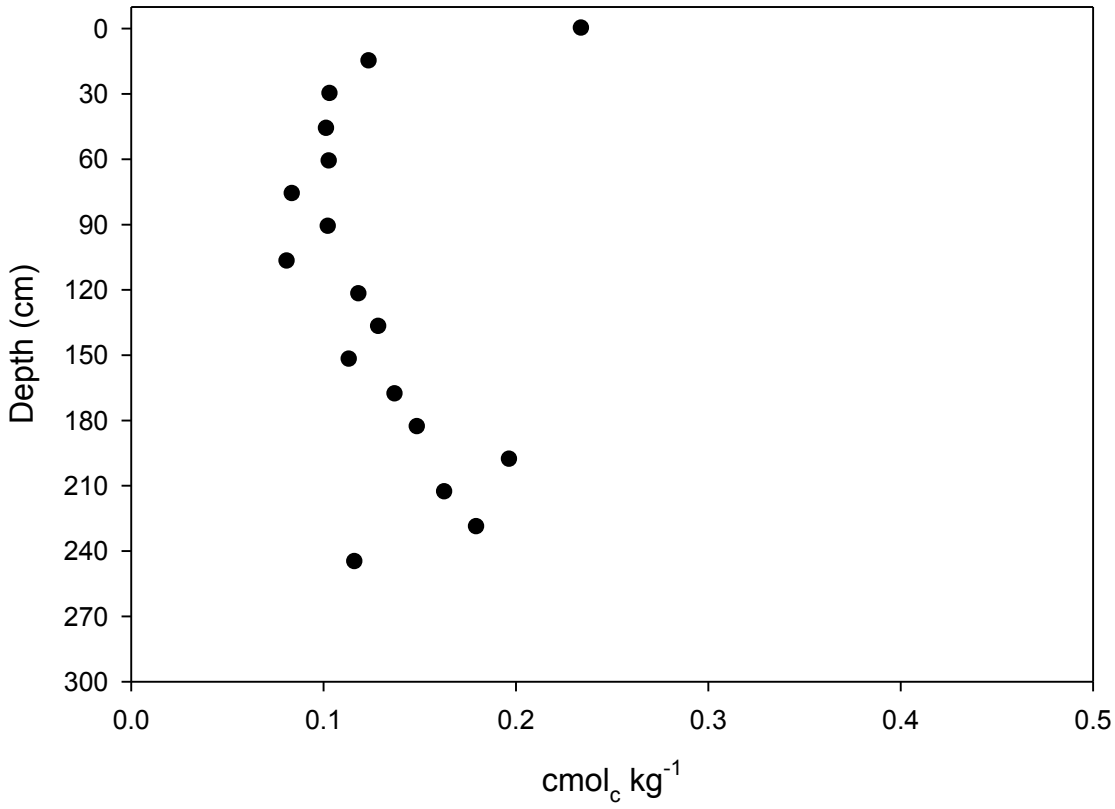

Figure 23. Effective anion exchange capacity (EAEC) of Plot 8

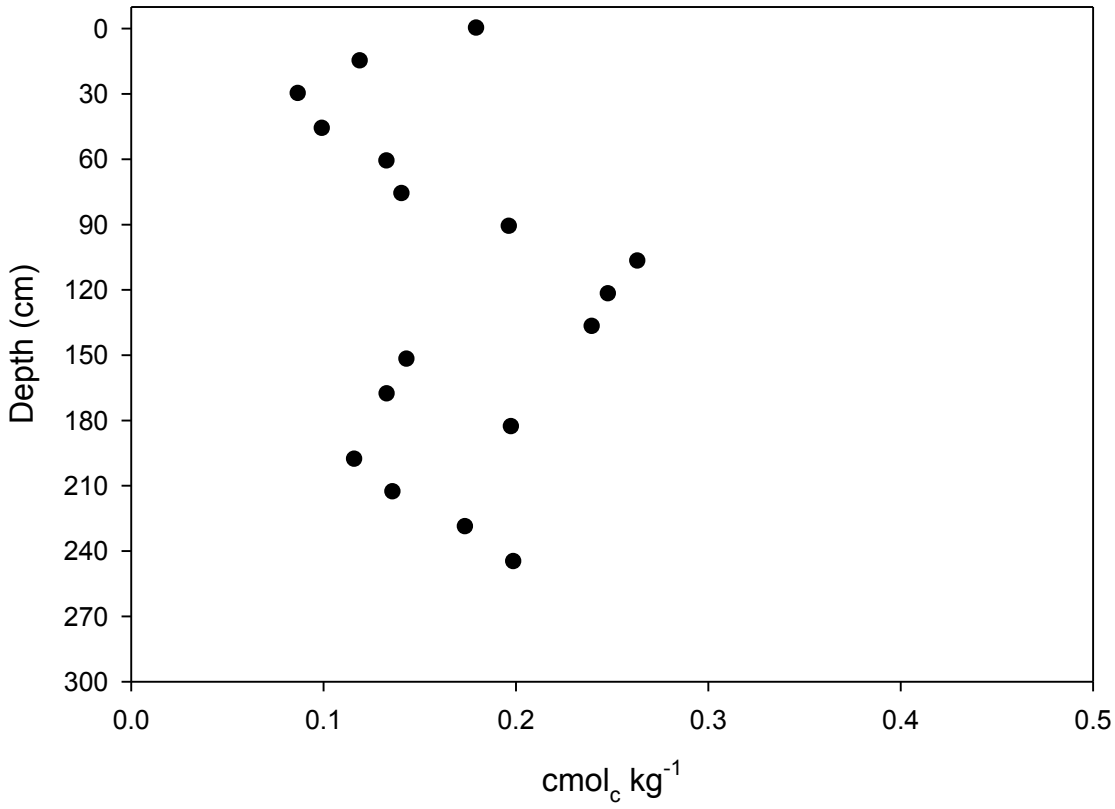

Figure 24. Effective anion exchange capacity (EAEC) of Plot 9

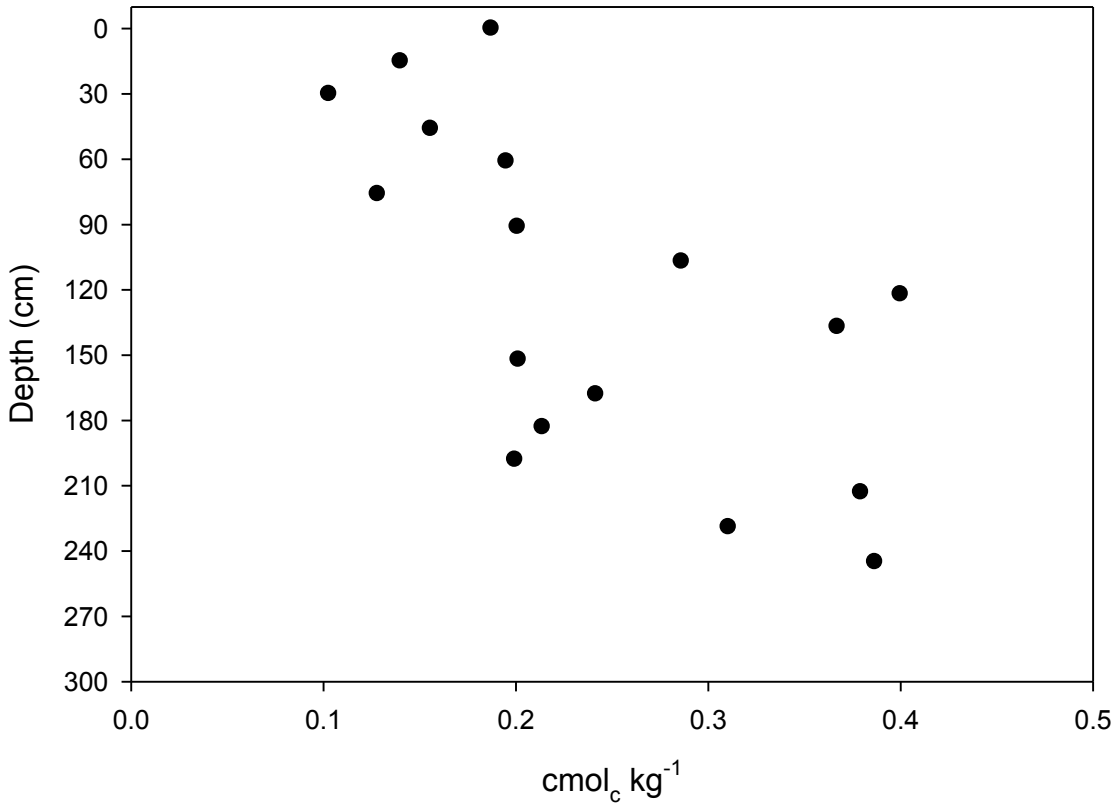

Figure 25. Effective anion exchange capacity (EAEC) of Plot 10

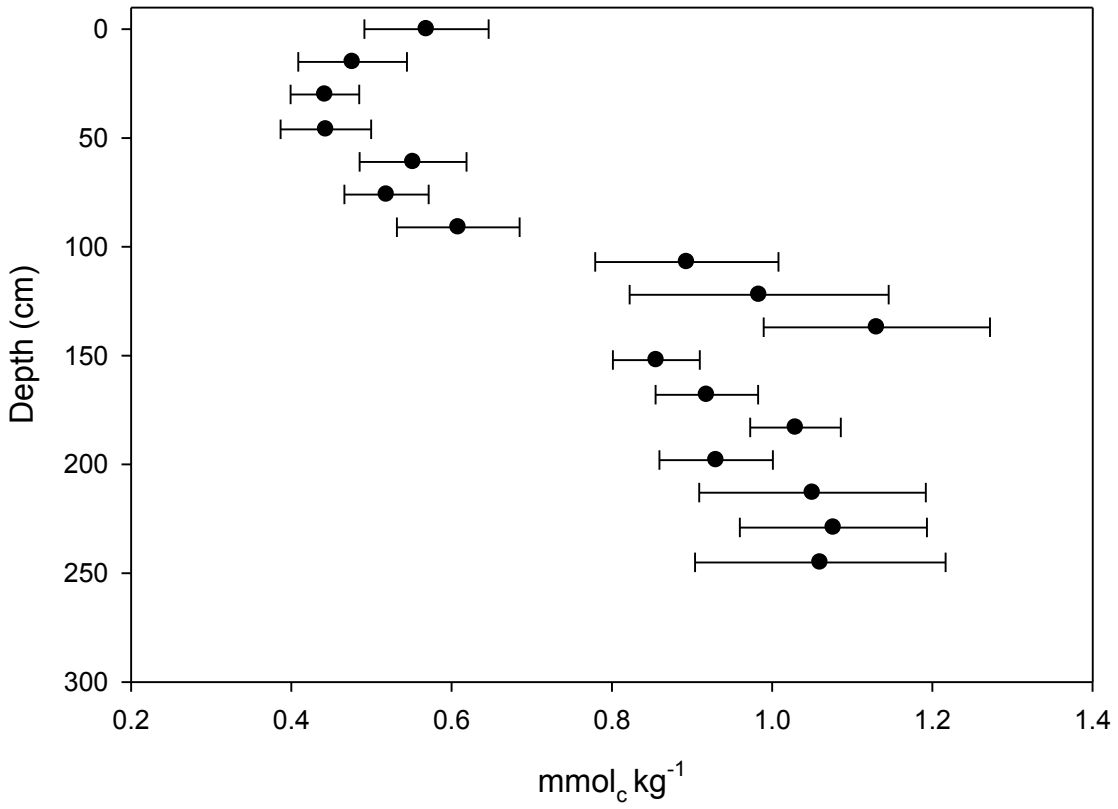

Figure 26. Mean exchangeable sulfate (SO_4) of the 10 depth-incremented plots. Error bars represent standard error.

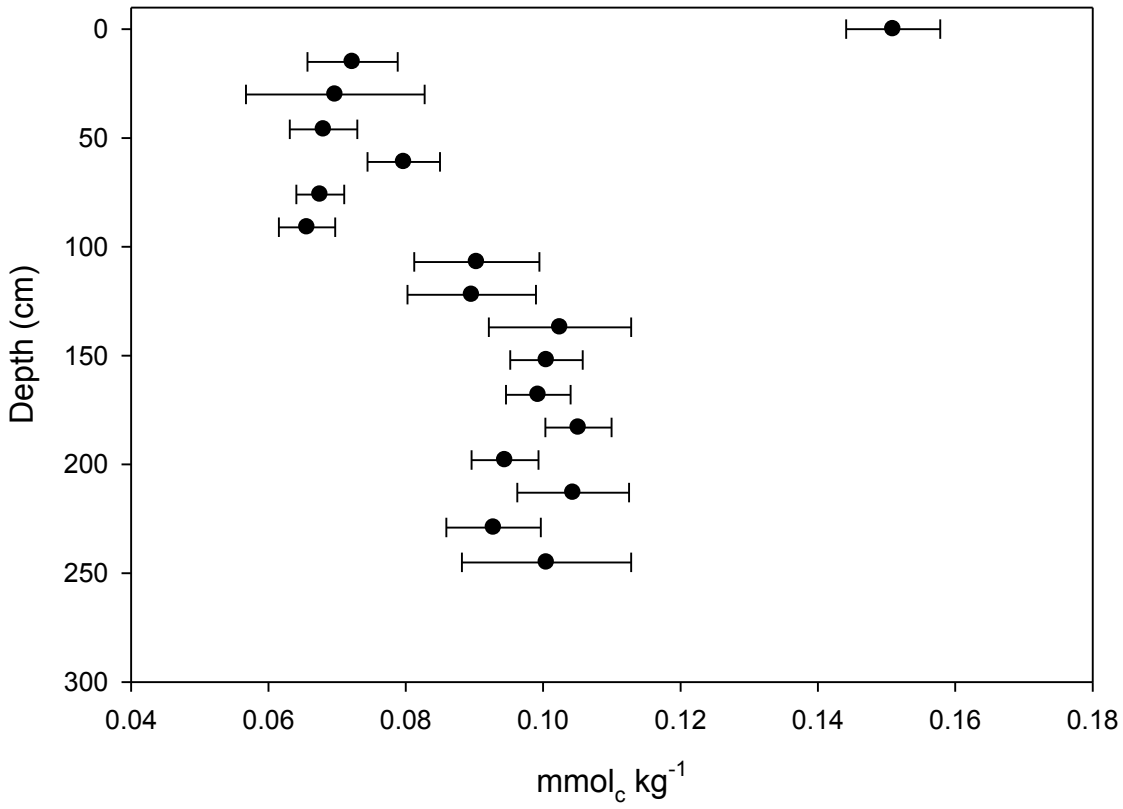

Figure 27. Mean exchangeable nitrate (NO_3) of the 10 depth-incremented plots. Error bars represent standard error.

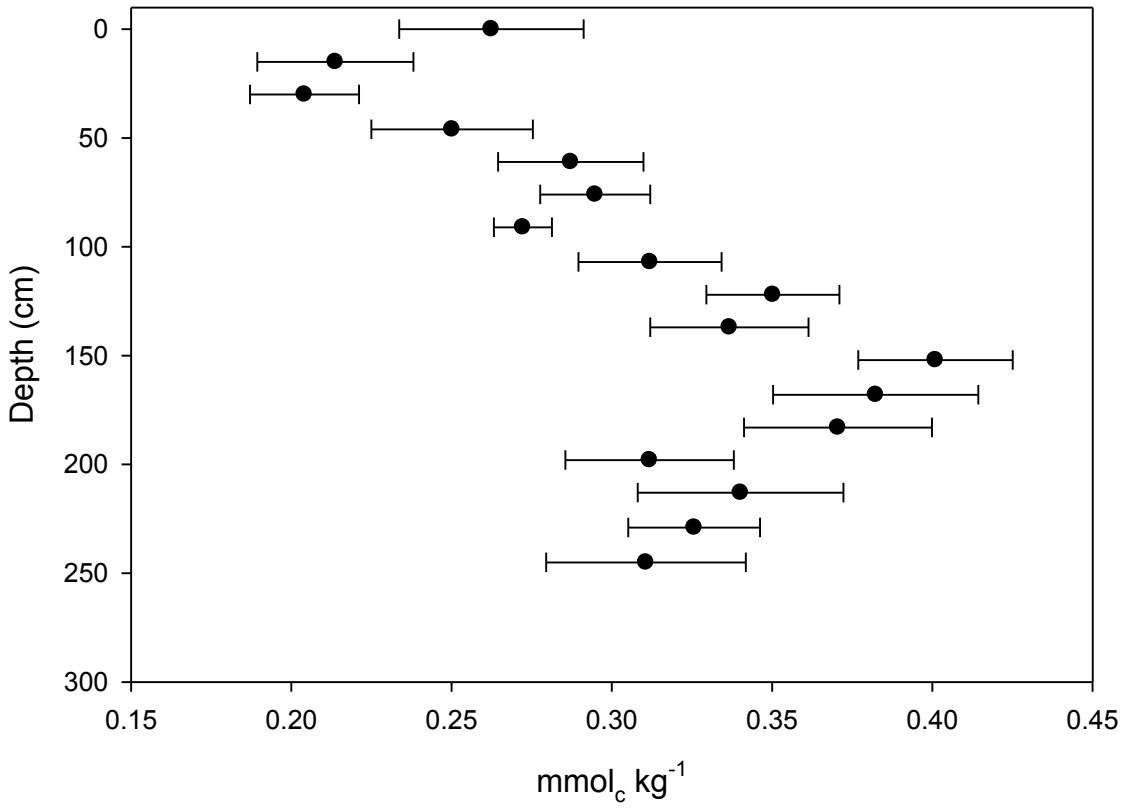

Figure 28. Mean exchangeable chloride (Cl) of the 10 depth-incremented plots. Error bars represent standard error.

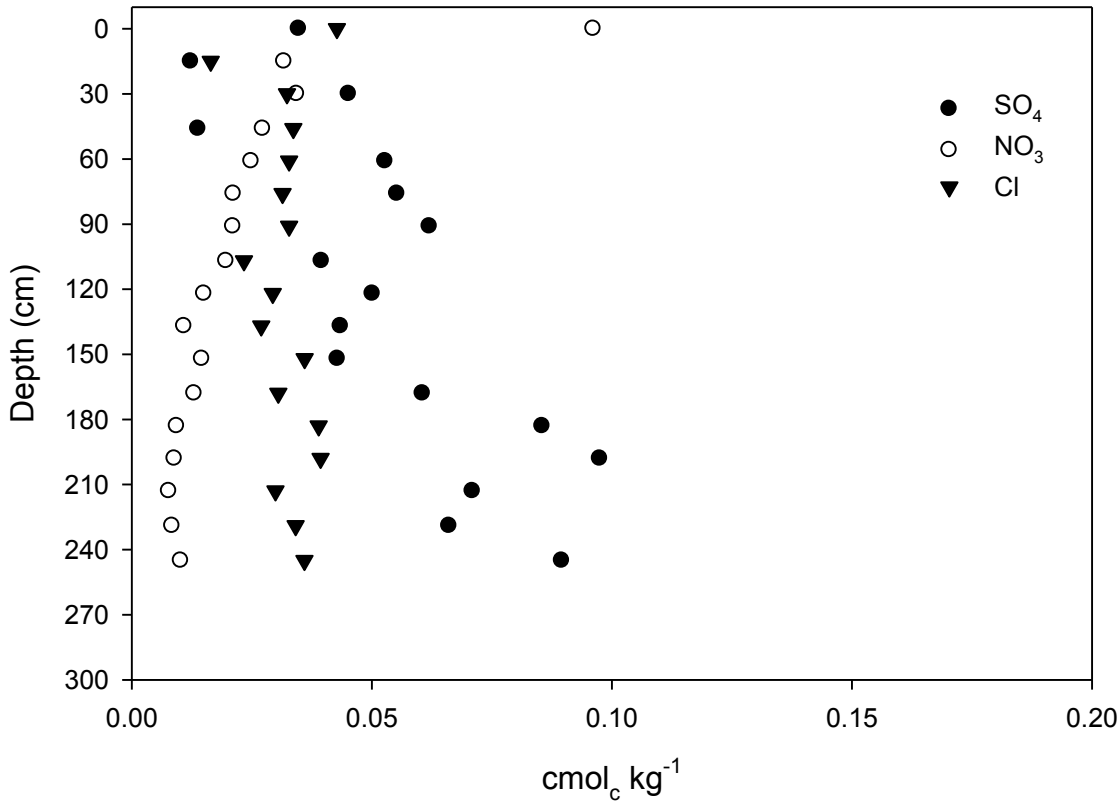

Figure 29. Exchangeable anion composition of Plot 1

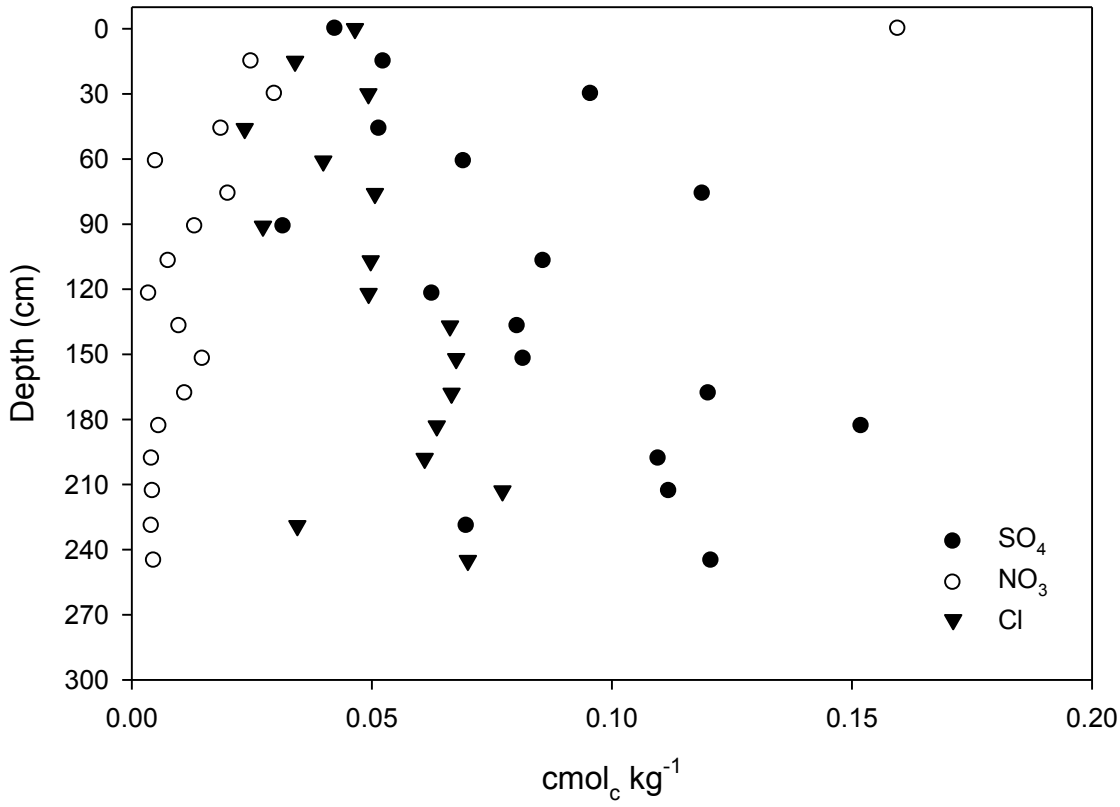

Figure 30. Exchangeable anion composition of Plot 2

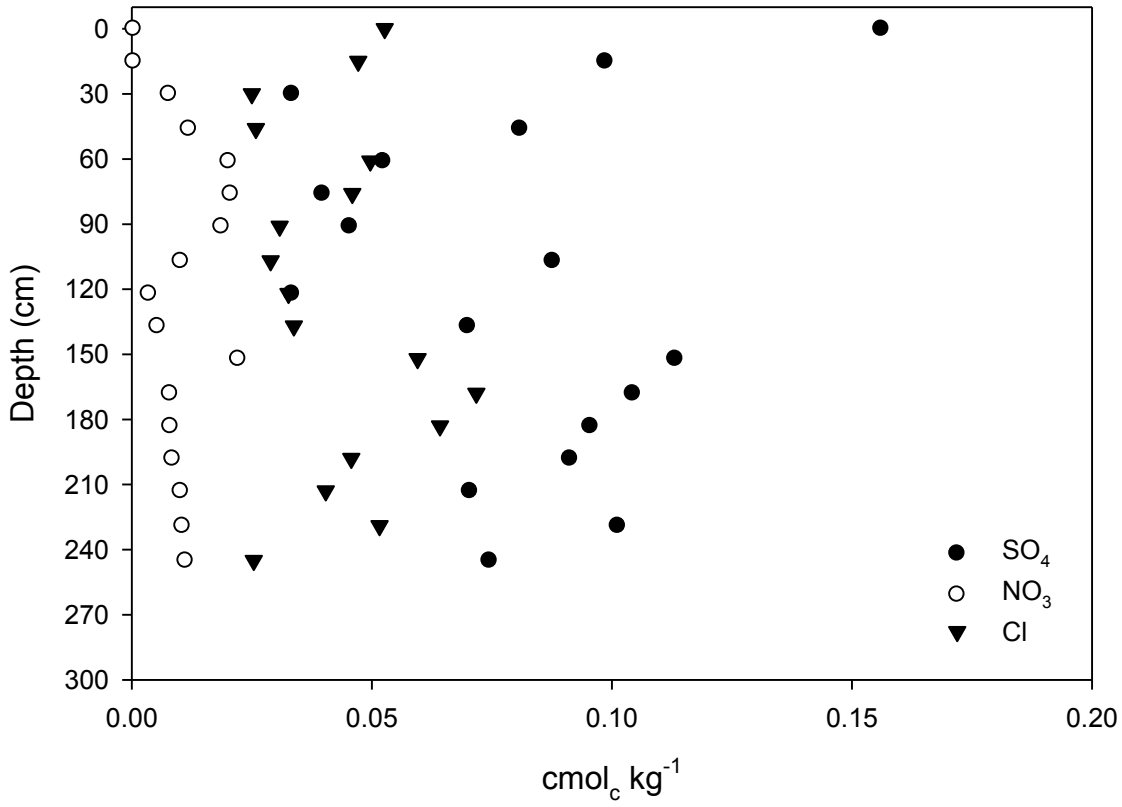

Figure 31. Exchangeable anion composition of Plot 3

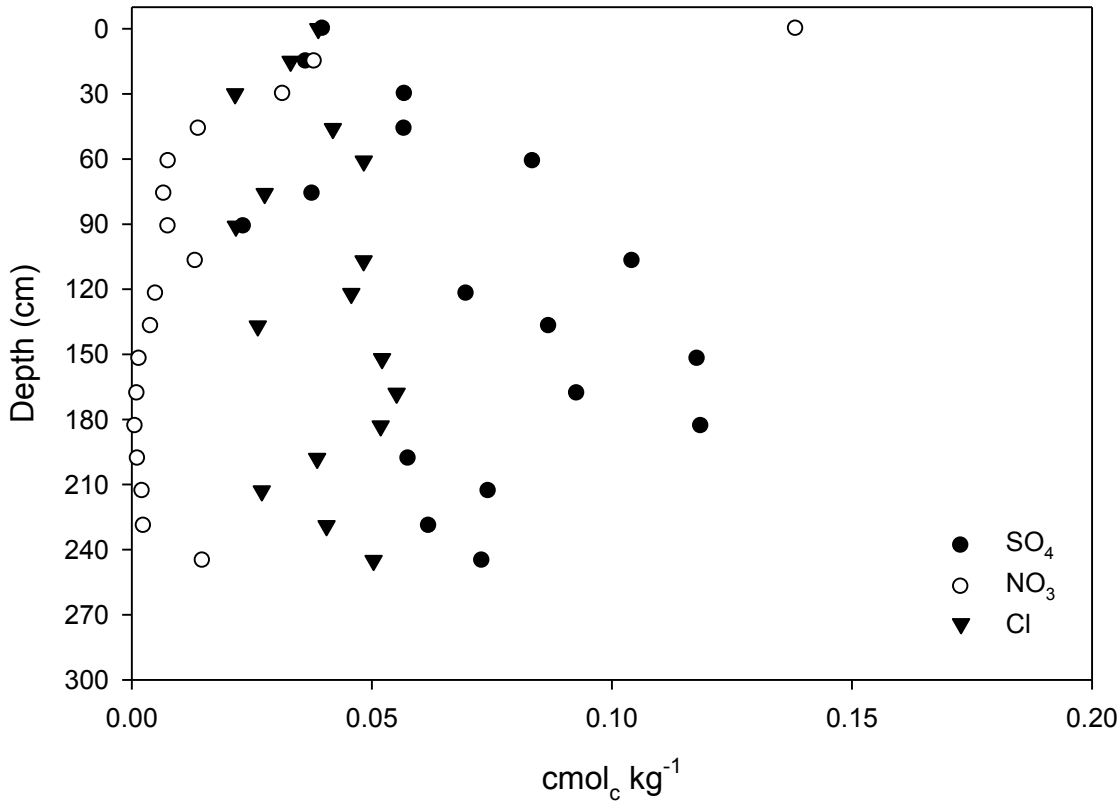

Figure 32. Exchangeable anion composition of Plot 4

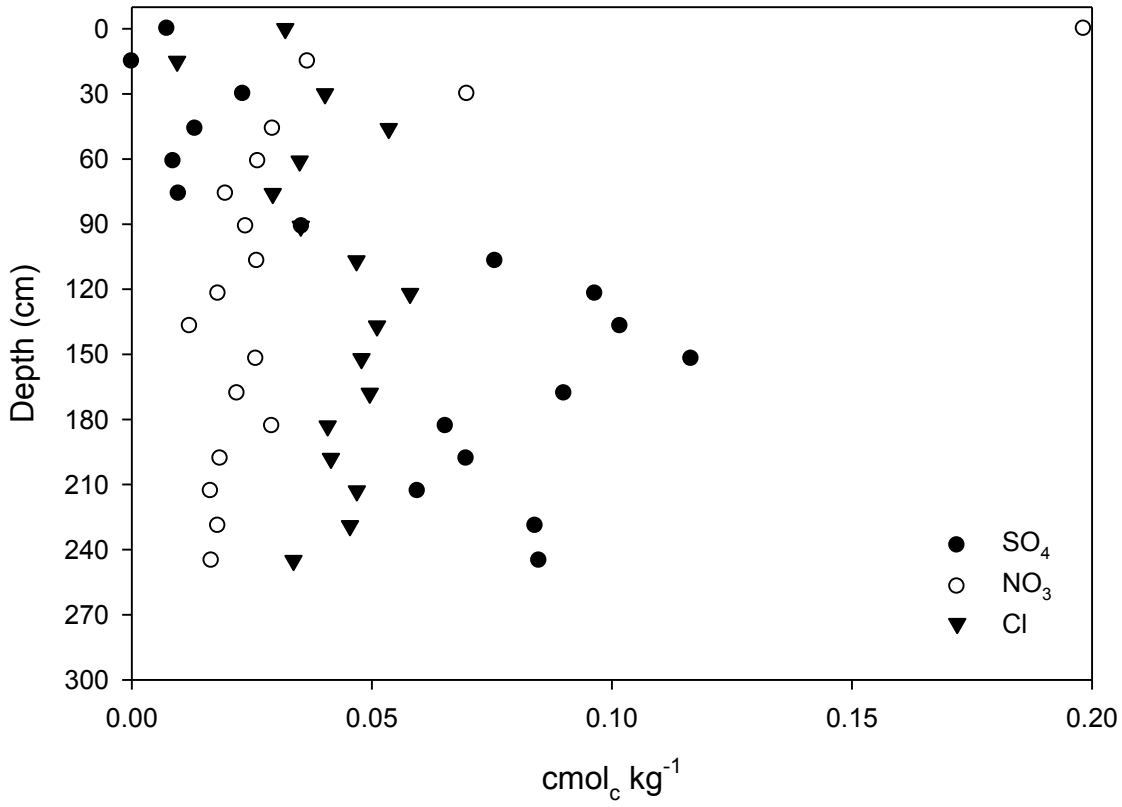

Figure 33. Exchangeable anion composition of Plot 5

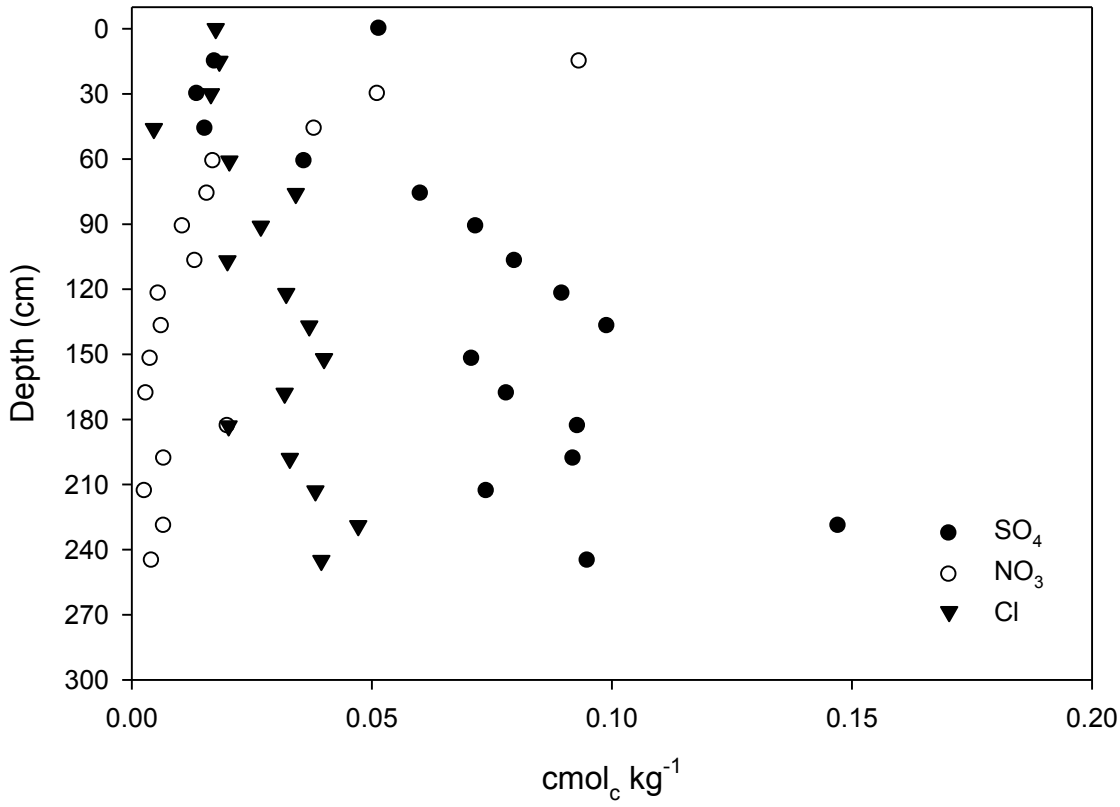

Figure 34. Exchangeable anion composition of Plot 6

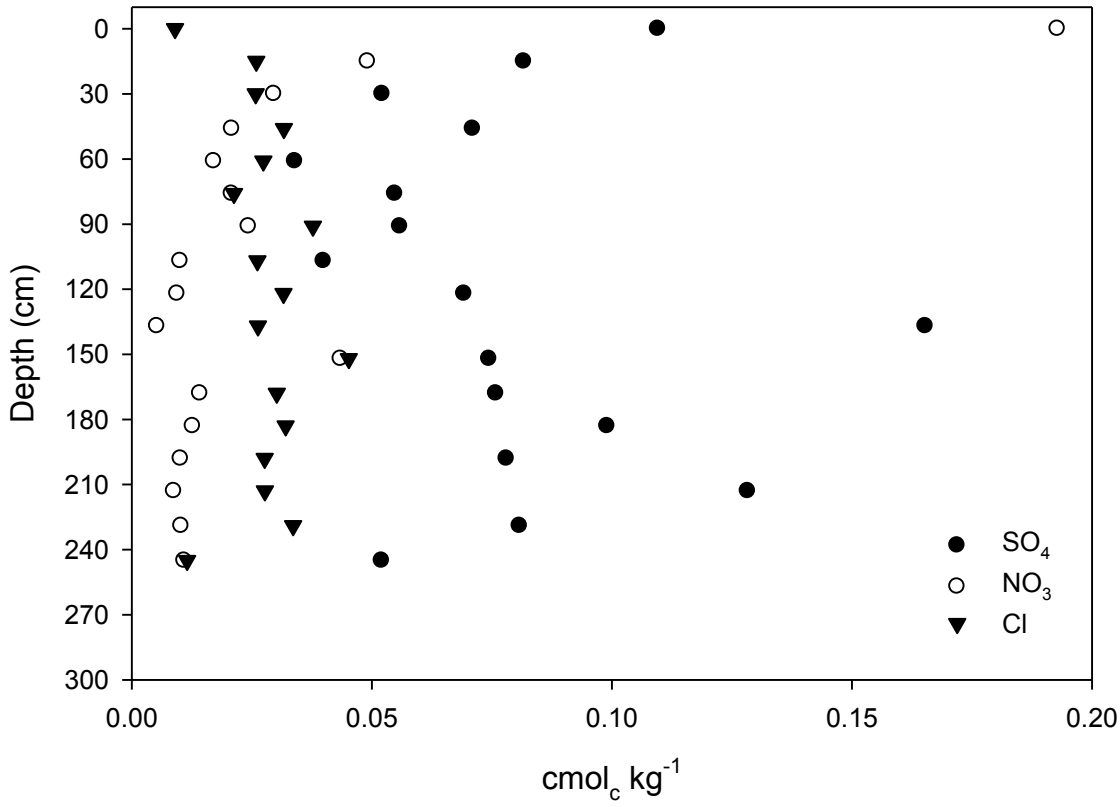

Figure 35. Exchangeable anion composition of Plot 7

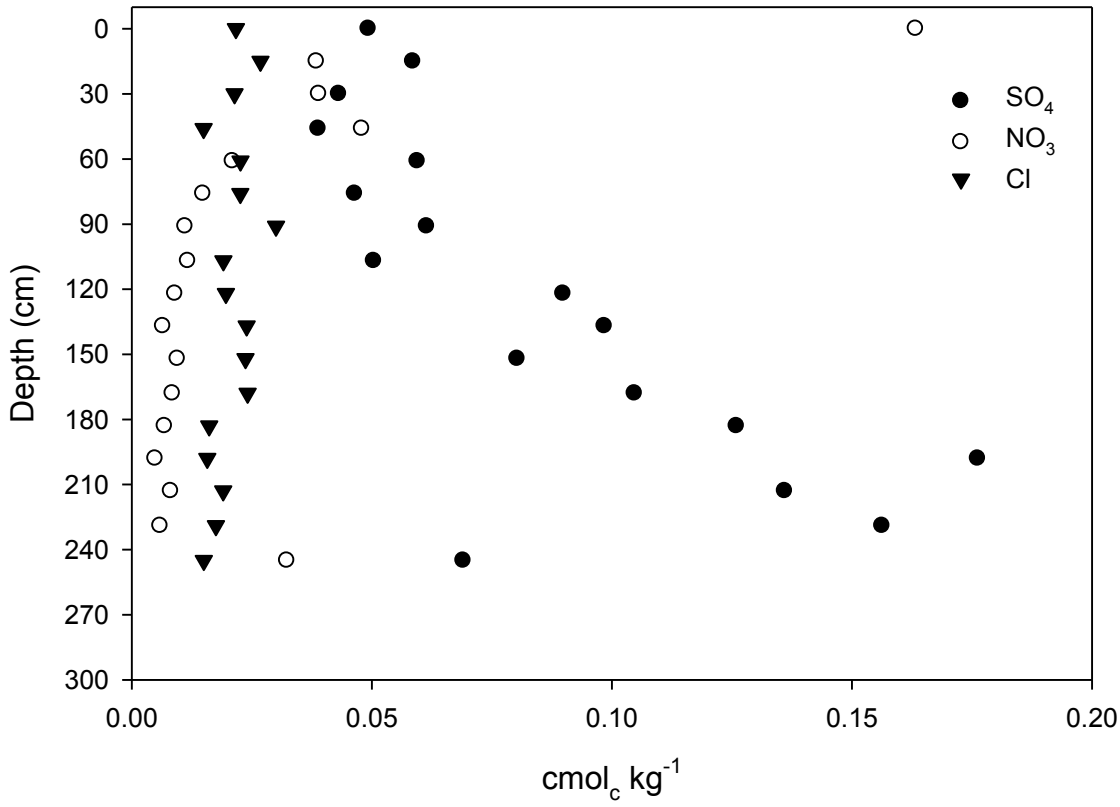

Figure 36. Exchangeable anion composition of Plot 8

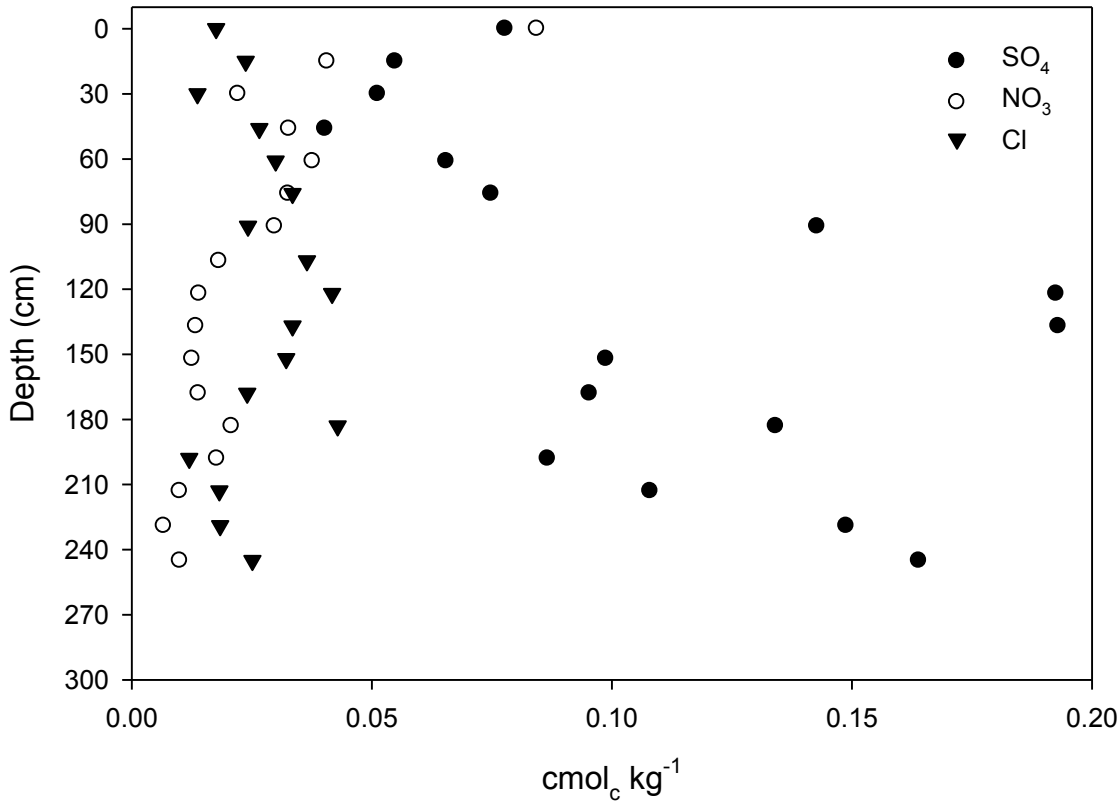

Figure 37. Exchangeable anion composition of Plot 9

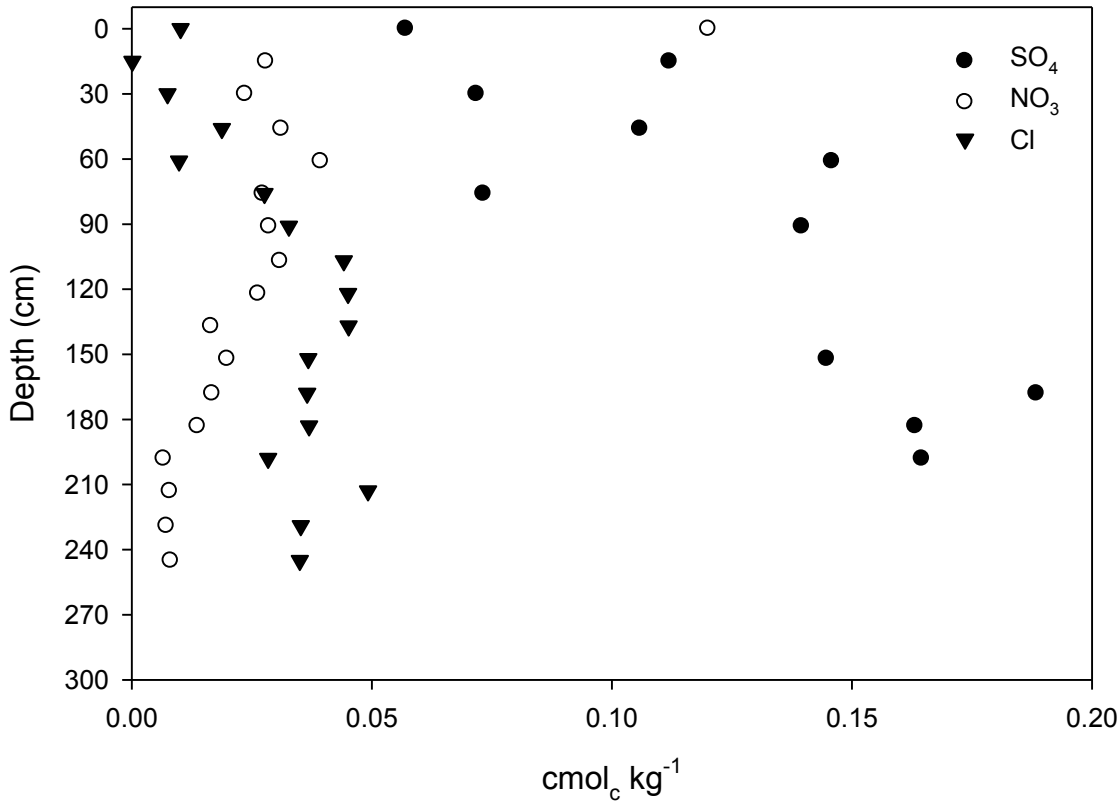

Figure 38. Exchangeable anion composition of Plot 10

Table 5. Mean cation exchange capacity (CEC), effective cation exchange capacity (ECEC) and cation exchange phase composition for the 10 depth-incremented plots using the ammonium chloride extraction method. †

Depth	Ca ‡	K	Mg	Na	Mn	CEC	ECEC
cm	———	———	———	$cmol_c/kg$	———	———	———
0-15	13.15 ± 0.7	0.75 ± 0.01	0.43 ± 0.01	0.03 ± 0.002	0.029 ± 0.009	7.27 ± 0.4	14.40 ± 0.7
15-30	17.35 ± 0.9	0.66 ± 0.02	0.45 ± 0.02	0.04 ± 0.002	0.006 ± 0.002	10.26 ± 0.6	18.50 ± 0.9
30-46	13.53 ± 0.3	0.63 ± 0.02	0.73 ± 0.06	0.04 ± 0.002	0.013 ± 0.003	12.31 ± 0.2	14.95 ± 0.2
46-61	11.20 ± 0.2	0.50 ± 0.02	0.75 ± 0.08	0.04 ± 0.002	0.007 ± 0.002	10.71 ± 0.5	12.50 ± 0.2
61-76	9.17 ± 0.2	0.43 ± 0.02	0.81 ± 0.09	0.04 ± 0.002	0.004 ± 0.001	9.33 ± 0.5	10.45 ± 0.2
76-91	8.09 ± 0.2	0.42 ± 0.02	0.98 ± 0.11	0.04 ± 0.003	0.003 ± 0.001	8.79 ± 0.3	9.54 ± 0.2
91-107	7.58 ± 0.2	0.49 ± 0.03	1.37 ± 0.17	0.04 ± 0.002	0.008 ± 0.003	8.65 ± 0.4	9.48 ± 0.2
107-122	6.83 ± 0.3	0.57 ± 0.05	1.64 ± 0.20	0.05 ± 0.004	0.014 ± 0.005	8.17 ± 0.4	9.10 ± 0.3
122-137	6.00 ± 0.3	0.63 ± 0.06	1.79 ± 0.19	0.05 ± 0.004	0.028 ± 0.010	8.07 ± 0.5	8.50 ± 0.2
137-152	5.53 ± 0.2	0.66 ± 0.07	1.89 ± 0.20	0.06 ± 0.006	0.028 ± 0.009	7.53 ± 0.3	8.17 ± 0.2
152-168	5.19 ± 0.2	0.69 ± 0.08	1.98 ± 0.19	0.05 ± 0.005	0.03 ± 0.009	7.32 ± 0.3	7.94 ± 0.1
168-183	4.78 ± 0.1	0.69 ± 0.09	1.90 ± 0.16	0.05 ± 0.005	0.023 ± 0.006	7.56 ± 0.7	7.45 ± 0.1
183-198	4.81 ± 0.1	0.78 ± 0.09	2.04 ± 0.14	0.04 ± 0.005	0.02 ± 0.005	7.26 ± 0.3	7.70 ± 0.1
198-213	4.78 ± 0.2	0.82 ± 0.09	2.02 ± 0.11	0.04 ± 0.004	0.015 ± 0.004	7.29 ± 0.2	7.68 ± 0.1
213-229	4.42 ± 0.2	0.82 ± 0.10	1.95 ± 0.11	0.04 ± 0.003	0.013 ± 0.004	7.33 ± 0.2	7.25 ± 0.2
229-245	4.54 ± 0.2	0.89 ± 0.11	2.05 ± 0.07	0.04 ± 0.003	0.014 ± 0.005	7.53 ± 0.3	7.53 ± 0.2
245-261	4.59 ± 0.2	0.97 ± 0.10	2.16 ± 0.06	0.04 ± 0.003	0.017 ± 0.005	7.77 ± 0.3	7.78 ± 0.2

† Al and Fe are below detectable levels, <0.001 $cmol_c/kg$. ECEC = summation of $cmol_c/kg$ from exchangeable Ca, Mg, K, and Na.

‡ Error term is the standard error

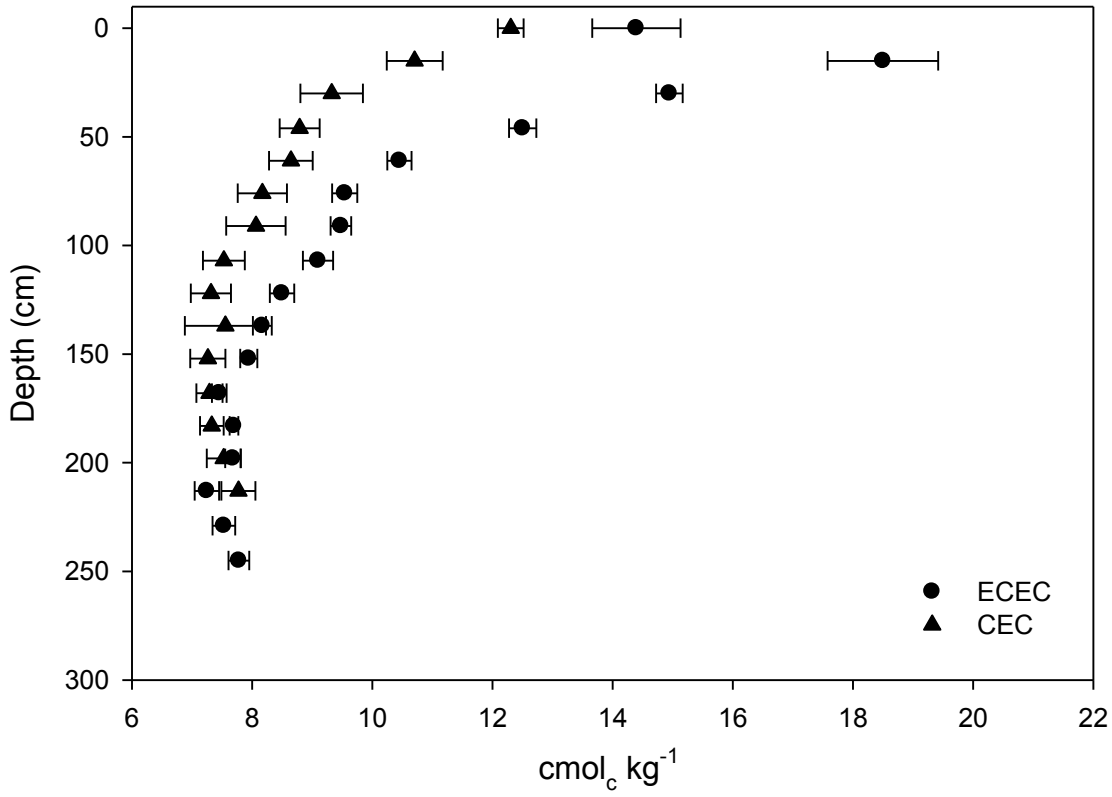

Figure 39. Mean cation exchange capacity (CEC) and mean effective cation exchange capacity (ECEC) of the 10 depth-incremented plots. Error bars represent standard error.

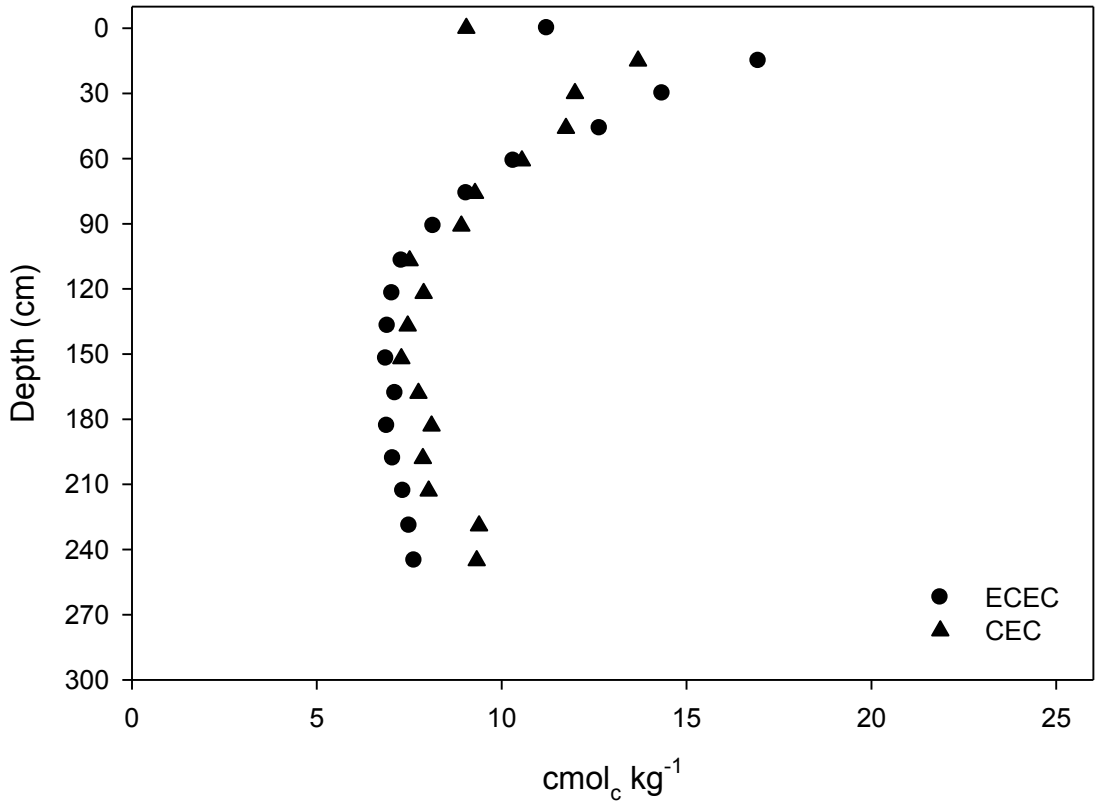

Figure 40. Effective cation exchange capacity (ECEC) and cation exchange capacity (CEC) of Plot 1.

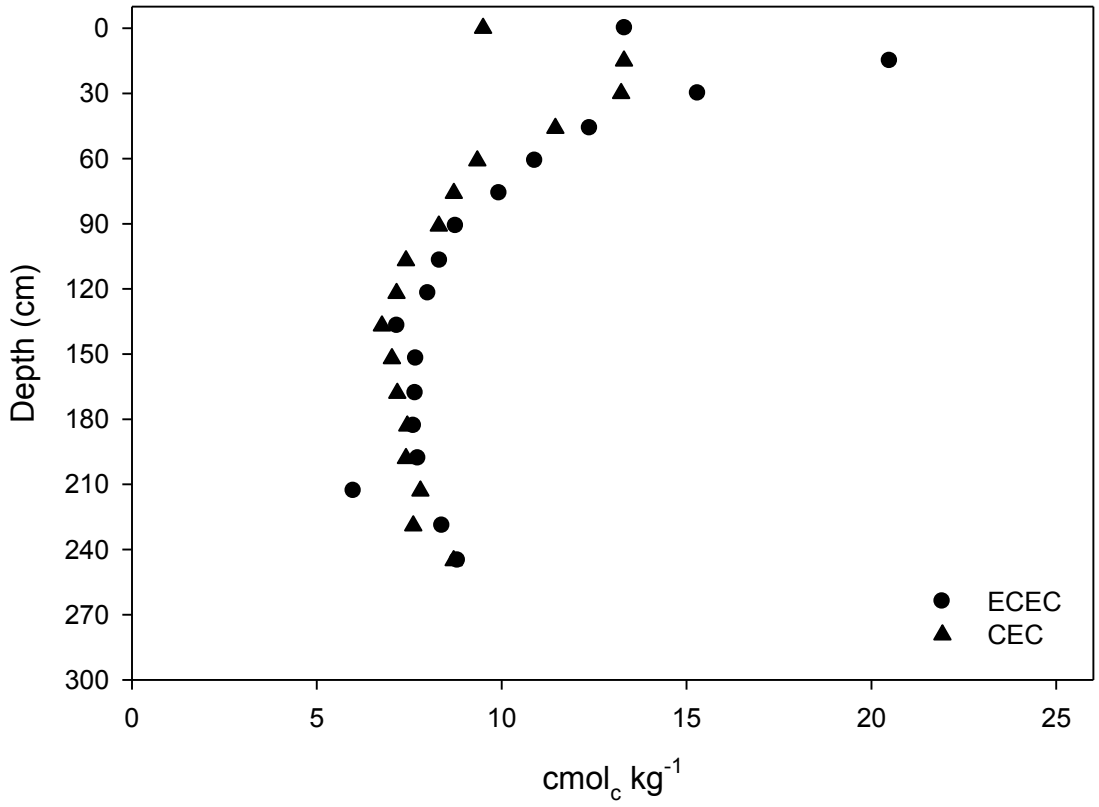

Figure 41. Effective cation exchange capacity (ECEC) and cation exchange capacity (CEC) of Plot 2.

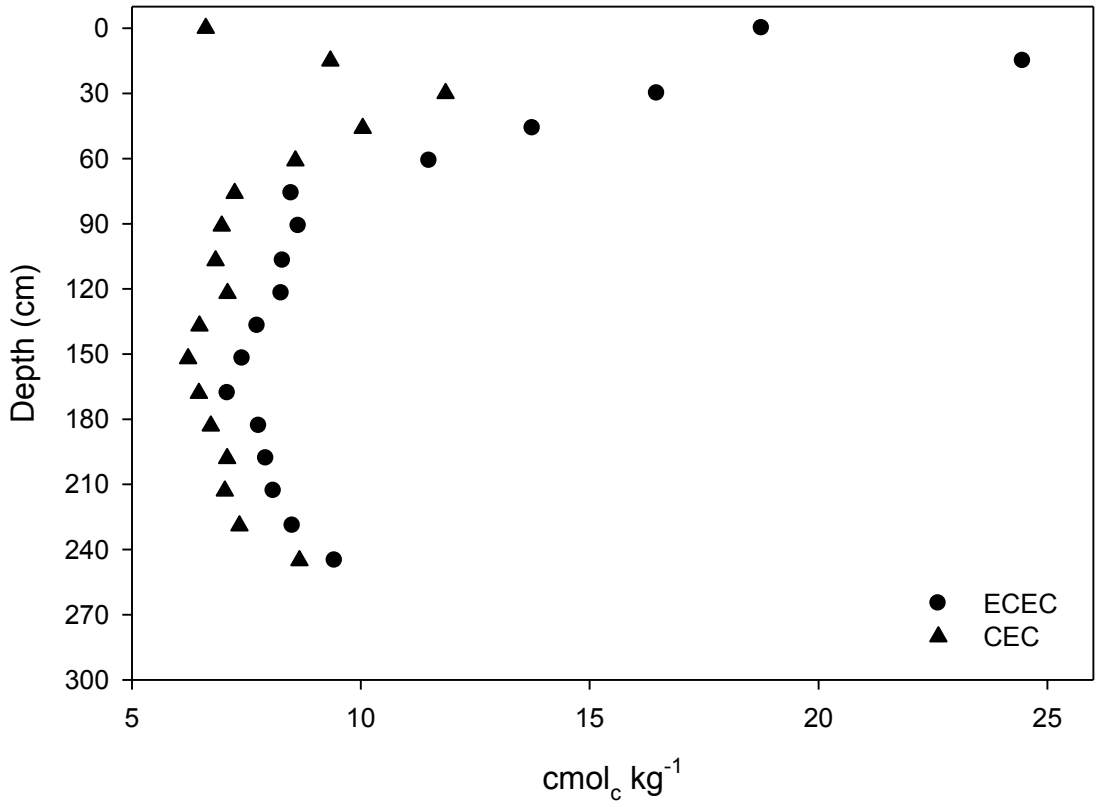

Figure 42. Effective cation exchange capacity (ECEC) and cation exchange capacity (CEC) of Plot 3.

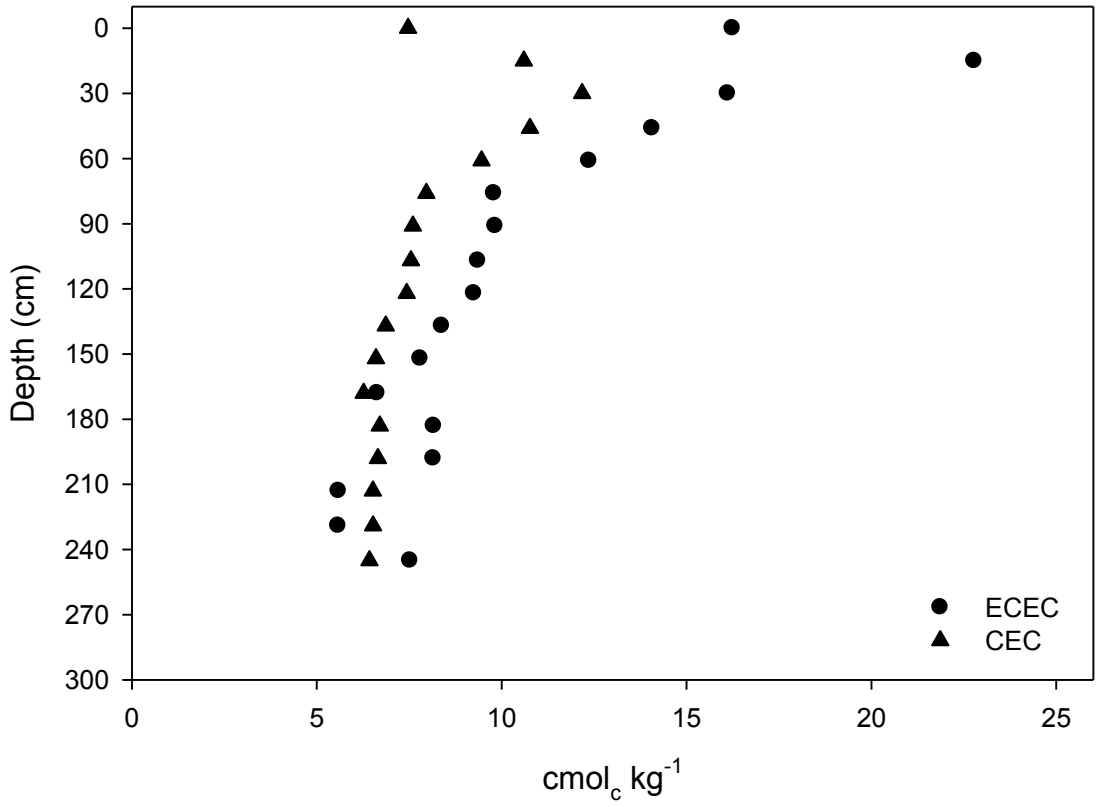

Figure 43. Effective cation exchange capacity (ECEC) and cation exchange capacity (CEC) of Plot 4.

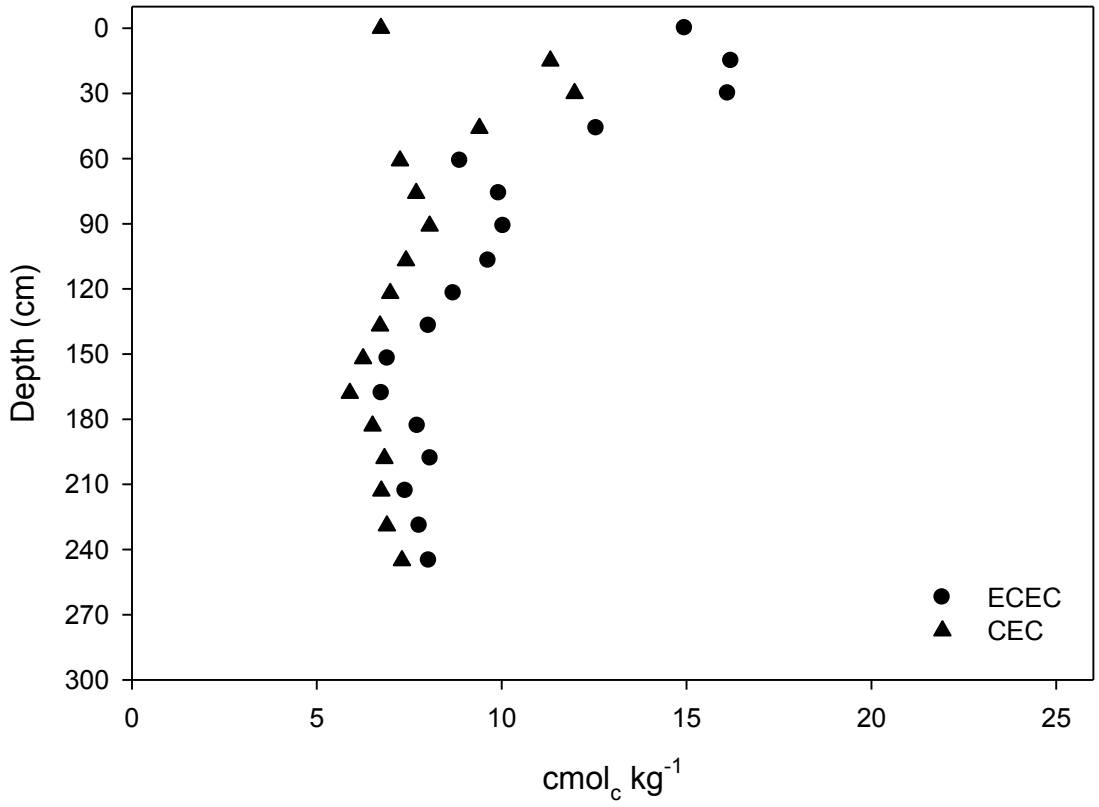

Figure 44. Effective cation exchange capacity (ECEC) and cation exchange capacity (CEC) of Plot 5.

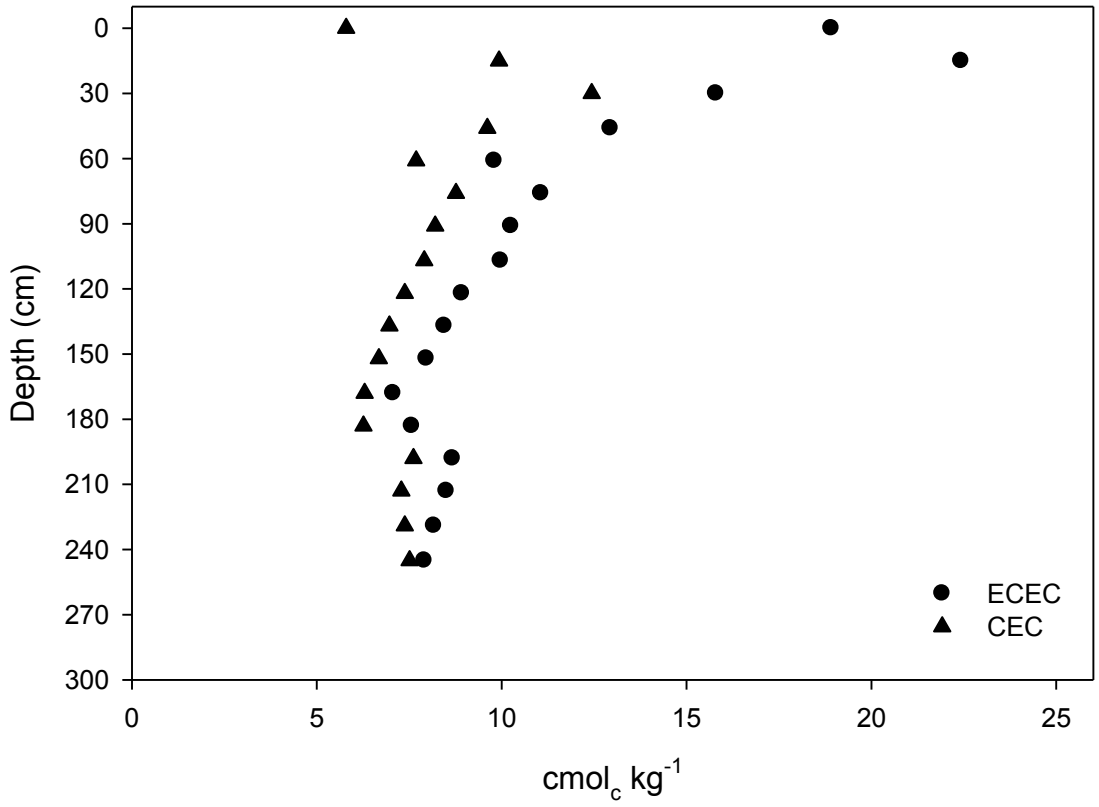

Figure 45. Effective cation exchange capacity (ECEC) and cation exchange capacity (CEC) of Plot 6.

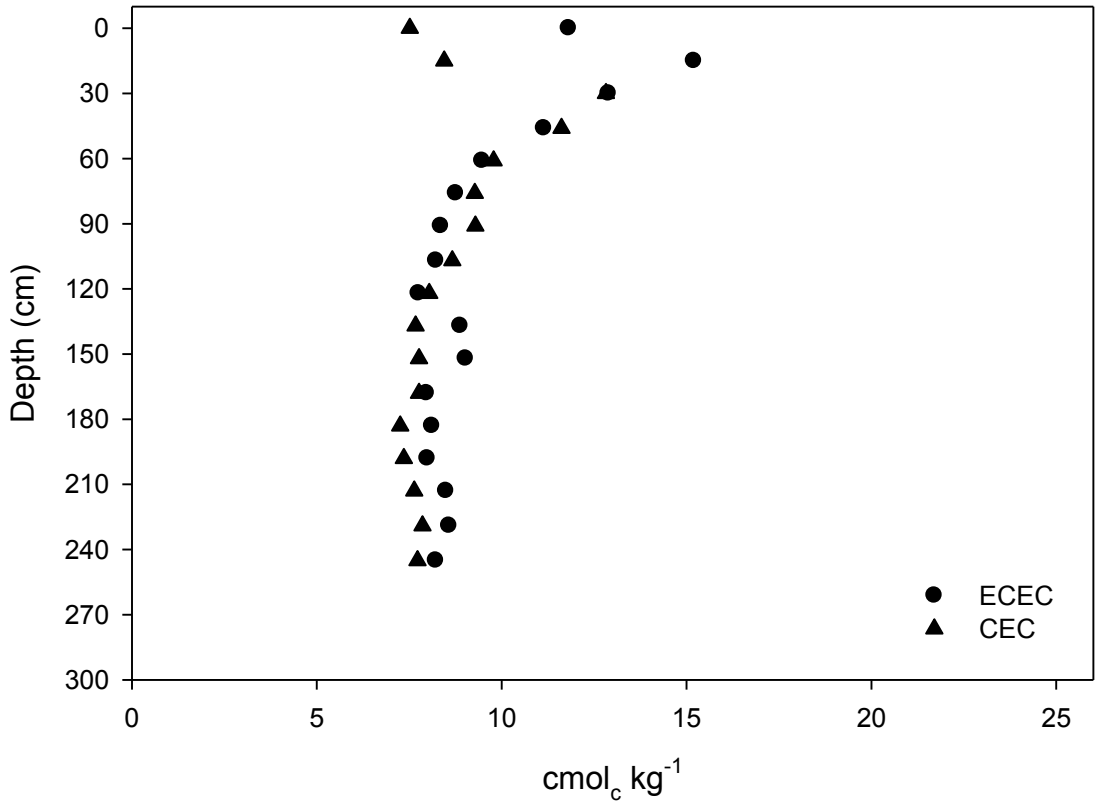

Figure 46. Effective cation exchange capacity (ECEC) and cation exchange capacity (CEC) of Plot 7.

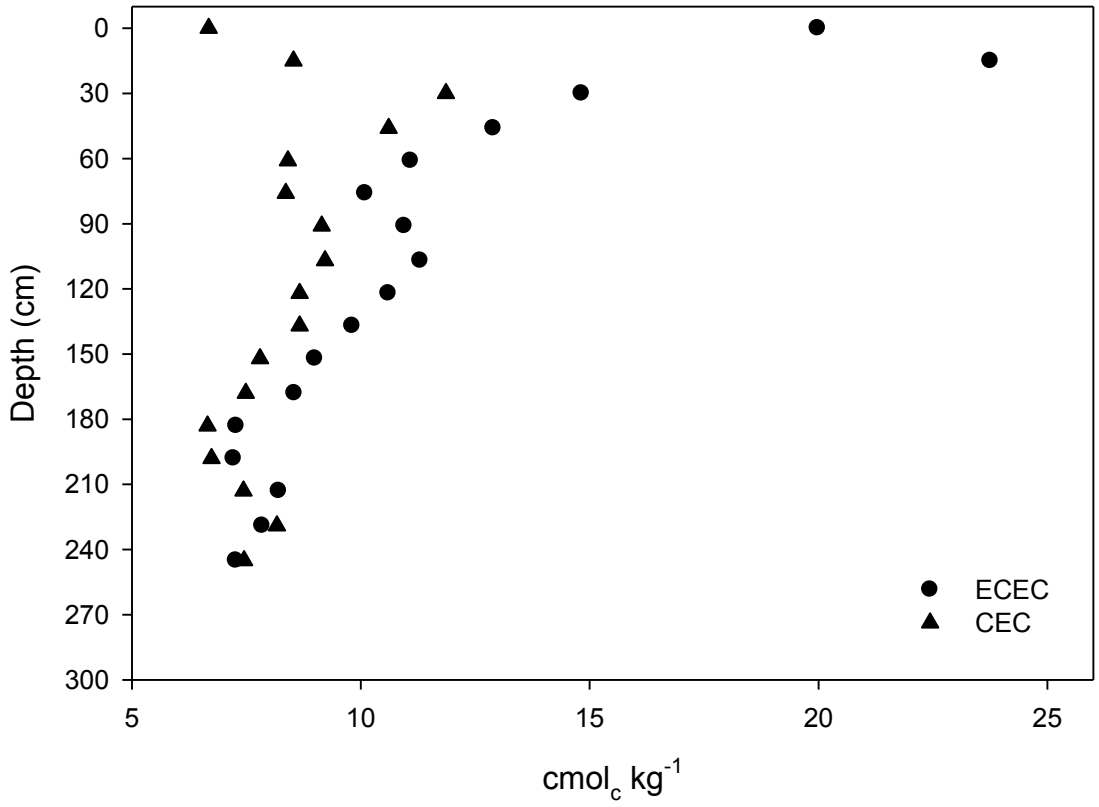

Figure 47. Effective cation exchange capacity (ECEC) and cation exchange capacity (CEC) of Plot 8.

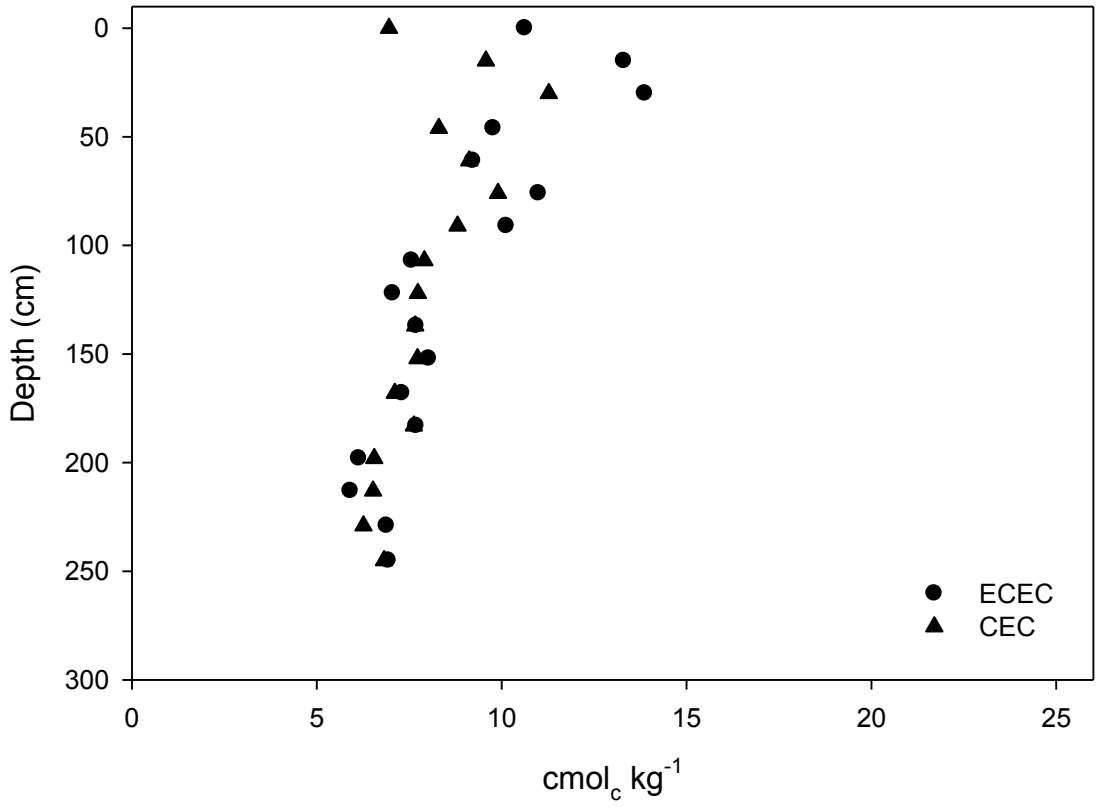

Figure 48. Effective cation exchange capacity (ECEC) and cation exchange capacity (CEC) of Plot 9.

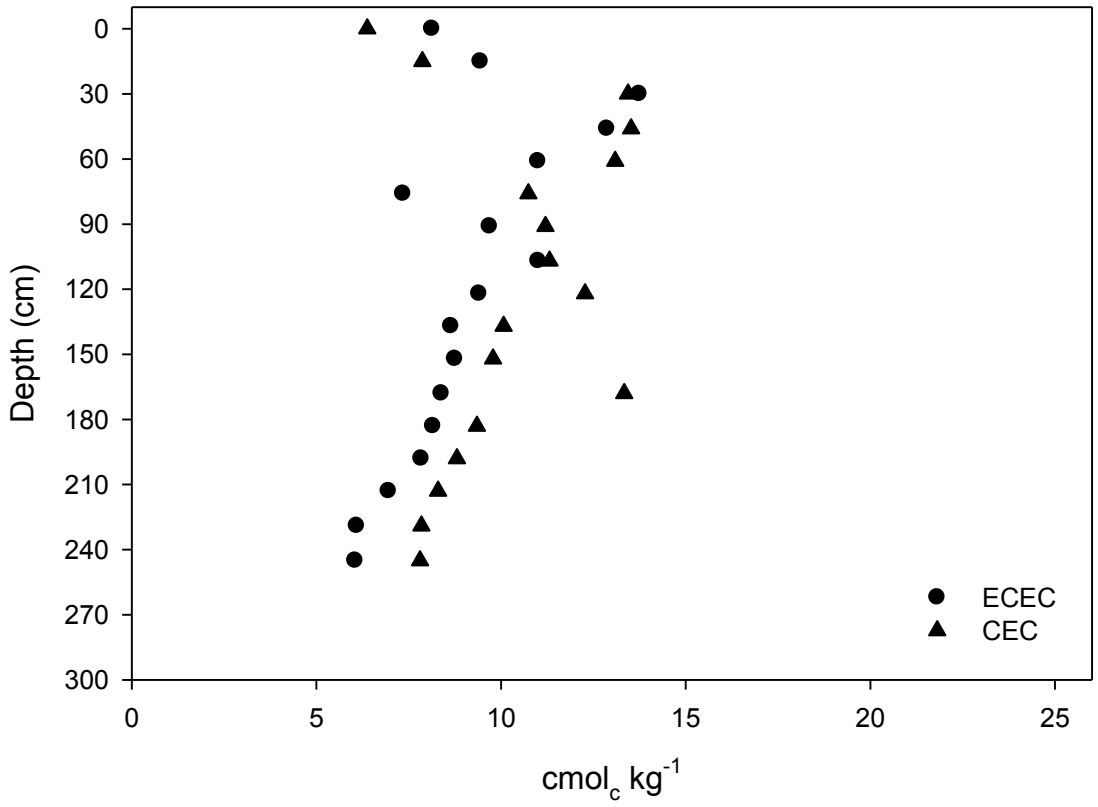

Figure 49. Effective cation exchange capacity (ECEC) and cation exchange capacity (CEC) of Plot 10.

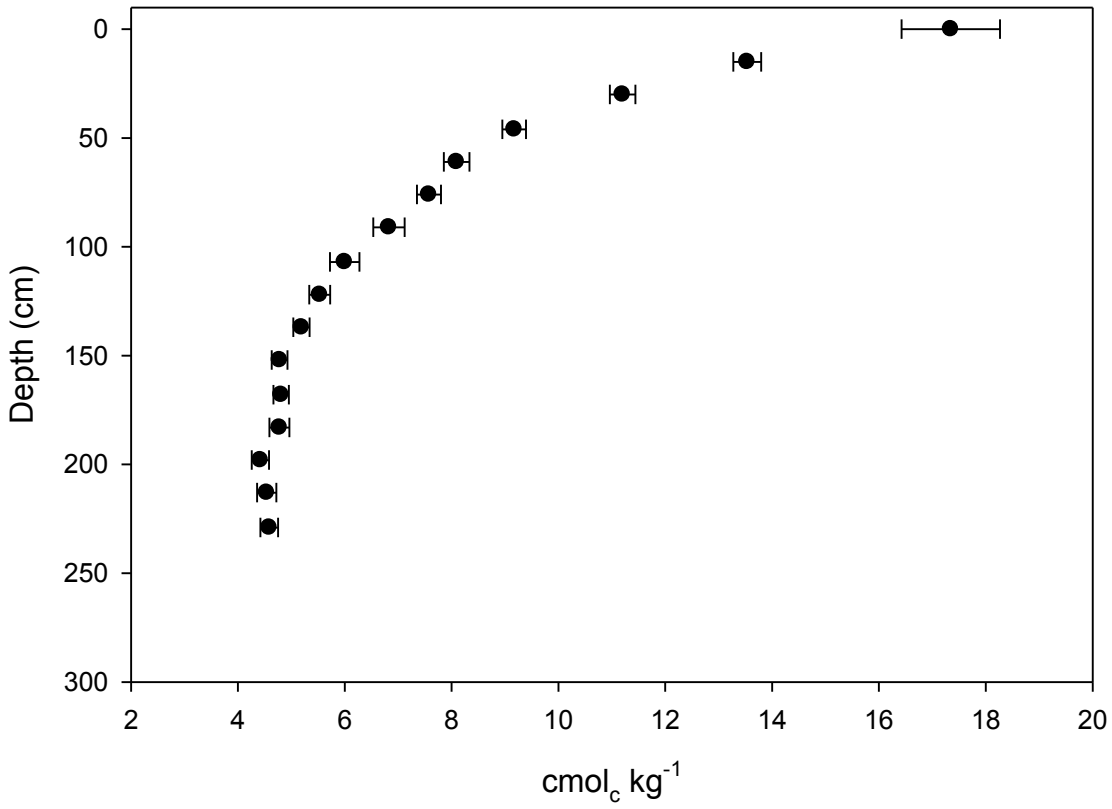

Figure 50. Mean exchangeable calcium (Ca) of the 10 depth-incremented plots. Error bars represent standard error.

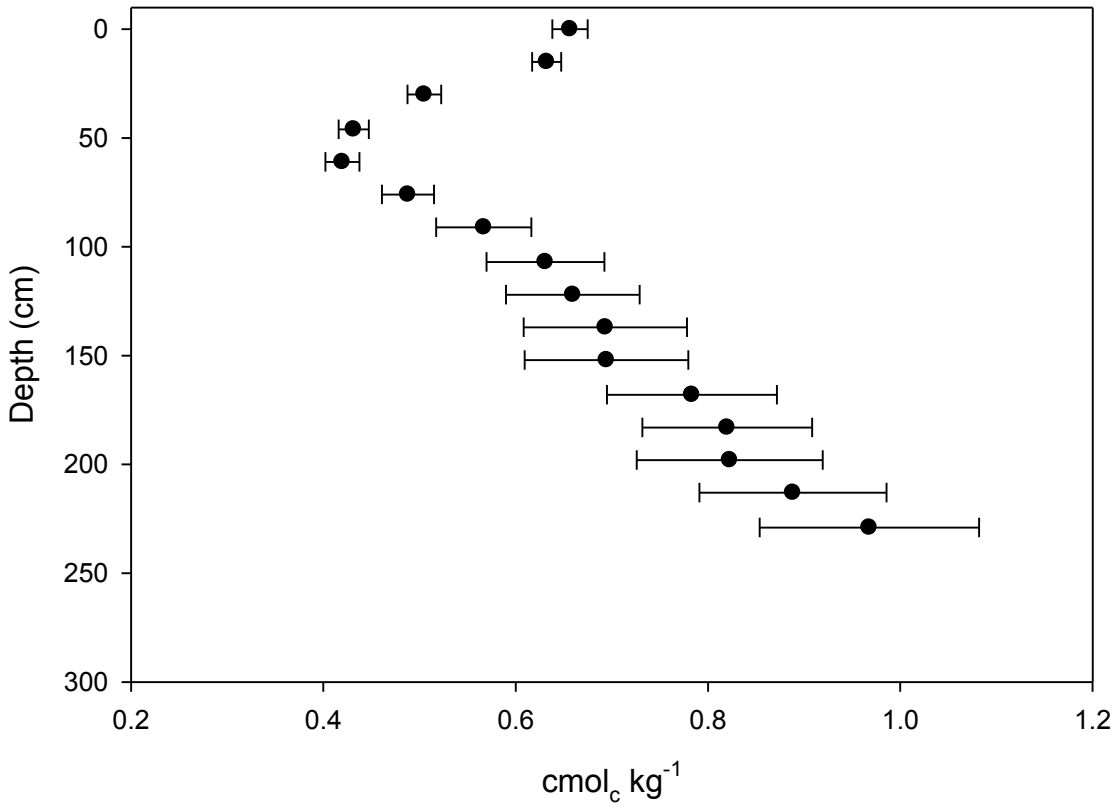

Figure 51. Mean exchangeable potassium (K) of the 10 depth-incremented plots. Error bars represent standard error.

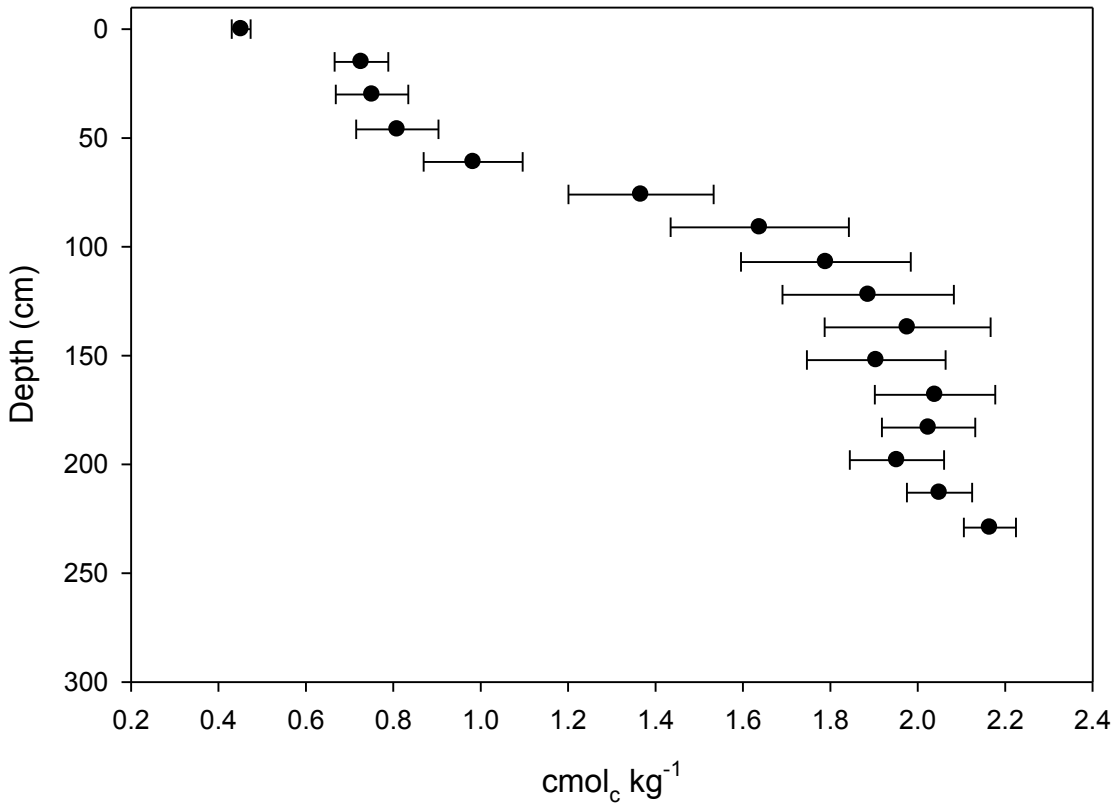

Figure 52. Mean exchangeable magnesium (Mg) of the 10 depth-incremented plots. Error bars represent standard error

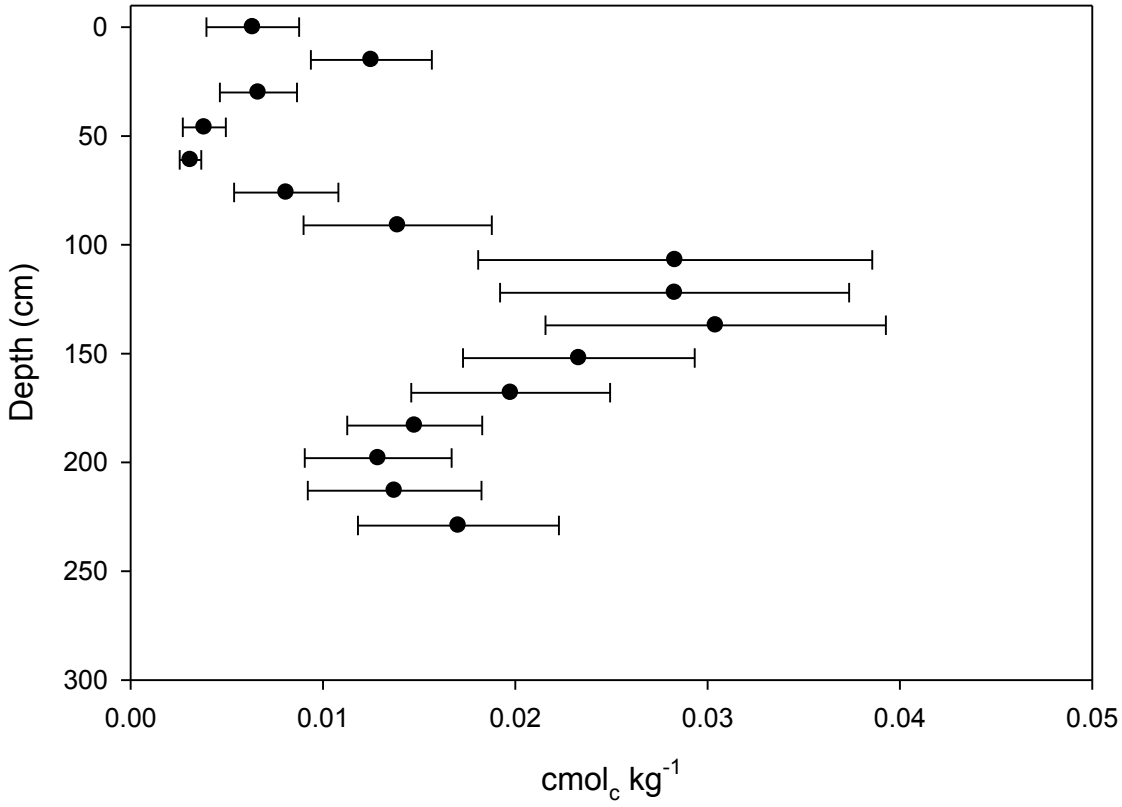

.

Figure 53. Mean exchangeable manganese (Mn) of the 10 depth-incremented plots. Error bars represent standard error.

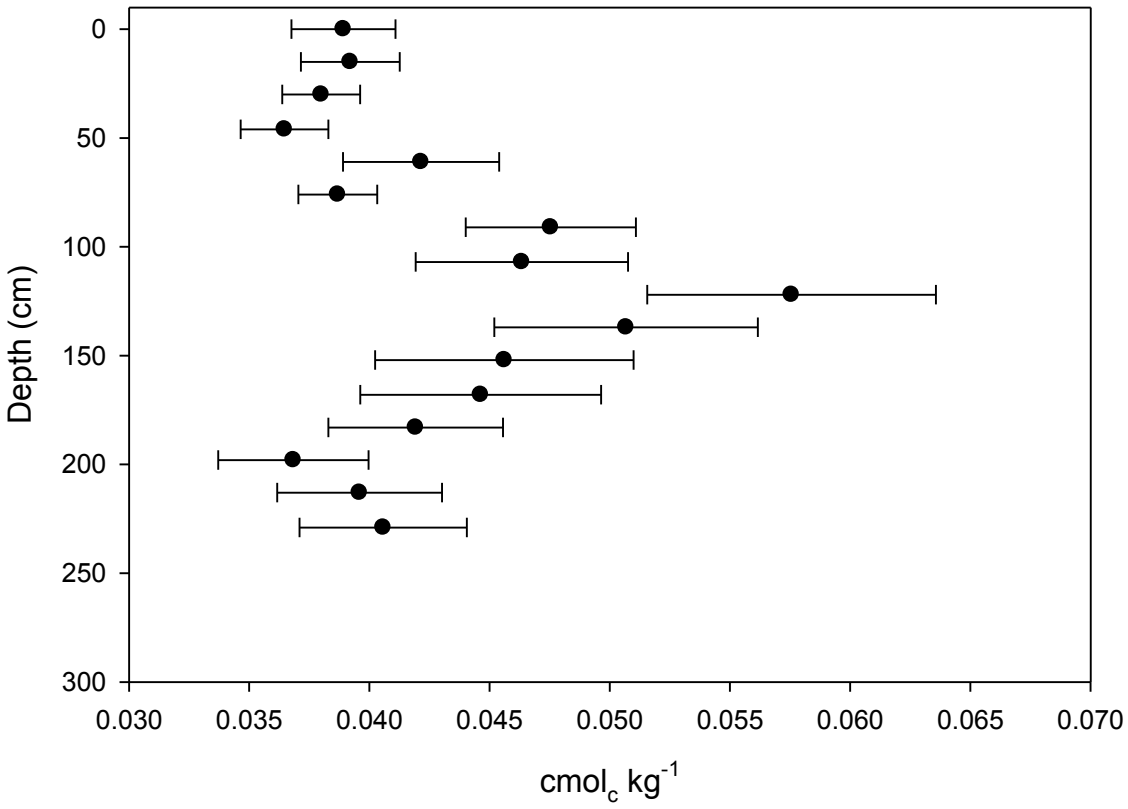

Figure 54. Mean exchangeable sodium (Na) of the 10 depth-incremented plots. Error bars represent standard error.

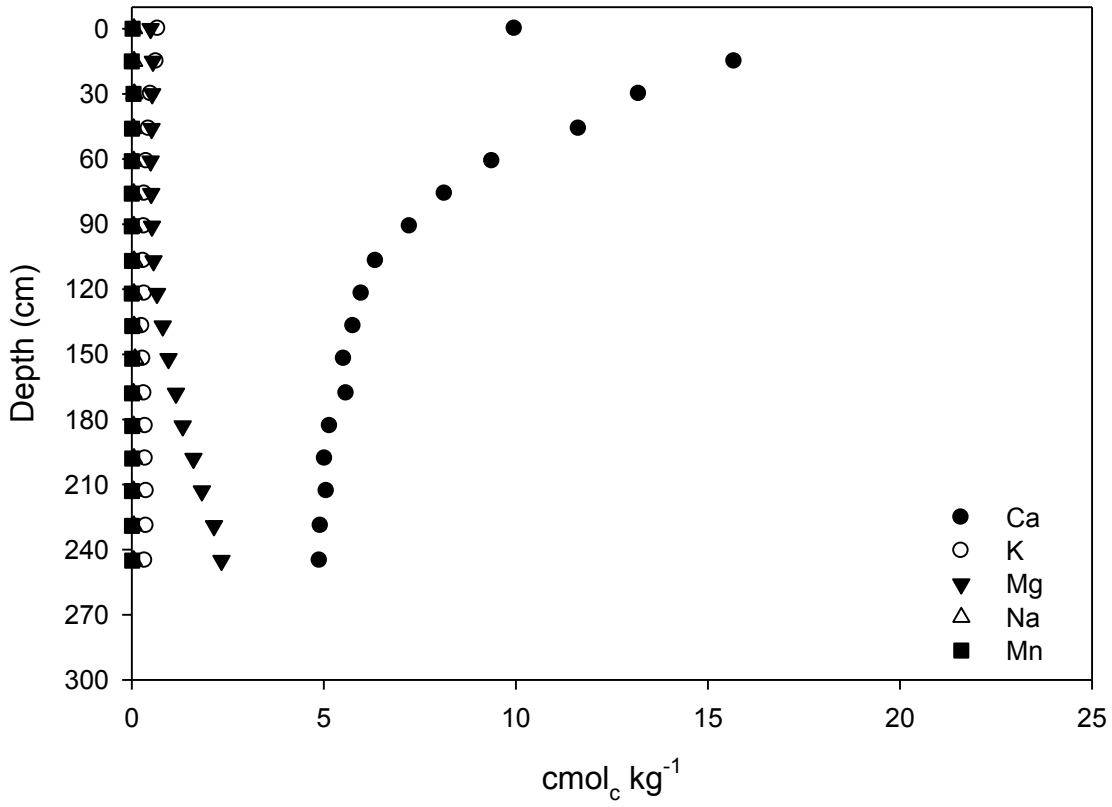

Figure 55. Cation exchange phase composition of Plot 1.

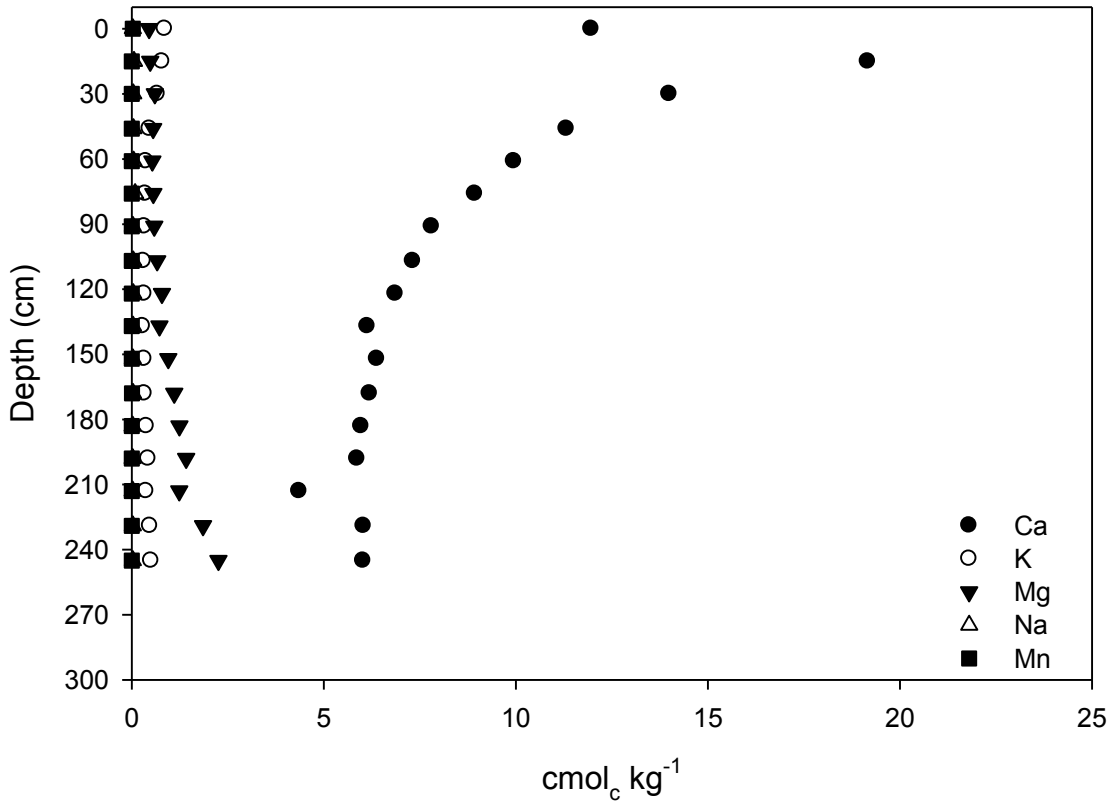

Figure 56. Cation exchange phase composition of Plot 2.

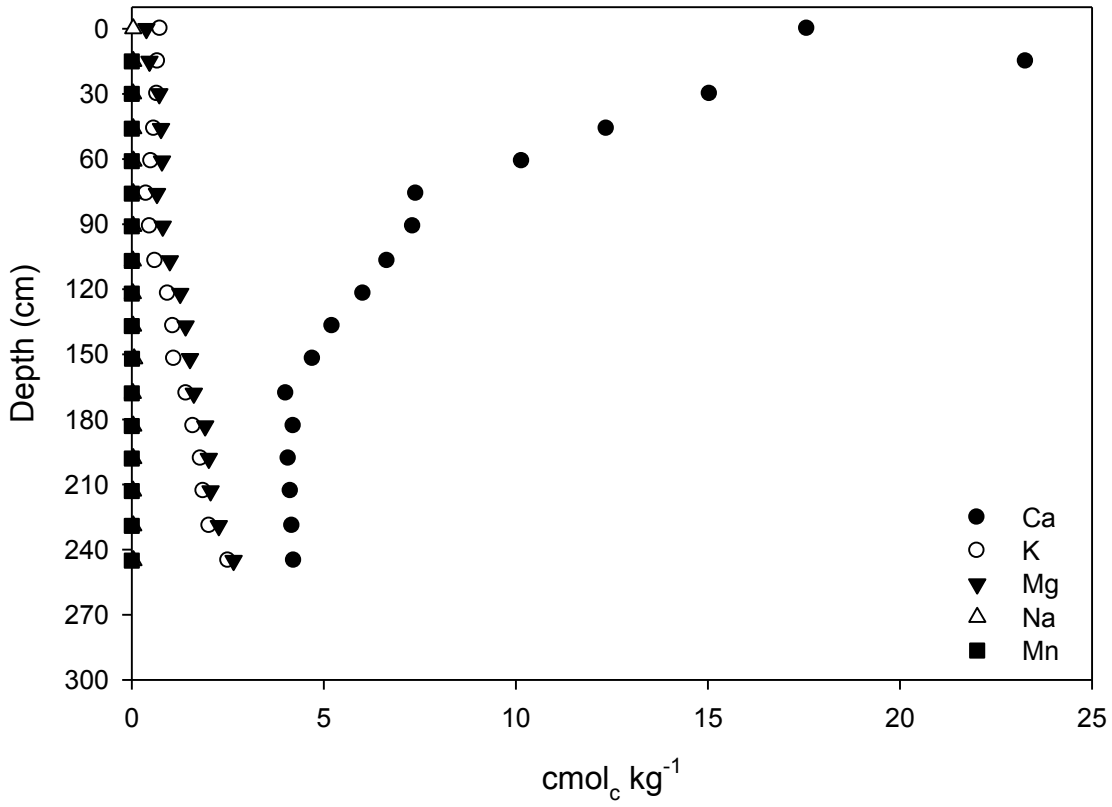

Figure 57. Cation exchange phase composition of Plot 3.

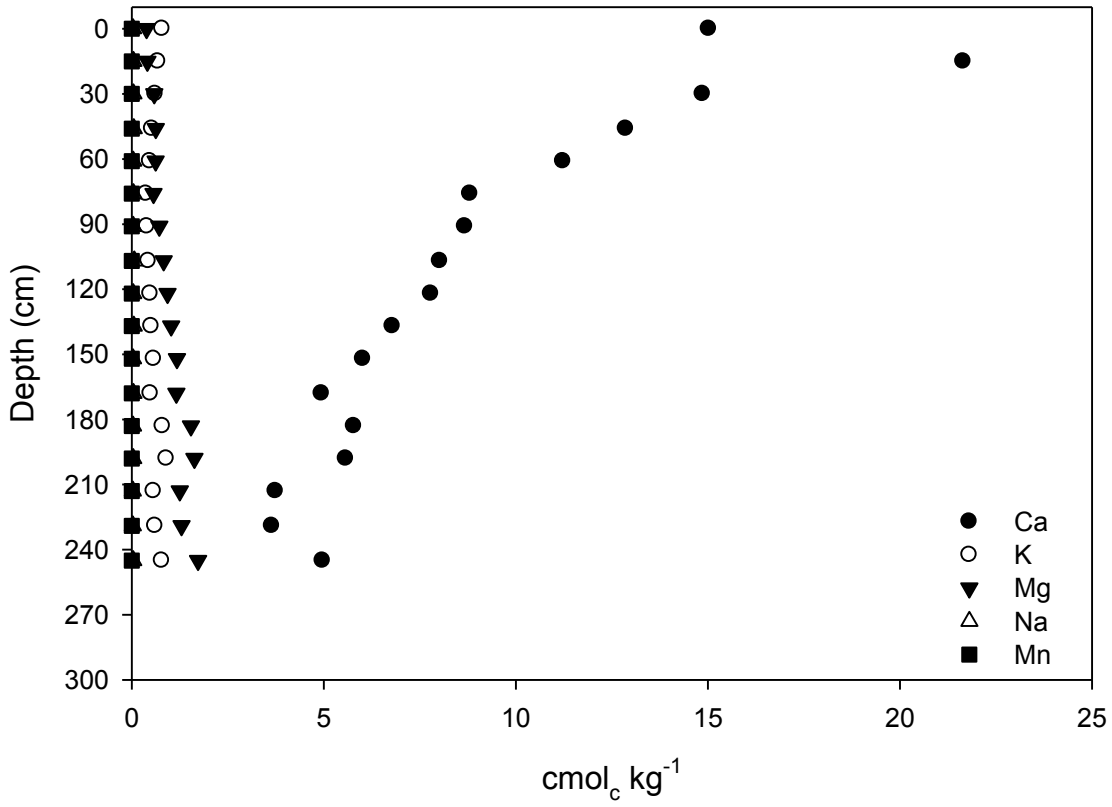

Figure 58. Cation exchange phase composition of Plot 4.

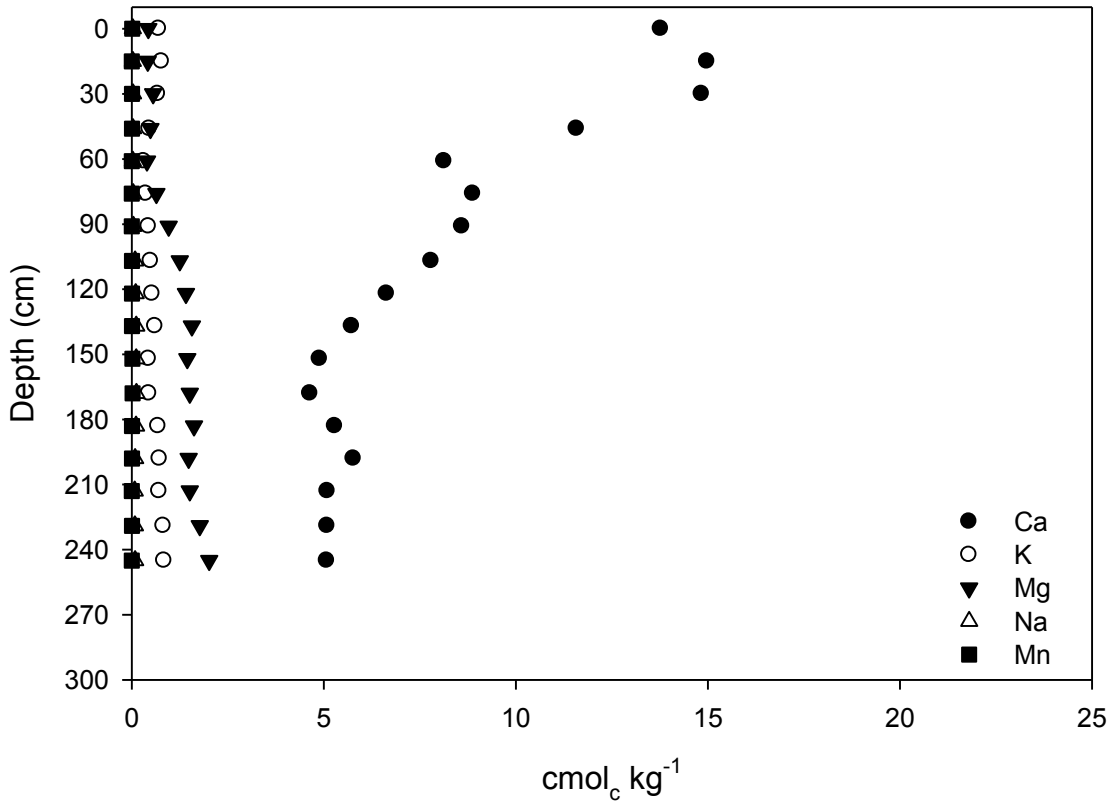

Figure 59. Cation exchange phase composition of Plot 5.

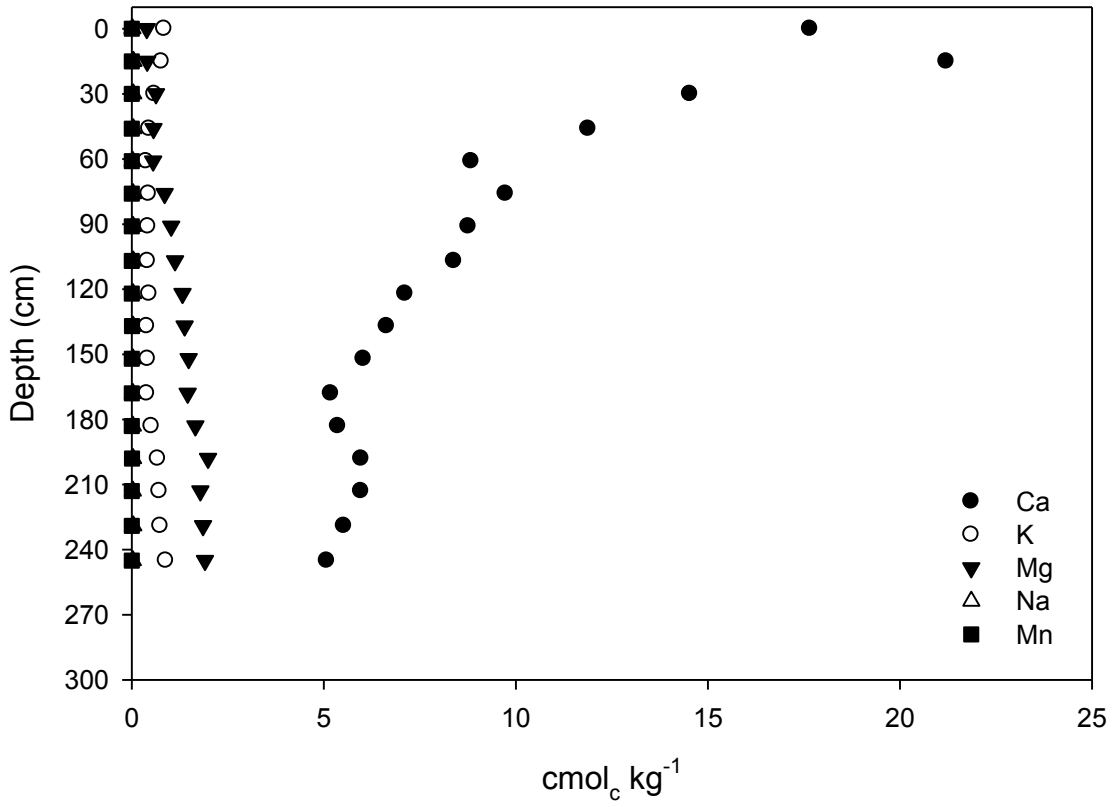

Figure 60. Cation exchange phase composition of Plot 6.

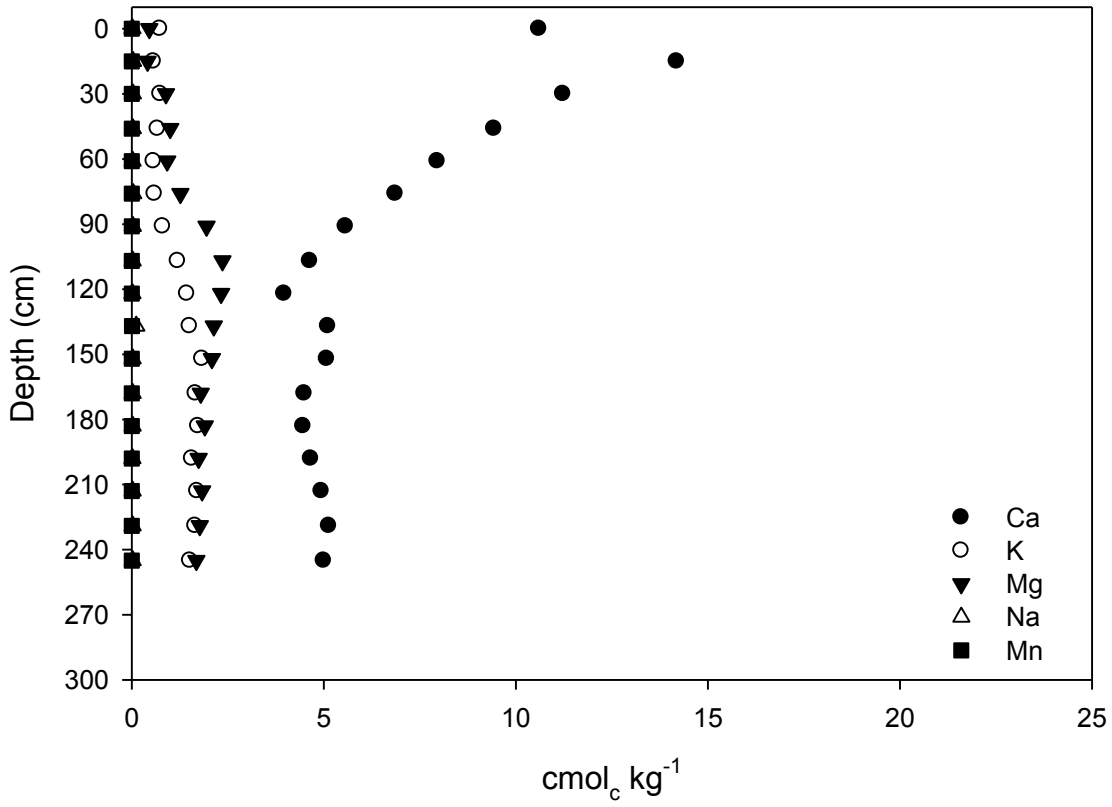

Figure 61. Cation exchange phase composition of Plot 7.

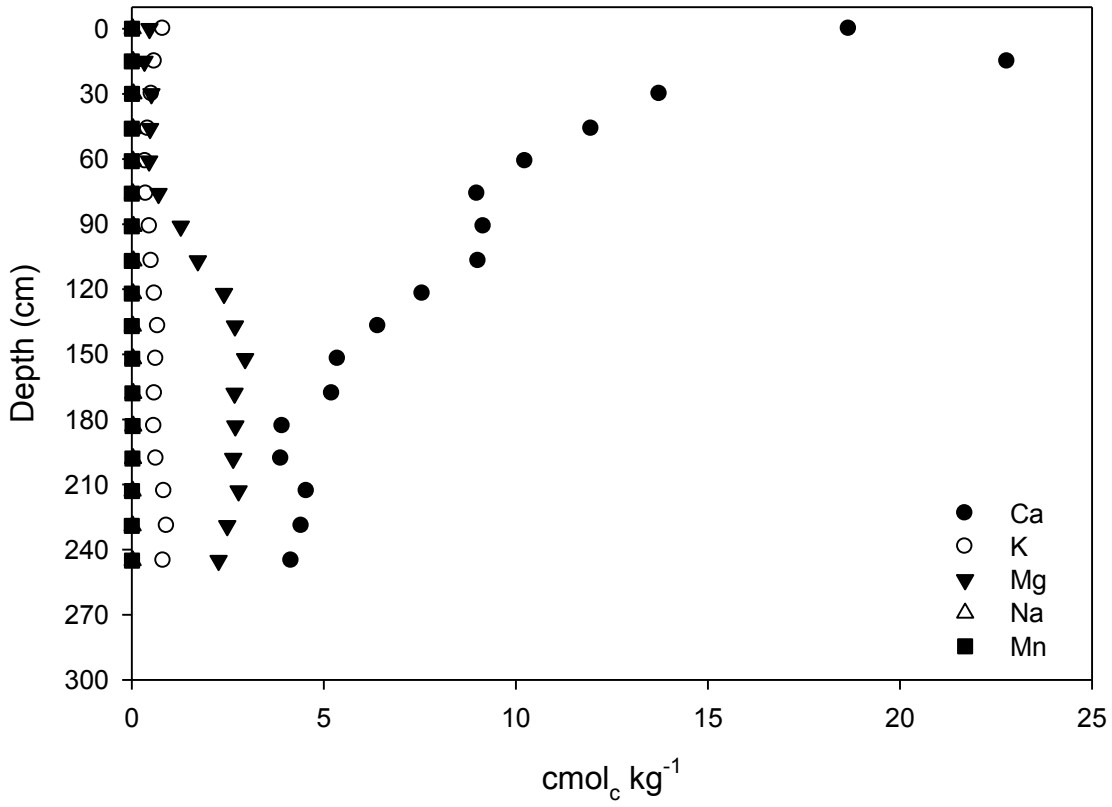

Figure 62. Cation exchange phase composition of Plot 8.

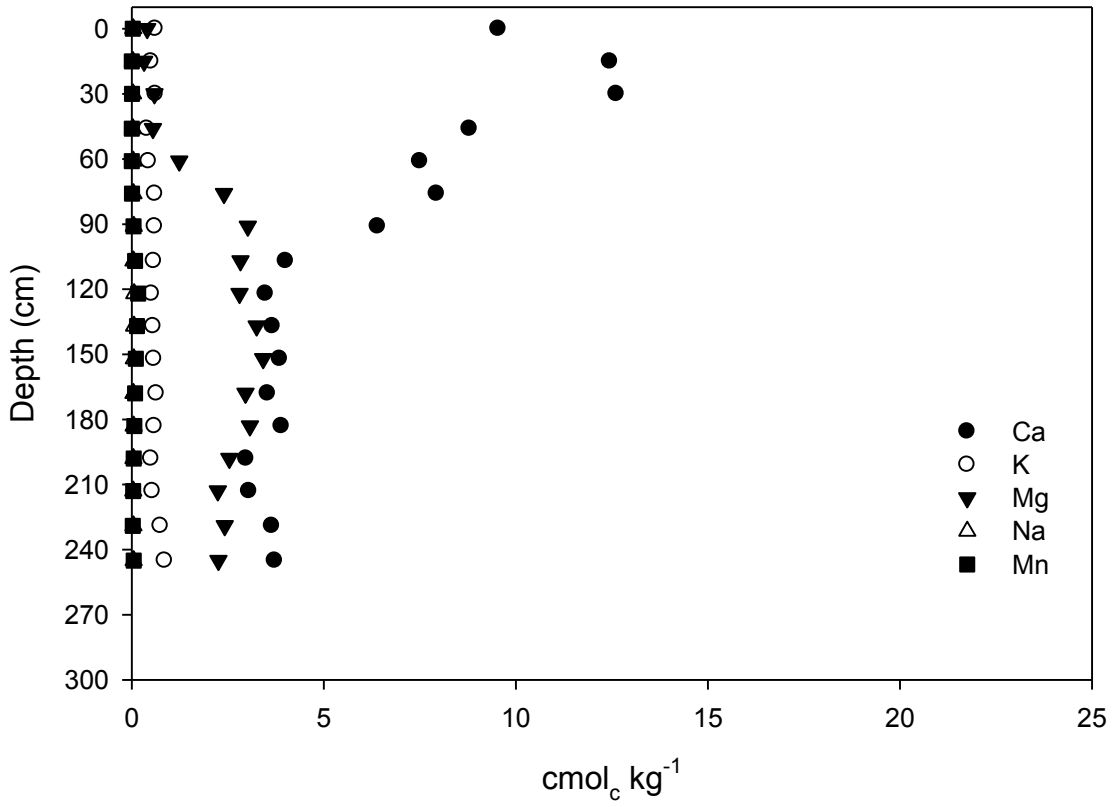

Figure 63. Cation exchange phase composition of Plot 9.

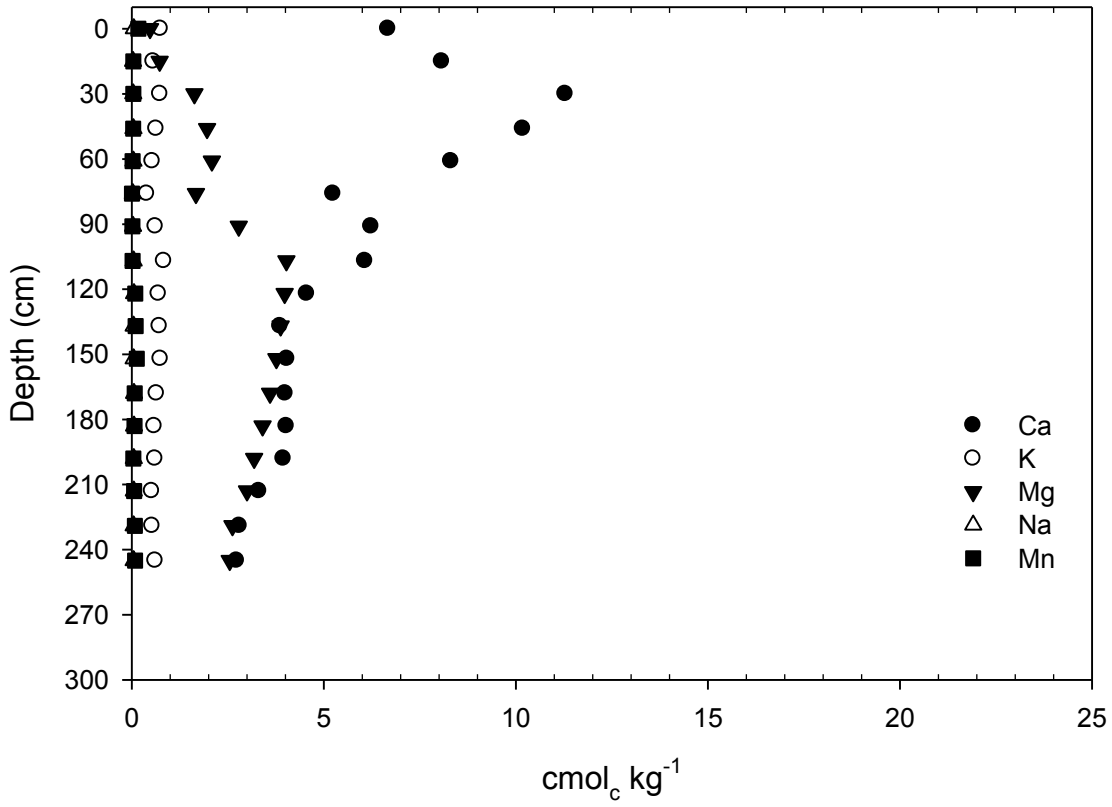

Figure 64. Cation exchange phase composition of Plot 10.

CHAPTER III
ANION EXCHANGE CHARACTERISTICS OF BINARY AND TERNARY NITRATE, CHLORIDE, AND SULFATE SYSTEMS IN A LOESS SOIL

ABSTRACT

Subsoil metal-oxide accumulations in the loess soils of west Tennessee may retain and restrict the movement of otherwise mobile anions, such as nitrate and bromide, from leaching into streams and groundwater. A detailed characterization of CBD and AAO Fe, Al, and Mn in these loess soils show that metal oxide concentrations peak in the argillic horizon (30 to 46 cm) and in the underlying tertiary sands (245 to 261 Soils included in a Catena are said to have been developed from similar parent material under similar climatic conditions, but whose characteristics differ because of variations in relief and drainage (Brady and Weil, 2002).cm). This study examined the anion exchange characteristics of binary and ternary nitrate, sulfate, and chloride systems in the high metal-oxide horizons in the loess soils. Exchange isotherms were constructed by equilibrating varying ratios of two (binary) or three (ternary) anions containing solutions with soil samples, and by determining the solution and anion exchange composition at equilibrium. Exchange isotherms indicate that chloride and nitrate are preferred relative to sulfate, and that chloride is preferred relative to nitrate, where preference is established by the Vanselow selectivity coefficients. Although not preferred, sulfate predominates on the anion exchange phase due to its divalent charge. These findings will enhance our knowledge of how the addition of sulfate to soil will possibly impact conservative anion behavior in loess soils.

INTRODUCTION

The addition of industrial and agricultural by-products, such as sewage sludge, dairy and swine manure, poultry litter, yard waste, and paper mill residues, to soil have been shown to enhance soil nutrient levels and physical characteristics. Flue-gas desulfurization (FGD) gypsum has been produced in increasing volumes over the past decade due to the implementation of Clean Air Act standards. The impact of gypsum on soil has been well documented, but little is known about the impact of FGD gypsum on the anion exchange behavior in the loess soils of west Tennessee.

Soils of west Tennessee are characterized as coastal plain deposits overlain by loess (Springer and Elder, 1980). These soils are highly susceptible to erosion, which has resulted in the implementation of no-till management (Ammons et al., 1994). A potential method of enhancing erosion control is the addition of FGD gypsum. Rhoton and McChesney (2011) showed the gypsum amendments can improve physical properties by increasing aggregation. While the physical conditions of the soil might be improved, it is important to determine the effects of gypsum application on the chemical properties of the soil. A potential concerned associated with gypsum application is the enhanced leaching of nitrate into streams and groundwater.

The loess-derived soils of west Tennessee contain variable charge minerals, such as Fe- and Al-oxides, that bear net positive surface charge under neutral to acidic soil solution pH conditions (Donn and Menzies, 2005a and b). The presence of variable charge minerals leads to the retention of otherwise mobile anions, such as nitrate (NO_3) and bromide (Br) through outer-sphere (anion exchange) retention mechanisms. Specifically, long-term studies have shown that loess soils in west Tennessee

accumulate NO_3 and Br in subsoil horizons (Ammons et al., 1994; Tyner et al., 2007). This is thought to be due to the presence of hydrous Fe-oxides acting as a barrier against NO_3 leaching into the groundwater.

The ability to predict how the addition of sulfate from FGD gypsum ($CaSO_4$) will affect soil-bound nitrate can be evaluated by examining anion exchange behavior, commonly by the development of exchange isotherms. An exchange isotherm is a plot of the equivalent fraction of an ion on the exchange phase (E) versus the equivalent fraction of that ion in the aqueous phase (Ẽ) (Essington, 2003). These isotherms can be constructed for binary exchange (two ions present) or for ternary exchange (three ions present). In addition, the Vanselow selectivity coefficient (K_V) can be determined. In general,an anion exchange reaction may be described as:

$$aB^{b-}(aq) + bAX_a(ex) \rightarrow aBX_b(ex) + bA^{a-}(aq) \quad [1]$$

where X^+ represents an equivalent of anion exchanger. The Vanselow selectivity coefficient for this reaction is:

$$K_V = \frac{N_B^a (A^{a-})^b}{N_A^b (B^{b-})^a} \quad [2]$$

where, (A^{a-}) and (B^{b-}) are the activities of the soluble species, and N_A and N_B represent the mole fractions of A^{a-} and B^{b-} on the exchange complex at equilibrium. If K_V is greater than 1 for the reaction in Eq. [1], B^{b-} is preferred on the exchange complex; whereas, if K_V is less than 1, A^{a-} is preferred (Essington, 2003). The exchange isotherm illustrates both the preference and magnitude of K_V. Exchange isotherms commonly include the nonpreference isotherm: a theoretically derived line which represents the condition

where K_V is equal to 1(neither A^{a-} or B^{b-} are preferred by the exchange phase). The data are then evaluated relative to the nonpreference isotherm to establish preference.

The anion exchange characteristics of soil have only received limited interest in the scientific literature, primarily because cation exchange processes predominate in most soils. Katou et al. (1996) examined NO_3 – Cl – SO_4 exchange in an Andisol. They found that NO_3 had a lower affinity for the exchange phase than did Cl. They also concluded that SO_4 dominated the exchange phase relative to NO_3 and Cl. Katou et al. (1996) concluded that the ease of replaceability of anion was NO_3 > Cl > SO_4. Feder and Findeling (2006) examined the NO_3 – Cl binary exchange system. They found that NO_3 was retained to a greater extent than Cl in an andic soil. Ishiguru et al. (2003) added SO_4 and NO_3 to soil columns and observed the leaching of NO_3 was accelerated. They postulated that the added SO_4 was strongly retained relative to NO_3, enhancing NO_3 immobilization.

Charlet and Sposito (1987) conducted a study on an Oxisol in which a slight preference for NO_3 over Cl was observed. They determined the exchange coefficients of NO_3 and Cl were $\mathrm{K_{NO_3}} = 10^{2.4}$ and $\mathrm{K_{Cl}} = 10^{1.8}$ for $X^+ + NO_3^- = XNO_3$ and $X^+ + Cl^- = XCl$. Therefore, the equilibrium exchange coefficient for the NO_3 - Cl reaction (Eq. [1]) is $\mathrm{K_{NO_3-Cl}} = 10^{0.6}$ which indicated that the Oxisol prefers NO_3 relative to Cl. Toner et al. (1989) evaluated the exchange properties associated with a Cecil soil. They found the Cecil soil to have a slight preference for Cl over NO_3. They also observed that the presence of SO_4 drastically reduced the retention of NO_3. Toner et al. (1989) also found that there was evidence of competition between NO_3 and SO_4 for the exchange sites, which was more evident in soil samples containing high levels of Fe-oxides. Rasiah et

al. (2004) examined SO_4 – NO_3 – Cl exchange in Australian Ferrosols and found that Cl and NO_3 could not compete with SO_4 for anion exchange sites, but that Cl was more competitive than NO_3.

Based on previous studies, NO_3 is most effectively displaced from soil, followed by Cl then SO_4. In order to test this hypothesis, binary and ternary anion exchange isotherms were examined in Memphis Catena soils using the soil depth increments of 30 to 46 cm and 245 to 261 cm. These increments have been shown to contain high concentrations of metal (Fe, Al, and Mn) oxides (Chapter II). The isotherms were developed by saturating the soils with two ions for binary systems, and with one ion for ternary systems. After saturation, the systems received varying ratios of two anions and were then equilibrated for 16 hours. Supernatant from the equilibrations was analyzed to calculate the equivalent fraction of the anions in the solution phase. The samples were then rinsed of entrained solution and saturated with acetate to replace anions on the exchange phase. These supernatants were then analyzed to generate the equivalent fraction of the anions in the aqueous phase. From this information, the isotherms were generated by plotting the equivalent fraction in solution against the equivalent fraction on the exchange phase. Vanselow selectivity coefficients were also computed with this data to identify preference.

MATERIALS AND METHODS

Binary Exchange Isotherms

Binary NO_3 – SO_4, NO_3 – Cl, and Cl – SO_4 equilibrium anion exchange was examined using an exchange isotherm method. A 5 g sample of soil from either the 30-

46 cm or 259-274 cm depth of the Memphis Catena soils (described in Chapter II) was placed into a preweighed 50 mL polypropylene centrifuge tube. The soils were then saturated with a monoionic saturating solution [0.2 M KCl, 0.2 M K_2SO_4, or 0.2 M KNO_3]. This was achieved by adding 30 mL of the saturating solution to each tube, mixing on a vortex mixer for 5 minutes, and centrifuging for 5 minutes. The supernatant was then decanted and this washing process was repeated three additional times. After saturation, the samples were centrifuge-washed with Type I deionized water three times to remove any entrained solution. The tubes were then weighed to determine the mass of entrained water. Additional water was then added to bring the total mass of entrained water to 5 g. Salt solutions containing varying ratios of anions (NO_3 - SO_4, NO_3 - Cl, and Cl^-SO_4) were then added (Appendix III), such that one anion in the pair was always the saturating anion. The tubes were equilibrated for 16 hours on a reciprocating shaker.

After equilibration, the tubes were centrifuged and the supernatants were collected and analyzed for the anions on either a DIONEX IC (for Cl and SO_4) or a Skalar CFA (for NO_3). The tubes were then centrifuge-washed with 30 mL aliquots of a 20% ethanol (EtOH) solution a total of three times to remove entrained solution. After the EtOH washings, the tubes are centrifuge-washed four times with 0.2 M $C_2H_3O_2K$ (potassium acetate) and the supernatant collected in a 100mL volumetric flask. The flask was then brought to volume with extracting solution and analyzed for the exchangeable anions using either a Dionex Model Ion Chromatography ICS-5000 Reagent-Free™ system (Sunnyvale, CA) for SO_4 and Cl and a Skalar San^{++} Automated Wet Chemistry Analyzer – Continuous Flow Analyzer (CFA) (Buford, GA) for NO_3. The operating conditions for the Dionex and Skalar are described in Chapter II.

Ternary Exchange Isotherms

The ternary anion exchange isotherms were conducted in a manner similar to that of the binary exchange isotherms. A 5 g soil sample was placed into a preweighed 50 mL polypropylene centrifuge tube and the soil was saturated with a monoionic saturating solution [0.2 M KCl, 0.2 M K_2SO_4, or 0.2 M KNO_3]. The tubes were then vortexed, placed on a reciprocal shaker for 5 minutes, and centrifuged for 5 minutes. This centrifuge washing was repeated two additional times and the supernatants were discarded. After saturation, the tubes were centrifuge-washed three times with Type I water to remove entrained salts, and the supernatants were discarded. The tubes were weighed and additional aliquots of Type I water was added to bring the total volume of entrained liquid to 5 mL. Next, different concentration ratios of anions, (Appendix III), other than the saturating anion, were added to the tubes. The tubes were vortexed and equilibrated on a reciprocating shaker for 16 hours. After equilibration, the tubes were centrifuged and the supernatants collected and analyzed for Cl and SO_4 using a DIONEX IC and for NO_3 using a Skalar CFA. The remaining soil was then centrifuge-washed with 30 mL of 20% EtOH a total of four times and supernatants discarded. The tubes were then centrifuge-washed with 30 mL of 0.2 M $C_2H_3O_2K$ three times and the supernatants were collected into 100 mL volumetric flasks. The flasks were brought to volume with the extracting solution and analyzed for Cl and SO_4 using a DIONEX IC and for NO_3 using a Skalar CFA.

Computations

Consider the binary, NO_3-SO_4 bivalent anion exchange reaction:

$$\mathbf{2XNO_3 + SO_4^{2-} = XSO_4 + 2NO_3^-} \quad \textbf{[3]}$$

where X represents an equivalent of the anion exchanger phase charge (X^+). The thermodynamic anion exchange equilibrium constant is expressed as:

$$\mathbf{K_{ex} = \frac{(XSO_4)(NO_3^-)^2}{(XNO_3)^2(SO_4^{2-})}} \quad \textbf{[4]}$$

where the parentheses () denote activities. The exchanger phase may be treated as a non-ideal solid solution (Essington, 2003). Thus, the activity of the adsorbed anions is given by

$$\mathbf{(XSO_4) \equiv f_{SO_4} N_{SO_4}; \qquad (XNO_3) \equiv f_{NO_3} N_{NO_3}} \quad \textbf{[5]}$$

where f is the rational activity coefficient and N is the mole fraction of the ions on the exchanger phase. Similarly, the activities of the soluble species are related to their free concentrations by

$$\mathbf{\left(SO_4^{2-}\right) \equiv \gamma_{SO_4}\left[SO_4^{2-}\right]; \quad (NO_3^-) \equiv \gamma_{NO_3}[NO_3^-]} \quad \textbf{[6]}$$

where γ is the single ion activity coefficient and the brackets [ ] denote molar (mol L^{-1}) concentrations. In a binary NO_3-SO_4 exchange system, the mole fractions are defined as

$$\mathbf{N_{SO_4}} \equiv \frac{\{\mathbf{X_2SO_4}\}}{\{\mathbf{X_2SO_4}\}+\{\mathbf{XNO_3}\}}; \quad \mathbf{N_{NO_3}} \equiv \frac{\{\mathbf{XNO_3}\}}{\{\mathbf{X_2SO_4}\}+\{\mathbf{XNO_3}\}} \qquad \textbf{[7]}$$

where the braces {} denote the concentrations of adsorbed anions in mol kg^{-1}, with N_{SO4} + N_{NO3} = 1. Substituting equations [5], [6] and [7] into equation [4] yields:

$$\mathbf{K_{ex}} = \frac{\mathbf{f_{SO_4} N_{SO_4} \gamma_{NO_3}^2 [NO_3^-]^2}}{\mathbf{f_{NO_3}^2 N_{NO_3}^2 \gamma_{SO_4} [SO_4^{2-}]}} \qquad \textbf{[8]}$$

With the exception of the rational activity coefficients, the variables are measurable or predicted from analytical results (total exchanger and solution phase concentrations), the application of the ion association model (ion speciation and the solution concentrations), and the application of the Davies equation (single-ion activity coefficients).

The rational activity coefficients will be unity (f=1) if the exchangeable anions form an ideal mixture on the surface. When this assumption is imposed, equation [8] becomes the Vanselow selectivity coefficient:

$$\mathbf{K_V} = \frac{\mathbf{N_{SO_4} \gamma_{NO_3}^2 [NO_3^-]^2}}{\mathbf{N_{NO_3}^2 \gamma_{SO_4} [SO_4^{2-}]}} \qquad \textbf{[9]}$$

which is related to the exchange equilibrium constant by

$$\mathbf{K_{ex}} = \frac{\mathbf{f_{SO_4}}}{\mathbf{f_{NO_3}^2}} \mathbf{K_V} \qquad \textbf{[10]}$$

Both K_{ex} and K_V can be obtained by constructing an exchange isotherm. This plot represents the equivalent fraction of SO_4 on the exchanger phase (E_{XSO4}) versus the equivalent fraction of SO_4 in the solution phase ($\tilde{E}_{SO4}$), at equilibrium and at a constant total normality (TN):

$$\mathbf{E_{SO_4}} \equiv \frac{\mathbf{2\{XSO_4\}}}{\mathbf{2\{XSO_4\}+\{XNO_3\}}}; \qquad \mathbf{E_{NO_3}} \equiv \frac{\mathbf{\{XNO_3\}}}{\mathbf{2\{XSO_4\}+\{XNO_3\}}} \qquad \textbf{[11]}$$

$$\mathbf{E_{XSO_4}} \equiv \frac{\mathbf{2[SO_4^{2-}]}}{\mathbf{2[SO_4^{2-}]+[NO_3^-]}}; \qquad \mathbf{E_{XNO_3}} \equiv \frac{\mathbf{[NO_3^-]}}{\mathbf{2[SO_4^{2-}]+[NO_3^-]}} \qquad \textbf{[12]}$$

These isotherms also aid in determining anion preference for the exchanger phase, when the data are plotted relative to the non-preference isotherm (the exchange isotherm that would result if K_V=1). Because, the K_v selectivity coefficient is a conditional equilibrium constant that varies with exchange phase composition, it may be employed to predict the effects of leachate water quality on soil exchanger phase composition.

RESULTS AND CONCLUSIONS

Nitrate-Sulfate Exchange

Binary exchange isotherms were generated using soils at 30 to 46 cm and 245 to 261 cm depths as a function of total normality and initial anion saturation. The NO_3 –

SO_4 exchange isotherms for soils at a depth of 30 to 46 cm below the surface are shown in Fig. 1. For the soils initially saturated with SO_4, the isotherm indicated that there is a preference for NO_3 on the exchange phase relative to SO_4, as indicated by the nonpreference isotherm. The preference for NO_3 relative to SO_4 is less pronounced when samples were initially saturated with NO_3. The $\ln K_V$ (Fig. 2) values for the XNO_3 to X_2SO_4 reaction range from -4.08 to 0.73.

The NO_3 – SO_4 exchange isotherm for soils at a depth of 245 to 261 cm (Fig. 3) followed the same trend of preference as the 30 to 46 cm samples. Soils saturated with SO_4 show a preference for NO_3, and soils initially saturated with NO_3 are above and below the nonpreference line. The $\ln K_V$ values for this depth are shown in Fig. 4. The $\ln K_V$ values for the XNO_3 to X_2SO_4 reaction range from -5.79 to -0.87.

The $\ln K_V$ values generated for NO_3 – SO_4 exchange isotherms were less than 1 for the XNO_3 – X_2SO_4 reaction, indicating that NO_3 is thermodynamically preferred on the exchange phase; however, SO_4 dominates the exchange phase due to its higher valence. It was also evident (Figs. 2 and 4) that the $\ln K_V$ values did not stratify based on initial anion saturation of the exchanger phase. This suggests that NO_3 – SO_4 exchange is either ideal or non-hysteretic.

Chloride-Sulfate Exchange

The Cl – SO_4 exchange isotherm for soils at a depth of 30 to 46 cm is shown in Fig. 5. These isotherms indicate that the soil has a strong preference for Cl on the exchange phase relative to SO_4, as indicated by the location of the data relative to the nonpreference isotherm. The $\ln K_V$ (Fig. 6) range from -18.93 to -2.79 for XCl to X_2SO_4

exchange. The $\ln K_V$ values for the Cl-saturated systems differ from those of the SO_4-saturated, indicating the X_2SO_4 – XCl exchange is either hysteretic or non-ideal.

The Cl – SO_4 exchange isotherms for soils at a depth of 245 to 261 cm (Fig. 7) follow the same trend as the isotherms for the 30 to 46 cm soil. Again, a preference for Cl on the exchange phase relative to SO_4 is evident from the location of the data relative to the nonpreference isotherm. The $\ln K_V$ values (Fig. 8) ranged from -16.95 to -1.79 for XCl to X_2SO_4 exchange. Also, the $\ln K_V$ values are a function of initial anion saturation.

As were observed for X_2SO_4 – XNO_3 exchange, although Cl is preferred, there is more sulfate present on the exchange phase due to the greater negative charge associated with the SO_4 anion.

Nitrate-Chloride Exchange

The NO_3 – Cl exchange isotherm for soils at a depth of 30 to 46 cm is shown in Fig. 9. The Cl-saturated samples show a clear preference for NO_3 relative to Cl. However, for the NO_3-saturated samples there was preference for Cl. The $\ln K_V$ values for the system (Fig. 10) range from -3.06 to 8.48. The large range in $\ln K_V$ values, and the dependence of $\ln K_V$ on initial saturation, suggests hysteresis or non-ideal behavior within the XCl to XNO_3 exchange system.

The NO_3 – Cl isotherm for a depth of 245 to 261 cm is shown in Fig. 11. The isotherms follow the same trend as the isotherms generated from the 30 to 46 cm depth. Samples initially saturated with Cl generally show no preference, as the data tend to straddle the nonpreference line. Samples initially saturated with NO_3 are below the nonpreference line indicating a preference for Cl. Chloride-saturated samples have

$\ln K_V$ (Fig. 12) values that range from -1.66 to 12.21. Nitrate-saturated samples have a $\ln K_V$ that range from -1.66 to 12.21.

The $\ln K_V$ values of the NO_3 – Cl system were dependent on the initial saturation, suggesting the XCl to XNO_3 exchange is hysteretic or non-ideal.

Chloride-Saturated Nitrate-Sulfate Exchange

The NO_3 – SO_4 exchange isotherm with initial Cl-saturation at a depth of 30 to 46 cm is shown on Fig. 13. The isotherm indicates a preference on the exchanger phase for NO_3 relative to SO_4. The $\ln K_V$ values (Fig. 14) range from -9.83 to -0.55 for XNO_3 to X_2SO_4 exchange. This also indicates that NO_3 is preferred on the exchange phase relative to SO_4 when the anion exchange phase is initially saturated with Cl.

The NO_3 – SO_4 exchange isotherm with initial Cl-saturation at a depth of 245 to 246 cm is shown in Fig. 15. The isotherms follow the same trend observed in the 30 to 46 cm depth, with preference primarily observed for NO_3. The $\ln K_V$ (Fig. 16) values range from -8.46 to 2.89. Nitrate – sulfate exchange in the presence of chloride at a depth of 245 to 261 cm yields an average $\ln K_V$ value that is 0.03 units greater than that in the absence of chloride.

Nitrate-saturated Chloride-Sulfate Exchange

The Cl – SO_4 exchange isotherm in the presence of NO_3 at a depth of 30 to 46 cm is shown in Fig. 17. The isotherm indicates a clear preference of Cl relative to SO_4. The $\ln K_V$ values (Fig. 18) also reflect this, ranging from -14.87 to -2.78 for XCl to X_2SO_4

exchange. Without nitrate present in the system, the $\ln K_V$ values were similar to those shown in Fig. 18, indicating that NO_3 does not impact Cl – SO_4 exchange.

The Cl – SO_4 exchange isotherm in the presence of NO_3 at a depth of 245 to 261 cm is shown in Fig. 19. These data indicate a preference for Cl relative to SO_4. The $\ln K_V$ values in Fig. 20 range from -17.21 to -2.96. In the absence of nitrate, the $\ln K_V$ values were similar to those shown in Fig. 20, indicating that NO_3 does not impact Cl – SO_4 exchange. Both soil depths show a strong preference for Cl relative to SO_4 in the absence of NO_3 or when saturated with NO_3 initially.

Sulfate-saturated Nitrate-Chloride Exchange

The NO_3 – Cl exchange isotherm in the presence of SO_4 at a depth of 30 to 46 cm is shown in Fig. 21. The isotherm shows a preference for Cl relative to NO_3. The $\ln K_V$ values (Fig. 22) for XNO_3 to XCl exchange varied from 0.54 to 7.34, also indicate a preference for Cl on the exchange phase relative to NO_3.

The NO_3 – Cl exchange isotherm in the presence of SO_4 at a depth of 245 to 261 cm is shown in Fig. 23. The data plotted on the exchange isotherm show a preference for Cl in relation to NO_3 when compared to the nonpreference line. The $\ln K_V$ values (Fig. 24) for XNO_3 to XCl exchange range from -3.64 to 8.59 indicate a preference for Cl over NO_3 on the exchange phase in the presence of SO_4. The average $\ln K_V$ for NO_3 – Cl exchange in the absence of sulfate are similar to those shown in Fig. 24, indicating that SO_4 does not impact NO_3 – Cl exchange.

SUMMARY

The binary exchange isotherms indicated that NO_3 is preferred relative to SO_4, Cl is preferred relative to SO_4, and Cl is preferred relative to NO_3 irrespective of soil depth. The results from the Cl – NO_3 exchange system suggest hysteresis in the 30 to 46 cm depth increment based on initial saturating solution. When initially saturated with Cl, NO_3 is preferred, but when initially saturated with NO_3 the opposite occurs and Cl is preferred on the exchange complex. Ternary isotherms provided similar conclusions. Thermodynamically, the preferential sequence is Cl > NO_3 > SO_4 on the exchange complex. However, SO_4 is the predominate anion on the exchange phase due to its divalent charge.

LITERATURE CITED

Ammons, J.T., A.O. Gallagher, R.L. Livingston, J.L. Branson, and R.J. Lewis. 1994.Background levels of nitrate-nitrogen and selected heavy metals for the Ames Plantation watershed project. Tenn. Farm Home Sci. 169:30-33.

Charlet, L., and G. Sposito. 1987. Monovalent ion adsorption by an Oxisol. Soil Sci. Soc. Am. J. 51:1155-1160.

Donn, M.J., and N.W. Menzies. 2005a. Simulated rainfall effects on anion exchange capacity and nitrate retention in Ferrosols. Aust. J. Soil. Res. 43:33-42.

Donn, M.J., and N.W. Menzies. 2005b. The effect of ionic strength variation and anion competition on the development of nitrate accumulations in variable charge subsoils. Aust. J. Soil. Res. 43:43-50.

Essington, M.E. 2003. Soil and water chemistry: an integrated approach. CRC Press, Boca Raton, FL.

Feder, F., and A. Findeling. 2007. Retention and leaching of nitrate and chloride in an andic soil after pig manure amendment. European Journal of Soil Science. 58:393-404.

Gale, P.M., M.D. Mullen, C. Cieslik, D.D. Tyler, B.N. Duck, M. Kirchner, and J. McClure. . Phosphorus distribution and availability in response to dairy manure applications. Comm. Soil Sci. and Plant Analysis. 31:553-565.

Ishiguro, M., Y. Manabe, S. Seo, and T. Akae. 2003. Effect of sulfate on nitrate transport in volcanic ash soils sampled from the A and the B horizons. Soil Science and Plant Nutrition. 49:249-254.

Katou, H., B.E. Clothier, and S.R. Green. 1996. Anion transport involving competitive adsorption during transient water flow in an andisol. Soil Sci. Soc. Am. J. 60:1368-1375.

Nightingale, E.R., 1959. Phenomenological theory of ion salvation. Effective radii of hydrated ions. J.Phys. Chem. 63:1381-1387.

Rasiah, V., J.D. Armour, N.W. Menzies, D.H. Heiner, and M.J. Donn. 2004. Impact of pre-existing sulphate on retention of imported chloride and nitrate in variable charge soil profiles. Geoderma. 123:205-218.

Rhoton, F.E., and D.S. McChesney. 2011. Erodibility of a sodic soil amended with flue gas desulfurization gypsum. Soil Science. 176:190-195.

Springer, M.E., and J.A. Elder. 1980. Soils of Tennessee. Bulletin 596. Tennessee Agriculture Experiment Station, Knoxville, TN.

Toner IV, C.V., D.L. Sparks, and T.H. Carski. 1989. Anion exchange chemistry of middle Atlantic soils: charge properties and nitrate retention kinetics. Soil Sci. Soc. Am. J. 53:1061-1067.

Tyner, J.S., W.C. Wright, and R.E. Yoder. 2007. Identifying long-term preferential and matrix flow recharge at the field scale. Trans. ASABE. 50:2001-2006.

APPENDIX II

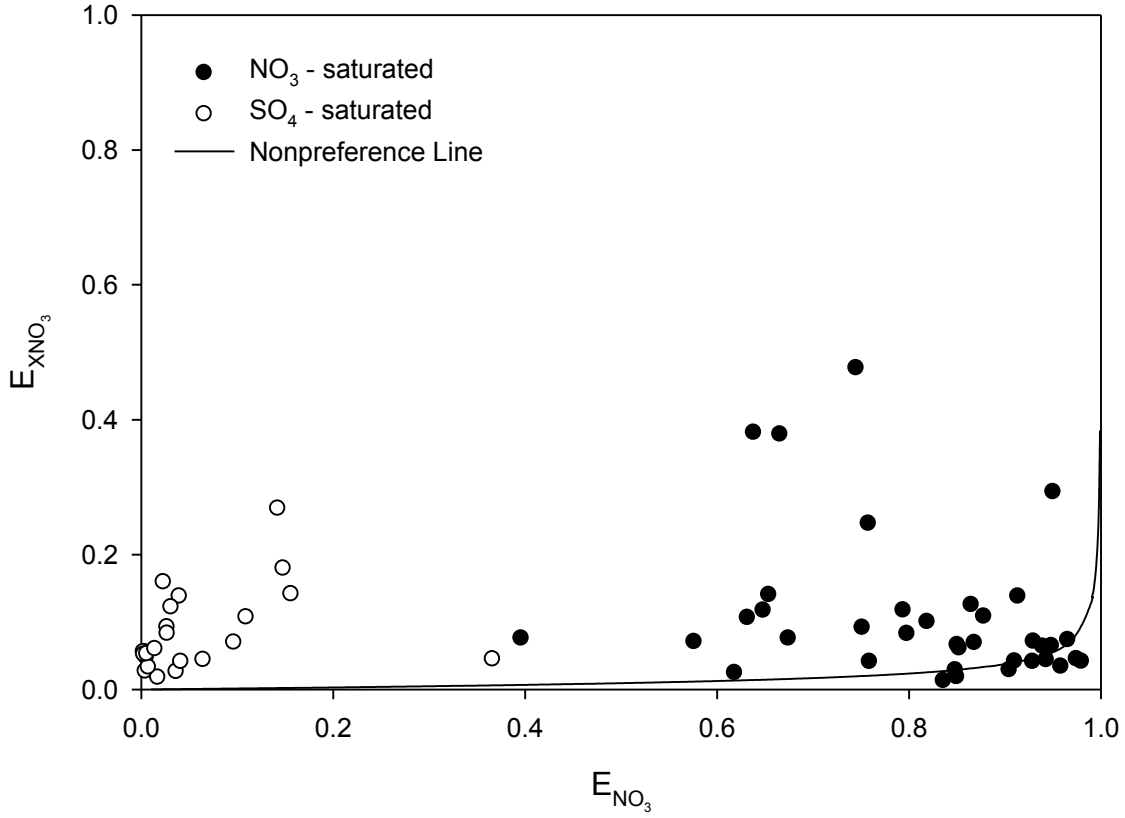

Figure 1. NO_3-SO_4 exchange for 0.0002 TN at a depth of 30 to 46 cm, where E_{NO3} is the equivalent fraction of NO_3 in solution and E_{XNO3} is the equivalent fraction of NO_3 on the exchanger phase for the reaction $2XNO_3 + SO_4^{2-} = X_2SO_4 + 2NO_3^-$.

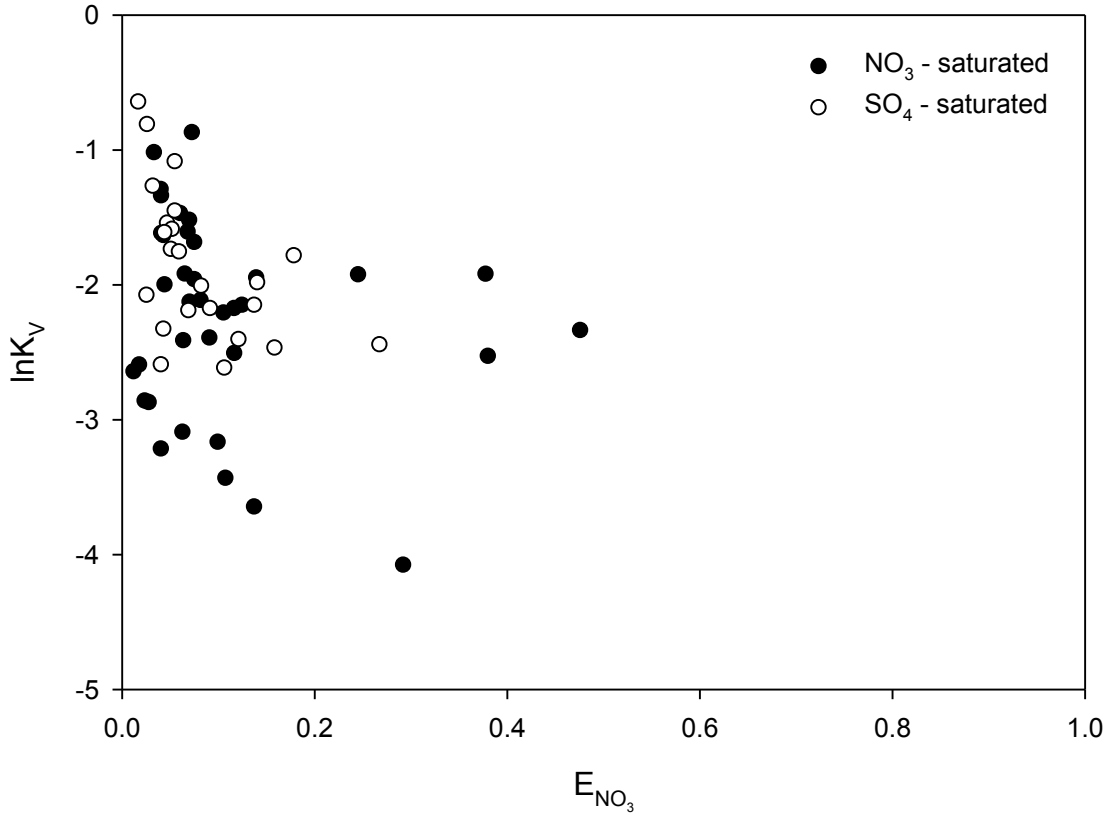

Figure 2. $\ln K_V$ vs. E_{XNO3} data plotted for NO_3-SO_4 exchange for 0.0002 TN at a depth of 30 to 46 cm, where K_V is the Vanselow selectivity coefficient for the exchange isotherm and E_{XNO3} is the equivalent fraction of NO_3 on the exchange phase for the reaction $2XNO_3 + SO_4^{2-} = X_2SO_4 + 2NO_3^-$.

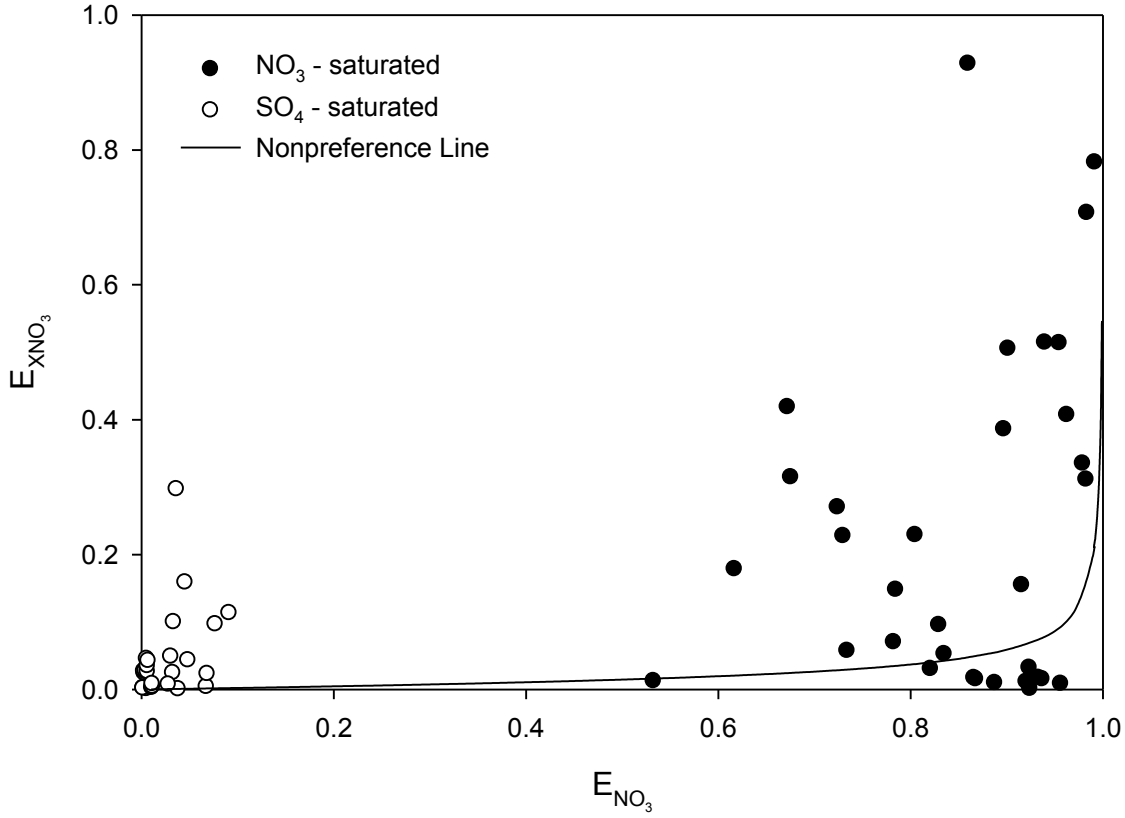

Figure 3. NO_3-SO_4 exchange for 0.0002 TN at a depth of 245 to 261 cm, where E_{NO3} is the equivalent fraction of NO_3 in solution and E_{XNO3} is the equivalent fraction of NO_3 on the exchange phase for the reaction $2XNO_3 + SO_4^{2-} = X_2SO_4 + 2NO_3^-$.

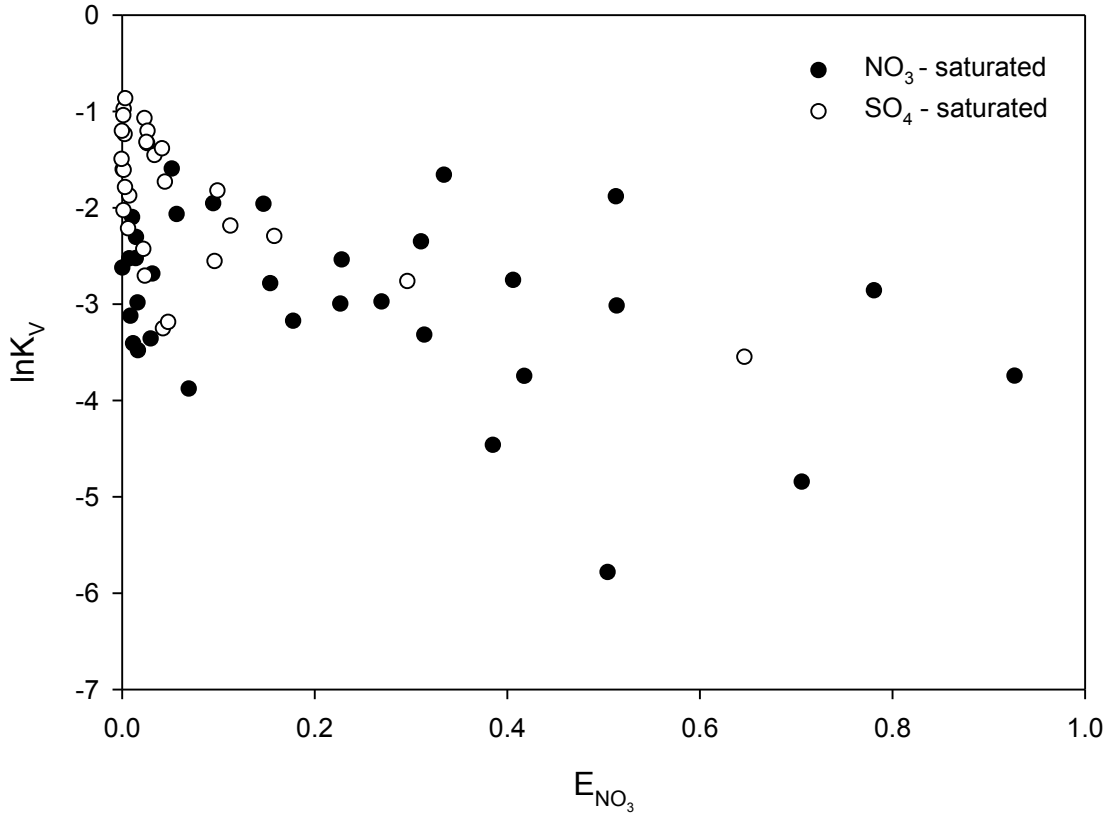

Figure 4. $\ln K_V$ vs. E_{XNO3} data plotted for NO_3-SO_4 exchange for 0.0002 TN at a depth of 245 to 261 cm, where $\ln K_V$ is the natural log of the Vanselow selectivity coefficient for the exchange isotherm and E_{XNO3} is the equivalent fraction of NO_3 on the exchange phase for the reaction $2XNO_3 + SO_4^{2-} = X_2SO_4 + NO_3^-$.

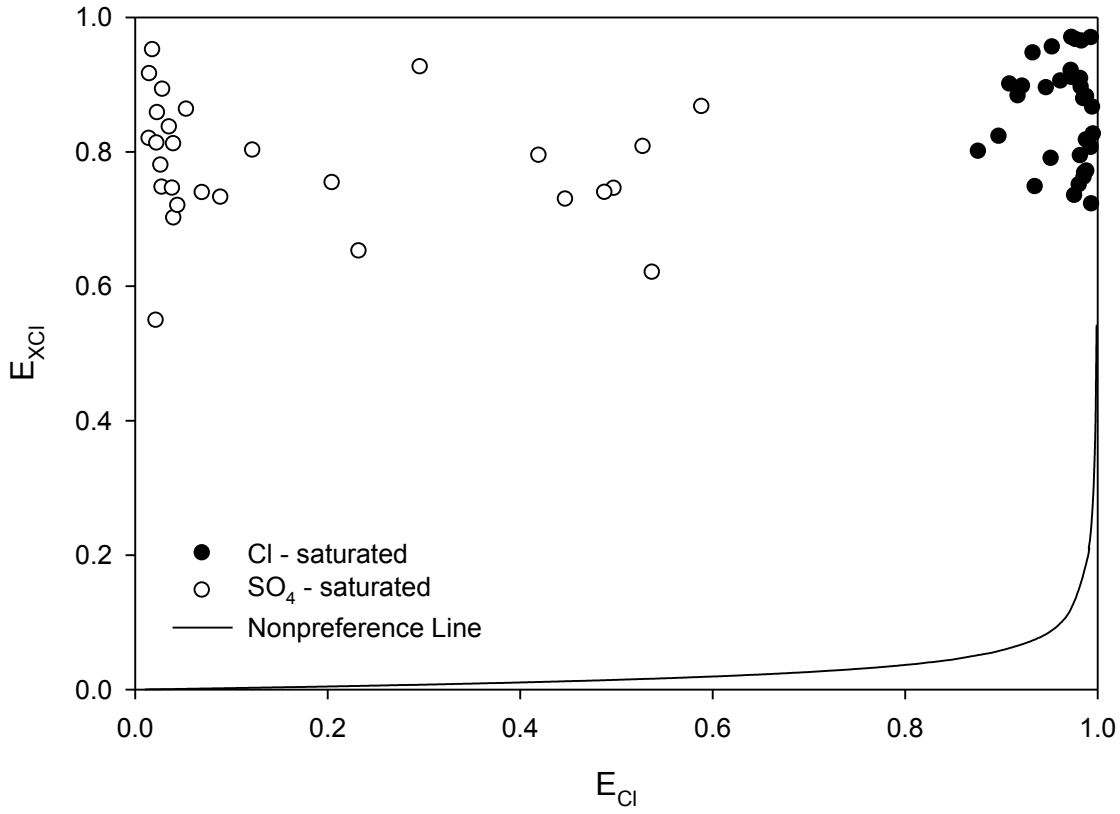

Figure 5. Cl-SO_4 exchange for 0.0002 TN at a depth of 30 to 46 cm, where E_{Cl} is the equivalent fraction of Cl in solution and E_{XCl} is the equivalent fraction of Cl on the exchange phase for the reaction $2XCl + SO_4^{2-} = X_2SO_4 + 2Cl^-$.

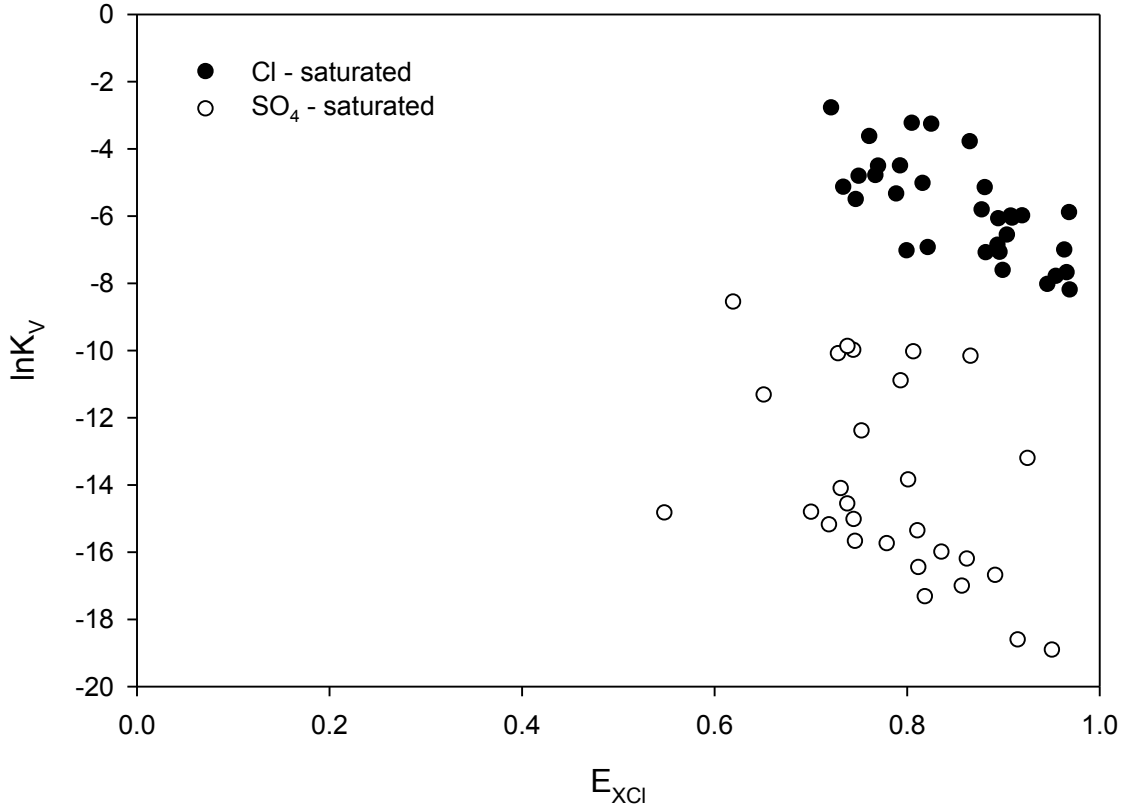

Figure 6. $\ln K_V$ vs. E_{XCl} data plotted for Cl-SO_4 exchange for 0.0002 TN at a depth of 30 to 46 cm, where $\ln K_V$ is the natural log of the Vanselow selectivity coefficient for the exchange isotherm and E_{XCl} is the equivalent fraction of Cl on the exchange phase for the reaction $2XCl + SO_4^{2-} = X_2SO_4 + 2Cl^-$.

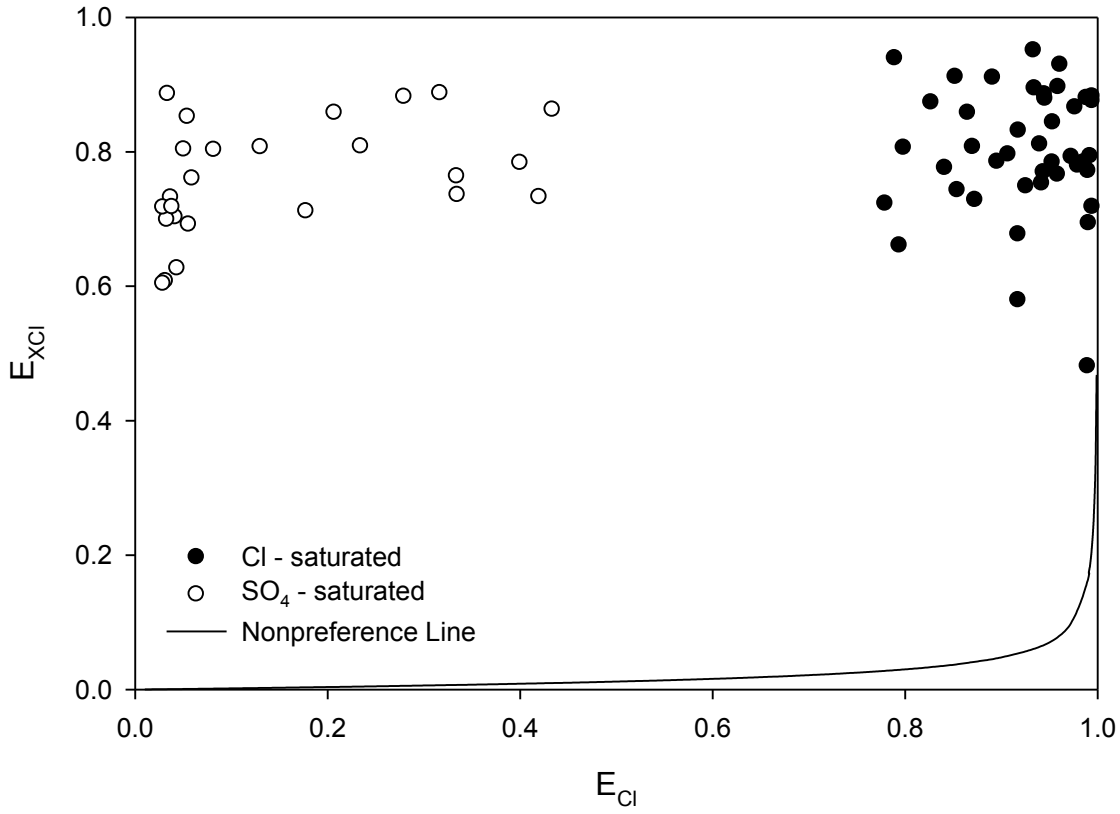

Figure7. Cl-SO_4 exchange for 0.0002 TN at a depth of 245 to 261 cm, where E_{Cl} is the equivalent fraction of Cl in solution and E_{XCl} is the equivalent fraction of Cl on the exchange phase for the reaction $2XCl + SO_4^{2-} = X_2SO_4 + 2Cl^-$.

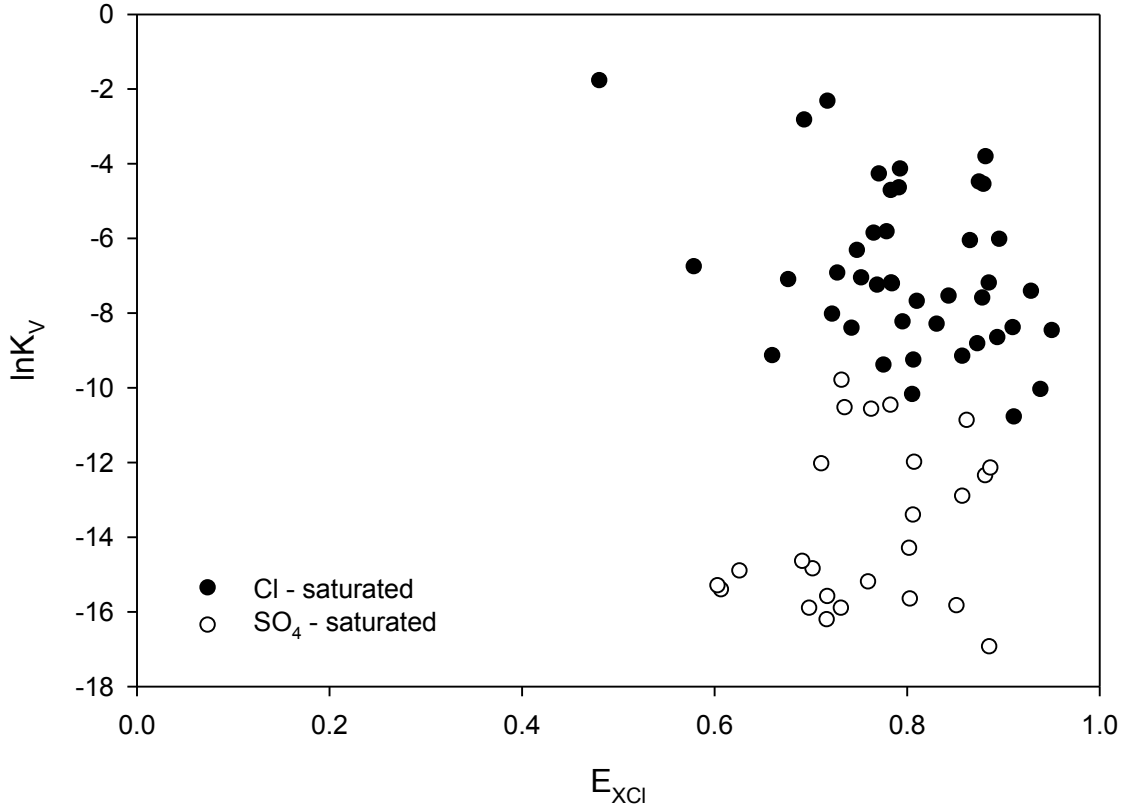

Figure 8. $\ln K_V$ vs. E_{XCl} data plotted for Cl-SO_4 exchange for 0.0002 TN at a depth of 245 to 261 cm, where $\ln K_V$ is the natural log of the Vanselow selectivity coefficient for the exchange isotherm and E_{XCl} is the equivalent fraction of Cl on the exchange phase for the reaction $2XCl + SO_4^{2-} = X_2SO_4 + 2Cl^-$.

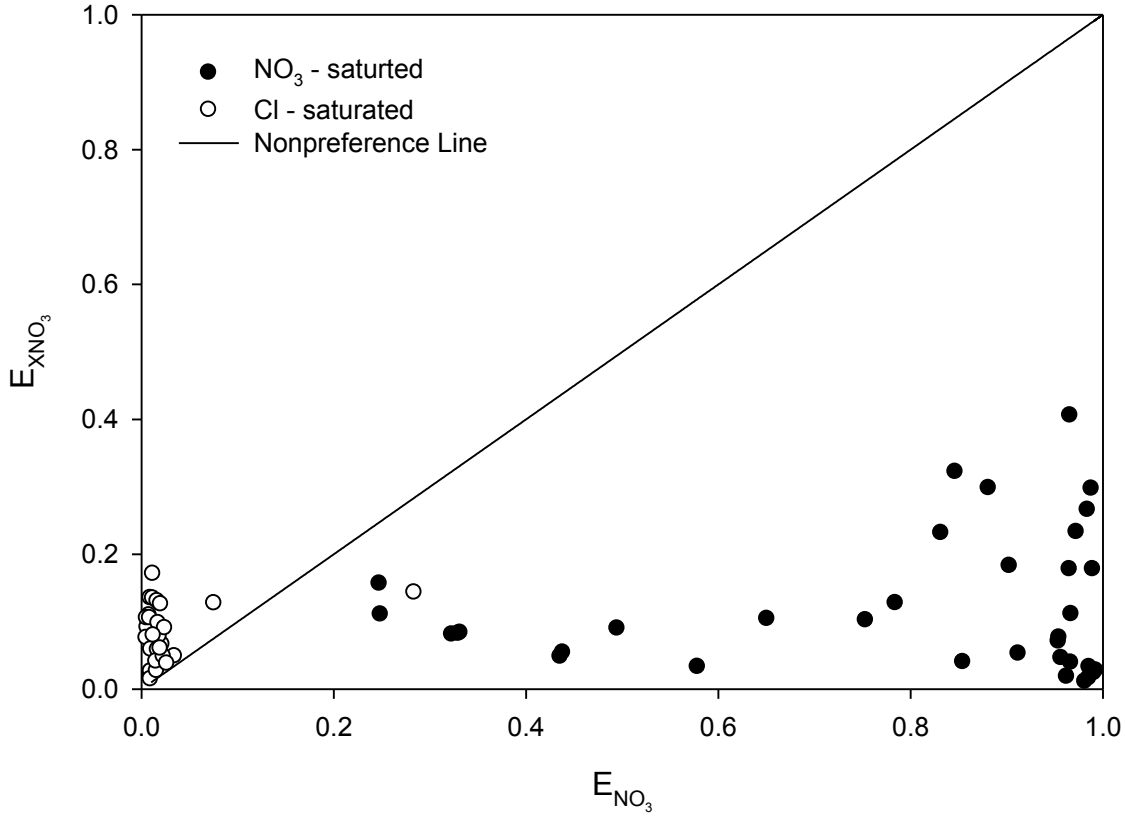

Figure 9. NO_3-Cl exchange for 0.0002 TN at a depth of 30 to 46 cm, where E_{NO3} is the equivalent fraction of NO_3 in solution and E_{XNO3} is the equivalent fraction of NO_3 on the exchange phase for the reaction $XCl + NO_3^- = XNO_3 + Cl^-$.

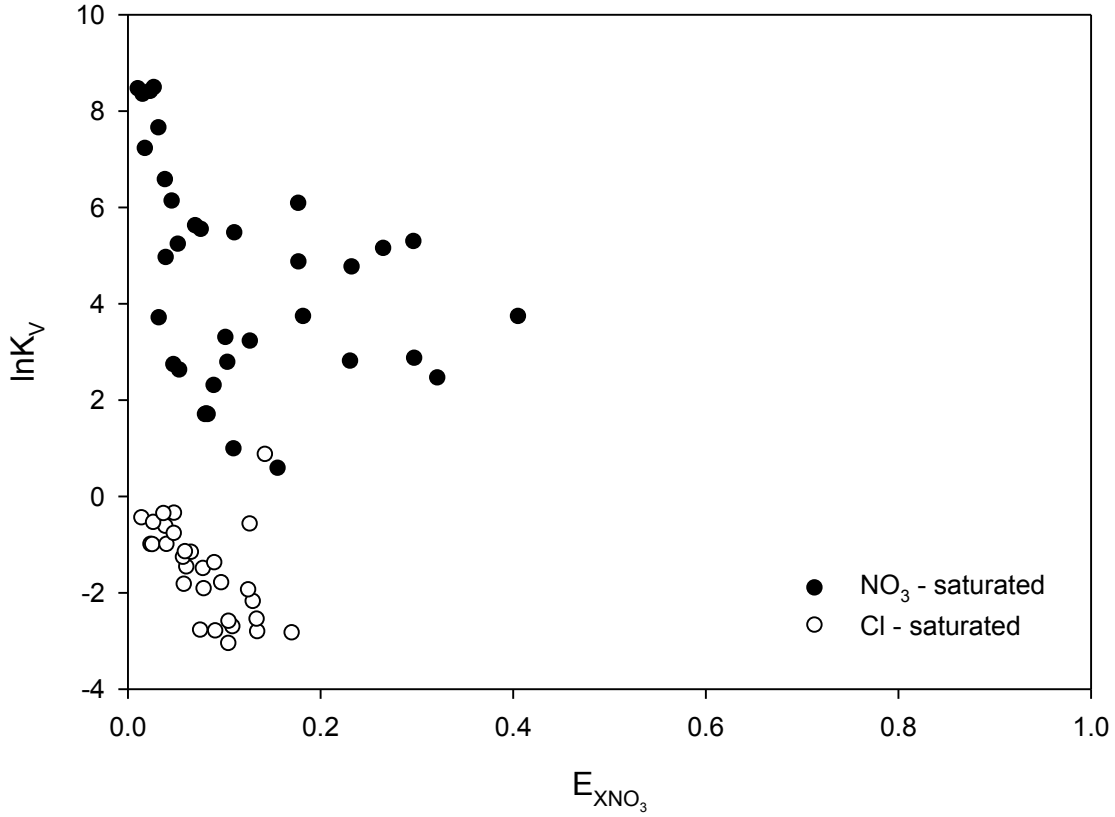

Figure 10. $\ln K_V$ vs. E_{XNO3} data plotted for NO_3-Cl exchange for 0.0002 TN at a depth of 30 to 46 cm, where $\ln K_V$ is the natural log of the Vanselow selectivity coefficient for the exchange isotherm and E_{XNO3} is the equivalent fraction of NO_3 on the exchange phase for the reaction $XCl + NO_3^- + XNO_3 + Cl^-$.

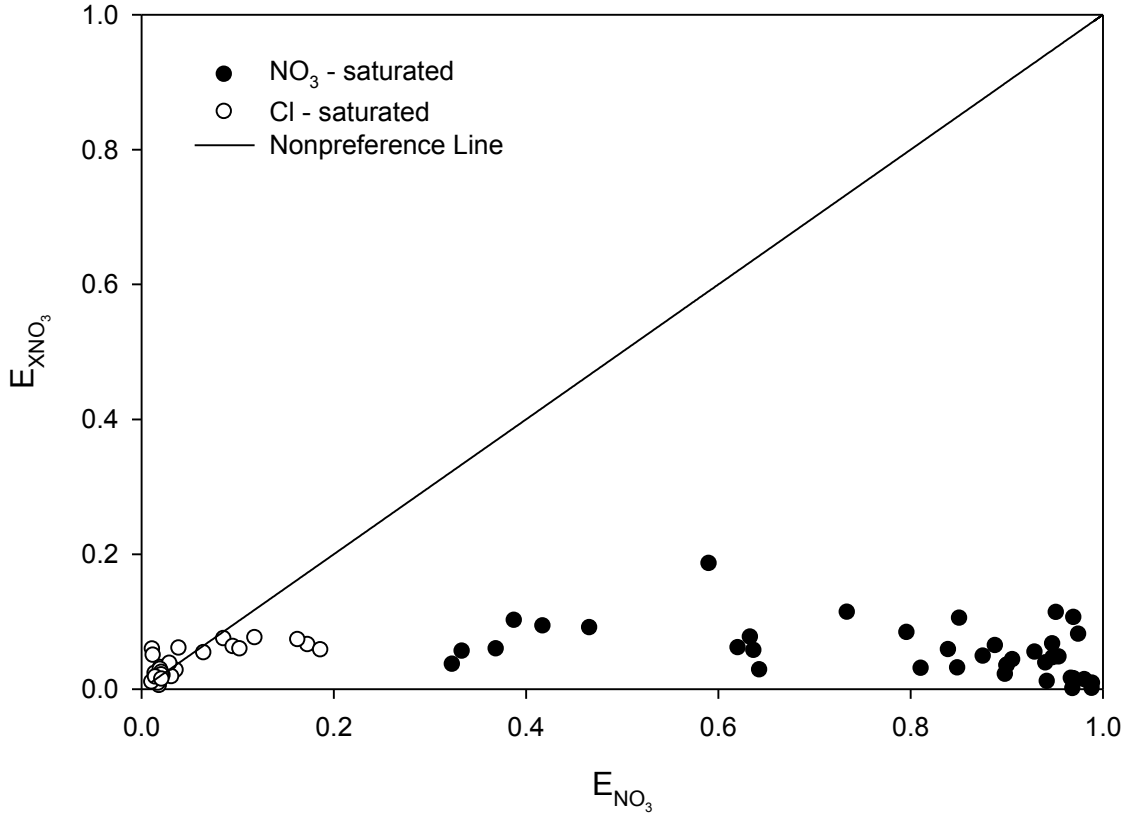

Figure 11. NO_3-Cl exchange for 0.0002 TN at a depth of 245 to 261 cm, where E_{NO3} is the equivalent fraction of NO_3 in solution and E_{XNO3} is the equivalent fraction of NO_3 on the exchange phase for the reaction $XCl + NO_3^- = XNO_3 + Cl^-$.

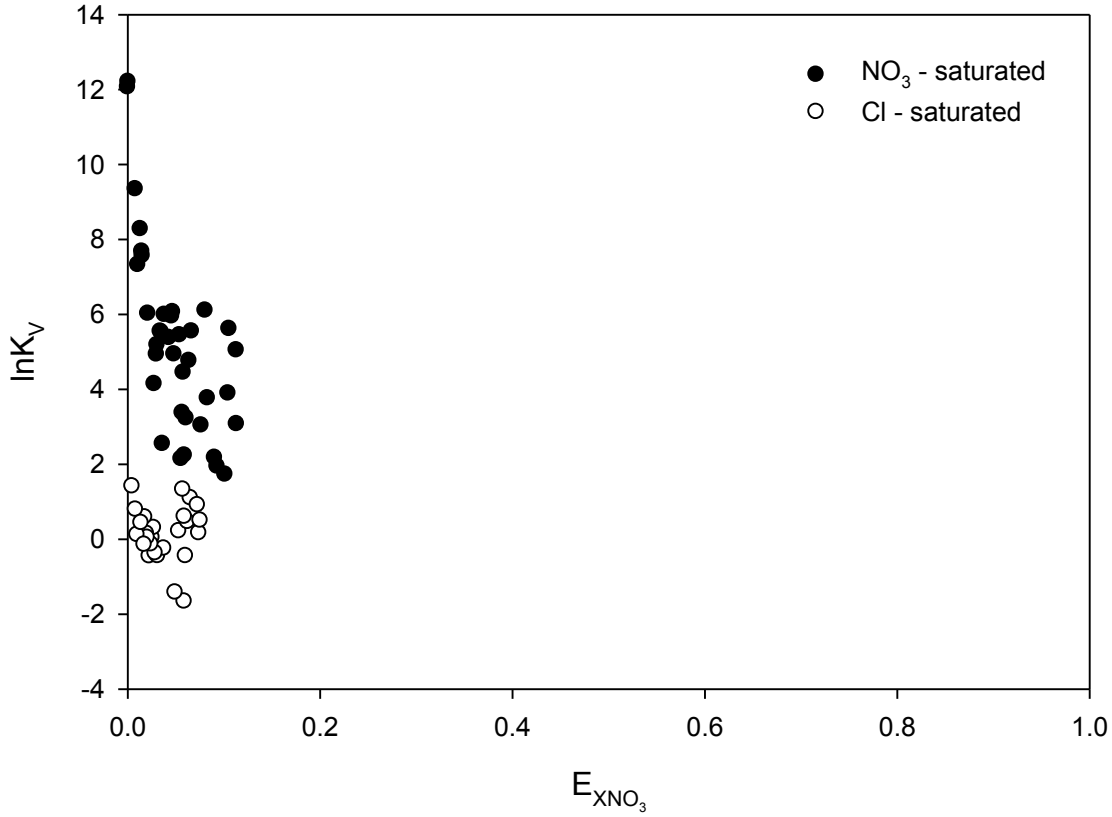

Figure 12. $\ln K_V$ vs. E_{XNO3} data plotted for NO_3-Cl exchange for 0.0002 TN at a depth of 245 to 261 cm, where $\ln K_V$ is the natural log of the Vanselow selectivity coefficient for the exchange isotherm and E_{XNO3} is the equivalent fraction of NO_3 on the exchange phase for the reaction $XCl + NO_3^- + XNO_3 + Cl^-$.

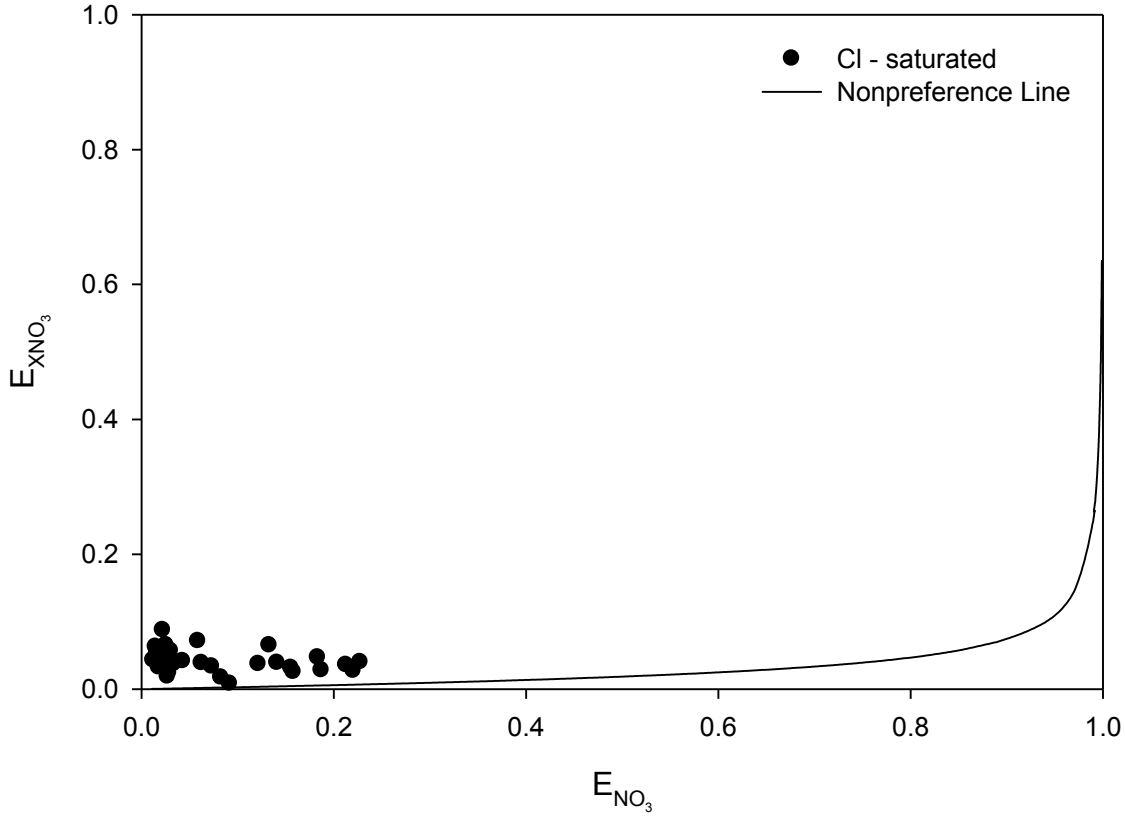

Figure 13. NO_3-SO_4 exchange in the presence of Cl for 0.0002 TN at a depth of 30 to 46 cm, where E_{NO3} is the equivalent fraction of NO_3 in solution and E_{XNO3} is the equivalent fraction of NO_3 on the exchange phase for the reaction $X_2SO_4 + 2NO_3^- = 2XNO_3 + SO_4^{2-}$.

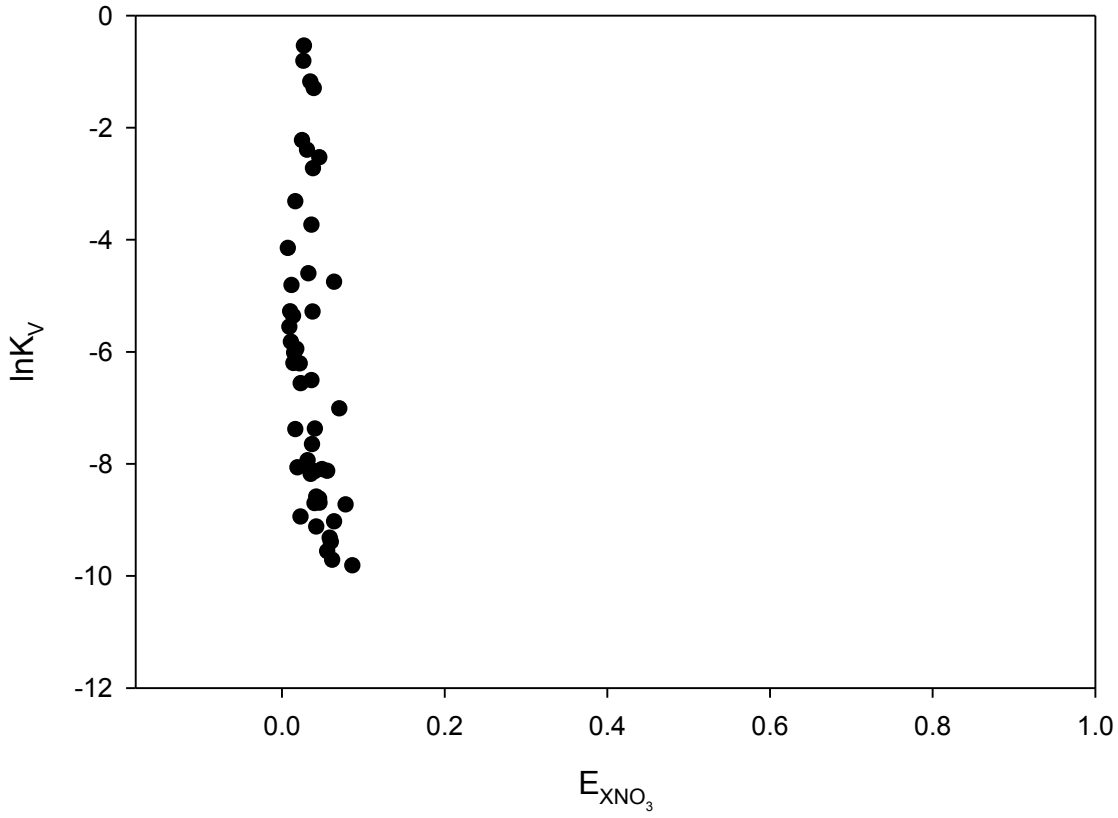

Figure 14. $\ln K_V$ vs. E_{XNO3} data plotted for NO_3-SO_4 exchange in the presence of Cl for 0.0002 TN at a depth of 30 to 46 cm, where $\ln K_V$ is the natural log of the Vanselow selectivity coefficient for the exchange isotherm and E_{XNO3} is the equivalent fraction of NO_3 on the exchange phase for the reaction $2XNO_3 + SO_4^{2-} = X_2SO_4 + 2NO_3^-$.

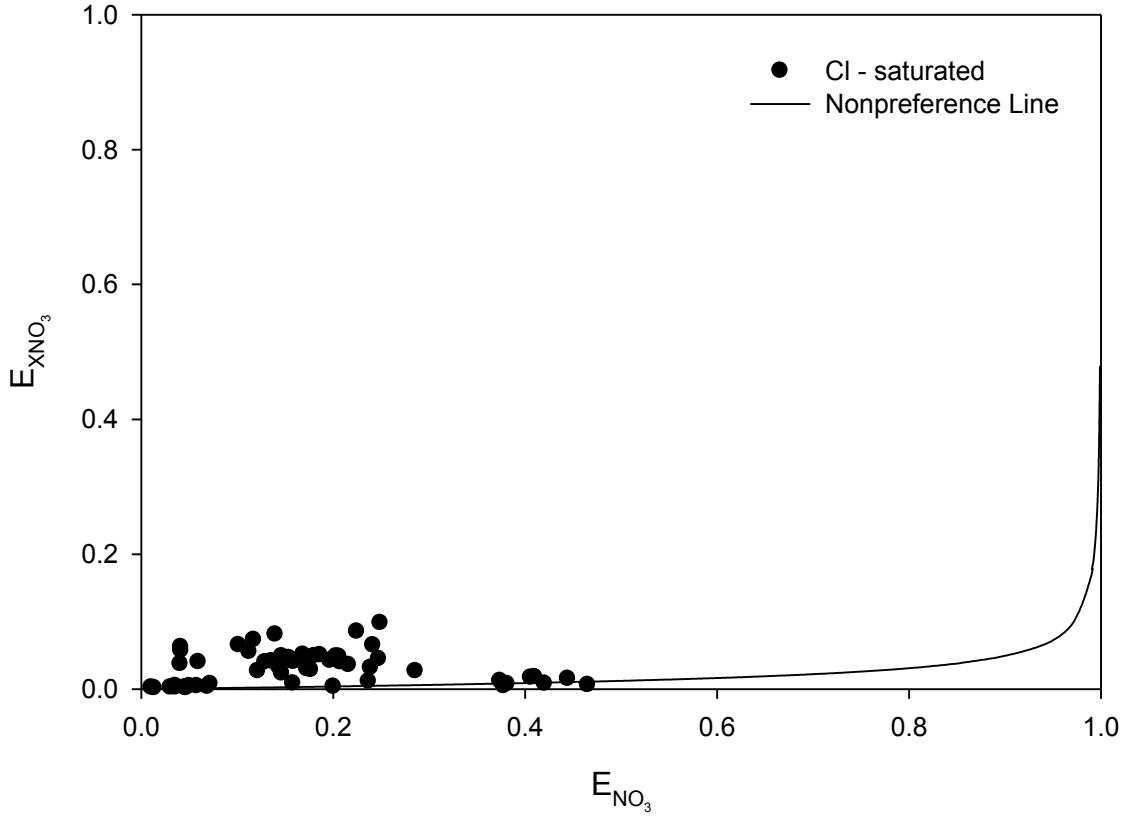

Figure 15. NO_3-SO_4 exchange in the presence of Cl for 0.0002 TN at a depth of 245 to 261 cm, where E_{NO3} is the equivalent fraction of NO_3 in solution and E_{XNO3} is the equivalent fraction of NO_3 on the exchange phase for the reaction $2XNO_3 + SO_4^- = X_2SO_4 + 2NO_3^-$.

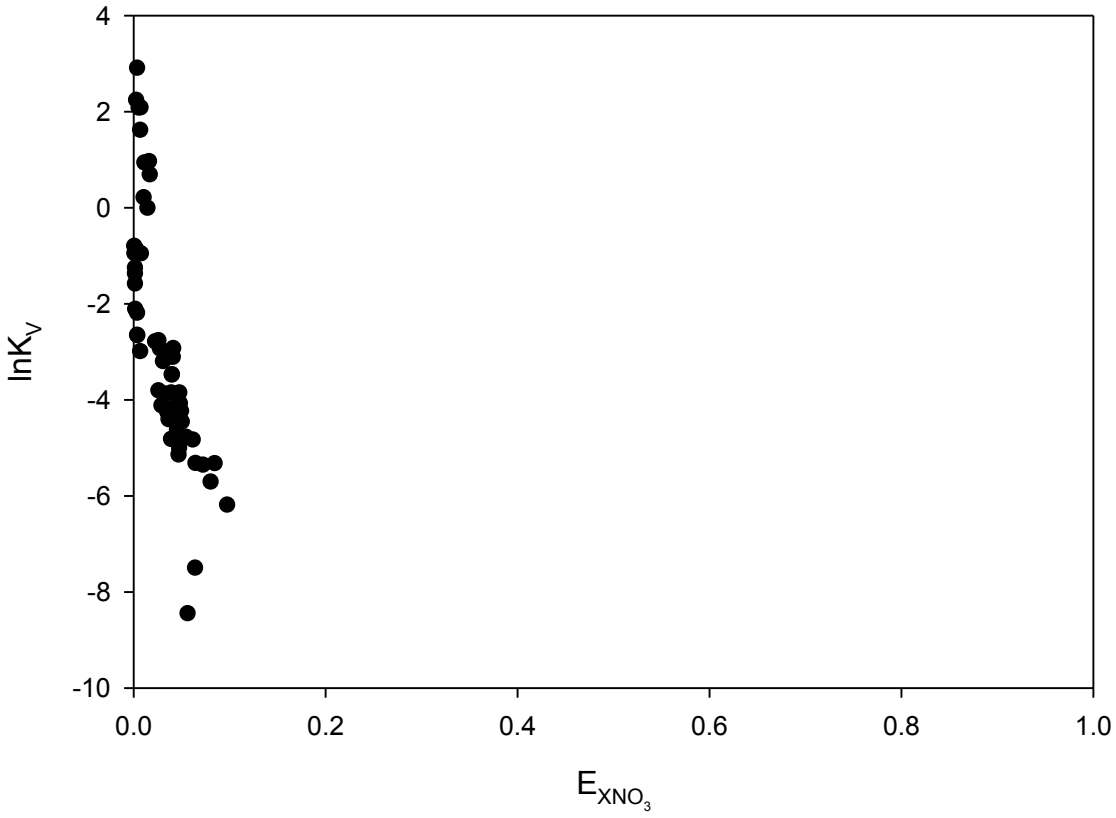

Figure 16. $\ln K_V$ vs. E_{XNO3} data plotted for NO_3-SO_4 exchange in the presence of Cl for 0.0002 TN at a depth of 245 to 261 cm, where $\ln K_V$ is the natural log of the Vanselow selectivity coefficient for the exchange isotherm and E_{XNO3} is the equivalent fraction of NO_3 on the exchange phase for the reaction $2XNO_3 + SO_4^{2-} = X_2SO_4 + 2NO_3^-$.

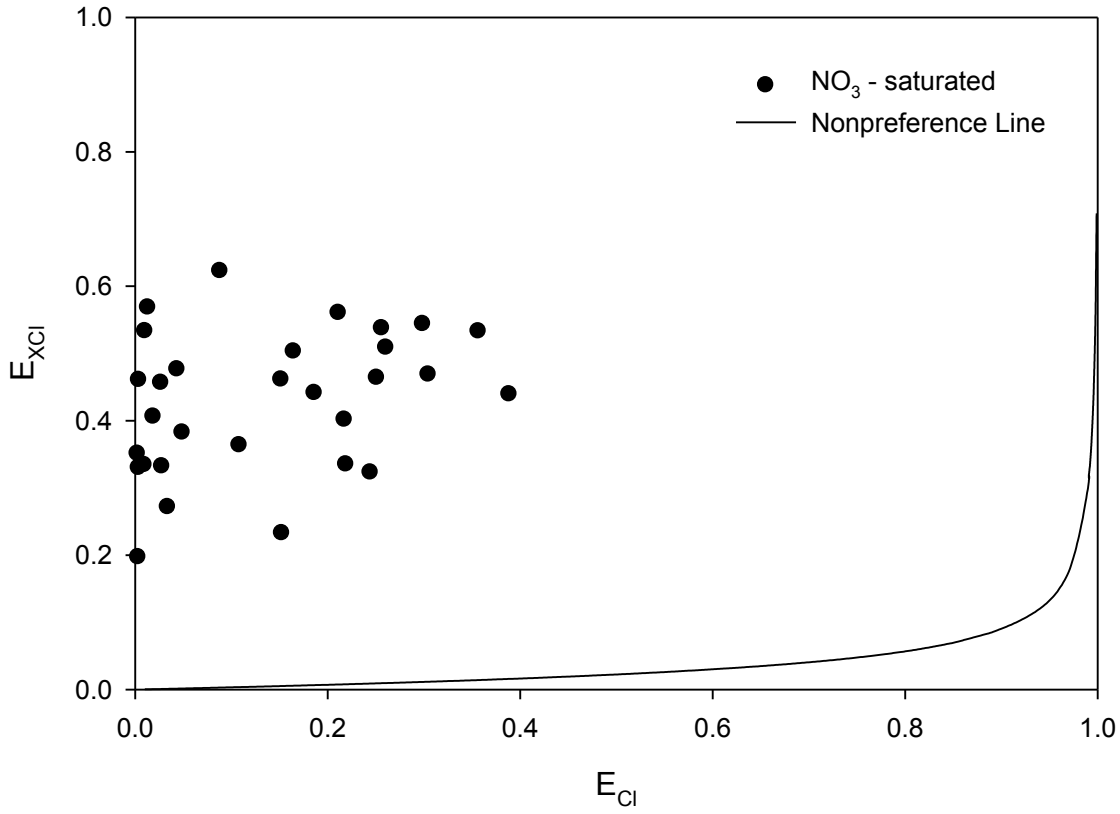

Figure 17. Cl-SO_4 exchange in the presence of NO_3 for 0.0002 TN at a depth of 30 to 46 cm, where E_{Cl} is the equivalent fraction of Cl in solution and E_{XCl} is the equivalent fraction of Cl on the exchange phase for the reaction $2XCl + SO_4^{2-} = X_2SO_4 + 2Cl^-$.

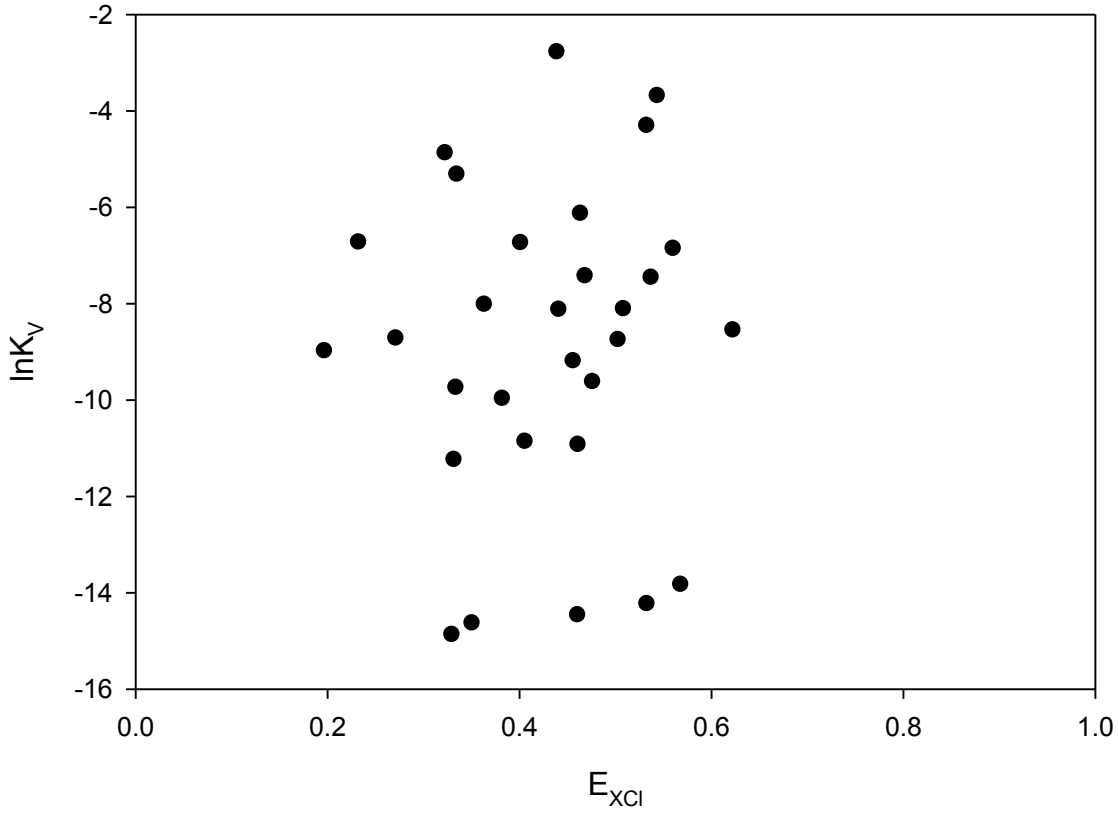

Figure 18. $\ln K_V$ vs. E_{XCl} data plotted for Cl-SO_4 exchange in the presence of NO_3 for 0.0002 TN at a depth of 30 to 46 cm, where $\ln K_V$ is the natural log of the Vanselow selectivity coefficient for the exchange isotherm and E_{XCl} is the equivalent fraction of Cl on the exchange phase for the reaction $2XCl + SO_4^{2-} = X_2SO_4 + 2Cl^-$.

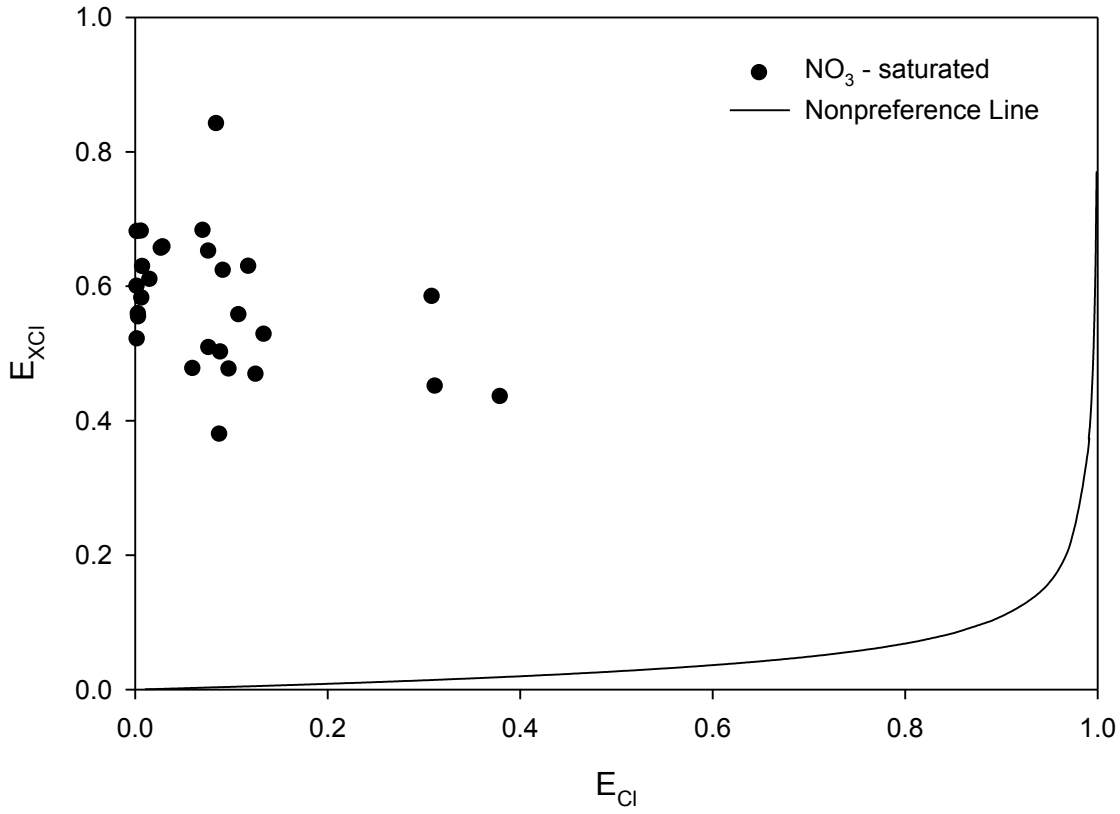

Figure 19. Cl-SO_4 exchange in the presence of NO_3 for 0.0002 TN at a depth of 245 to 261 cm, where E_{Cl} is the equivalent fraction of Cl in solution and E_{XCl} is the equivalent fraction of Cl on the exchange phase for the reaction $2XCl + SO_4^{2-} = X_2SO_4 + 2Cl^-$.

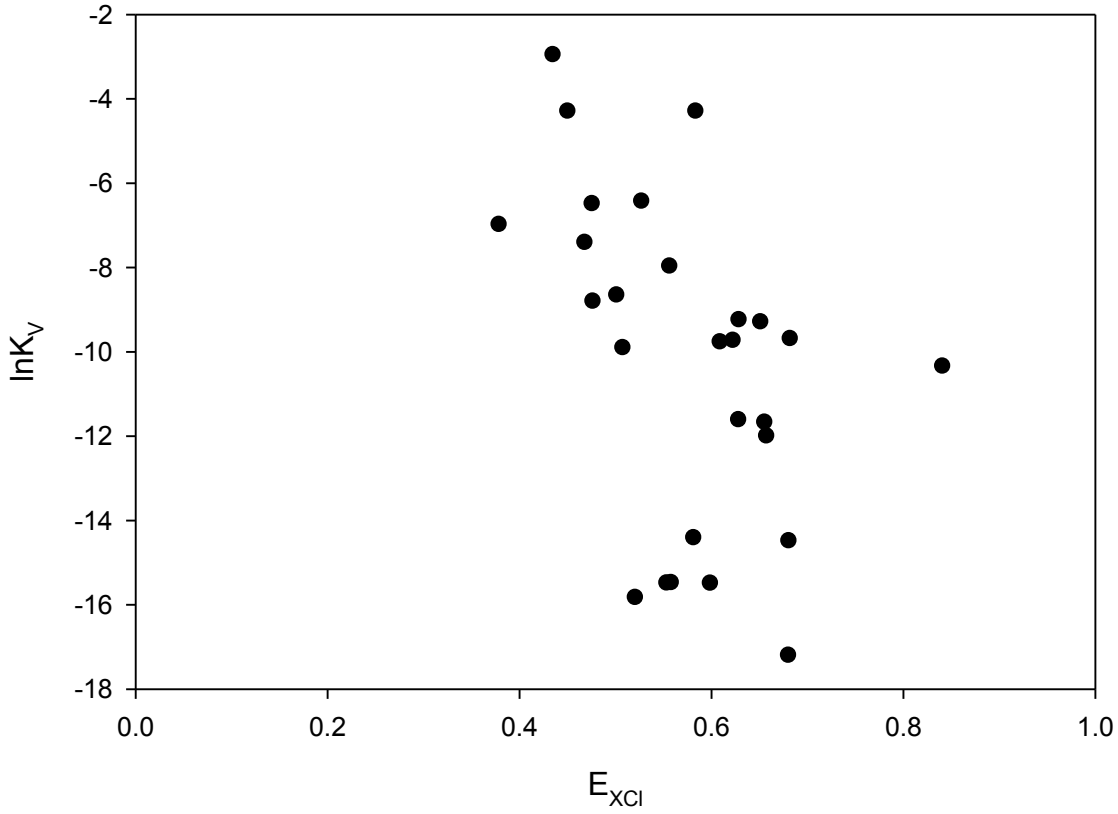

Figure 20. $\ln K_V$ vs. E_{XCl} data plotted for Cl-SO_4 exchange in the presence of NO_3 for 0.0002 TN at a depth of 245 to 261 cm, where $\ln K_V$ is the natural log of the Vanselow selectivity coefficient for the exchange isotherm and E_{XCl} is the equivalent fraction of Cl on the exchange phase for the reaction $2XCl + SO_4^{2-} = X_2SO_4 + 2Cl^-$.

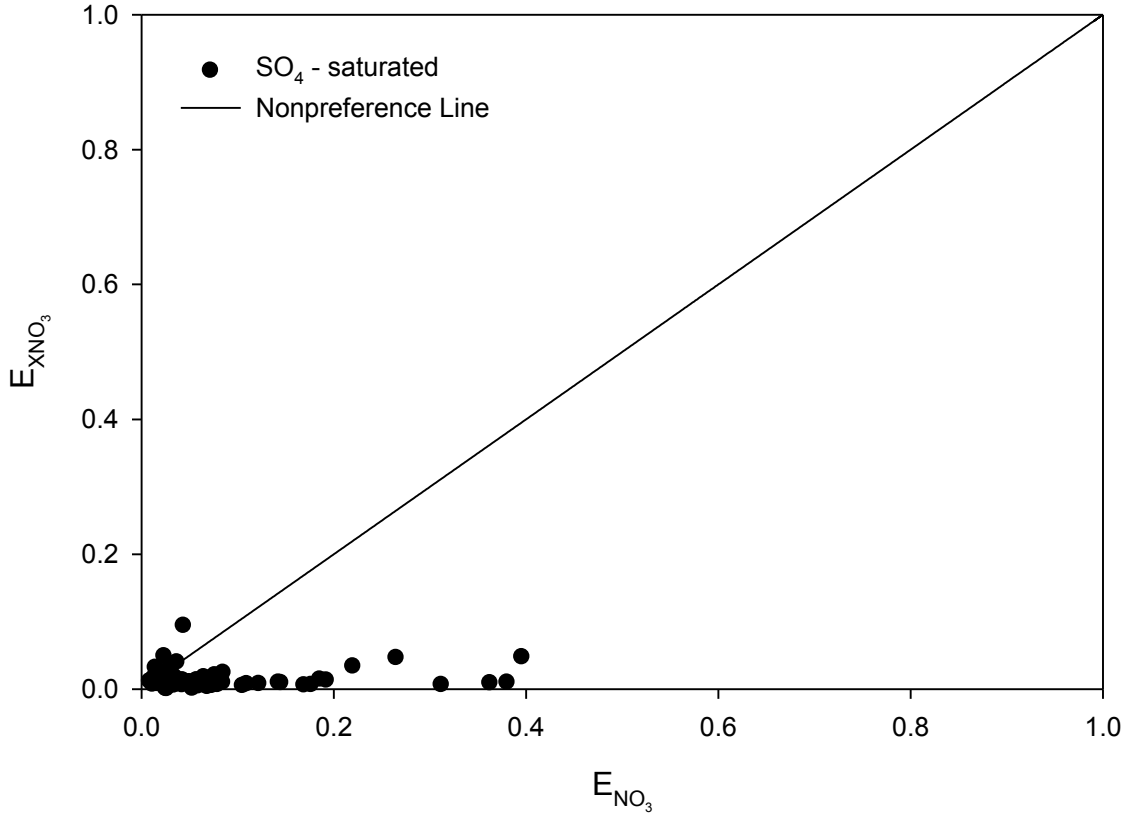

Figure 21. NO_3-Cl exchange in the presence of SO_4 for 0.0002 TN at a depth of 30 to 46 cm, where E_{NO3} is the equivalent fraction of NO_3 in solution and E_{XNO3} is the equivalent fraction of NO_3 on the exchange phase for the reaction $XNO_3 + Cl^- = XCl + NO_3^-$.

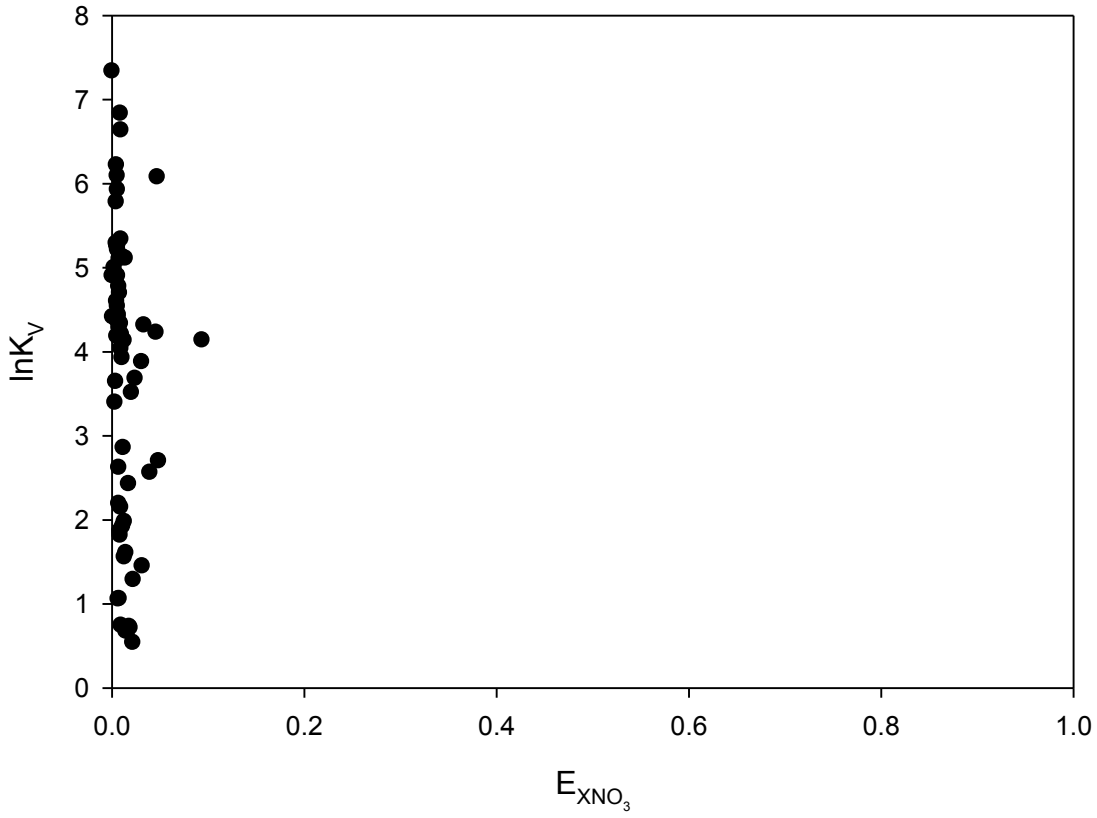

Figure 22. lnK_V vs. E_{XNO3} data plotted for NO_3-Cl exchange in the presence of SO_4 for 0.0002 TN at a depth of 30 to 46 cm, where lnK_V is the natural log of the Vanselow selectivity coefficient for the exchange isotherm and E_{XNO3} is the equivalent fraction of NO_3 on the exchange phase for the reaction $XNO_3 + Cl^- = XCl + NO_3^-$.

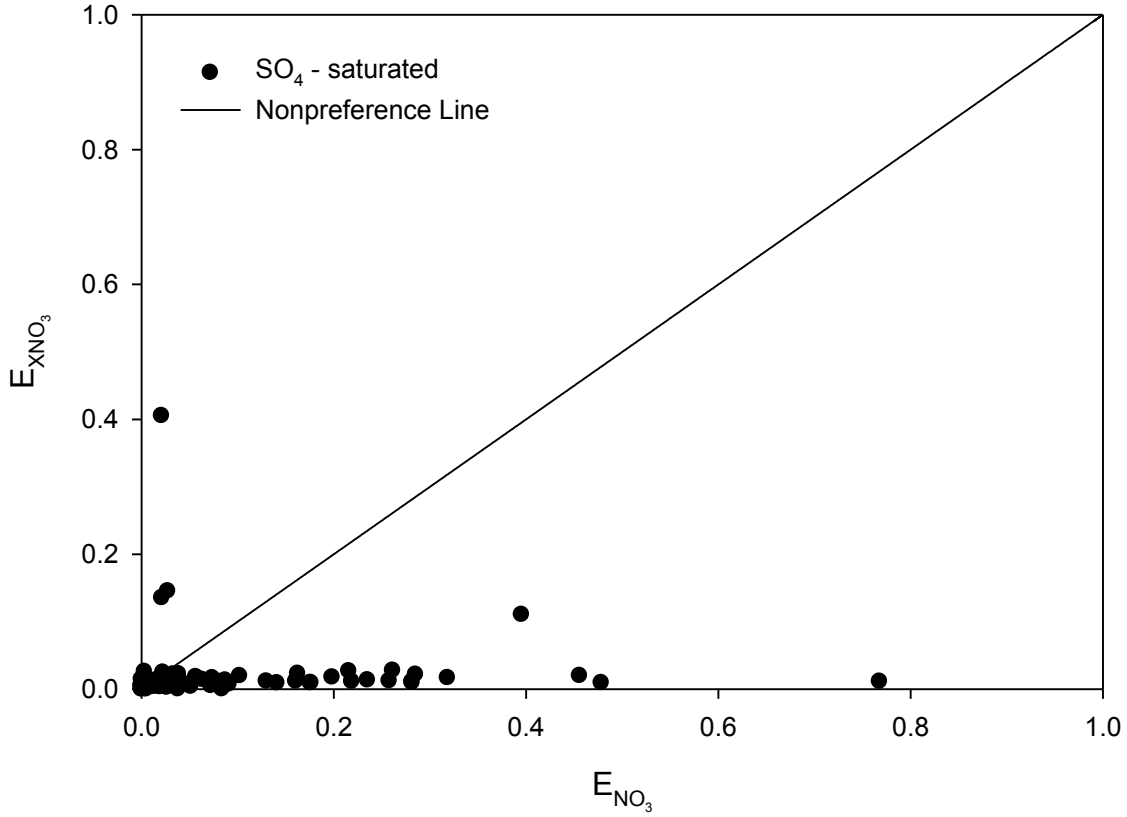

Figure 23. NO_3-Cl exchange in the presence of SO_4 for 0.0002 TN at a depth of 245 to 261 cm, where E_{NO3} is the equivalent fraction of NO_3 in solution and E_{XNO3} is the equivalent fraction of NO_3 on the exchange phase for the reaction $XNO_3 + Cl^- = XCl + NO_3^-$.

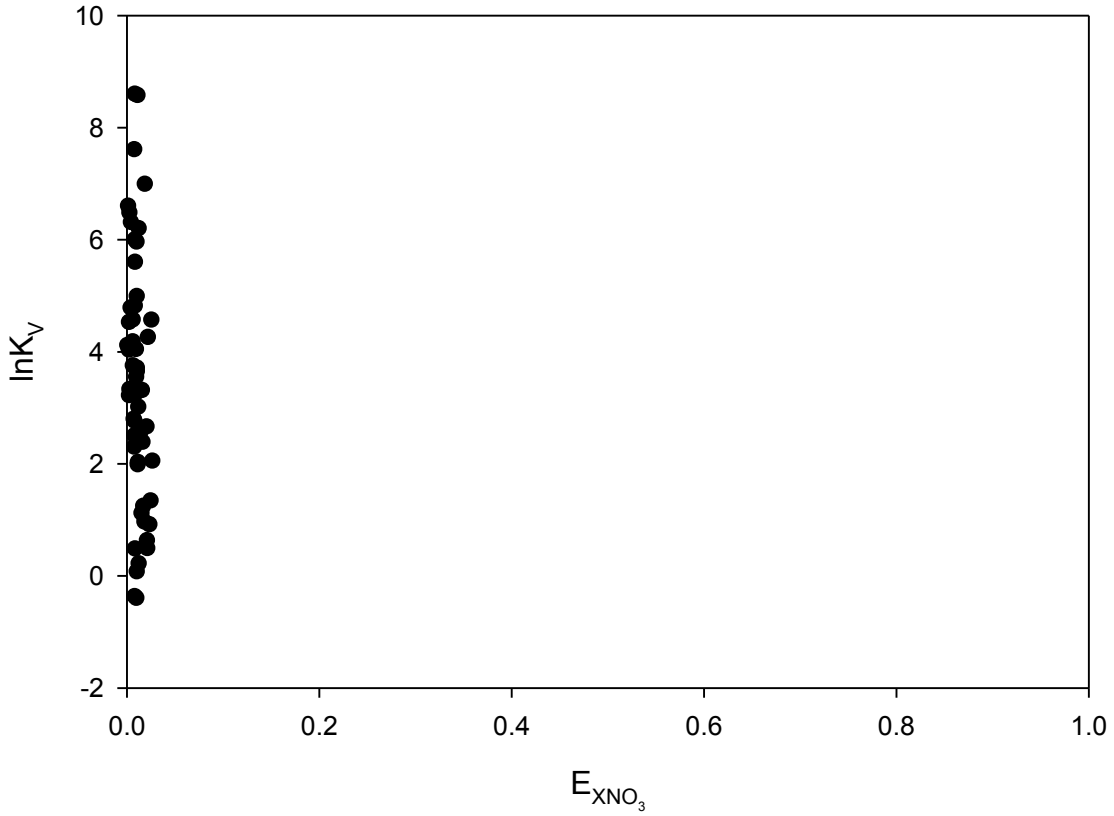

Figure 24. $\ln K_V$ vs. E_{XNO3} data plotted for NO_3-Cl exchange in the presence of SO_4 for 0.0002 TN at a depth of 245 to 261 cm, where $\ln K_V$ is the natural log of the Vanselow selectivity coefficient for the exchange isotherm and E_{XNO3} is the equivalent fraction of NO_3 on the exchange phase for the reaction $XNO_3 + Cl^- = XCl + NO_3^-$.

LITERATURE CITED

American Coal Ash Association. 2011. Coal ash recycling rates remain stalled as regulatory uncertainty continues. Washington, DC.

Ammons, J.T., A.O. Gallagher, R.L. Livingston, J.L. Branson, and R.J. Lewis. 1994. Background levels of nitrate-nitrogen and selected heavy metals for the Ames Plantation Watershed Project. Tenn. Farm Home Sci. 169:30-33.

Bellini, G., M.E. Sumner, D.E. Radcliffe, and N.P. Qafoku. 1996. Anion transport through columns of highly weathered acid soil: Adsorption and retardation. Soil Sci. Soc. Am. J.60:132-137.

Clark, R.B., K.D. Ritchey, and V.C. Baligar. 2001. Benefits and constraints for use of FGD products on agricultural land. Fuel. 80:821-828.

Donn, M.J. and N.W. Menzies. 2005. The effect of ionic strength variation and anion competition on the development of nitrate accumulations in variable charge subsoils. Australian Journal of Soil Research. 43:43-50.

Essington, M.E. 2003. Soil and water chemistry: an integrated approach. CRC Press, Boca Raton, FL.

Essington, M.E., and D.D. Howard. 2000. Phosphorus availability and speciation in long-term no-till and disk-till soil. Soil Sci. 165:144-152

Grove, J.H., C.S. Fowler, and M.E. Sumner. 1982. Determination of the charge character of selected acid soils. Soil Sci. Soc. Am. J. 46:32-38.

He, B., S. Kanae, T. Oki, Y. Hirabayashi, Y. Yamashiki, and K. Tarara. 2011. Assessment of global nitrogen pollution in rivers using an integrated biogeochemical modeling framework. Water Research. 45:2573-2586.

Hingston, F.J., A.M. Posner, and J.P. Quirk. 1942.Influence of potassium chloride on nitrification in Bedford loam. J. Soil Sci. 23:117-192.

Lee, S.S., C.J. Gantzer, A.L. Thompson, and S.H. Anderson. 2010. Polyacrylamide and gypsum amendments for erosion and runoff control on two soil series. Journal of Soil and Water Conservation. 65(4):233-242.

Singh, B.R., and Y. Kanehiro. 1969. Adsorption of nitrate in amorphous and kaolinitic Hawaiian soils. Soil Sci. Soc. Am. Proc. 33:681-683.

Suba, J.D., and M.E. Essington. 1999. Adsorption of Mercury(II) by variable charged surfaces of quartz and gibbsite. Soil Sci. 164:145-155

Sumner, M.E., and J.C. Davidtz. 1965. Positive and negative charges in some Natal soils. S. Afr. J. Agric. Sci. 8:1045-1050.

Truman, C.C., R.C. Nuti, L.R. Truman, and J.D. Dean. 2010. Feasibility of using FDG gypsum to conserve water and reduce erosion from an agricultural soil in Georgia. Catena. 81:234-239.

Tyner, J.S., W.C. Wright, and R.E. Yoder. 2007. Identifying long-term preferential and matrix flow recharge at the field scale. Trans. ASABE 50:2001-2006.

Uehara, G., and G.P. Gillman. 1980. Charge characteristics of soils with variable and permanent charge minerals: II. Experimental. Soil Sci. Soc. Am. J. 44:252-255.

APPENDIX III

Table 1. pH of 10 g sample using 1:1 solid-to-solution with 0.1 M $CaCl_2$

Depth	Plot									
(cm)	1	2	3	4	5	6	7	8	9	10
0-15	6.24	6.59	6.99	6.79	6.70	6.85	6.89	6.84	6.40	5.56
15-30	6.43	6.94	7.00	6.88	6.70	6.91	6.94	7.02	6.70	6.06
30-46	6.15	6.23	6.90	6.60	6.46	6.72	6.71	6.58	6.46	6.08
46-61	6.06	6.53	6.67	6.65	6.91	6.81	6.70	6.67	6.55	6.03
61-76	6.09	6.63	6.78	6.66	6.65	6.74	6.83	6.67	6.46	5.97
76-91	6.32	6.64	6.47	6.53	6.55	6.63	6.75	6.72	6.19	6.15
91-107	6.07	6.66	6.71	6.55	6.39	6.58	6.77	6.68	5.49	6.18
107-122	6.25	6.60	6.71	6.48	6.28	6.57	6.61	6.66	4.64	5.57
122-137	6.27	6.55	6.48	6.44	6.08	6.47	6.46	6.23	4.66	5.06
137-152	6.29	6.50	6.22	6.48	5.98	6.54	6.49	6.30	4.60	4.60
152-168	6.12	6.56	6.52	6.22	6.03	6.40	6.52	6.08	4.64	4.60
168-183	6.14	6.49	6.49	6.36	6.08	6.37	6.48	6.08	4.55	4.84
183-198	6.19	6.48	6.51	6.45	6.08	6.40	6.45	5.91	4.78	5.00
198-213	6.13	6.18	6.34	6.19	6.16	6.47	6.49	5.91	4.66	5.17
213-229	6.14	6.47	6.31	6.20	6.15	6.47	6.43	5.99	5.13	5.01
244-259	6.01	6.40	6.44	6.28	6.13	6.45	6.40	6.15	5.32	4.75
259-274	6.10	6.30	6.40	6.24	6.17	6.36	6.47	6.10	5.30	4.56

Table 2. Concentration (mg/kg) of Fe-, Al-, and Mn-oxide in plot 1 using the sodium citrate-bicarbonate-dithionite (CBD) method.

	Fe			Al			Mn		
Depth	Rep 1	Rep 2	Rep 3	Rep 1	Rep 2	Rep 3	Rep 1	Rep 2	Rep 3
cm	mg/kg								
0-15	7870	8310	8350	1056	1074	1078	988	1030	1039
15-30	14580	13330	14150	1983	1857	2028	817	742	791
30-46	16250	15770	16050	2091	1965	2029	811	758	781
46-61	15420	15130	15220	2018	2019	2020	470	461	465
61-76	14140	14010	14490	1881	1833	1776	447	450	471
76-91	11060	12510	11420	1706	1683	1543	468	478	482
91-107	12260	12090	12410	1659	1545	1622	643	669	687
107-122	11670	10760	10830	1556	1337	1310	571	540	530
122-137	9220	7770	9790	1294	970	1314	481	404	498
137-152	9410	8340	9560	1155	1029	1088	468	409	478
152-168	9080	8650	9490	1113	980	1112	483	448	491
168-183	8890	8850	6610	1101	1170	802	410	447	326
183-198	10450	10370	10120	1203	1214	1144	434	458	416
198-213	10660	10050	10530	1258	1103	1224	354	316	342
213-229	11660	11740	11460	1376	1207	1190	274	276	272
229-245	12330	11390	11670	1507	1274	1332	152	141	137
245-261	13240	13370	13990	1544	1341	1413	147	142	146

Table 3. Concentration (mg/kg) of Fe-, Al-, and Mn-oxide in plot 2 using the sodium citrate-bicarbonate-dithionite (CBD) method.

	Fe			Al			Mn		
Depth	Rep 1	Rep 2	Rep 3	Rep 1	Rep 2	Rep 3	Rep 1	Rep 2	Rep 3
cm	mg/kg								
0-15	7940	7770	7570	910	933	931	1136	1118	1094
15-30	14760	14720	14580	1921	1875	1837	813	828	801
30-46	17950	17840	18090	2304	2279	2344	517	526	533
46-61	13560	14320	14330	1996	2097	2017	413	452	467
61-76	14130	13750	10650	1967	1824	1289	401	413	318
76-91	13570	12810	13110	1644	1481	1552	598	565	573
91-107	11810	11450	11660	1451	1446	1446	649	645	664
107-122	10130	9680	10030	1315	1240	1284	484	453	479
122-137	10750	10060	10620	1167	1143	1072	449	437	446
137-152	8920	8540	8680	1107	1051	1065	331	314	334
152-168	8720	8740	8700	968	1080	1102	408	397	399
168-183	9420	9240	9730	1062	1022	955	507	463	511
183-198	11020	10770	11480	1113	1102	1174	534	508	556
198-213	11430	11320	11440	1057	1094	1116	418	420	417
213-229	11330	12540	10170	1061	1125	970	289	291	255
229-245	13130	11350	13050	1238	1064	1215	199	170	192
245-261	13700	13840	13650	1473	1465	1472	140	133	138

Table 4. Concentration (mg/kg) of Fe-, Al-, and Mn-oxide in plot 3 using the sodium citrate-bicarbonate-dithionite (CBD) method.

	Fe			Al			Mn		
Depth	Rep 1	Rep 2	Rep 3	Rep 1	Rep 2	Rep 3	Rep 1	Rep 2	Rep 3
cm	mg/kg								
0-15	8020	8160	8370	930	923	989	1243	1313	1291
15-30	13030	12020	12550	1621	1448	1601	983	909	950
30-46	16490	16820	16600	2130	2088	2060	641	655	641
46-61	15400	13590	15340	2062	1820	2122	567	489	558
61-76	12060	14600	14120	1644	1864	1831	327	404	390
76-91	13980	12910	13310	1716	1663	1756	490	461	475
91-107	12420	11980	11900	1425	1522	1515	469	444	433
107-122	11710	11680	11520	1273	1309	1356	530	530	533
122-137	11000	10930	10890	1376	1214	1234	619	601	601
137-152	10340	8680	10740	1139	972	1300	587	536	606
152-168	8410	9410	9520	932	1051	1047	513	571	614
168-183	9900	9790	9850	1072	1065	1255	595	527	605
183-198	11250	11780	11000	1186	1146	1165	522	571	502
198-213	11760	12560	11920	1270	1203	1219	389	455	427
213-229	13170	13270	13240	1357	1347	1471	302	318	300
229-245	15210	15260	14740	1664	1490	1613	187	185	197
245-261	15590	14200	17110	1689	1638	1796	142	126	151

Table 5. Concentration (mg/kg) of Fe-, Al-, and Mn-oxide in plot 4 using the sodium citrate-bicarbonate-dithionite (CBD) method.

	Fe			Al			Mn		
Depth	Rep 1	Rep 2	Rep 3	Rep 1	Rep 2	Rep 3	Rep 1	Rep 2	Rep 3
cm	mg/kg								
0-15	8270	8550	8440	1041	1090	1126	1029	1068	1037
15-30	15510	15190	13690	1918	1822	1599	840	886	762
30-46	17440	17080	16510	2093	2084	1974	758	750	725
46-61	15390	16310	15150	1911	1982	1796	511	534	505
61-76	14270	14160	14110	1817	1833	1854	564	532	533
76-91	13510	13410	12760	1752	1792	1672	478	466	446
91-107	11520	12940	12360	1280	1473	1335	482	561	521
107-122	12110	12370	9450	1345	1421	973	607	639	493
122-137	11200	11390	10680	1275	1350	1252	637	639	606
137-152	10700	10050	10290	1342	1196	1254	597	573	604
152-168	9910	9640	8900	1071	1039	865	489	503	459
168-183	9000	9630	9030	987	1097	1095	486	492	449
183-198	13040	10780	10570	1365	1140	1008	677	571	586
198-213	13310	11520	10640	1369	1203	1002	724	622	585
213-229	11430	11690	11660	1442	1192	1239	480	495	469
229-245	12990	12200	10480	1427	1323	970	411	367	310
245-261	11870	12040	11940	1454	1311	1327	377	408	381

Table 6. Concentration (mg/kg) of Fe-, Al-, and Mn-oxide in plot 5 using the sodium citrate-bicarbonate-dithionite (CBD) method.

	Fe			Al			Mn		
Depth	Rep 1	Rep 2	Rep 3	Rep 1	Rep 2	Rep 3	Rep 1	Rep 2	Rep 3
cm	mg/kg								
0-15	6330	6210	6450	717	750	797	1227	1252	1222
15-30	13790	13620	13610	1736	1733	1746	643	637	652
30-46	18620	17870	19680	2945	2345	3117	701	692	741
46-61	19790	12930	15800	3162	2003	2140	678	523	556
61-76	13620	9000	13490	1785	1281	1779	441	343	439
76-91	12490	12800	12120	1487	1450	1495	358	361	356
91-107	11730	10680	12520	1259	1224	1283	450	463	478
107-122	11840	13990	14340	1166	1821	1473	641	739	801
122-137	10170	10640	10600	1162	1188	1178	557	604	604
137-152	10120	9290	9130	1140	1095	1144	560	517	537
152-168	9180	9200	8060	1022	1185	1100	557	555	539
168-183	9340	8880	8630	1084	1021	1057	592	592	546
183-198	10450	10490	10760	1222	1195	1139	679	620	670
198-213	11290	11310	11560	1239	1246	1260	614	624	664
213-229	11800	11070	11220	1251	1233	1245	435	438	396
229-245	12440	11990	12190	1332	1229	1360	345	334	357
245-261	13970	13270	13620	1603	1437	1567	197	188	205

Table 7. Concentration (mg/kg) of Fe-, Al-, and Mn-oxide in plot 6 using the sodium citrate-bicarbonate-dithionite (CBD) method.

	Fe			Al			Mn		
Depth	Rep 1	Rep 2	Rep 3	Rep 1	Rep 2	Rep 3	Rep 1	Rep 2	Rep 3
cm	mg/kg								
0-15	6690	6230	6450	751	777	801	1384	1274	1331
15-30	13760	13600	14190	1658	1646	1715	908	1005	989
30-46	15830	17300	17180	2409	2379	2431	879	854	852
46-61	16520	14360	15720	2142	1833	2019	578	536	573
61-76	11990	12230	11710	1526	1516	1819	464	463	444
76-91	12580	12700	12730	1354	1423	1477	432	456	443
91-107	11990	11840	11790	1289	1255	1299	578	584	564
107-122	10210	12650	11350	1640	1445	1134	362	740	660
122-137	10220	10720	10040	1226	1158	1056	622	590	578
137-152	9320	9480	9740	898	945	985	523	533	545
152-168	9040	9160	8700	934	963	994	582	546	512
168-183	9120	8820	9360	838	777	834	449	456	506
183-198	9380	8800	9210	936	1013	1108	588	621	672
198-213	11210	13070	12280	1258	1472	1058	663	816	755
213-229	10930	10740	11540	1092	1064	1108	537	558	567
229-245	12020	12690	13200	1259	1360	1276	289	312	310
245-261	13400	14370	13570	1435	1602	1801	272	284	272

Table 8. Concentration (mg/kg) of Fe-, Al-, and Mn-oxide in plot 7 using the sodium citrate-bicarbonate-dithionite (CBD) method.

	Fe			Al			Mn		
Depth	Rep 1	Rep 2	Rep 3	Rep 1	Rep 2	Rep 3	Rep 1	Rep 2	Rep 3
cm	mg/kg								
0-15	6380	6930	6810	777	877	791	1244	1384	1393
15-30	10450	10950	10950	1464	1313	1320	947	902	951
30-46	17350	17840	18630	2174	2429	2370	509	590	576
46-61	16840	16420	17410	2240	2251	2538	662	653	705
61-76	15660	14920	15830	1876	1857	1993	798	769	800
76-91	13500	13240	12730	1381	1456	1477	594	578	443
91-107	12610	12570	12320	1126	1280	1238	458	490	458
107-122	11550	11890	12100	1168	1177	1205	431	428	454
122-137	11670	11880	12550	1238	1187	1222	675	654	701
137-152	11190	11460	10900	1029	1244	1078	643	675	665
152-168	10100	10040	10870	1373	1161	1121	650	637	649
168-183	10880	10410	10510	1221	1309	1243	634	638	666
183-198	9270	9380	9740	1126	1247	1206	587	671	630
198-213	10120	10710	10230	1187	1296	1235	809	771	708
213-229	11530	11520	11000	1574	1280	1392	746	801	782
229-245	12940	12700	13310	1403	1512	1537	679	679	773
245-261	13410	13660	14110	1467	1492	1673	337	356	402

Table 9. Concentration (mg/kg) of Fe-, Al-, and Mn-oxide in plot 8 using the sodium citrate-bicarbonate-dithionite (CBD) method.

	Fe			Al			Mn		
Depth	Rep 1	Rep 2	Rep 3	Rep 1	Rep 2	Rep 3	Rep 1	Rep 2	Rep 3
cm	mg/kg								
0-15	6030	6680	6640	763	820	802	1405	1442	1467
15-30	10540	11210	9320	1443	1618	1296	1069	1200	952
30-46	15520	16070	16440	2390	2274	2317	667	684	719
46-61	16540	17080	17020	2195	2217	2253	658	645	673
61-76	12010	11220	13730	1566	1514	1737	614	591	734
76-91	10320	10880	11570	1201	1307	1304	487	486	516
91-107	11830	11450	11980	1269	1251	1248	679	656	691
107-122	13260	12780	12550	1345	1245	1275	801	759	748
122-137	13220	12130	12840	1058	1025	1105	673	649	679
137-152	11040	11320	10490	990	964	982	463	480	478
152-168	10350	10510	10530	1035	944	1051	512	518	498
168-183	11200	10960	10800	1045	1009	943	592	609	610
183-198	9380	9080	8720	1068	956	987	638	658	647
198-213	9810	9130	9580	1082	1048	1175	936	950	923
213-229	11970	11020	11560	1450	1229	1302	1004	947	921
229-245	11890	12560	11440	1388	1536	1314	924	933	794
245-261	13070	12360	13740	1404	1384	1481	693	697	737

Table 10. Concentration (mg/kg) of Fe-, Al-, and Mn-oxide in plot 9 using the sodium citrate-bicarbonate-dithionite (CBD) method.

	Fe			Al			Mn		
Depth	Rep 1	Rep 2	Rep 3	Rep 1	Rep 2	Rep 3	Rep 1	Rep 2	Rep 3
cm	mg/kg								
0-15	6540	5810	6570	695	596	692	1211	1156	1265
15-30	10600	10090	11390	1536	1502	1547	835	802	863
30-46	18300	13820	17160	2608	1900	2389	946	742	861
46-61	14830	13960	15730	2009	1987	2043	736	751	817
61-76	11850	12080	11930	1393	1502	1349	416	384	364
76-91	10640	13010	11920	1121	1367	1217	384	464	406
91-107	15470	13860	12570	1449	1280	1179	720	617	564
107-122	13520	13180	13460	1411	1413	1267	854	792	789
122-137	12390	12120	12660	1177	1111	1195	946	935	1016
137-152	13610	11660	13220	1278	1069	1206	1026	850	1047
152-168	12480	10840	10820	1141	932	957	893	791	771
168-183	11490	11450	12110	1281	1293	1212	885	856	901
183-198	11090	10910	11250	965	960	992	924	868	901
198-213	10680	10070	9860	1031	1005	932	900	871	876
213-229	10640	10990	10610	1190	1230	1166	949	995	934
229-245	11960	11920	12310	1375	1471	1371	1214	1352	1126
245-261	12990	12710	13220	1593	1507	1654	1332	1184	1249

Table 11. Concentration (mg/kg) of Fe-, Al-, and Mn-oxide in plot 10 using the sodium citrate-bicarbonate-dithionite (CBD) method.

	Fe			Al			Mn		
Depth	Rep 1	Rep 2	Rep 3	Rep 1	Rep 2	Rep 3	Rep 1	Rep 2	Rep 3
cm	mg/kg								
0-15	7080	7520	6840	804	844	786	1196	1227	1136
15-30	9820	9740	9630	1375	1437	1308	1021	1002	1032
30-46	15820	15590	15050	2255	2223	2220	479	486	449
46-61	17600	17750	17070	2435	2540	2319	713	715	720
61-76	17990	17410	18690	2307	2237	2345	935	948	968
76-91	12570	11860	11380	1357	1405	1314	369	372	372
91-107	10840	11480	11180	1256	1171	1276	232	252	248
107-122	11940	12550	11980	1199	1190	1144	304	316	294
122-137	11470	11610	11990	1003	976	1090	366	372	373
137-152	11020	11440	10300	937	999	945	393	438	388
152-168	11050	11550	11120	1063	1082	1112	573	579	642
168-183	10870	10130	10130	1037	943	927	567	500	511
183-198	11040	11610	11180	975	1038	956	622	665	659
198-213	9890	10580	10490	1080	1089	1056	532	601	554
213-229	9340	10050	9880	939	1068	1038	710	842	822
229-245	10340	10770	10350	1325	1371	1315	1156	1246	1157
245-261	11130	12260	11700	1531	1606	1577	1536	1752	1649

Table 12. Concentration (mg/kg) of Si extracted using the sodium citrate-bicarbonate-dithionite (CBD) method.

		Plot									
Depth	Rep	1	2	3	4	5	6	7	8	9	10
cm		mg/kg									
0-15	1	592	513	569	615	141	212	260	625	438	231
	2	632	574	525	646	506	294	777	667	355	182
	3	609	552	592	655	578	354	604	675	422	165
15-30	1	773	814	720	551	410	403	390	698	506	230
	2	714	834	702	550	664	674	613	802	440	225
	3	795	765	756	479	665	683	670	622	439	174
30-46	1	675	796	474	517	1171	554	381	836	520	312
	2	636	772	470	548	633	789	911	738	383	283
	3	624	783	486	482	1249	874	669	792	414	267
46-61	1	800	720	711	498	1166	619	277	509	491	252
	2	727	764	628	516	608	480	651	485	423	308
	3	719	735	718	416	545	548	702	558	376	239
61-76	1	688	817	330	688	256	208	370	409	513	234
	2	619	765	338	631	466	472	652	568	495	276
	3	635	567	370	605	576	906	661	461	454	256
76-91	1	767	594	607	680	413	325	404	628	476	192
	2	607	533	613	698	349	360	722	490	536	218
	3	594	578	613	638	379	392	392	658	554	145
91-107	1	710	594	509	325	625	536	435	635	657	328
	2	595	572	627	457	657	518	837	772	585	257
	3	523	529	641	330	649	565	817	538	574	305
107-122	1	704	665	291	458	580	270	463	1014	715	452
	2	546	621	283	533	1190	1257	839	996	639	443
	3	488	668	343	339	706	750	861	939	552	454
122-137	1	701	538	760	560	373	589	953	704	660	528
	2	534	523	680	560	665	681	910	674	584	466
	3	674	478	664	484	677	579	870	748	664	549
137-152	1	612	631	607	695	370	409	327	873	690	549
	2	556	606	558	629	670	789	757	916	614	583
	3	540	606	729	655	679	810	662	918	671	550
152-168	1	632	558	502	464	310	442	440	896	758	524
	2	496	631	602	441	816	579	677	847	603	575
	3	546	648	625	319	789	569	589	999	628	637
168-183	1	774	491	580	568	294	701	354	689	777	656
	2	648	479	637	653	582	636	798	795	714	523
	3	473	431	699	651	594	637	693	597	668	516
183-198	1	725	489	335	488	305	345	216	975	739	486
	2	610	474	300	423	319	722	634	846	666	571
	3	590	519	311	296	275	762	621	863	746	536

Table 12. Concentration (mg/kg) of Si extracted using the sodium citrate-bicarbonate-dithionite (CBD) method. (continued)

		Plot									
Depth	Rep	1	2	3	4	5	6	7	8	9	10
cm		mg/kg									
198-213	1	685	415	301	431	281	441	267	731	663	465
	2	554	448	273	366	259	895	560	761	606	482
	3	754	428	286	330	292	548	594	859	585	479
213-229	1	669	438	587	676	230	245	357	867	552	304
	2	511	411	615	473	524	529	541	680	569	409
	3	474	383	616	414	505	559	591	727	484	378
229-245	1	790	403	709	391	153	230	227	752	497	304
	2	537	363	536	422	449	576	734	792	474	318
	3	560	415	611	149	471	490	742	656	453	308
245-261	1	616	553	573	566	243	146	168	507	454	261
	2	484	590	554	452	483	508	526	619	394	257
	3	474	564	617	454	567	794	615	414	462	235

Table 13. Concentration (mg/kg) of Fe-, Al-, and Mn-oxide in plot 1 using the ammonium oxalate extraction (AAO) method.

	Fe			Al			Mn		
Depth	Rep 1	Rep 2	Rep 3	Rep 1	Rep 2	Rep 3	Rep 1	Rep 2	Rep 3
cm	mg/kg								
0-15	1634	1558	969	648	621	762	887	888	897
15-30	2585	2548	1625	1118	1103	1280	776	817	771
30-46	2405	2429	1947	1085	1117	1444	524	535	577
46-61	2324	2245	1492	1084	1043	1127	298	286	270
61-76	2149	1994	1690	943	944	1176	274	252	305
76-91	2248	1827	982	979	872	902	284	281	237
91-107	2020	1915	1420	878	874	1025	373	374	377
107-122	1702	1580	1057	785	748	805	324	326	294
122-137	1928	1771	1224	797	826	921	377	389	380
137-152	1607	1601	949	706	749	774	345	363	297
152-168	1718	1651	860	748	757	719	389	397	323
168-183	1742	1739	1136	822	839	919	431	454	421
183-198	1689	1039	1072	940	978	1008	496	508	458
198-213	1306	845	3108	931	1025	610	389	427	607
213-229	1286	943	794	788	977	947	300	343	374
229-245	949	718	790	818	981	868	105	123	283
245-261	925	653	735	798	924	974	81	97	112

Table 14. Concentration (mg/kg) of Fe-, Al-, and Mn-oxide in plot 2 using the ammonium oxalate extraction (AAO) method.

	Fe			Al			Mn		
Depth	Rep 1	Rep 2	Rep 3	Rep 1	Rep 2	Rep 3	Rep 1	Rep 2	Rep 3
cm	mg/kg								
0-15	1455	1415	757	625	623	654	1014	994	917
15-30	2872	2170	1295	1274	1019	1094	938	769	772
30-46	3108	2623	1442	1540	1352	1300	399	342	335
46-61	1970	1845	1119	1010	1013	1061	303	290	299
61-76	1981	1887	1091	922	944	940	249	241	237
76-91	2058	1843	1210	946	882	973	358	309	365
91-107	1976	2122	1391	902	930	1071	397	436	486
107-122	1732	1701	943	788	803	812	360	359	344
122-137	1773	1705	1005	796	795	841	319	292	306
137-152	1478	1553	914	722	773	806	257	273	281
152-168	1509	1667	1028	737	812	859	323	346	349
168-183	1625	1712	890	777	814	753	416	431	373
183-198	1466	626	1006	881	894	962	475	82	500
198-213	1203	1037	809	861	1000	1007	412	512	421
213-229	1097	758	658	834	917	898	269	422	257
229-245	1100	644	634	843	880	919	249	252	141
245-261	1035	592	639	920	961	995	78	74	81

Table 15. Concentration (mg/kg) of Fe-, Al-, and Mn-oxide in plot 3 using the ammonium oxalate extraction (AAO) method.

	Fe			Al			Mn		
Depth	Rep 1	Rep 2	Rep 3	Rep 1	Rep 2	Rep 3	Rep 1	Rep 2	Rep 3
cm	mg/kg								
0-15	1600	1467	1431	737	722	656	1001	941	915
15-30	2261	1678	1894	1006	854	855	862	821	715
30-46	2966	2704	2830	1330	1240	1307	453	412	416
46-61	2404	2578	2345	1173	1270	1119	332	381	332
61-76	2291	1976	2057	1020	930	926	235	213	214
76-91	1604	1500	1422	771	754	681	246	241	210
91-107	1588	1609	1660	693	756	758	262	266	259
107-122	2047	1951	1924	786	786	739	335	338	314
122-137	2313	2552	2723	850	953	969	417	475	491
137-152	2501	2188	2881	909	838	1041	469	392	492
152-168	1930	2102	2327	790	866	920	426	453	473
168-183	2020	2250	2297	905	949	945	464	473	487
183-198	1753	1876	1900	940	977	973	443	469	464
198-213	1312	1258	1356	970	878	969	343	315	342
213-229	1145	1226	1351	889	908	970	224	221	235
229-245	1270	1177	1298	979	875	998	120	105	119
245-261	1380	1393	1396	1012	979	991	84	86	83

Table 16. Concentration (mg/kg) of Fe-, Al-, and Mn-oxide in plot 4 using the ammonium oxalate extraction (AAO) method.

	Fe			Al			Mn		
Depth	Rep 1	Rep 2	Rep 3	Rep 1	Rep 2	Rep 3	Rep 1	Rep 2	Rep 3
cm	mg/kg								
0-15	1723	1526	1536	745	902	612	984	368	890
15-30	2883	2911	3114	1264	1099	1135	783	781	749
30-46	3108	3240	3402	1363	1215	1274	556	574	525
46-61	2707	2870	3588	1240	866	1262	347	460	382
61-76	2711	3264	3042	1149	1268	1092	370	405	344
76-91	2684	2742	2509	1154	1072	897	362	360	319
91-107	2321	2033	2837	803	776	823	349	272	359
107-122	2913	2427	3186	957	784	936	457	361	431
122-137	3018	2996	3246	918	868	922	477	455	454
137-152	2834	2530	3162	888	793	897	469	444	464
152-168	2565	2336	2842	874	746	873	416	376	400
168-183	2303	2234	2751	827	812	839	431	435	444
183-198	2184	2049	2635	947	845	994	481	449	509
198-213	1933	1739	2202	956	844	955	577	516	550
213-229	1696	1619	78	868	824	10	471	442	16
229-245	1479	1510	1396	563	893	769	860	361	328
245-261	1629	1613	1646	923	898	884	375	377	373

Table 17. Concentration (mg/kg) of Fe-, Al-, and Mn-oxide in plot 5 using the ammonium oxalate extraction (AAO) method.

	Fe			Al			Mn		
Depth	Rep 1	Rep 2	Rep 3	Rep 1	Rep 2	Rep 3	Rep 1	Rep 2	Rep 3
cm	mg/kg								
0-15	1928	1889	1838	772	659	765	1228	1288	1304
15-30	2897	2611	3072	1069	989	1195	749	671	784
30-46	3558	3516	3594	1341	1347	1537	635	619	623
46-61	2838	2614	2595	1220	1121	1285	423	367	360
61-76	1585	1361	1459	739	625	746	208	169	178
76-91	1979	1763	2111	698	600	814	238	204	229
91-107	3102	3252	3486	785	820	999	361	365	370
107-122	3282	3204	3432	824	780	984	514	496	524
122-137	3408	3444	3942	847	872	1102	526	512	592
137-152	3330	3456	3672	909	919	1031	515	522	549
152-168	2759	2984	2798	815	951	907	537	556	523
168-183	2410	2752	2733	815	917	992	512	560	559
183-198	2958	2626	2508	1044	1115	1062	716	634	604
198-213	2210	1826	2194	1020	1120	1130	649	464	653
213-229	1842	2273	1622	1050	1220	1022	453	682	412
229-245	1651	1690	1610	985	1108	1012	418	446	421
245-261	1726	1586	1658	1027	1071	1080	195	183	181

Table 18. Concentration (mg/kg) of Fe-, Al-, and Mn-oxide in plot 6 using the ammonium oxalate extraction (AAO) method.

	Fe			Al			Mn		
Depth	Rep 1	Rep 2	Rep 3	Rep 1	Rep 2	Rep 3	Rep 1	Rep 2	Rep 3
cm	mg/kg								
0-15	1806	2993	1517	715	1110	668	1456	1042	1315
15-30	2864	1998	2400	1087	764	1103	1112	1474	1052
30-46	3612	3402	2810	1438	1303	1351	689	617	583
46-61	2131	2011	1745	1061	953	1032	333	295	303
61-76	2251	1498	1144	1147	773	689	334	229	197
76-91	3078	2632	1998	998	908	808	382	335	293
91-107	3546	3774	2802	905	982	835	435	484	404
107-122	3558	3714	3078	903	915	871	529	580	535
122-137	3126	3030	2533	813	802	769	469	485	449
137-152	2614	2735	2114	695	760	697	416	461	406
152-168	2953	2500	2010	791	779	730	524	477	437
168-183	2293	2046	1696	722	714	671	337	338	300
183-198	2248	2187	1892	841	914	862	528	544	512
198-213	2307	1810	1670	1024	896	890	688	583	577
213-229	1946	1642	1616	985	932	1026	588	546	583
229-245	1844	1546	1459	953	950	976	308	281	290
245-261	1610	1331	1235	890	895	895	236	234	228

Table 19. Concentration (mg/kg) of Fe-, Al-, and Mn-oxide in plot 7 using the ammonium oxalate extraction (AAO) method.

	Fe			Al			Mn		
Depth	Rep 1	Rep 2	Rep 3	Rep 1	Rep 2	Rep 3	Rep 1	Rep 2	Rep 3
cm	mg/kg								
0-15	1760	1692	1703	719	679	722	1250	1132	1187
15-30	1864	2164	1765	892	970	811	746	772	695
30-46	3636	4140	3450	1561	1709	1518	398	424	388
46-61	2872	3486	3072	1448	1610	1476	423	488	472
61-76	2062	2727	2059	982	1155	965	390	475	379
76-91	2022	2392	2098	758	818	755	313	343	322
91-107	2825	3534	3894	719	866	925	286	347	380
107-122	2969	3834	3732	786	876	847	317	366	344
122-137	3120	3300	3720	764	785	853	464	466	507
137-152	2945	3342	3834	792	854	929	452	489	515
152-168	3390	3522	4050	994	1037	1081	518	538	581
168-183	3870	3144	3786	1180	1009	1139	576	512	565
183-198	3210	2884	3096	1127	1067	1120	553	527	533
198-213	2845	2401	2824	1120	1035	1144	647	572	626
213-229	2285	2174	2321	1100	1117	1117	650	673	658
229-245	2023	1775	2119	1081	1006	1126	646	644	668
245-261	1651	1493	1710	1037	988	1047	348	352	371

Table 20. Concentration (mg/kg) of Fe-, Al-, and Mn-oxide in plot 8 using the ammonium oxalate extraction (AAO) method.

	Fe			Al			Mn		
Depth	Rep 1	Rep 2	Rep 3	Rep 1	Rep 2	Rep 3	Rep 1	Rep 2	Rep 3
cm	mg/kg								
0-15	1994	1765	1745	748	664	686	1216	1115	1079
15-30	2423	2365	2268	1052	1027	1063	1049	1058	997
30-46	2923	2558	2720	1493	1290	1408	491	451	475
46-61	1894	2054	1912	1039	1162	1164	406	451	425
61-76	1343	1369	1331	725	773	793	292	307	302
76-91	1589	1436	1421	658	617	635	252	224	231
91-107	2218	2064	2389	757	719	838	389	385	433
107-122	3438	3054	3150	859	837	874	548	513	520
122-137	3042	2625	2845	740	710	775	473	424	451
137-152	2426	2307	2458	706	697	767	326	316	338
152-168	2280	2226	2136	753	720	733	348	356	336
168-183	2516	2299	2315	812	787	799	400	391	383
183-198	2234	2104	2116	743	727	736	482	473	475
198-213	2128	2005	2160	829	801	850	693	689	689
213-229	1873	1889	2145	883	971	1025	656	673	719
229-245	1814	1566	1792	1039	944	1026	729	630	692
245-261	1572	1559	1648	910	964	976	567	559	580

Table 21. Concentration (mg/kg) of Fe-, Al-, and Mn-oxide in plot 9 using the ammonium oxalate extraction (AAO) method.

	Fe			Al			Mn		
Depth	Rep 1	Rep 2	Rep 3	Rep 1	Rep 2	Rep 3	Rep 1	Rep 2	Rep 3
cm	mg/kg								
0-15	2095	2252	2606	639	688	809	895	963	1106
15-30	2301	2407	1997	936	947	831	743	752	631
30-46	2659	2712	2666	1456	1442	1415	539	533	499
46-61	1315	1505	1631	788	857	957	350	380	397
61-76	1159	1193	1223	632	638	670	186	185	181
76-91	2051	2096	2317	728	756	816	249	240	300
91-107	2995	3180	3078	778	805	797	365	371	389
107-122	3378	3492	3894	869	860	979	593	572	691
122-137	2997	3162	3300	752	767	782	752	745	860
137-152	2731	3360	3090	773	914	841	625	680	724
152-168	2989	2929	2605	855	860	775	628	608	626
168-183	3612	4176	3066	1028	1198	910	636	719	593
183-198	2277	2479	2204	706	813	690	562	632	623
198-213	2202	2402	2027	808	896	776	542	568	557
213-229	2015	2507	1688	860	1132	758	576	707	532
229-245	1777	2248	1421	898	1155	748	725	888	638
245-261	2102	2337	2086	979	1099	957	1058	1145	1180

Table 22. Concentration (mg/kg) of Fe-, Al-, and Mn-oxide in plot 10 using the ammonium oxalate extraction (AAO) method.

	Fe			Al			Mn		
Depth	Rep 1	Rep 2	Rep 3	Rep 1	Rep 2	Rep 3	Rep 1	Rep 2	Rep 3
cm	mg/kg								
0-15	2294	2395	2350	610	638	619	779	799	787
15-30	2015	2345	2026	853	994	884	903	1011	838
30-46	2686	3234	2670	1253	1454	1286	318	359	472
46-61	2961	2912	2797	1470	1451	1297	529	530	314
61-76	2146	2192	1927	1027	1079	948	518	541	458
76-91	947	994	938	425	458	448	129	146	138
91-107	1268	1205	1244	533	562	533	122	116	120
107-122	2441	2245	2481	724	685	724	185	174	188
122-137	2373	2035	2153	611	547	566	218	200	202
137-152	2039	2096	2027	541	553	529	232	241	218
152-168	2327	2368	2339	708	703	676	439	463	437
168-183	2359	2097	2059	670	633	614	388	369	333
183-198	2062	2161	2160	715	664	638	357	419	391
198-213	2638	2069	2324	742	741	785	475	372	370
213-229	2109	1827	2183	847	681	772	857	560	599
229-245	1974	2249	2231	714	887	870	591	887	844
245-261	2041	2077	2398	960	926	1045	1232	1198	1332

Table 23. Concentration (mg/kg) of Si extracted using the ammonium oxalate extraction (AAO) method.

		Plot									
Depth	Replicate	1	2	3	4	5	6	7	8	9	10
cm		mg/kg									
0-15	1	156	213	302	266	294	241	284	274	286	177
	2	132	173	332	329	290	572	277	290	254	182
	3	158	192	316	370	629	421	289	247	233	178
15-30	1	308	418	367	438	469	395	312	378	293	232
	2	306	303	393	405	403	430	387	395	334	265
	3	370	468	373	530	421	542	349	353	336	221
30-46	1	274	459	500	458	575	451	425	445	383	313
	2	271	425	448	422	486	617	658	466	399	370
	3	362	502	460	514	478	688	431	402	406	310
46-61	1	295	379	446	476	459	336	467	395	337	324
	2	288	295	497	353	386	490	494	326	304	360
	3	307	341	429	498	437	534	436	376	276	348
61-76	1	302	349	386	398	305	239	359	275	282	273
	2	273	302	405	451	262	239	421	245	271	307
	3	392	329	391	450	277	546	345	263	267	283
76-91	1	278	376	307	366	388	352	362	288	344	184
	2	267	275	318	361	276	337	380	257	330	184
	3	289	349	306	460	329	544	339	246	319	180
91-107	1	265	458	343	352	518	381	672	410	331	215
	2	263	286	352	303	385	420	510	337	349	316
	3	320	278	299	270	408	560	406	344	324	227
107-122	1	250	328	339	416	481	431	476	496	366	337
	2	241	250	349	320	377	431	484	472	332	313
	3	272	277	337	356	428	635	442	454	319	330
122-137	1	268	358	457	434	671	395	432	465	323	261
	2	272	268	436	371	382	379	416	416	322	263
	3	316	286	380	366	404	628	401	401	307	310
137-152	1	242	331	507	416	512	361	417	440	345	260
	2	279	255	425	388	430	344	382	382	373	257
	3	291	272	422	365	420	529	377	381	331	347
152-168	1	266	340	451	412	438	397	454	370	330	316
	2	267	297	397	341	422	350	442	356	387	314
	3	255	236	366	380	364	577	405	353	367	426
168-183	1	270	288	444	395	462	344	441	380	357	290
	2	289	246	407	363	382	330	386	374	523	304
	3	344	261	424	340	370	527	446	359	401	329
183-198	1	406	395	450	425	500	398	435	344	293	305
	2	323	313	392	343	439	367	403	332	338	316
	3	377	294	409	383	472	541	410	323	305	332

Table 23. Concentration (mg/kg) of Si extracted using the ammonium oxalate extraction (AAO) method. (continued)

		Plot									
Depth	Replicate	1	2	3	4	5	6	7	8	9	10
cm		mg/kg									
198-213	1	352	414	441	397	476	394	430	371	326	361
	2	344	368	361	341	491	335	387	341	355	326
	3	630	273	403	356	426	589	400	325	327	362
213-229	1	271	363	454	44	497	418	417	395	288	329
	2	324	352	371	326	497	335	433	338	419	300
	3	352	291	381	327	426	551	400	365	350	299
244-259	1	263	360	462	335	481	386	439	370	279	308
	2	328	328	369	338	547	307	382	367	380	313
	3	293	275	422	238	404	517	403	338	317	308
259-274	1	271	377	467	355	472	338	419	359	343	302
	2	323	365	411	340	438	329	388	326	383	272
	3	347	291	434	338	425	472	408	355	326	274

Table 24. The cation exchange capacity (CEC), effective cation exchange capacity (ECEC) and cation exchange phase composition ($cmol_c/kg$) of plot 1 with the ammonium chloride extraction method. †

Depth	Replicate	Ca	K	Mg	Mn	Na	CEC	ECEC
cm		—— $cmol_c/kg$ ——						
0-15	1	9.99	0.6982	0.49	0.0194	0.0800	7.85	11.27
	2	9.98	0.6854	0.50	0.0222	0.0635	9.61	11.25
	3	9.94	0.6675	0.49	0.0219	0.0268	9.69	11.14
15-30	1	15.39	0.6573	0.55	0.0022	0.0678	12.25	16.67
	2	15.69	0.6611	0.56	0.0036	0.0836	13.95	17.00
	3	15.99	0.5992	0.55	0.0025	0.0300	14.87	17.17
30-46	1	12.77	0.5345	0.53	0.0451	0.0859	9.41	13.97
	2	13.22	0.4918	0.53	0.0457	0.0713	12.93	14.36
	3	13.62	0.4587	0.54	0.0465	0.0451	13.61	14.70
46-61	1	11.58	0.4517	0.52	0.0067	0.0572	10.25	12.62
	2	11.72	0.4535	0.52	0.0069	0.0584	12.58	12.76
	3	11.61	0.4194	0.51	0.0074	0.0316	12.39	12.57
61-76	1	9.27	0.4045	0.50	0.0030	0.0605	9.36	10.24
	2	9.28	0.3868	0.48	0.0030	0.0667	11.04	10.22
	3	9.60	0.3563	0.49	0.0061	0.0371	11.25	10.49
76-91	1	8.07	0.3483	0.51	0.0019	0.0731	8.11	9.00
	2	8.11	0.3364	0.50	0.0023	0.0574	9.63	9.01
	3	8.27	0.3162	0.50	0.0023	0.0334	10.09	9.12
91-107	1	7.56	0.3723	0.56	0.0039	0.0701	8.22	8.56
	2	7.61	0.3254	0.56	0.0041	0.0638	9.46	8.57
	3	6.54	0.2772	0.47	0.0031	0.0308	9.05	7.32
107-122	1	5.88	0.3308	0.53	0.0062	0.0612	6.16	6.80
	2	6.35	0.2909	0.58	0.0068	0.0634	7.85	7.29
	3	6.84	0.2813	0.60	0.0070	0.0606	8.52	7.79
122-137	1	5.24	0.3804	0.59	0.0029	0.0686	6.95	6.28
	2	6.43	0.3258	0.70	0.0045	0.0696	8.13	7.53
	3	6.28	0.2896	0.68	0.0044	0.0378	8.60	7.30
137-152	1	5.69	0.2733	0.80	0.0108	0.0669	6.48	6.84
	2	5.81	0.2738	0.81	0.0110	0.0648	7.84	6.97
	3	5.80	0.2517	0.81	0.0101	0.0540	8.06	6.93
152-168	1	5.45	0.3343	0.96	0.0137	0.0831	6.38	6.84
	2	5.69	0.2786	0.98	0.0143	0.0867	7.60	7.05
	3	5.43	0.2687	0.93	0.0127	0.0875	7.89	6.72
168-183	1	5.53	0.3331	1.14	0.0060	0.0495	6.88	7.07
	2	5.62	0.3414	1.15	0.0070	0.0608	8.10	7.18
	3	5.62	0.2886	1.16	0.0075	0.0373	8.27	7.11
183-198	1	4.73	0.4083	1.25	0.0067	0.0501	6.76	6.45
	2	5.27	0.3288	1.34	0.0121	0.0432	8.59	6.99
	3	5.47	0.3292	1.39	0.0125	0.0518	8.96	7.26

† Al and Fe are below detectable levels, <0.001 $cmol_c/kg$.

Table 24. The cation exchange capacity (CEC), effective cation exchange capacity (ECEC) and cation exchange phase composition ($cmol_c/kg$) of plot 1 with the ammonium chloride extraction method. (continued) †

Depth	Replicate	Ca	K	Mg	Mn	Na	CEC	ECEC
cm		——————————---------- $cmol_c/kg$ ——————————----------						
198-213	1	5.06	0.3902	1.61	0.0084	0.0560	7.09	7.13
	2	5.00	0.3483	1.60	0.0098	0.0284	8.40	6.98
	3	5.02	0.3306	1.61	0.0178	0.0890	8.12	7.06
213-229	1	5.07	0.4091	1.80	0.0066	0.0630	6.12	7.35
	2	5.14	0.3702	1.84	0.0083	0.0311	9.14	7.39
	3	5.00	0.3708	1.83	0.0084	0.0412	8.82	7.26
229-245	1	4.78	0.4036	2.11	0.0059	0.0875	8.83	7.40
	2	5.00	0.3648	2.14	0.0059	0.0298	9.83	7.54
	3	4.97	0.3683	2.17	0.0054	0.0455	9.51	7.56
245-261	1	4.78	0.3683	2.32	0.0120	0.0746	9.07	7.56
	2	4.88	0.3243	2.32	0.0117	0.0309	9.17	7.56
	3	5.03	0.3304	2.37	0.0121	0.0450	9.73	7.78

† Al and Fe are below detectable levels, <0.001 $cmol_c/kg$.

Table 25. The cation exchange capacity (CEC), effective cation exchange capacity (ECEC) and cation exchange phase composition ($cmol_c/kg$) of plot 2 with the ammonium chloride extraction method. †

Depth	Replicate	Ca	K	Mg	Mn	Na	CEC	ECEC
cm		——————————— $cmol_c/kg$ ———————————						
0-15	1	12.10	0.8312	0.41	0.0239	0.0345	10.45	13.41
	2	11.41	0.8593	0.46	0.0250	0.0310	10.13	12.78
	3	12.38	0.8875	0.48	0.0261	0.0181	7.91	13.81
15-30	1	19.83	0.7890	0.45	0.0040	0.0705	13.84	21.14
	2	17.81	0.7609	0.48	0.0043	0.0586	14.65	19.11
	3	19.85	0.8133	0.52	0.0049	0.0483	11.44	21.24
30-46	1	14.24	0.6624	0.56	0.0031	0.0439	14.46	15.51
	2	14.21	0.6969	0.64	0.0033	0.0393	14.45	15.60
	3	13.52	0.6483	0.61	0.0029	0.0274	10.80	14.81
46-61	1	11.31	0.4614	0.51	0.0029	0.0505	12.30	12.33
	2	11.16	0.4830	0.58	0.0035	0.0463	12.44	12.28
	3	11.48	0.4486	0.58	0.0031	0.0331	9.62	12.55
61-76	1	10.00	0.3691	0.50	0.0013	0.0542	10.67	10.92
	2	9.76	0.3723	0.56	0.0018	0.0436	8.77	10.74
	3	10.09	0.3614	0.55	0.0017	0.0373	8.59	11.04
76-91	1	8.94	0.3540	0.51	0.0016	0.1092	10.41	9.92
	2	8.90	0.3616	0.58	0.0022	0.0772	7.87	9.92
	3	8.96	0.3468	0.59	0.0019	0.0746	7.84	9.97
91-107	1	8.57	0.3454	0.59	0.0012	0.0418	9.72	9.54
	2	6.34	0.3020	0.51	0.0016	0.0210	7.87	7.18
	3	8.52	0.3423	0.66	0.0017	0.0236	7.32	9.55
107-122	1	7.06	0.3116	0.66	0.0022	0.0519	8.59	8.08
	2	7.34	0.3074	0.67	0.0020	0.0304	6.79	8.35
	3	7.55	0.2937	0.66	0.0016	0.0344	6.85	8.54
122-137	1	7.05	0.3494	0.79	0.0020	0.0466	8.16	8.23
	2	6.84	0.3234	0.78	0.0017	0.0226	6.68	7.97
	3	6.70	0.2880	0.79	0.0029	0.0372	6.62	7.83
137-152	1	6.71	0.3160	0.82	0.0032	0.0543	8.27	7.90
	2	5.44	0.2399	0.66	0.0029	0.0319	5.72	6.38
	3	6.25	0.2847	0.70	0.0013	0.0179	6.30	7.25
152-168	1	6.21	0.3381	0.94	0.0032	0.0411	8.38	7.53
	2	6.35	0.3173	0.95	0.0033	0.0215	6.38	7.64
	3	6.59	0.3120	0.96	0.0027	0.0195	6.34	7.88
168-183	1	6.10	0.3354	1.09	0.0054	0.0421	8.63	7.57
	2	6.34	0.3295	1.13	0.0058	0.0301	6.59	7.84
	3	6.13	0.3111	1.11	0.0049	0.0268	6.32	7.58
183-198	1	6.28	0.4198	1.30	0.0025	0.0336	8.73	8.04
	2	6.33	0.4012	1.33	0.0027	0.0200	6.79	8.09
	3	5.30	0.3249	1.09	0.0019	0.0166	6.83	6.74

† Al and Fe are below detectable levels, <0.001 $cmol_c/kg$.

Table 25. The cation exchange capacity (CEC), effective cation exchange capacity (ECEC) and cation exchange phase composition ($cmol_c/kg$) of plot 2 with the ammonium chloride extraction method. (continued) †

Depth	Replicate	Ca	K	Mg	Mn	Na	CEC	ECEC
cm		$cmol_c/kg$						
198-213	1	6.18	0.4600	1.47	0.0021	0.0347	8.47	8.15
	2	6.00	0.4497	1.49	0.0024	0.0194	6.82	7.96
	3	5.42	0.3711	1.29	0.0019	0.0164	6.95	7.10
213-229	1	5.67	0.4446	1.61	0.0022	0.0320	9.40	7.77
	2	1.53	0.2239	0.44	0.0018	0.0103	6.95	2.20
	3	5.87	0.4487	1.67	0.0046	0.0198	7.05	8.01
229-245	1	6.02	0.4894	1.86	0.0021	0.0384	8.57	8.41
	2	5.99	0.4650	1.87	0.0020	0.0193	7.13	8.34
	3	6.08	0.4651	1.85	0.0017	0.0197	7.13	8.42
245-261	1	5.96	0.5179	2.26	0.0015	0.0385	10.47	8.78
	2	5.99	0.5082	2.28	0.0015	0.0203	7.76	8.80
	3	6.12	0.4804	2.23	0.0012	0.0222	7.87	8.85

† Al and Fe are below detectable levels, <0.001 $cmol_c/kg$.

Table 26. The cation exchange capacity (CEC), effective cation exchange capacity (ECEC) and cation exchange phase composition ($cmol_c/kg$) of plot 3 with the ammonium chloride extraction method. †

Depth	Replicate	Ca	K	Mg	Mn	Na	CEC	ECEC
cm		———	———	———	$cmol_c/kg$	———	———	———
0-15	1	15.59	0.7174	0.37	0.0094	0.0271	6.40	16.71
	2	18.33	0.7596	0.39	0.0126	0.0405	6.39	19.54
	3	18.83	0.7506	0.39	0.0108	0.0410	7.06	20.02
15-30	1	21.55	0.6688	0.46	0.0010	0.0277	9.07	22.70
	2	23.84	0.6765	0.46	0.0035	0.0453	9.36	25.03
	3	24.44	0.6905	0.47	0.0009	0.0393	9.58	25.64
30-46	1	15.29	0.6726	0.75	0.0017	0.0258	10.92	16.74
	2	13.37	0.6090	0.64	0.0039	0.0401	12.13	14.66
	3	16.48	0.7084	0.77	0.0016	0.0373	12.52	18.00
46-61	1	11.68	0.5609	0.74	0.0019	0.0272	9.79	13.01
	2	12.62	0.5988	0.77	0.0042	0.0453	9.75	14.04
	3	12.79	0.5871	0.78	0.0018	0.0394	10.59	14.20
61-76	1	9.60	0.4786	0.76	0.0008	0.0296	8.52	10.86
	2	10.47	0.5251	0.78	0.0032	0.0466	8.22	11.84
	3	10.41	0.5127	0.82	0.0006	0.0451	8.96	11.79
76-91	1	5.71	0.2862	0.52	0.0010	0.0198	7.08	6.53
	2	8.43	0.4298	0.72	0.0030	0.0436	7.38	9.63
	3	8.08	0.4330	0.73	0.0005	0.0447	7.27	9.29
91-107	1	6.68	0.4120	0.76	0.0008	0.0240	6.84	7.87
	2	7.53	0.4958	0.83	0.0032	0.0463	7.00	8.91
	3	7.75	0.5033	0.84	0.0006	0.0390	7.04	9.14
107-122	1	6.58	0.5934	0.99	0.0011	0.0207	6.66	8.18
	2	6.88	0.6471	1.03	0.0036	0.0361	6.91	8.60
	3	6.50	0.5999	0.96	0.0008	0.0272	6.91	8.10
122-137	1	5.84	0.9757	1.29	0.0009	0.0187	6.67	8.12
	2	6.46	1.0128	1.32	0.0035	0.0383	7.39	8.84
	3	5.79	0.8363	1.18	0.0006	0.0302	7.21	7.84
137-152	1	4.61	1.0243	1.28	0.0016	0.0194	6.63	6.93
	2	5.56	1.1228	1.48	0.0045	0.0416	5.95	8.22
	3	5.50	1.0780	1.45	0.0015	0.0336	6.85	8.06
152-168	1	4.58	1.0729	1.49	0.0064	0.0433	6.38	7.19
	2	5.00	1.0767	1.53	0.0088	0.0771	6.52	7.70
	3	4.57	1.1650	1.53	0.0057	0.0697	5.78	7.35
168-183	1	3.66	1.2685	1.47	0.0011	0.0152	6.07	6.41
	2	4.31	1.4207	1.68	0.0012	0.0321	6.71	7.44
	3	4.09	1.5857	1.71	0.0004	0.0356	6.61	7.42
183-198	1	4.14	1.5742	1.88	0.0034	0.0229	6.44	7.62
	2	4.35	1.5422	1.92	0.0036	0.0420	7.03	7.86
	3	4.16	1.6957	1.94	0.0030	0.0405	6.70	7.84

† Al and Fe are below detectable levels, <0.001 $cmol_c/kg$.

Table 26. The cation exchange capacity (CEC), effective cation exchange capacity (ECEC) and cation exchange phase composition ($cmol_c/kg$) of plot 3 with the ammonium chloride extraction method. (continued) †

Depth	Replicate	Ca	K	Mg	Mn	Na	CEC	ECEC
cm		——— $cmol_c/kg$ ———						
198-213	1	4.03	1.7711	1.95	0.0011	0.0410	6.76	7.80
	2	4.25	1.7046	2.02	0.0011	0.0311	7.26	8.01
	3	3.97	1.9194	2.05	0.0007	0.0370	7.23	7.99
213-229	1	4.17	1.9182	2.01	0.0033	0.0361	6.99	8.15
	2	4.28	1.7647	2.08	0.0011	0.0316	7.20	8.15
	3	3.96	1.9258	2.06	0.0002	0.0337	6.91	7.98
229-245	1	4.29	1.9655	2.27	0.0031	0.0376	7.24	8.58
	2	4.29	1.9463	2.27	0.0007	0.0314	7.06	8.54
	3	3.95	2.1547	2.26	0.0003	0.0375	7.74	8.41
245-261	1	4.25	2.4936	2.62	0.0004	0.0384	8.90	9.41
	2	4.32	2.5281	2.71	0.0005	0.0409	8.40	9.61
	3	4.09	2.5102	2.62	0.0005	0.0413	8.68	9.27

† Al and Fe are below detectable levels, <0.001 $cmol_c/kg$.

Table 27. The cation exchange capacity (CEC), effective cation exchange capacity (ECEC) and cation exchange phase composition ($cmol_c/kg$) of plot 4 with the ammonium chloride extraction method. †

Depth	Replicate	Ca	K	Mg	Mn	Na	CEC	ECEC
cm		——————————— $cmol_c/kg$ ———————————						
0-15	1	15.56	0.7928	0.39	0.0050	0.0372	8.06	16.79
	2	14.34	0.7711	0.37	0.0044	0.0237	7.31	15.51
	3	15.16	0.8210	0.40	0.0042	0.0417	7.04	16.43
15-30	1	21.75	0.6893	0.41	0.0001	0.0478	11.60	22.89
	2	19.90	0.6662	0.39	0.0001	0.0340	9.64	20.99
	3	23.29	0.6918	0.42	0.0001	0.0394	10.56	24.45
30-46	1	14.79	0.6352	0.59	0.0040	0.0535	12.99	16.07
	2	13.77	0.5610	0.54	0.0039	0.0328	11.62	14.90
	3	16.03	0.6483	0.63	0.0048	0.0463	11.92	17.37
46-61	1	12.97	0.5368	0.64	0.0023	0.0565	11.78	14.20
	2	13.47	0.5497	0.66	0.0022	0.0564	9.97	14.73
	3	12.15	0.4900	0.59	0.0020	0.0438	10.54	13.28
61-76	1	10.86	0.4648	0.60	0.0003	0.0385	10.22	11.96
	2	11.35	0.4803	0.63	0.0001	0.0399	9.11	12.50
	3	11.47	0.4770	0.64	0.0000	0.0371	9.04	12.63
76-91	1	8.78	0.3642	0.56	0.0002	0.0378	8.72	9.75
	2	8.20	0.3463	0.53	0.0002	0.0460	7.65	9.13
	3	9.45	0.4005	0.60	0.0003	0.0439	7.52	10.50
91-107	1	8.48	0.3908	0.68	0.0000	0.0310	7.63	9.58
	2	8.33	0.3877	0.70	0.0002	0.0443	7.38	9.46
	3	9.21	0.4142	0.76	0.0003	0.0428	7.78	10.44
107-122	1	7.95	0.4426	0.85	0.0007	0.0616	7.65	9.30
	2	7.32	0.3894	0.76	0.0007	0.0693	7.53	8.54
	3	8.80	0.4645	0.89	0.0014	0.0770	7.45	10.23
122-137	1	7.43	0.4735	0.89	0.0009	0.0317	7.11	8.83
	2	7.84	0.4849	0.93	0.0010	0.0474	7.84	9.31
	3	8.10	0.4939	0.97	0.0012	0.0408	7.35	9.61
137-152	1	6.89	0.4930	1.05	0.0013	0.0260	6.99	8.45
	2	6.53	0.5390	1.00	0.0009	0.1004	6.81	8.17
	3	6.94	0.4962	1.04	0.0015	0.0330	6.79	8.51
152-168	1	6.15	0.5907	1.20	0.0013	0.0284	6.85	7.97
	2	5.52	0.5157	1.09	0.0007	0.0346	6.41	7.17
	3	6.38	0.6064	1.24	0.0015	0.0331	6.55	8.26
168-183	1	5.58	0.5503	1.30	0.0028	0.0301	6.38	7.46
	2	4.81	0.4739	1.15	0.0015	0.0538	6.31	6.49
	3	4.43	0.4362	1.03	0.0044	0.0373	6.13	5.95
183-198	1	5.61	0.7136	1.51	0.0018	0.0250	6.74	7.86
	2	5.84	1.0013	1.57	0.0011	0.0377	6.87	8.45
	3	5.90	0.6905	1.55	0.0021	0.0353	6.52	8.18

† Al and Fe are below detectable levels, <0.001 $cmol_c/kg$.

Table 27. The cation exchange capacity (CEC), effective cation exchange capacity (ECEC) and cation exchange phase composition ($cmol_c/kg$) of plot 4 with the ammonium chloride extraction method. (continued) †

Depth	Replicate	Ca	K	Mg	Mn	Na	CEC	ECEC
cm		——————————— $cmol_c/kg$ ———————————						
198-213	1	5.43	0.7788	1.60	0.0029	0.0274	6.68	7.85
	2	5.49	1.1343	1.61	0.0018	0.0465	6.84	8.28
	3	5.81	0.7916	1.68	0.0040	0.0442	6.45	8.33
213-229	1	3.83	0.5536	1.28	0.0026	0.0218	6.47	5.70
	2	2.04	0.3786	0.69	0.0004	0.0162	6.49	3.13
	3	5.35	0.7762	1.78	0.0050	0.0386	6.59	7.95
229-245	1	3.60	0.5988	1.26	0.0020	0.0221	6.61	5.48
	2	2.07	0.3451	0.76	0.0004	0.0163	6.58	3.20
	3	5.27	0.8734	1.86	0.0035	0.0406	6.39	8.06
245-261	1	5.09	0.8107	1.77	0.0042	0.0291	6.56	7.70
	2	4.63	0.7391	1.65	0.0033	0.0410	6.36	7.07
	3	5.19	0.7928	1.77	0.0054	0.0389	6.36	7.79

† Al and Fe are below detectable levels, <0.001 $cmol_c/kg$.

Table 28. The cation exchange capacity (CEC), effective cation exchange capacity (ECEC) and cation exchange phase composition ($cmol_c/kg$) of plot 5 with the ammonium chloride extraction method. †

Depth	Replicate	Ca	K	Mg	Mn	Na	CEC	ECEC
cm		——————————— $cmol_c/kg$ ———————————						
0-15	1	13.84	0.6867	0.46	0.0131	0.0343	6.37	15.04
	2	13.99	0.7097	0.43	0.0148	0.0210	6.89	15.17
	3	13.49	0.7046	0.41	0.0154	0.0218	6.95	14.65
15-30	1	15.34	0.7801	0.46	0.0004	0.0338	11.06	16.61
	2	14.91	0.7928	0.41	0.0028	0.0251	11.22	16.14
	3	14.69	0.7621	0.39	0.0031	0.0235	11.67	15.87
30-46	1	14.99	0.6893	0.60	0.0070	0.0405	11.52	16.33
	2	14.61	0.6535	0.53	0.0093	0.0260	12.15	15.84
	3	14.91	0.6880	0.54	0.0096	0.0298	12.24	16.19
46-61	1	11.51	0.4451	0.52	0.0033	0.0358	9.38	12.51
	2	11.64	0.4687	0.47	0.0061	0.0288	9.33	12.62
	3	11.60	0.4546	0.46	0.0062	0.0275	9.49	12.55
61-76	1	7.15	0.2714	0.37	0.0004	0.0319	7.36	7.83
	2	8.62	0.3450	0.42	0.0028	0.0289	7.19	9.42
	3	8.63	0.3141	0.40	0.0022	0.0251	7.21	9.37
76-91	1	8.39	0.3423	0.64	0.0004	0.0377	7.59	9.41
	2	9.14	0.3604	0.65	0.0021	0.0334	7.71	10.19
	3	9.11	0.3931	0.64	0.0027	0.0386	7.77	10.18
91-107	1	7.78	0.3942	0.92	0.0004	0.0444	7.98	9.14
	2	9.15	0.4678	1.00	0.0033	0.0418	8.14	10.67
	3	8.86	0.4549	0.96	0.0033	0.0410	8.04	10.32
107-122	1	7.86	0.4798	1.33	0.0053	0.0882	7.25	9.76
	2	7.74	0.4964	1.23	0.0075	0.0828	7.59	9.56
	3	7.80	0.4941	1.21	0.0087	0.0852	7.40	9.60
122-137	1	6.38	0.5528	1.49	0.0024	0.0969	7.18	8.53
	2	6.70	0.4834	1.36	0.0092	0.0973	7.00	8.65
	3	6.83	0.5593	1.39	0.0114	0.1135	6.79	8.91
137-152	1	5.74	0.5877	1.67	0.0037	0.1216	6.77	8.12
	2	5.76	0.6043	1.53	0.0069	0.1096	6.68	8.01
	3	5.69	0.6260	1.50	0.0076	0.1155	6.68	7.95
152-168	1	5.36	0.4806	1.68	0.0171	0.1279	6.46	7.67
	2	4.06	0.3664	1.15	0.0161	0.0917	6.18	5.68
	3	5.26	0.4665	1.51	0.0219	0.1259	6.11	7.39
168-183	1	4.84	0.4734	1.66	0.0209	0.1368	6.00	7.13
	2	4.67	0.4526	1.50	0.0255	0.1205	5.87	6.77
	3	4.41	0.4193	1.39	0.0261	0.1122	5.81	6.36
183-198	1	5.37	0.6893	1.64	0.0068	0.1133	6.33	7.82
	2	5.40	0.7775	1.69	0.0083	0.1277	6.57	8.00
	3	5.10	0.5941	1.54	0.0074	0.1034	6.62	7.35

† Al and Fe are below detectable levels, <0.001 $cmol_c/kg$.

Table 28. The cation exchange capacity (CEC), effective cation exchange capacity (ECEC) and cation exchange phase composition ($cmol_c/kg$) of plot 5 with the ammonium chloride extraction method. (continued) †

Depth	Replicate	Ca	K	Mg	Mn	Na	CEC	ECEC
cm		——————————— $cmol_c/kg$ ———————————						
198-213	1	5.79	0.7494	1.52	0.0049	0.0897	6.66	8.15
	2	5.70	0.7340	1.47	0.0051	0.0883	6.98	8.00
	3	5.83	0.6905	1.46	0.0054	0.0845	6.85	8.07
213-229	1	5.37	0.7545	1.57	0.0044	0.0770	6.63	7.78
	2	5.15	0.6957	1.47	0.0041	0.0699	6.69	7.40
	3	4.75	0.6944	1.50	0.0015	0.0782	6.91	7.02
229-245	1	5.24	0.8440	1.77	0.0061	0.0812	6.87	7.95
	2	5.11	0.8286	1.72	0.0066	0.0827	6.89	7.75
	3	4.92	0.7928	1.83	0.0098	0.0845	6.93	7.63
245-261	1	5.05	0.8529	1.99	0.0044	0.0821	7.01	7.99
	2	5.24	0.8325	1.98	0.0046	0.0824	7.53	8.14
	3	4.95	0.8440	2.08	0.0018	0.0934	7.37	7.97

† Al and Fe are below detectable levels, <0.001 $cmol_c/kg$.

Table 29. The cation exchange capacity (CEC), effective cation exchange capacity (ECEC) and cation exchange phase composition ($cmol_c/kg$) of plot 6 with the ammonium chloride extraction method. †

Depth	Replicate	Ca	K	Mg	Mn	Na	CEC	ECEC
cm		——————————— $cmol_c/kg$ ———————————						
0-15	1	17.96	0.8824	0.40	0.0013	0.0231	5.80	19.26
	2	17.41	0.8389	0.39	0.0029	0.0171	5.68	18.66
	3	17.61	0.8031	0.39	0.0028	0.0189	5.91	18.82
15-30	1	21.77	0.8235	0.42	0.0007	0.0374	10.09	23.05
	2	21.10	0.7788	0.40	0.0027	0.0446	9.94	22.33
	3	20.75	0.7148	0.38	0.0029	0.0394	9.76	21.89
30-46	1	14.41	0.5900	0.64	0.0018	0.0356	12.02	15.68
	2	13.97	0.5545	0.60	0.0040	0.0338	12.73	15.16
	3	15.21	0.6157	0.66	0.0043	0.0417	12.55	16.54
46-61	1	11.86	0.4444	0.56	0.0003	0.0363	9.35	12.90
	2	11.90	0.4492	0.57	0.0026	0.0401	9.93	12.96
	3	11.88	0.4581	0.57	0.0028	0.0378	9.55	12.95
61-76	1	9.09	0.4032	0.58	0.0005	0.0262	7.59	10.10
	2	8.23	0.3457	0.53	0.0015	0.0256	7.72	9.13
	3	9.19	0.3756	0.57	0.0017	0.0228	7.76	10.17
76-91	1	9.66	0.4453	0.86	0.0005	0.0306	8.38	11.00
	2	9.78	0.4271	0.84	0.0018	0.0301	8.98	11.09
	3	9.76	0.4344	0.87	0.0020	0.0316	8.93	11.10
91-107	1	8.68	0.4299	1.04	0.0020	0.0286	7.98	10.18
	2	8.54	0.4170	1.00	0.0021	0.0407	8.23	10.00
	3	9.07	0.4238	1.04	0.0024	0.0292	8.40	10.57
107-122	1	8.22	0.4142	1.12	0.0042	0.0352	7.75	9.79
	2	8.36	0.4054	1.13	0.0045	0.0368	8.03	9.94
	3	8.58	0.4202	1.14	0.0045	0.0368	7.95	10.18
122-137	1	7.32	0.4653	1.36	0.0029	0.0263	7.41	9.18
	2	6.49	0.4105	1.20	0.0030	0.0319	7.52	8.14
	3	7.54	0.4771	1.40	0.0034	0.0318	7.21	9.45
137-152	1	6.77	0.3949	1.39	0.0058	0.0340	6.87	8.60
	2	6.67	0.3950	1.42	0.0061	0.0365	7.06	8.53
	3	6.47	0.3829	1.33	0.0062	0.0318	6.96	8.22
152-168	1	6.06	0.4125	1.48	0.0036	0.0252	6.57	7.98
	2	5.89	0.4078	1.46	0.0039	0.0304	6.78	7.80
	3	6.15	0.4191	1.52	0.0042	0.0261	6.69	8.12
168-183	1	5.39	0.4082	1.54	0.0037	0.0254	6.20	7.37
	2	4.58	0.3509	1.29	0.0036	0.0241	6.31	6.25
	3	5.58	0.4151	1.55	0.0042	0.0258	6.37	7.57
183-198	1	4.84	0.4501	1.48	0.0024	0.0223	5.20	6.80
	2	5.65	0.5444	1.74	0.0028	0.0271	6.80	7.97
	3	5.61	0.5404	1.76	0.0031	0.0264	6.78	7.94

† Al and Fe are below detectable levels, <0.001 $cmol_c/kg$.

Table 29. The cation exchange capacity (CEC), effective cation exchange capacity (ECEC) and cation exchange phase composition ($cmol_c/kg$) of plot 6 with the ammonium chloride extraction method. (continued) †

Depth	Replicate	Ca	K	Mg	Mn	Na	CEC	ECEC
cm		——————————————— $cmol_c/kg$ ———————————————						
198-213	1	5.91	0.6726	1.97	0.0051	0.0286	7.55	8.59
	2	5.96	0.6765	1.98	0.0055	0.0308	7.77	8.65
	3	6.04	0.6803	2.01	0.0058	0.0336	7.53	8.78
213-229	1	5.97	0.7263	1.78	0.0019	0.0254	7.47	8.50
	2	6.00	0.7136	1.78	0.0021	0.0331	7.37	8.53
	3	5.94	0.7174	1.80	0.0023	0.0247	7.03	8.49
229-245	1	5.33	0.7161	1.82	0.0041	0.0331	7.29	7.90
	2	5.56	0.7634	1.88	0.0046	0.0405	7.52	8.25
	3	5.68	0.7519	1.88	0.0050	0.0361	7.34	8.35
245-261	1	5.35	0.9309	2.02	0.0026	0.0266	7.94	8.33
	2	5.45	0.9501	2.02	0.0031	0.0291	7.27	8.45
	3	4.43	0.7864	1.68	0.0029	0.0287	7.33	6.94

† Al and Fe are below detectable levels, <0.001 $cmol_c/kg$.

Table 30. The cation exchange capacity (CEC), effective cation exchange capacity (ECEC) and cation exchange phase composition ($cmol_c/kg$) of plot 7 with the ammonium chloride extraction method. †

Depth	Replicate	Ca	K	Mg	Mn	Na	CEC	ECEC
cm		——————————— $cmol_c/kg$ ———————————						
0-15	1	1.56	0.6765	0.48	0.0005	0.0125	7.69	2.73
	2	14.91	0.7545	0.45	0.0011	0.0159	7.58	16.13
	3	15.34	0.7685	0.44	0.0005	0.0222	7.29	16.57
15-30	1	2.09	0.5188	0.42	0.0012	0.0275	8.71	3.06
	2	20.85	0.5919	0.40	0.0008	0.0297	8.37	21.88
	3	19.63	0.5843	0.41	0.0010	0.0370	8.26	20.66
30-46	1	1.46	0.6201	0.84	0.0024	0.0228	12.99	2.95
	2	15.89	0.7941	0.90	0.0019	0.0236	12.73	17.61
	3	16.33	0.8184	0.94	0.0019	0.0291	12.75	18.12
46-61	1	1.42	0.6248	1.05	0.0016	0.0228	11.75	3.12
	2	13.47	0.7033	0.97	0.0014	0.0252	11.58	15.17
	3	13.42	0.6957	0.99	0.0013	0.0294	11.53	15.13
61-76	1	1.20	0.5220	0.95	0.0026	0.0167	9.80	2.70
	2	11.26	0.5983	0.91	0.0023	0.0222	9.72	12.79
	3	11.42	0.5824	0.90	0.0023	0.0271	9.83	12.93
76-91	1	1.02	0.5349	1.30	0.0024	0.0282	9.34	2.88
	2	9.75	0.6145	1.23	0.0021	0.0350	9.19	11.63
	3	9.81	0.6247	1.26	0.0020	0.0511	9.29	11.75
91-107	1	0.89	0.7647	2.10	0.0024	0.0191	9.23	3.77
	2	8.43	0.8747	1.96	0.0021	0.0213	9.30	11.29
	3	7.39	0.7852	1.78	0.0019	0.0416	9.34	10.00
107-122	1	0.69	1.0985	2.46	0.0026	0.0203	8.61	4.28
	2	6.62	1.2353	2.32	0.0023	0.0231	8.65	10.20
	3	6.60	1.2570	2.31	0.0023	0.0233	8.74	10.19
122-137	1	0.59	1.3159	2.44	0.0014	0.0164	8.13	4.37
	2	5.72	1.5192	2.28	0.0012	0.0211	8.10	9.54
	3	5.60	1.4719	2.26	0.0012	0.0205	7.89	9.35
137-152	1	5.08	1.5064	2.13	0.0075	0.1127	7.70	8.84
	2	5.09	1.4910	2.14	0.0079	0.1201	7.56	8.85
	3	5.15	1.5269	2.14	0.0071	0.1157	7.75	8.95
152-168	1	5.02	1.8427	2.10	0.0019	0.0199	7.91	8.99
	2	5.18	1.8389	2.11	0.0015	0.0260	7.46	9.15
	3	5.03	1.8197	2.06	0.0018	0.0204	7.93	8.94
168-183	1	5.00	1.8875	2.03	0.0019	0.0207	7.80	8.94
	2	5.08	1.8542	2.00	0.0016	0.0247	7.58	8.96
	3	3.40	1.2417	1.36	0.0021	0.0166	7.92	6.01
183-198	1	4.43	1.7366	1.91	0.0019	0.0186	7.36	8.10
	2	4.50	1.7289	1.90	0.0017	0.0253	7.11	8.16
	3	4.45	1.7238	1.90	0.0018	0.0187	7.30	8.09

† Al and Fe are below detectable levels, <0.001 $cmol_c/kg$.

Table 30. The cation exchange capacity (CEC), effective cation exchange capacity (ECEC) and cation exchange phase composition ($cmol_c/kg$) of plot 7 with the ammonium chloride extraction method. (continued) †

Depth	Replicate	Ca	K	Mg	Mn	Na	CEC	ECEC
cm		$cmol_c/kg$						
198-213	1	4.80	1.5921	1.76	0.0018	0.0164	7.31	8.17
	2	4.71	1.6087	1.79	0.0016	0.0232	7.30	8.13
	3	4.47	1.5026	1.68	0.0018	0.0173	7.46	7.67
213-229	1	4.92	1.7020	1.82	0.0020	0.0259	7.68	8.47
	2	4.97	1.7327	1.88	0.0017	0.0256	7.71	8.61
	3	4.92	1.6662	1.80	0.0019	0.0176	7.51	8.40
229-245	1	5.16	1.6458	1.79	0.0024	0.0201	7.87	8.62
	2	5.02	1.6586	1.72	0.0022	0.0226	7.84	8.43
	3	5.21	1.6496	1.81	0.0023	0.0194	7.86	8.69
245-261	1	4.78	1.3926	1.56	0.0024	0.0168	7.74	7.75
	2	5.10	1.5499	1.75	0.0022	0.0238	7.86	8.43
	3	5.11	1.6125	1.73	0.0022	0.0194	7.58	8.48

† Al and Fe are below detectable levels, <0.001 $cmol_c/kg$.

Table 31. The cation exchange capacity (CEC), effective cation exchange capacity (ECEC) and cation exchange phase composition ($cmol_c/kg$) of plot 8 with the ammonium chloride extraction method. †

Depth	Replicate	Ca	K	Mg	Mn	Na	CEC	ECEC
cm		$cmol_c/kg$						
0-15	1	18.20	0.8107	0.46	0.0073	0.0214	6.82	19.50
	2	17.41	0.7864	0.45	0.0058	0.0195	6.60	18.67
	3	20.40	0.8465	0.48	0.0161	0.0279	6.61	21.77
15-30	1	22.47	0.5958	0.33	0.0013	0.0282	8.27	23.42
	2	22.37	0.5821	0.33	0.0011	0.0320	8.54	23.31
	3	23.54	0.6043	0.34	0.0037	0.0363	8.79	24.52
30-46	1	11.67	0.4281	0.45	0.0021	0.0362	11.66	12.60
	2	14.71	0.5772	0.52	0.0034	0.0466	11.82	15.86
	3	14.84	0.5509	0.56	0.0104	0.0427	12.12	16.01
46-61	1	12.92	0.4618	0.50	0.0011	0.0290	10.52	13.91
	2	12.99	0.4503	0.51	0.0013	0.0318	10.44	13.99
	3	9.97	0.3563	0.42	0.0057	0.0303	10.88	10.79
61-76	1	10.27	0.3552	0.43	0.0015	0.0261	8.06	11.09
	2	10.43	0.3708	0.46	0.0013	0.0309	8.57	11.29
	3	10.03	0.3471	0.47	0.0035	0.0336	8.59	10.88
76-91	1	8.32	0.3418	0.62	0.0018	0.0200	8.35	9.31
	2	9.19	0.3785	0.72	0.0015	0.0269	8.30	10.31
	3	9.46	0.3913	0.76	0.0038	0.0328	8.43	10.65
91-107	1	9.40	0.4951	1.31	0.0011	0.0471	8.97	11.26
	2	9.56	0.4848	1.30	0.0011	0.0350	9.02	11.38
	3	8.52	0.4297	1.21	0.0043	0.0387	9.44	10.21
107-122	1	8.93	0.4992	1.72	0.0007	0.0381	8.87	11.19
	2	8.94	0.5115	1.70	0.0004	0.0428	8.89	11.20
	3	9.19	0.5205	1.74	0.0057	0.0441	9.89	11.50
122-137	1	7.47	0.5813	2.38	0.0001	0.0255	8.51	10.46
	2	7.51	0.6169	2.39	0.0009	0.0342	8.63	10.55
	3	7.72	0.6012	2.43	0.0065	0.0363	8.86	10.80
137-152	1	5.75	0.6054	2.45	0.0011	0.0197	8.66	8.82
	2	6.85	0.7110	2.87	0.0020	0.0264	8.56	10.46
	3	6.64	0.7289	2.75	0.0090	0.0319	8.77	10.16
152-168	1	5.30	0.6160	2.96	0.0086	0.0264	7.85	8.92
	2	5.38	0.6293	2.98	0.0105	0.0343	7.78	9.04
	3	5.41	0.6496	2.92	0.0204	0.0395	7.77	9.04
168-183	1	5.25	0.5919	2.76	0.0143	0.0325	7.43	8.65
	2	5.10	0.5731	2.58	0.0141	0.0374	7.50	8.31
	3	5.29	0.6231	2.69	0.0288	0.0473	7.54	8.68
183-198	1	3.90	0.5776	2.70	0.0179	0.0399	6.66	7.26
	2	3.91	0.5852	2.74	0.0188	0.0345	6.58	7.29
	3	3.95	0.5903	2.66	0.0350	0.0440	6.72	7.29

† Al and Fe are below detectable levels, <0.001 $cmol_c/kg$.

Table 31. The cation exchange capacity (CEC), effective cation exchange capacity (ECEC) and cation exchange phase composition ($cmol_c/kg$) of plot 8 with the ammonium chloride extraction method. (continued) †

Depth	Replicate	Ca	K	Mg	Mn	Na	CEC	ECEC
cm		——— $cmol_c/kg$ ———						
198-213	1	3.90	0.6354	2.69	0.0139	0.0250	6.76	7.28
	2	3.82	0.6419	2.64	0.0159	0.0308	6.79	7.15
	3	3.95	0.6302	2.59	0.0254	0.0387	6.67	7.23
213-229	1	4.58	0.8465	2.83	0.0026	0.0192	7.50	8.27
	2	4.56	0.8478	2.82	0.0036	0.0255	7.48	8.26
	3	4.52	0.8286	2.70	0.0109	0.0297	7.34	8.09
229-245	1	4.60	0.9923	2.66	0.0012	0.0193	7.62	8.27
	2	4.85	0.9949	2.76	0.0060	0.0250	9.19	8.64
	3	3.80	0.7442	2.04	0.0071	0.0267	7.70	6.62
245-261	1	4.24	0.8632	2.34	0.0018	0.0194	7.27	7.47
	2	4.48	0.9130	2.51	0.0078	0.0270	8.05	7.95
	3	3.74	0.6931	1.93	0.0081	0.0269	7.03	6.39

† Al and Fe are below detectable levels, <0.001 $cmol_c/kg$.

Table 32. The cation exchange capacity (CEC), effective cation exchange capacity (ECEC) and cation exchange phase composition ($cmol_c/kg$) of plot 9 with the ammonium chloride extraction method. †

Depth	Replicate	Ca	K	Mg	Mn	Na	CEC	ECEC
cm		——— $cmol_c/kg$ ———						
0-15	1	9.57	0.6097	0.39	0.0242	0.0339	6.73	10.63
	2	8.89	0.5661	0.37	0.0241	0.0341	6.96	9.88
	3	10.18	0.6586	0.46	0.0268	0.0383	7.17	11.36
15-30	1	12.64	0.5091	0.32	0.0053	0.0319	9.98	13.51
	2	13.84	0.5703	0.35	0.0050	0.0279	9.29	14.79
	3	10.85	0.4289	0.30	0.0004	0.0294	9.45	11.61
30-46	1	12.89	0.6066	0.57	0.0072	0.0346	11.57	14.11
	2	12.57	0.6082	0.58	0.0073	0.0271	11.05	13.79
	3	12.39	0.6393	0.63	0.0035	0.0380	11.20	13.70
46-61	1	8.75	0.3958	0.52	0.0041	0.0303	8.33	9.70
	2	8.53	0.3717	0.50	0.0041	0.0249	8.02	9.44
	3	9.09	0.4219	0.64	0.0001	0.0341	8.57	10.19
61-76	1	8.55	0.4868	1.34	0.0040	0.0429	9.10	10.43
	2	5.32	0.2967	0.84	0.0034	0.0251	9.13	6.48
	3	8.63	0.5353	1.55	0.0001	0.0497	9.14	10.76
76-91	1	7.93	0.5957	2.37	0.0094	0.0424	9.99	10.95
	2	7.56	0.5554	2.18	0.0090	0.0351	9.52	10.34
	3	8.32	0.6560	2.66	0.0064	0.0485	10.20	11.70
91-107	1	6.46	0.5853	2.92	0.0472	0.0512	8.80	10.07
	2	6.32	0.5793	2.94	0.0474	0.0474	8.80	9.94
	3	6.43	0.6244	3.21	0.0491	0.0546	8.81	10.36
107-122	1	4.56	0.6364	3.12	0.0928	0.0448	8.00	8.49
	2	3.15	0.4390	2.08	0.0719	0.0385	7.62	5.80
	3	4.30	0.6391	3.29	0.0988	0.0491	8.11	8.41
122-137	1	2.83	0.4038	2.21	0.1265	0.0575	7.82	5.65
	2	4.08	0.6116	3.25	0.1999	0.0732	7.71	8.24
	3	3.53	0.5334	2.97	0.1693	0.0518	7.67	7.27
137-152	1	3.91	0.5712	3.34	0.1391	0.0646	7.54	8.05
	2	3.22	0.4817	2.81	0.1307	0.0500	7.60	6.72
	3	3.86	0.6153	3.60	0.1456	0.0568	7.83	8.30
152-168	1	3.86	0.5565	3.37	0.1027	0.0458	7.80	7.95
	2	3.93	0.5822	3.34	0.1152	0.0553	7.50	8.03
	3	3.77	0.5969	3.55	0.1092	0.0515	7.86	8.09
168-183	1	3.64	0.6376	2.87	0.0886	0.0353	7.08	7.30
	2	3.50	0.6458	2.99	0.0869	0.0447	7.16	7.30
	3	3.47	0.6496	3.02	0.0899	0.0410	7.09	7.31
183-198	1	3.98	0.5825	3.06	0.0675	0.0404	7.34	7.74
	2	3.94	0.6267	3.22	0.0741	0.0640	7.65	7.93
	3	3.78	0.5579	2.95	0.0661	0.0420	7.89	7.40

† Al and Fe are below detectable levels, <0.001 $cmol_c/kg$.

Table 32. The cation exchange capacity (CEC), effective cation exchange capacity (ECEC) and cation exchange phase composition ($cmol_c/kg$) of plot 9 with the ammonium chloride extraction method. (continued) †

Depth	Replicate	Ca	K	Mg	Mn	Na	CEC	ECEC
cm		——————————— $cmol_c/kg$ ———————————						
198-213	1	2.41	0.3754	1.92	0.0402	0.0295	6.56	4.79
	2	3.29	0.5703	2.85	0.0608	0.0485	6.36	6.87
	3	3.23	0.5641	2.85	0.0631	0.0453	6.74	6.77
213-229	1	2.30	0.3845	1.58	0.0260	0.0254	6.50	4.33
	2	3.37	0.5836	2.49	0.0388	0.0433	6.57	6.53
	3	3.48	0.6373	2.65	0.0458	0.0470	6.50	6.87
229-245	1	3.67	0.7123	2.32	0.0234	0.0354	6.94	6.76
	2	3.61	0.7609	2.45	0.0247	0.0481	6.59	6.90
	3	3.66	0.7621	2.50	0.0302	0.0403	5.26	6.99
245-261	1	3.62	0.7852	2.04	0.0415	0.0373	6.45	6.53
	2	3.81	0.8990	2.37	0.0573	0.0512	6.77	7.19
	3	3.73	0.8926	2.37	0.0565	0.0478	7.23	7.09

† Al and Fe are below detectable levels, <0.001 $cmol_c/kg$.

Table 33. The cation exchange capacity (CEC), effective cation exchange capacity (ECEC) and cation exchange phase composition ($cmol_c/kg$) of plot 10 with the ammonium chloride extraction method. †

Depth	Replicate	Ca	K	Mg	Mn	Na	CEC	ECEC
cm		$cmol_c/kg$						
0-15	1	6.91	0.7967	0.49	0.2044	0.0802	6.34	8.48
	2	6.62	0.7379	0.47	0.1551	0.0433	6.54	8.03
	3	6.48	0.7148	0.47	0.1625	0.0403	6.43	7.88
15-30	1	8.50	0.6003	0.76	0.0523	0.0363	7.91	9.95
	2	7.50	0.5208	0.69	0.0378	0.0289	8.07	8.78
	3	8.22	0.5729	0.74	0.0412	0.0266	7.63	9.60
30-46	1	11.38	0.7519	1.66	0.0471	0.0422	18.47	13.87
	2	11.37	0.7391	1.64	0.0431	0.0395	10.80	13.83
	3	11.12	0.7148	1.61	0.0426	0.0378	11.04	13.52
46-61	1	10.71	0.6752	2.06	0.0399	0.0456	19.08	13.53
	2	10.33	0.6445	1.98	0.0384	0.0466	10.63	13.04
	3	9.52	0.5876	1.86	0.0342	0.0378	10.86	12.03
61-76	1	8.70	0.5653	2.15	0.0223	0.0434	20.67	11.48
	2	7.79	0.5092	1.98	0.0199	0.0406	9.30	10.34
	3	8.45	0.5326	2.13	0.0208	0.0392	9.31	11.17
76-91	1	5.52	0.4313	1.77	0.0107	0.0309	14.43	7.77
	2	4.88	0.3533	1.55	0.0084	0.0260	10.98	6.82
	3	5.33	0.3885	1.70	0.0090	0.0249	6.82	7.45
91-107	1	6.38	0.6362	2.88	0.0185	0.0352	16.09	9.95
	2	5.86	0.5785	2.56	0.0162	0.0330	9.08	9.05
	3	6.46	0.6445	2.93	0.0171	0.0322	8.44	10.08
107-122	1	5.55	0.7724	3.77	0.0226	0.0468	14.51	10.16
	2	6.29	0.8593	4.14	0.0244	0.0516	9.60	11.37
	3	6.38	0.8734	4.17	0.0232	0.0449	9.83	11.49
122-137	1	4.20	0.6624	3.69	0.0891	0.0538	19.54	8.71
	2	4.71	0.7302	4.14	0.0977	0.0584	8.63	9.75
	3	4.77	0.6995	4.12	0.0970	0.0543	8.64	9.76
137-152	1	3.97	0.7302	3.99	0.1008	0.0484	14.26	8.87
	2	3.92	0.7442	3.93	0.1056	0.0489	8.03	8.78
	3	3.71	0.6867	3.72	0.1054	0.0388	7.92	8.29
152-168	1	4.17	0.7813	4.00	0.1407	0.0517	13.40	9.16
	2	4.18	0.7826	3.90	0.1363	0.0517	8.01	9.06
	3	3.77	0.6714	3.41	0.1227	0.0448	7.94	8.02
168-183	1	4.19	0.6803	3.80	0.0853	0.0581	24.67	8.82
	2	4.13	0.6777	3.77	0.0841	0.0598	7.76	8.73
	3	3.66	0.5770	3.24	0.0696	0.0548	7.59	7.61
183-198	1	3.79	0.5446	3.19	0.0681	0.0528	13.27	7.64
	2	4.13	0.6036	3.52	0.0779	0.0582	7.47	8.39
	3	4.17	0.6153	3.51	0.0778	0.0615	7.31	8.44

† Al and Fe are below detectable levels, <0.001 $cmol_c/kg$.

Table 33. The cation exchange capacity (CEC), effective cation exchange capacity (ECEC) and cation exchange phase composition ($cmol_c/kg$) of plot 10 with the ammonium chloride extraction method. (continued) †

Depth	Replicate	Ca	K	Mg	Mn	Na	CEC	ECEC
cm		——————————— $cmol_c/kg$ ———————————						
198-213	1	3.84	0.5921	3.07	0.0438	0.0500	12.41	7.60
	2	4.07	0.6141	3.26	0.0450	0.0520	7.20	8.04
	3	3.93	0.6202	3.23	0.0440	0.0542	6.80	7.88
213-229	1	3.30	0.5235	3.01	0.0637	0.0573	12.01	6.95
	2	3.38	0.5335	3.06	0.0648	0.0524	6.56	7.09
	3	3.25	0.5051	2.94	0.0638	0.0524	6.32	6.82
229-245	1	2.48	0.4895	2.36	0.0301	0.0447	11.61	5.41
	2	2.92	0.5494	2.67	0.1056	0.0505	5.86	6.30
	3	3.01	0.5554	2.84	0.1074	0.0520	6.05	6.57
245-261	1	2.73	0.6185	2.56	0.0844	0.0488	11.60	6.06
	2	2.75	0.6141	2.53	0.0848	0.0472	5.69	6.05
	3	2.72	0.5987	2.56	0.0884	0.0480	6.13	6.04

† Al and Fe are below detectable levels, <0.001 $cmol_c/kg$.

Table 34. Effective anion exchange capacity (EAEC), and anion exchange phase composition ($cmol_c/kg$) of plot 1 using the potassium acetate extraction method.

Depth	Replicate	SO_4	NO_3	Cl	EAEC
cm		——— $cmol_c/kg$ ———			
0-15	1	0.0421	0.0891	0.0535	0.1265
	2	0.0100	0.0995	0.0374	0.1570
	3	0.0000	0.0998	0.0374	0.2375
15-30	1	0.0000	0.0277	0.0000	0.0485
	2	0.0118	0.0322	0.0420	0.0977
	3	0.0067	0.0353	0.0073	0.0353
30-46	1	0.0373	0.0260	0.0379	0.0938
	2	0.0000	0.0389	0.0523	0.0912
	3	0.0305	0.0382	0.0068	0.1507
46-61	1	0.0155	0.0219	0.0405	0.0449
	2	0.0000	0.0322	0.0480	0.0802
	3	0.0053	0.0278	0.0126	0.0992
61-76	1	0.0219	0.0168	0.0436	0.0662
	2	0.0326	0.0303	0.0547	0.1502
	3	0.0247	0.0275	0.0000	0.1149
76-91	1	0.0265	0.0158	0.0457	0.0672
	2	0.0307	0.0250	0.0485	0.1348
	3	0.0257	0.0228	0.0000	0.1215
91-107	1	0.0382	0.0159	0.0434	0.0899
	2	0.0178	0.0260	0.0549	0.1164
	3	0.0370	0.0214	0.0000	0.1413
107-122	1	0.0354	0.0188	0.0372	0.0505
	2	0.0080	0.0204	0.0329	0.0692
	3	0.0159	0.0198	0.0000	0.1279
122-137	1	0.0385	0.0120	0.0441	0.0239
	2	0.0367	0.0182	0.0322	0.1238
	3	0.0000	0.0150	0.0118	0.1361
137-152	1	0.0321	0.0014	0.0410	0.0106
	2	0.0332	0.0185	0.0307	0.1157
	3	0.0000	0.0127	0.0092	0.1179
152-168	1	0.0265	0.0114	0.0546	0.0368
	2	0.0299	0.0178	0.0439	0.1214
	3	0.0079	0.0147	0.0096	0.1222
168-183	1	0.0377	0.0113	0.0618	0.0383
	2	0.0397	0.0138	0.0299	0.1231
	3	0.0135	0.0139	0.0000	0.1511
183-198	1	0.0403	0.0086	0.0598	0.1077
	2	0.0424	0.0067	0.0489	0.1404
	3	0.0455	0.0129	0.0080	0.1533

Table 34. Effective anion exchange capacity (EAEC), and anion exchange phase composition ($cmol_c/kg$) of plot 1 using the potassium acetate extraction method. (continued)

Depth	Replicate	SO_4	NO_3	Cl	EAEC
cm		——— $cmol_c/kg$ ———			
198-213	1	0.0405	0.0088	0.0580	0.1236
	2	0.0533	0.0057	0.0501	0.1624
	3	0.0524	0.0122	0.0100	0.1513
213-229	1	0.0386	0.0059	0.0509	0.0593
	2	0.0473	0.0039	0.0267	0.1252
	3	0.0206	0.0135	0.0123	0.1415
229-245	1	0.0349	0.0072	0.0567	0.1242
	2	0.0150	0.0041	0.0272	0.0615
	3	0.0492	0.0139	0.0185	0.1404
245-261	1	0.0474	0.0118	0.0647	0.1216
	2	0.0403	0.0044	0.0267	0.1117
	3	0.0466	0.0145	0.0165	0.1741

Table 35. Effective anion exchange capacity (EAEC), and anion exchange phase composition ($cmol_c/kg$) of plot 2 using the potassium acetate extraction method.

Depth	Replicate	SO_4	NO_3	Cl	EAEC
cm		——— $cmol_c/kg$ ———			
0-15	1	0.0130	0.1257	0.0237	0.3336
	2	0.0000	0.1760	0.0090	0.1850
	3	0.0506	0.1772	0.1068	0.2268
15-30	1	0.0145	0.0006	0.0000	0.1977
	2	0.0167	0.0423	0.0000	0.0756
	3	0.0475	0.0318	0.1020	0.0607
30-46	1	0.0859	0.0146	1.4179	0.1588
	2	0.0162	0.0413	0.0000	0.0737
	3	0.0413	0.0335	0.0615	1.6232
46-61	1	0.0177	0.0124	0.0133	0.1586
	2	0.0151	0.0245	0.0000	0.0548
	3	0.0444	0.0191	0.0573	0.0678
61-76	1	0.0236	0.0008	0.0159	0.1588
	2	0.0332	0.0007	0.0394	0.1066
	3	0.0468	0.0136	0.0643	0.0768
76-91	1	0.0478	0.0189	0.0179	0.2524
	2	0.0558	0.0187	0.0500	0.1803
	3	0.0747	0.0227	0.0841	0.1362
91-107	1	0.0091	0.0121	0.0200	0.1507
	2	0.0000	0.0048	0.0000	0.0048
	3	0.0383	0.0227	0.0620	0.0609
107-122	1	0.0273	0.0006	0.0189	0.2054
	2	0.0378	0.0064	0.0526	0.1346
	3	0.0635	0.0160	0.0778	0.0895
122-137	1	0.0000	0.0015	0.0126	0.1550
	2	0.0525	0.0002	0.0648	0.1700
	3	0.0414	0.0091	0.0706	0.0216
137-152	1	0.0180	0.0115	0.0300	0.2304
	2	0.0469	0.0050	0.0612	0.1600
	3	0.0556	0.0132	0.1077	0.0792
152-168	1	0.0301	0.0182	0.0329	0.2211
	2	0.0387	0.0057	0.0743	0.1574
	3	0.0536	0.0205	0.0957	0.1135
168-183	1	0.0353	0.0124	0.0267	0.2223
	2	0.0844	0.0060	0.0842	0.2591
	3	0.0605	0.0150	0.0889	0.1122
183-198	1	0.1044	0.0047	0.0221	0.2408
	2	0.0562	0.0010	0.0674	0.1807
	3	0.0675	0.0114	0.1011	0.2423

Table 35. Effective anion exchange capacity (EAEC), and anion exchange phase composition ($cmol_c/kg$) of plot 2 using the potassium acetate extraction method. (continued)

Depth	Replicate	SO_4	NO_3	Cl	EAEC
cm		——— $cmol_c/kg$ ———			
198-213	1	0.0357	0.0006	0.0230	0.2456
	2	0.0549	0.0019	0.0629	0.1746
	3	0.0739	0.0101	0.0972	0.1044
213-229	1	0.0272	0.0007	0.0243	0.2530
	2	0.0699	0.0009	0.0966	0.2373
	3	0.0707	0.0115	0.1108	0.0902
229-245	1	0.0411	0.0007	0.0259	0.2052
	2	0.0000	0.0010	0.0000	0.0010
	3	0.0635	0.0108	0.0775	0.1190
245-261	1	0.0442	0.0012	0.0375	0.2481
	2	0.0632	0.0017	0.0728	0.2010
	3	0.0736	0.0110	0.0998	0.1370

Table 36. Effective anion exchange capacity (EAEC), and anion exchange phase composition ($cmol_c/kg$) of plot 3 using the potassium acetate extraction method.

Depth	Replicate	SO_4	NO_3	Cl	EAEC
cm		——— $cmol_c/kg$ ———			
0-15	1	0.0527	0.0003	0.1035	0.2461
	2	0.0585	0.0001	0.0546	0.1718
	3	0.1229	0.0006	0.0000	0.2095
15-30	1	0.0994	0.0004	0.0652	0.0820
	2	0.0250	0.0002	0.0418	0.0918
	3	0.0236	0.0006	0.0345	0.2646
30-46	1	0.0059	0.0224	0.0000	0.1045
	2	0.0212	0.0002	0.0387	0.0813
	3	0.0229	0.0005	0.0363	0.0123
46-61	1	0.0126	0.0234	0.0444	0.2028
	2	0.0190	0.0109	0.0333	0.0822
	3	0.0897	0.0013	0.0000	0.0708
61-76	1	0.0295	0.0210	0.0670	0.1003
	2	0.0259	0.0192	0.0489	0.1199
	3	0.0230	0.0201	0.0332	0.1462
76-91	1	0.0121	0.0208	0.0431	0.1233
	2	0.0232	0.0194	0.0407	0.1064
	3	0.0242	0.0216	0.0540	0.0888
91-107	1	0.0150	0.0168	0.0524	0.1034
	2	0.0298	0.0203	0.0000	0.0800
	3	0.0233	0.0189	0.0401	0.1013
107-122	1	0.0190	0.0113	0.0509	0.0921
	2	0.0901	0.0058	0.0000	0.1860
	3	0.0224	0.0134	0.0359	0.1022
122-137	1	0.0261	0.0019	0.0470	0.1006
	2	0.0000	0.0007	0.0000	0.0007
	3	0.0239	0.0082	0.0510	0.1074
137-152	1	0.0372	0.0074	0.0521	0.1486
	2	0.0217	0.0009	0.0000	0.0443
	3	0.0460	0.0077	0.0492	0.1343
152-168	1	0.0345	0.0260	0.0489	0.2065
	2	0.0763	0.0178	0.0671	0.2375
	3	0.0590	0.0226	0.0626	0.1406
168-183	1	0.0682	0.0164	0.1094	0.1749
	2	0.0385	0.0006	0.0473	0.1248
	3	0.0499	0.0068	0.0587	0.2526
183-198	1	0.0558	0.0191	0.0856	0.1620
	2	0.0407	0.0007	0.0577	0.1398
	3	0.0467	0.0043	0.0494	0.2016

Table 36. Effective anion exchange capacity (EAEC), and anion exchange phase composition ($cmol_c/kg$) of plot 3 using the potassium acetate extraction method. (continued)

Depth	Replicate	SO_4	NO_3	Cl	EAEC
cm		$cmol_c/kg$			
198-213	1	0.0437	0.0203	0.0485	0.1421
	2	0.0559	0.0009	0.0415	0.1543
	3	0.0373	0.0041	0.0472	0.1400
213-229	1	0.0306	0.0253	0.0462	0.1403
	2	0.0368	0.0006	0.0364	0.1107
	3	0.0381	0.0046	0.0386	0.1121
229-245	1	0.0446	0.0296	0.0399	0.2214
	2	0.0421	0.0007	0.0535	0.1384
	3	0.0651	0.0012	0.0615	0.1302
245-261	1	0.0393	0.0300	0.0507	0.1447
	2	0.0151	0.0014	0.0256	0.0571
	3	0.0574	0.0021	0.0000	0.1315

Table 37. Effective anion exchange capacity (EAEC), and anion exchange phase composition ($cmol_c/kg$) of plot 4 using the potassium acetate extraction method.

Depth	Replicate	SO_4	NO_3	Cl	EAEC
cm		——————————— $cmol_c/kg$ ———————————			
0-15	1	0.0125	0.1346	0.0416	0.1779
	2	0.0472	0.1362	0.0316	0.2623
	3	0.0000	0.1442	0.0433	0.2108
15-30	1	0.0193	0.0420	0.0403	0.0717
	2	0.0352	0.0273	0.0293	0.1271
	3	0.0000	0.0449	0.0298	0.1237
30-46	1	0.0376	0.0359	0.0340	0.0773
	2	0.0422	0.0260	0.0000	0.1105
	3	0.0054	0.0325	0.0306	0.1418
46-61	1	0.0683	0.0226	0.0442	0.0584
	2	0.0169	0.0009	0.0457	0.0804
	3	0.0000	0.0183	0.0358	0.1990
61-76	1	0.1039	0.0094	0.0392	0.0570
	2	0.0214	0.0037	0.0581	0.1047
	3	0.0000	0.0100	0.0477	0.2570
76-91	1	0.0400	0.0117	0.0000	0.0504
	2	0.0164	0.0014	0.0444	0.0786
	3	0.0000	0.0071	0.0386	0.0872
91-107	1	0.0238	0.0099	0.0349	0.0099
	2	0.0111	0.0063	0.0302	0.0587
	3	0.0000	0.0068	0.0000	0.0894
107-122	1	0.1250	0.0193	0.0631	0.1093
	2	0.0116	0.0060	0.0315	0.0606
	3	0.0198	0.0147	0.0503	0.3277
122-137	1	0.0652	0.0055	0.0392	0.0763
	2	0.0225	0.0034	0.0609	0.1093
	3	0.0169	0.0061	0.0371	0.1757
137-152	1	0.0919	0.0038	0.0000	0.0822
	2	0.0164	0.0032	0.0444	0.0804
	3	0.0220	0.0049	0.0344	0.1888
152-168	1	0.1115	0.0020	0.0576	0.0659
	2	0.0490	0.0020	0.0673	0.1673
	3	0.0162	0.0009	0.0316	0.2816
168-183	1	0.0760	0.0014	0.0704	0.1173
	2	0.0229	0.0013	0.0597	0.1068
	3	0.0402	0.0007	0.0355	0.2231
183-198	1	0.0849	0.0001	0.0528	0.0991
	2	0.0585	0.0016	0.0728	0.1914
	3	0.0345	0.0006	0.0300	0.2231

Table 37. Effective anion exchange capacity (EAEC), and anion exchange phase composition ($cmol_c/kg$) of plot 4 using the potassium acetate extraction method. (continued)

Depth	Replicate	SO_4	NO_3	Cl	EAEC
cm		$cmol_c/kg$			
198-213	1	0.0469	0.0019	0.0354	0.0379
	2	0.0215	0.0011	0.0804	0.1246
	3	0.0180	0.0008	0.0000	0.1299
213-229	1	0.0457	0.0012	0.0332	0.0831
	2	0.0247	0.0024	0.0481	0.1000
	3	0.0410	0.0030	0.0000	0.1277
229-245	1	0.0530	0.0057	0.0407	0.0873
	2	0.0183	0.0015	0.0426	0.0807
	3	0.0215	0.0002	0.0385	0.1470
245-261	1	0.0494	0.0150	0.0544	0.1193
	2	0.0315	0.0187	0.0495	0.1312
	3	0.0285	0.0106	0.0472	0.1639

Table 38. Effective anion exchange capacity (EAEC), and anion exchange phase composition ($cmol_c/kg$) of plot 5 using the potassium acetate extraction method.

Depth	Replicate	SO_4	NO_3	Cl	EAEC
cm		——— $cmol_c/kg$ ———			
0-15	1	0.0000	0.2002	0.0393	0.2789
	2	0.0000	0.1668	0.0000	0.1668
	3	0.0111	0.2278	0.0566	0.2671
15-30	1	0.0000	0.0403	0.0000	0.0687
	2	0.0000	0.0679	0.0000	0.0679
	3	0.0000	0.0017	0.0283	0.0017
30-46	1	0.0162	0.0553	0.0401	0.0921
	2	0.0186	0.0767	0.0439	0.1577
	3	0.0000	0.0776	0.0368	0.1500
46-61	1	0.0000	0.0284	0.0908	0.0501
	2	0.0198	0.0345	0.0481	0.1222
	3	0.0000	0.0252	0.0217	0.1160
61-76	1	0.0130	0.0224	0.1049	0.0224
	2	0.0000	0.0277	0.0000	0.0277
	3	0.0000	0.0288	0.0000	0.1597
76-91	1	0.0147	0.0064	0.0580	0.0366
	2	0.0000	0.0272	0.0000	0.0272
	3	0.0000	0.0250	0.0302	0.1124
91-107	1	0.0355	0.0270	0.0384	0.0863
	2	0.0058	0.0225	0.0316	0.0658
	3	0.0118	0.0218	0.0357	0.1312
107-122	1	0.0401	0.0254	0.0309	0.1652
	2	0.0354	0.0264	0.0457	0.1430
	3	0.0379	0.0265	0.0639	0.1376
122-137	1	0.0342	0.0245	0.0454	0.2275
	2	0.0523	0.0149	0.0420	0.1615
	3	0.0583	0.0147	0.0865	0.1285
137-152	1	0.0374	0.0170	0.0427	0.1921
	2	0.0582	0.0089	0.0496	0.1749
	3	0.0570	0.0103	0.0609	0.1278
152-168	1	0.0597	0.0299	0.0420	0.1833
	2	0.0671	0.0234	0.0441	0.2019
	3	0.0480	0.0244	0.0574	0.1858
168-183	1	0.0461	0.0188	0.0509	0.1686
	2	0.0408	0.0258	0.0444	0.1519
	3	0.0482	0.0213	0.0535	0.1644
183-198	1	0.0390	0.0260	0.0327	0.1616
	2	0.0209	0.0351	0.0303	0.1072
	3	0.0381	0.0266	0.0594	0.1374

Table 38. Effective anion exchange capacity (EAEC), and anion exchange phase composition ($cmol_c/kg$) of plot 5 using the potassium acetate extraction method. (continued)

Depth	Replicate	SO_4	NO_3	Cl	EAEC
cm		——— $cmol_c/kg$ ———			
198-213	1	0.0258	0.0219	0.0401	0.1504
	2	0.0403	0.0146	0.0329	0.1281
	3	0.0385	0.0188	0.0516	0.1105
213-229	1	0.0362	0.0173	0.0440	0.1330
	2	0.0216	0.0131	0.0440	0.1003
	3	0.0315	0.0190	0.0527	0.1355
229-245	1	0.0495	0.0207	0.0457	0.1427
	2	0.0375	0.0144	0.0467	0.1361
	3	0.0390	0.0189	0.0440	0.1636
245-261	1	0.0368	0.0192	0.0000	0.1644
	2	0.0414	0.0139	0.0540	0.1507
	3	0.0491	0.0167	0.0471	0.0903

Table 39. Effective anion exchange capacity (EAEC), and anion exchange phase composition ($cmol_c/kg$) of plot 6 using the potassium acetate extraction method.

Depth	Replicate	SO_4	NO_3	Cl	EAEC
cm		——— $cmol_c/kg$ ———			
0-15	1	0.0407	0.2342	0.0000	0.3932
	2	0.0000	0.2310	0.0000	0.2342
	3	0.0366	0.2594	0.0525	0.3043
15-30	1	0.0000	0.0891	0.0000	0.1271
	2	0.0000	0.0867	0.0317	0.0891
	3	0.0260	0.1040	0.0231	0.1703
30-46	1	0.0000	0.0473	0.0000	0.0921
	2	0.0000	0.0476	0.0161	0.0473
	3	0.0204	0.0587	0.0334	0.1045
46-61	1	0.0000	0.0321	0.0000	0.0464
	2	0.0000	0.0356	0.0139	0.0321
	3	0.0229	0.0464	0.0000	0.0954
61-76	1	0.0000	0.0068	0.0505	0.0276
	2	0.0319	0.0166	0.0105	0.1210
	3	0.0221	0.0276	0.0000	0.0712
76-91	1	0.0147	0.0112	0.0338	0.0938
	2	0.0437	0.0118	0.0285	0.1326
	3	0.0318	0.0241	0.0402	0.1040
91-107	1	0.0236	0.0093	0.0392	0.0576
	2	0.0438	0.0120	0.0414	0.1362
	3	0.0401	0.0105	0.0000	0.1337
107-122	1	0.0255	0.0136	0.0333	0.0574
	2	0.0479	0.0196	0.0265	0.1427
	3	0.0463	0.0065	0.0000	0.1386
122-137	1	0.0287	0.0028	0.0331	0.0957
	2	0.0479	0.0066	0.0325	0.1315
	3	0.0579	0.0074	0.0309	0.1549
137-152	1	0.0274	0.0056	0.0318	0.0934
	2	0.0392	0.0118	0.0418	0.1157
	3	0.0820	0.0013	0.0372	0.2175
152-168	1	0.0067	0.0010	0.0359	0.0497
	2	0.0477	0.0078	0.0509	0.1323
	3	0.0519	0.0030	0.0333	0.1624
168-183	1	0.0220	0.0008	0.0302	0.0757
	2	0.0404	0.0060	0.0359	0.1118
	3	0.0548	0.0023	0.0295	0.1515
183-198	1	0.0219	0.0247	0.0141	0.0548
	2	0.0445	0.0243	0.0464	0.1279
	3	0.0729	0.0110	0.0000	0.2165

Table 39. Effective anion exchange capacity (EAEC), and anion exchange phase composition ($cmol_c/kg$) of plot 6 using the potassium acetate extraction method. (continued)

Depth	Replicate	SO_4	NO_3	Cl	EAEC
cm		——— $cmol_c/kg$ ———			
198-213	1	0.0344	0.0046	0.0310	0.1050
	2	0.0450	0.0109	0.0362	0.1257
	3	0.0585	0.0046	0.0316	0.1642
213-229	1	0.0271	0.0012	0.0242	0.1470
	2	0.0443	0.0047	0.0000	0.1141
	3	0.0394	0.0022	0.0905	0.0835
229-245	1	0.0468	0.0083	0.0315	0.1497
	2	0.0493	0.0100	0.0557	0.1385
	3	0.1246	0.0018	0.0543	0.3149
245-261	1	0.0473	0.0028	0.0000	0.1379
	2	0.0446	0.0077	0.0771	0.0920
	3	0.0505	0.0021	0.0413	0.1860

Table 40. Effective anion exchange capacity (EAEC), and anion exchange phase composition ($cmol_c/kg$) of plot 7 using the potassium acetate extraction method.

Depth	Replicate	SO_4	NO_3	Cl	EAEC
cm		——— $cmol_c/kg$ ———			
0-15	1	0.1038	0.1866	0.0000	0.2350
	2	0.0242	0.2035	0.0000	0.3033
	3	0.0363	0.1883	0.0271	0.3960
15-30	1	0.0879	0.0446	0.0502	0.1044
	2	0.0161	0.0572	0.0276	0.0941
	3	0.0184	0.0456	0.0000	0.2718
30-46	1	0.0447	0.0301	0.0336	0.1090
	2	0.0175	0.0276	0.0439	0.0598
	3	0.0161	0.0311	0.0000	0.1540
46-61	1	0.0747	0.0261	0.0552	0.0773
	2	0.0130	0.0236	0.0252	0.0760
	3	0.0188	0.0129	0.0147	0.2174
61-76	1	0.0231	0.0169	0.0299	0.0650
	2	0.0126	0.0170	0.0230	0.0770
	3	0.0153	0.0174	0.0293	0.0936
76-91	1	0.0457	0.0212	0.0000	0.0847
	2	0.0149	0.0212	0.0336	0.0946
	3	0.0216	0.0201	0.0303	0.1116
91-107	1	0.0335	0.0250	0.0431	0.1036
	2	0.0204	0.0238	0.0378	0.1159
	3	0.0299	0.0243	0.0322	0.1343
107-122	1	0.0313	0.0157	0.0439	0.0157
	2	0.0000	0.0130	0.0000	0.1048
	3	0.0285	0.0015	0.0347	0.1081
122-137	1	0.0252	0.0108	0.0646	0.0895
	2	0.0380	0.0109	0.0028	0.1198
	3	0.0407	0.0067	0.0275	0.1217
137-152	1	0.0485	0.0065	0.0503	0.1346
	2	0.0617	0.0081	0.0047	0.3074
	3	0.1377	0.0012	0.0239	0.1485
152-168	1	0.0378	0.0428	0.0638	0.1293
	2	0.0302	0.0447	0.0260	0.1777
	3	0.0436	0.0430	0.0458	0.1824
168-183	1	0.0273	0.0156	0.0420	0.1253
	2	0.0453	0.0144	0.0192	0.1264
	3	0.0413	0.0126	0.0295	0.1091
183-198	1	0.0255	0.0132	0.0485	0.1777
	2	0.0682	0.0124	0.0281	0.1416
	3	0.0548	0.0125	0.0196	0.1120

Table 40. Effective anion exchange capacity (EAEC), and anion exchange phase composition ($cmol_c/kg$) of plot 7 using the potassium acetate extraction method. (continued)

Depth	Replicate	SO_4	NO_3	Cl	EAEC
cm		——— $cmol_c/kg$ ———			
198-213	1	0.0315	0.0097	0.0502	0.0899
	2	0.0401	0.0105	0.0000	0.1344
	3	0.0455	0.0103	0.0328	0.1235
213-229	1	0.0705	0.0082	0.0000	0.1675
	2	0.0560	0.0096	0.0472	0.1775
	3	0.0659	0.0085	0.0360	0.1494
229-245	1	0.0305	0.0095	0.0505	0.1208
	2	0.0454	0.0134	0.0205	0.1339
	3	0.0453	0.0079	0.0298	0.1193
245-261	1	0.0242	0.0116	0.0346	0.0116
	2	0.0000	0.0116	0.0000	0.1195
	3	0.0539	0.0096	0.0000	0.0926

Table 41. Effective anion exchange capacity (EAEC), and anion exchange phase composition ($cmol_c/kg$) of plot 8 using the potassium acetate extraction method.

Depth	Replicate	SO_4	NO_3	Cl	EAEC
cm		——— $cmol_c/kg$ ———			
0-15	1	0.0292	0.1549	0.0297	0.2503
	2	0.0219	0.1874	0.0191	0.2168
	3	0.0228	0.1476	0.0162	0.2357
15-30	1	0.0205	0.0309	0.0400	0.1738
	2	0.0511	0.0499	0.0217	0.0822
	3	0.0163	0.0347	0.0188	0.1157
30-46	1	0.0198	0.0384	0.0310	0.1004
	2	0.0223	0.0392	0.0167	0.1002
	3	0.0227	0.0394	0.0166	0.1100
46-61	1	0.0357	0.0486	0.0264	0.1128
	2	0.0226	0.0490	0.0185	0.0486
	3	0.0000	0.0462	0.0000	0.1440
61-76	1	0.0461	0.0221	0.0291	0.0785
	2	0.0191	0.0184	0.0218	0.0873
	3	0.0240	0.0226	0.0171	0.1439
76-91	1	0.0198	0.0140	0.0316	0.0634
	2	0.0172	0.0150	0.0140	0.1017
	3	0.0327	0.0156	0.0222	0.0867
91-107	1	0.0310	0.0100	0.0452	0.0729
	2	0.0214	0.0126	0.0175	0.1170
	3	0.0397	0.0109	0.0275	0.1181
107-122	1	0.0381	0.0079	0.0261	0.1047
	2	0.0322	0.0139	0.0265	0.0232
	3	0.0053	0.0134	0.0047	0.1158
122-137	1	0.0428	0.0060	0.0300	0.1185
	2	0.0541	0.0103	0.0000	0.1108
	3	0.0380	0.0107	0.0289	0.1262
137-152	1	0.0414	0.0036	0.0269	0.1162
	2	0.0445	0.0082	0.0190	0.1530
	3	0.0617	0.0077	0.0260	0.1174
152-168	1	0.0524	0.0067	0.0239	0.1647
	2	0.0628	0.0111	0.0279	0.0364
	3	0.0053	0.0108	0.0192	0.1395
168-183	1	0.0641	0.0057	0.0225	0.1578
	2	0.0628	0.0105	0.0218	0.0943
	3	0.0302	0.0092	0.0281	0.1600
183-198	1	0.0678	0.0051	0.0256	0.1824
	2	0.0759	0.0078	0.0228	0.0957
	3	0.0453	0.0076	0.0000	0.1688

Table 41. Effective anion exchange capacity (EAEC), and anion exchange phase composition ($cmol_c/kg$) of plot 8 using the potassium acetate extraction method. (continued)

Depth	Replicate	SO_4	NO_3	Cl	EAEC
cm		——— $cmol_c/kg$ ———			
198-213	1	0.0548	0.0016	0.0000	0.2888
	2	0.1413	0.0062	0.0000	0.1852
	3	0.0682	0.0069	0.0472	0.1166
213-229	1	0.0706	0.0025	0.0206	0.2020
	2	0.0774	0.0107	0.0366	0.1145
	3	0.0560	0.0112	0.0000	0.1731
229-245	1	0.0571	0.0034	0.0256	0.2707
	2	0.1320	0.0067	0.0000	0.1212
	3	0.0454	0.0077	0.0271	0.1475
245-261	1	0.0511	0.0832	0.0265	0.1307
	2	0.0525	0.0070	0.0186	0.0832
	3	0.0000	0.0068	0.0000	0.1354

Table 42. Effective anion exchange capacity (EAEC), and anion exchange phase composition ($cmol_c/kg$) of plot 9 using the potassium acetate extraction method.

Depth	Replicate	SO_4	NO_3	Cl	EAEC
cm		——— $cmol_c/kg$ ———			
0-15	1	0.0363	0.0969	0.0000	0.1865
	2	0.0292	0.1113	0.0310	0.2351
	3	0.0511	0.0449	0.0217	0.1176
15-30	1	0.0184	0.0483	0.0000	0.1146
	2	0.0205	0.0478	0.0252	0.1805
	3	0.0433	0.0260	0.0461	0.0628
30-46	1	0.0068	0.0292	0.0148	0.0952
	2	0.0198	0.0293	0.0264	0.1297
	3	0.0502	0.0079	0.0000	0.0364
46-61	1	0.0161	0.0352	0.0293	0.0902
	2	0.0130	0.0331	0.0291	0.1171
	3	0.0313	0.0299	0.0213	0.0915
61-76	1	0.0188	0.0407	0.0303	0.1437
	2	0.0357	0.0381	0.0316	0.1536
	3	0.0438	0.0342	0.0281	0.1021
76-91	1	0.0153	0.0331	0.0322	0.0936
	2	0.0219	0.0344	0.0167	0.2361
	3	0.0751	0.0302	0.0515	0.0930
91-107	1	0.0299	0.0319	0.0275	0.1694
	2	0.0461	0.0283	0.0452	0.3044
	3	0.1381	0.0291	0.0000	0.1164
107-122	1	0.0285	0.0192	0.0239	0.1112
	2	0.0310	0.0193	0.0300	0.5822
	3	0.2537	0.0162	0.0556	0.0971
122-137	1	0.0407	0.0150	0.0458	0.1181
	2	0.0381	0.0145	0.0269	0.4869
	3	0.2100	0.0126	0.0525	0.1398
137-152	1	0.1377	0.0154	0.0503	0.1249
	2	0.0428	0.0125	0.0239	0.2568
	3	0.1090	0.0122	0.0263	0.3379
152-168	1	0.0436	0.0132	0.0295	0.1185
	2	0.0414	0.0122	0.0225	0.1830
	3	0.0632	0.0123	0.0445	0.1290
168-183	1	0.0168	0.0153	0.0196	0.1469
	2	0.0524	0.0120	0.0268	0.1853
	3	0.0738	0.0144	0.0258	0.0677
183-198	1	0.0413	0.0205	0.0328	0.1743
	2	0.0641	0.0202	0.0256	0.2821
	3	0.0958	0.0218	0.0703	0.1371

Table 42. Effective anion exchange capacity (EAEC), and anion exchange phase composition ($cmol_c/kg$) of plot 9 using the potassium acetate extraction method. (continued)

Depth	Replicate	SO_4	NO_3	Cl	EAEC
cm		$cmol_c/kg$			
198-213	1	0.0548	0.0124	0.0359	0.0450
	2	0.0163	0.0119	0.0000	0.1295
	3	0.0588	0.0290	0.0000	0.1746
213-229	1	0.0455	0.0109	0.0298	0.1670
	2	0.0678	0.0099	0.0205	0.1116
	3	0.0487	0.0092	0.0045	0.1300
229-245	1	0.0453	0.0072	0.0297	0.1425
	2	0.0548	0.0065	0.0256	0.2527
	3	0.1231	0.0063	0.0000	0.1267
245-261	1	0.0539	0.0104	0.0400	0.1437
	2	0.0571	0.0092	0.0191	0.2953
	3	0.1349	0.0104	0.0163	0.1582

Table 43. Effective anion exchange capacity (EAEC), and anion exchange phase composition ($cmol_c/kg$) of plot 10 using the potassium acetate extraction method.

Depth	Replicate	SO_4	NO_3	Cl	EAEC
cm		——— $cmol_c/kg$ ———			
0-15	1	0.0533	0.1213	0.0000	0.2141
	2	0.0323	0.1191	0.0305	0.1213
	3	0.0000	0.1198	0.0000	0.2264
15-30	1	0.0678	0.0314	0.0005	0.0243
	2	0.0000	0.0243	0.0000	0.2318
	3	0.1002	0.0281	0.0000	0.1641
30-46	1	0.0541	0.0238	0.0000	0.1528
	2	0.0536	0.0231	0.0224	0.0238
	3	0.0000	0.0239	0.0000	0.1320
46-61	1	0.0419	0.0349	0.0000	0.1719
	2	0.0505	0.0330	0.0378	0.1861
	3	0.0663	0.0254	0.0185	0.1093
61-76	1	0.0711	0.0408	0.0086	0.1923
	2	0.0662	0.0391	0.0209	0.2038
	3	0.0815	0.0381	0.0000	0.1889
76-91	1	0.0336	0.0337	0.0066	0.1212
	2	0.0359	0.0248	0.0245	0.1663
	3	0.0403	0.0232	0.0519	0.0970
91-107	1	0.0252	0.0297	0.0130	0.1430
	2	0.0409	0.0282	0.0330	0.3684
	3	0.1432	0.0279	0.0523	0.0911
107-122	1	0.1501	0.0317	0.0912	0.1896
	2	0.0682	0.0302	0.0230	0.2469
	3	0.0984	0.0306	0.0183	0.4220
122-137	1	0.1808	0.0274	0.0539	0.2048
	2	0.0767	0.0268	0.0245	0.5549
	3	0.2354	0.0247	0.0568	0.4401
137-152	1	0.0827	0.0183	0.0154	0.5037
	2	0.2100	0.0169	0.0668	0.4028
	3	0.1655	0.0142	0.0534	0.1950
152-168	1	0.0800	0.0211	0.0160	0.0827
	2	0.0147	0.0207	0.0327	0.3275
	3	0.1224	0.0178	0.0615	0.1939
168-183	1	0.0828	0.0184	0.0070	0.2043
	2	0.0692	0.0174	0.0486	0.3337
	3	0.1307	0.0145	0.0540	0.1871
183-198	1	0.0736	0.0154	0.0077	0.1748
	2	0.0556	0.0151	0.0484	0.3012
	3	0.1155	0.0106	0.0547	0.1655

Table 43. Effective anion exchange capacity (EAEC), and anion exchange phase composition ($cmol_c/kg$) of plot 10 using the potassium acetate extraction method. (continued)

Depth	Replicate	SO_4	NO_3	Cl	EAEC
cm		——————————— $cmol_c/kg$ ———————————			
198-213	1	0.1022	0.0087	0.0283	0.1828
	2	0.0742	0.0080	0.0263	0.1802
	3	0.0704	0.0031	0.0306	0.2357
213-229	1	0.1294	0.0096	0.0394	0.3352
	2	0.1387	0.0093	0.0486	0.4998
	3	0.2153	0.0048	0.0596	0.3030
229-245	1	0.0226	0.0102	0.0126	0.4250
	2	0.1833	0.0103	0.0480	0.4477
	3	0.1962	0.0011	0.0451	0.0588
245-261	1	0.0450	0.0114	0.0164	0.6936
	2	0.3141	0.0121	0.0534	0.3592
	3	0.1562	0.0009	0.0353	0.1072

Table 44. Volume (mL) of first saturating solution added and combined with 5g soil samples for equilibrium exchange isotherm studies at 0.0002 total normality. Where X and Y represent the two anions participating in the exchange.

Ratio #	0.0004 M KX	Entrained H_2O	0.0002 *M* K_2Y	Total
1	4.95	5	0.05	10
2	4.90	5	0.10	10
3	4.85	5	0.15	10
4	4.80	5	0.20	10
5	4.60	5	0.40	10
6	4.40	5	0.60	10
7	4.20	5	0.80	10
8	4.00	5	1.00	10
9	3.80	5	1.20	10
10	3.60	5	1.40	10
11	3.40	5	1.60	10
12	3.20	5	1.80	10
13	3.00	5	2.00	10
14	2.80	5	2.20	10
15	2.60	5	2.40	10
16	2.40	5	2.60	10
17	2.20	5	2.80	10
18	2.00	5	3.00	10
19	1.80	5	3.20	10
20	1.60	5	3.40	10

Table 45. Volume (mL) of second saturating solution added and combined with 5g soil samples for equilibrium exchange isotherm studies at 0.0002 total normality. Where X and Y represent the two anions participating in the exchange.

Ratio #	0.0004 M KX	Entrained H_2O	0.0002 *M* K_2Y	Total
21	0.05	5	4.95	10
22	0.10	5	4.90	10
23	0.15	5	4.85	10
24	0.20	5	4.80	10
25	0.40	5	4.60	10
26	0.60	5	4.40	10
27	0.80	5	4.20	10
28	1.00	5	4.00	10
29	1.20	5	3.80	10
30	1.40	5	3.60	10
31	1.60	5	3.40	10
32	1.80	5	3.20	10
33	2.00	5	3.00	10
34	2.20	5	2.80	10
35	2.40	5	2.60	10
36	2.60	5	2.40	10

Table 46. Volume (mL) of initial saturating solution added and combined with 5g soil samples for equilibrium exchange isotherm studies at 0.0002 total normality. Where X and Y represent the two anions participating in the exchange.

Ratio #	0.0004 M KX	Entrained H_2O	0.0004 M K_2Y	Total
1	4.95	5	0.05	10
2	4.90	5	0.10	10
3	4.85	5	0.15	10
4	4.80	5	0.20	10
5	4.60	5	0.40	10
6	4.40	5	0.60	10
7	4.20	5	0.80	10
8	4.00	5	1.00	10
9	3.80	5	1.20	10
10	3.60	5	1.40	10
11	3.40	5	1.60	10
12	3.20	5	1.80	10
13	3.00	5	2.00	10
14	2.80	5	2.20	10
15	2.60	5	2.40	10
16	2.40	5	2.60	10
17	2.20	5	2.80	10
18	2.00	5	3.00	10
19	1.80	5	3.20	10
20	1.60	5	3.40	10
21	0.05	5	4.95	10
22	0.10	5	4.90	10
23	0.15	5	4.85	10
24	0.20	5	4.80	10
25	0.40	5	4.60	10
26	0.60	5	4.40	10
27	0.80	5	4.20	10
28	1.00	5	4.00	10
29	1.20	5	3.80	10
30	1.40	5	3.60	10
31	1.60	5	3.40	10
32	1.80	5	3.20	10
33	2.00	5	3.00	10
34	2.20	5	2.80	10
35	2.40	5	2.60	10
36	2.60	5	2.40	10

VITA

Jessica Lynn Ottinger was born March 21st, 1988 in Cleveland, Tennessee, to David Lynn and Carla Mason Ottinger. Jessica grew up in Decatur, Tennessee, and received her high school diploma from The Baylor School in Chattanooga, Tennessee in 2006. Jessica attended the University of Tennessee in Knoxville, Tennessee, where she received her Bachelor's of Science in Environmental and Soil Science in May 2010. She then went on to receive a Master's of Science in Environmental and Soil Science in December 2012 from the same institution.